

NORTHERN AFFAIRS
GEOLOGY LIBRARY
DO NOT REMOVE

Grant 0114.68/60
Thanks for all your help
& friendship along the
way
Bob

QE 195

T87

**THE GENESIS OF STRATIFORM LEAD-ZINC DEPOSITS,
JASON PROPERTY, MACMILLAN PASS, YUKON**

**A DISSERTATION
SUBMITTED TO THE DEPARTMENT OF GEOLOGY
AND THE COMMITTEE ON GRADUATE STUDIES
OF STANFORD UNIVERSITY
IN PARTIAL FULFILLMENT OF THE REQUIREMENTS
FOR THE DEGREE OF
DOCTOR OF PHILOSOPHY**

By

Robert John Whitlock Turner

October 1986

DIAND - YUKON REGION, LIBRARY

I certify that I have read this thesis and that in my opinion it is fully adequate, in scope and quality, as a dissertation for the degree of Doctor of Philosophy.

Mart. Smadi
(Principal Adviser)

I certify that I have read this thesis and that in my opinion it is fully adequate, in scope and quality, as a dissertation for the degree of Doctor of Philosophy.

James Douglas

I certify that I have read this thesis and that in my opinion it is fully adequate, in scope and quality, as a dissertation for the degree of Doctor of Philosophy.

Stephen Alan Galt

Approved for the University Committee on Graduate Studies:

Elizabeth Cross Vrangos

Dean of Graduate Studies

THE GENESIS OF STRATIFORM LEAD-ZINC DEPOSITS
ON THE JASON PROPERTY, YUKON

Robert John Whitlock Turner, Ph. D.
Stanford University, 1986

In modern geothermal systems, the factor limiting the formation of metal sulfides is the availability of reduced sulfur; in anoxic watermasses, the limiting factor is the availability of metal. The coincidence, therefore, of an exhalative metal-bearing geothermal system and a reduced watermass is very favorable for the formation of stratiform sulfide mineralization. The occurrence of stratiform Pb-Zn sulfide deposits throughout the Proterozoic and Lower Paleozoic and their absence following the oxygenation of the world ocean in the middle Paleozoic supports the contention that anoxic ocean waters were prerequisite for the formation and preservation of stratiform Zn-Pb deposits.

Stratiform lead-zinc mineralization at the Jason property occurs within marine sediments of the Lower Earn Group of Middle to Late Devonian age that were deposited below a deep water, euxinic sea during rifting or wrench tectonism of the outer miogeocline of northwestern North America. Stratiform mineralization occurs adjacent to a synsedimentary fault and is interstratified with organic-rich siliceous shale, thin-bedded siltstone turbidite, and sedimentary breccias derived from the fault scarp. Mineralization includes veining and brecciation within and adjacent to the fault, thick bedded stratiform mineralization adjacent to the fault, and sheetlike bodies of finely laminated stratiform mineralization distal to the fault. Laminae and beds of quartz-sphalerite, sphalerite, sphalerite-galena, galena, galena-pyrite, pyrite, siderite, ankerite, barite, and carbonaceous quartz-pyrite comprise the deposit. The stratiform deposit is divided spatially into six distinctive assemblages of laminae types. Relative to the Jason fault, from proximal to distal they are: pyrite, iron carbonate, Pb-Zn-Fe sulfide, barite-sulfide, quartz-sulfide and quartz. Near the Jason fault, stratiform mineralization is cut by abundant irregular veinlets and nodules, and replacement of carbonates by sulfide, and sulfide by sulfide is common.

The presence of abundant resedimentation of stratiform mineralization, compositional and textural grading of stratiform laminae and beds, and lack of evidence of sequential deposition of minerals comprising the distal strata supports a sedimentary origin. The monominerallic tendency of laminae, the lateral zoning of lead:zinc within the stratiform bodies, and compositionally graded strata suggest effective segregation mechanisms, such as differential settling rates, during sedimentation. Formation of stratiform mineralization below a submarine brine pool is argued for by: (1) strontium isotopic data from stratiform carbonates and barite samples ; (2) the textural similarity of stratiform mineralization with modern brine pool sediments; (3) stratigraphic evidence for the deposition of stratiform mineralization within a bathymetric depression and (4) the quartz-rich nature of the stratiform mineralization. Hydrothermal discharge was cyclic throughout the formation of the deposit with individual cycles showing a gradual increase in discharge rate, followed by an abrupt decrease. Mixing with brine pool fluids caused quenching of these fluids.

TABLE OF CONTENTS

TITLE PAGE	i
SIGNATURE PAGE.....	ii
ACKNOWLEDGEMENTS.....	iii
ABSTRACT.....	iv
TABLE OF CONTENTS.....	vi
 CHAPTER 1. PALEOZOIC OCEANS AND THE FORMATION OF STRATIFORM SEDIMENT-HOSTED LEAD-ZINC DEPOSITS	
INTRODUCTION.....	1
CHARACTERISTICS OF STRATIFORM Pb-Zn DEPOSITS.....	1
Ore Deposit Character	1
Tectonic Setting.....	3
Age	5
SUBOXIC AND ANOXIC MARINE ENVIRONMENTS.....	9
Sedimentation in Anoxic Environments.....	11
ANOXIC PROTEROZOIC AND PALEOZOIC GLOBAL OCEAN	11
Lower Paleozoic Ocean	11
Proterozoic Ocean.....	12
Causes of Anoxia and Ventilation	13
Variations in Degree of Anoxia in Lower Paleozoic Ocean.....	13
ASSOCIATION OF STRATIFORM Pb-Zn DEPOSITS AND ANOXIC CONDITIONS	14
Textural and Stratigraphic Evidence.....	14

Temporal Association	16
Paleo-latitudinal Control.....	16
Selwyn Basin.....	18
ANOXIA, SULFUR SOURCE AND STRATIFORM DEPOSITS	18
CONCLUSIONS	20
REFERENCES	22
CHAPTER 2. SYNSEDIMENTARY FAULT CONTROL OF LATE DEVONIAN AGE SEDIMENTARY BRECCIAS AND STRATIFORM LEAD-ZINC DEPOSITS, JASON PROPERTY, MACMILLAN PASS YUKON	33
INTRODUCTION.....	33
GEOLOGICAL SETTING OF THE MACMILLAN PASS AREA.....	34
GEOLOGY OF THE JASON SYNCLINE AREA.....	41
Lithofacies.....	45
Siltstone Turbidite Lithofacies	45
Turbidite Channel Lithofacies.....	45
Sedimentary Breccia Lithofacies.....	46
Carbonaceous Shale Lithofacies.....	46
STRATIGRAPHY OF THE SEDIMENTARY BRECCIA LITHOFACIES	47
Lithologies.....	48
Fine-Grained Sedimentary Rocks.....	48
Homolithic Breccia.....	50
Heterolithic Breccia.....	50
Thick-Bedded Conglomerate and Sandstone.....	56
Lithologic Sub-Facies	57

Homolithic Sub-Facies.....	57
Heterolithic Sub-Facies.....	57
Origin of Sedimentary Breccia	61
JASON HYDROTHERMAL SYSTEM	64
Jason Fault	65
Breccia Body	74
Sulfide Cemented Conglomerate.....	74
Stratiform Ore Horizons.....	74
DISCUSSION	79
Temporal Link Between Fault Movement, Sedimentation and Hydrothermal Activity.....	79
Age of the Jason Fault Relative to Sedimentation.....	80
Age of Stratiform Mineralization Relative to Sedimentation.....	81
Age of Breccia Body Relative to Faulting and Stratiform Mineralization	81
Age of Veins Relative to Faulting and Sedimentation	82
Age of Infiltration Relative to the Formation of the Breccia Body and Stratiform Mineralization.....	82
Age of Hydrothermal Activity Relative to Fault Movement.....	83
Sedimentological Environment of Deposition of Stratiform Ores	84
Hydrothermal Infiltration of Sediments	85
Tectonic Setting of the Jason Fault	87
CONCLUSIONS	89
REFERENCES	92

CHAPTER 3. DEPOSITIONAL PROCESSES IN STRATIFORM SEDIMENT-HOSTED Pb-Zn DEPOSITS; EVIDENCE FROM THE JASON DEPOSIT, MACMILLAN PASS, YUKON	100
INTRODUCTION	100
GEOLOGICAL SETTING	101
STRATIFORM MINERALIZATION	104
STRATAL TYPES IN STRATIFORM ORES	106
Siltstone Strata	108
Carbonaceous Quartz-Pyrite Strata	108
Quartz-Sphalerite Strata	112
Sphalerite Strata	114
Sphalerite-Galena Strata	118
Galena Strata	118
Galena-Pyrite Strata	120
Pyrite Strata	120
Barite Strata	123
Siderite Strata	127
Ankerite Strata	127
SUMMARY OF MINERAL TEXTURES IN STRATA TYPES	127
Distal, Laminated Horizons	127
Proximal, Thick-Bedded Horizons	128
NON-STRATIFORM TEXTURES IN STRATIFORM HORIZONS	128
Distal Horizons	128
Disseminated and Banded Celsian/Hyalophane	130

Quartz-Celsian Bands.....	130
Quartz Veins.....	133
Disseminated Pyrite.....	133
Disseminated Iron Carbonate.....	133
Irregular Veinlets of Sphalerite, Galena, Quartz and Celsian.....	133
Proximal Stratiform Body.....	133
Quartz Nodules.....	135
Ankerite Nodules.....	135
Disseminated Barian Muscovite.....	135
Disseminated Pyrrhotite.....	135
Pyrite.....	135
Siderite-ankerite veinlets and breccia matrix.....	138
Carbonate-Muscovite-Sulfide Veinlets.....	138
Sulfide Veinlets.....	138
Quartz-Sulfide Veinlets.....	141
Carbonate-Quartz-Sulfide Veinlets.....	141
Pyrobitumen Veinlets.....	141
Quartz Veins.....	141
Breccia Body.....	141
Jason Fault.....	152
STRATIFORM FACIES.....	155
Pyrite Facies.....	155
Iron Carbonate Facies.....	156
Pb-Zn-Fe Sulfide Facies.....	157

Barite Facies	157
Quartz-Sulfide Facies	158
Quartz Facies	161
GRADED UNITS AND METAL CYCLES	161
STRONTIUM ISOTOPIC DATA	165
SEDIMENTARY ORIGIN OF THE STRATIFORM MINERALIZATION	165
SEDIMENTATION BELOW A BRINE POOL	169
Types of Exhalative Environments	169
Interpretation of Strontium Isotope Data	170
Textural Similarity to Modern Brine Pool Sediments	173
Stratigraphic Evidence for Bathymetric Control	173
Quartz-Rich Nature of Stratiform Mineralization	174
Formation of a Brine Pool From Hot, Low Density Fluids	175
Comparison to the Atlantis II Brine Pool	176
TEMPORAL AND SPATIAL MODEL FOR MINERALIZATION	177
Paragenesis Within Distal Stratiform Body	177
Paragenesis In Proximal Stratiform Body, Breccia Body and Fault	178
Variations in the Depositional Environments:Hydrothermal Facies	180
Subsurface Environment, Vent Complex	180
Iron Carbonate Facies	182
Pyrite Facies	182
Pb-Zn-Fe Facies	184
Barite Facies	184
Quartz-Sulfide Facies	187

Quartz Facies.....	189
ZONATION.....	190
EVIDENCE FOR GRAVITATIONAL SORTING.....	190
Strata Dominated by Single Minerals.....	191
Thicker, Polyminerallic Nature of Laminae Near the Vent Area.....	192
Compositionally and Texturally Graded Units.....	192
TEMPORAL FLUCTUATIONS IN HYDROTHERMAL DISCHARGE.....	193
HIGH RATES OF HYDROTHERMAL SEDIMENTATION.....	194
DURATION OF HYDROTHERMAL ACTIVITY.....	194
CONCLUSIONS.....	195
REFERENCES.....	199

CHAPTER 1

PALEOZOIC OCEANS AND THE FORMATION OF STRATIFORM SEDIMENT-HOSTED LEAD-ZINC DEPOSITS

INTRODUCTION

Stratiform sediment-hosted Pb-Zn deposits are generally interpreted to reflect submarine venting of hydrothermal fluids during the extensional faulting of continental crust (Large, 1981; Badham, 1981). It has been recognized that an anoxic depositional environment is prerequisite for the formation and preservation of stratiform Pb-Zn deposits (Large, 1981; Vaughan, 1981). Though widespread in strata of Proterozoic and Lower Paleozoic age, stratiform Pb-Zn deposits are absent in strata younger than Mississippian age. This paper presents data and interpretations which suggest that the disappearance of this class of ore deposit coincided with a middle Paleozoic global decrease in the extent of anoxic ocean waters (cf. Berry and Wilde, 1978).

CHARACTERISTICS OF STRATIFORM Pb-Zn DEPOSITS

Ore Deposit Character

Stratiform sediment-hosted Pb-Zn deposits (Table 1.1), also known as sediment-hosted submarine exhalative lead-zinc deposits, shale-hosted Pb-Zn deposits and sediment-hosted massive sulfide deposits, are regarded as a distinct class of ore deposit (Large, 1981; Smith, 1983; Sawkins, 1984). Although minor volcanic rocks are associated with some deposits, this class of deposits is distinguished from volcanogenic massive sulfide deposits by their general lack of association with volcanic rocks and by higher lead to copper ratios (Gustafson and Williams, 1981). Stratiform Pb-Zn deposits occur as concordant sheet-like to tabular bodies which commonly are adjacent to or overlie zones of discordant sulfide-bearing veins or breccias. The stratiform portions range up to tens of meters thick and up to thousands of

DEPOSIT NAME	AGE	METALS	ROCK	Org	Lat.	REFERENCE
Red Dog, Alaska	Early Miss.-Mid Penn.	Zn Pb Ag	S	0	40-45	Moore et al. (in press)
Lib, Alaska	Mississippian	Zn Pb Ag	S	0	40-45	Forrest, 1983
Brenchwater Cr., Alaska	Mississippian	Zn Pb Ag	S	0	40-45	Nockelberg and Winkler, 1982
Silvermines, Ireland	Early Mississippian	Zn Pb Ag	C	X	0-5	Taylor and Andrew, 1978
Jason/Too, Yukon	Late Devonian	Zn Pb Ag	S	0	25-30	Carne, 1979; Turner, 1985
Clear Lake, Yukon	Late Devonian	Fe Zn Pb	S	0	25-30	Abbott et al. (in press)
Cirque, D.C.	Late Devonian	Zn Pb Ag	S	0	25-30	Jefferson et al., 1983
Triumph, Idaho	Late Devonian	Zn Pb Ag	S	0	15-20	Kaibsgaard, 1951
Driftpile, B.C.	Late Devonian	Zn Pb Ag	S	0	25-30	MacIntyre, 1983
Chaudfontaine, Belgium	Late Devonian	Zn Pb	C	0	5-10	Dejonghe, 1979
Mirgaliosai, U.S.S.R.	Late Devonian	Pb Zn Ag	C	0	15-20	Saiznov and Gorzhersky, 1977
Tobeli, U.S.S.R.	Devonian	Zn Pb Cu	S	0	10-25	Saiznov and Gorzhersky, 1977
Reggen, G.D.R.	Middle Devonian	Fe Zn Pb	S	0	0-5	Krebs, 1981
Raamsberg, G.D.R.	Middle Devonian	Zn Pb Ag	S	0	0-5	Hannat, 1981
Howards Pass, Yukon	Early Silurian	Zn Pb	S	0	10-15	Goodfellow et al., (in press)
Cl/Ern, B.C.	Early Silurian	Fe Zn	S	0	10-15	MacIntyre, 1983
Reb, B.C.	Middle Ordovician	Fe Zn	S	0	5-10	MacIntyre, 1983
Blauvassli, Norway	Cambrian-Silurian	Zn Pb Cu	S	X	0-15	Laznicka, 1981
Hofjellet	Cambrian-Silurian	Zn Pb Cu	S	X	0-15	Laznicka, 1981
Anvil, Yukon	Lower Cambrian	Fe Zn Pb	S	0	20-25	Jennings and Jilson, (in press)
Nel, Yukon	Lower Cambrian	Zn Pb Ag	C	X	20-25	Miller and Wright, 1983
Reeves-MacDonald, B.C.	Lower Cambrian	Zn Pb	C	X	10-15	Hoy, 1982
Duncan, B.C.	Lower Cambrian	Zn Pb	C	X	10-15	Hoy, 1982
Aberfeldy, Scotland	Late Prot. (~600)	Zn Pb	S	0	35-40	Coats et al., 1984
Posh Pinah, Namibia	Late Prot. (~720)	Zn Pb	S	0	N.D.	Page and Watson, 1976
Ducktown, Tennessee	Late Prot. (800-850)	Fe Cu Zn	S	0	N.D.	Hesbitt and Kelly, 1980
Gossan Lead, Virginia	Late Prot. (800-850)	Fe Cu Zn	S	0	40-47	Feiss and Hauck, 1980
Black Angel, Greenland	Middle Prot. (1000-600)	Fe Zn Pb	C	0	N.D.	Pederson, 1980
Yholodnina, Siberia	Middle Prot. (1000-1050)	Zn Pb Ag	S	0	N.D.	Saiznov and Gorzhersky, 1977
Balsat-Edwards, New York	Middle Prot. (~1120)	Zn Pb	C	?	0-5	Lea and Brill, 1968
Anjhore, India	Middle-Late Prot. (1400-1600e (Zn, P		S	0	N.D.	Hair and Ray, 1977
Gansberg, F.S.A.	Middle Prot. (~1300)	Fe Zn Pb	S	0	45	Rozendaal, 1980
Aggeneys, F.S.A.	Middle Prot. (~1300)	Pb Zn Cu	S	1	45	Laznicka, 1981
Sullivan, B.C.	Middle Prot. (~1450)	Pb Zn	S	1	25	Hamilton et al., 1982
Highlands, Montana	Middle Prot. (1400-1450)	Zn Pb	S	0	25	Thorson, 1984
N.Y.C., Australia	Middle Prot. (~1650)	Zn Pb Cu	C	0	N.D.	Laubert, 1976
Mount Isa, Australia	Middle Prot. (~1650)	Zn Pb	C	0	N.D.	Mathias and Clark, 1975
Dugald River, Australia	Middle Prot. (1700-1600)	Zn Pb	C	1	N.D.	Whitcher, 1975
Lady Loretta, Australia	Middle Prot. (~1700)	Zn Pb	C	0	N.D.	Loudon et al., 1975
Sargipals, India	Middle Prot. (~1600)	Pb Cu	S	1	N.D.	Sarkar, 1974
Broken Hill, Australia	Early-Middle Prot. (1700)	Pb Zn Fe	S	1	N.D.	Johnson and Klinger, 1975
Zawar, India	Early Prot. (2400-1700)	Zn Pb Ag	C	1	N.D.	Mulherjee and Sen, 1980
Dariba-Pajpura, India	Early Prot. (2500-2000)	Zn Pb Ag	C	0	N.D.	Deb and Bhattacharya, 1980

Table 1.1 Selected characteristics of stratiform Pb-Zn deposits. AGE: Prot = Proterozoic, Miss. = Mississippian, Penn. = Pennsylvanian. METALS: major metals are listed in order of abundance. ROCK: lithology interbedded with sulfide strata: S = shale or metamorphosed equivalent, C = carbonate or metamorphosed equivalent. ORG: O = significant carbonaceous matter or graphite is present in strata interbedded with sulphides, X = absence of carbonaceous matter in host strata. LAT.: approximate paleolatitude of stratiform deposit during formation. Paleolatitudinal data for deposits of Paleozoic age from Scotese (1984); for North American deposits of Proterozoic age from Irving (1977) and for South African deposits of Proterozoic age from Piper (1973).

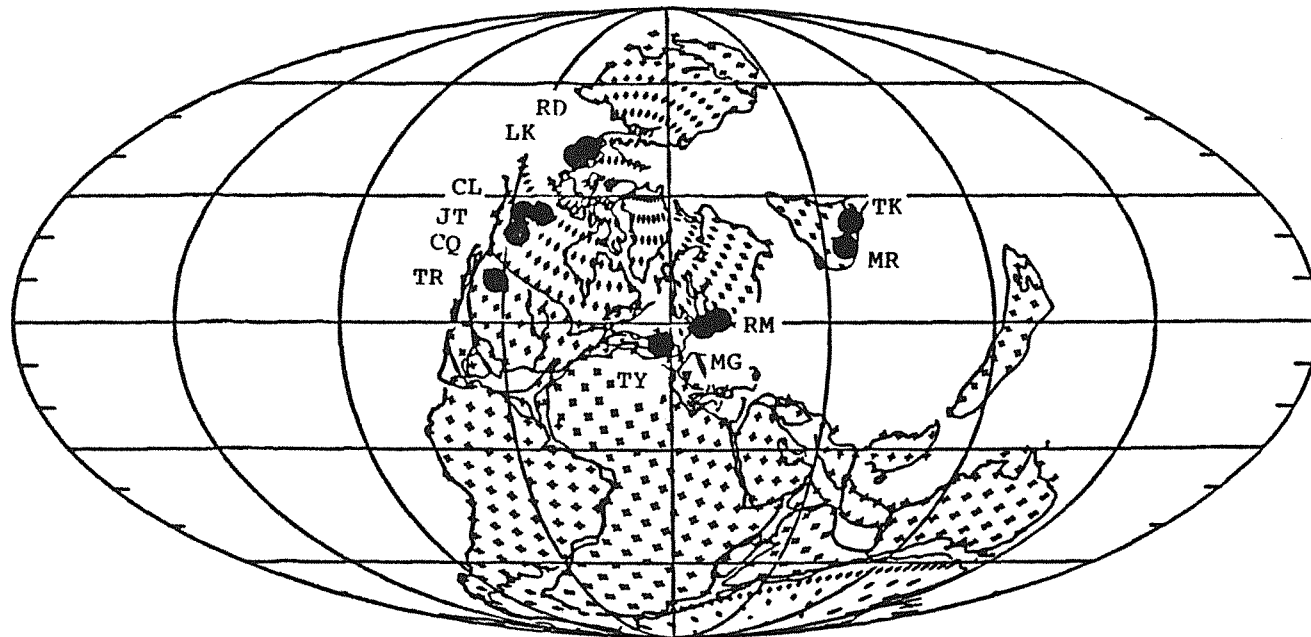
meters in lateral dimension.

Sphalerite, galena, pyrite and/or pyrrhotite are typically the dominant minerals; chert, barite, siderite and ankerite are important minerals in many deposits and chalcopyrite, tetrahedrite and arsenopyrite commonly are present as minor phases. The stratiform horizons are usually finely laminated, with monomineralic to polymineralic laminations of hydrothermal minerals ranging in thickness from a millimeter to a centimeter. Within unmetamorphosed deposits of this class such as McArthur River (Lambert, 1976), hydrothermal minerals are very fine-grained. Lead to zinc ratios range from 1:0.85 to 1:8 (Lydon, 1983). Most deposit-scale studies of stratiform deposits have led to the conclusion that mineralization reflects the sedimentary accumulation of sulfides from a submarine hydrothermal vent (Krebs, 1981; Hamilton et al, 1983; Turner, 1984; Goodfellow and Jonasson, in press).

Stratiform deposits are characteristically interbedded with and hosted by organic-rich mudrocks that lack evidence of bioturbation (Large, 1981; Smith, 1983). These carbonaceous mudrocks commonly occur in association with turbidites and are interpreted to reflect deep marine conditions; such is the interpretation at Sullivan (Hamilton, 1983), at deposits in the Selwyn basin (Turner, 1984; Goodfellow and Jonasson, in press) and at Rammelsberg (Hannak, 1981). At some other deposits, such as Meggen (Krebs, 1981), Silvermines (Taylor and Andrew, 1978) and McArthur River (Williams, 1978), organic rich strata hosting stratiform mineralization occur adjacent to shallow water carbonates interpreted to suggest that these stratiform Pb-Zn deposits formed in small, deep water basins within a platformal environment.

Tectonic Setting

The distribution of Paleozoic stratiform Pb-Zn deposits, combined with reconstructions of paleogeography by Scotese (1984), indicate that these Pb-Zn deposits formed predominantly in miogeoclinal strata along the rifted margins of continental masses (Fig. 1.1). Deposits of Paleozoic age in the Selwyn basin (Abbott, in press), the German Variscan basin



● STRATIFORM LEAD-ZINC DEPOSIT

Figure 1.1 The distribution of stratiform Pb-Zn deposits of Middle Devonian to Mississippian age plotted on the Late Devonian (Famennian) paleogeographic reconstruction of Scotese (1984). Stratiform deposits are labeled: Red Dog (RD), Lik (LK), Jason-Tom (JT), Clear Lake (CL), Cirque (CQ), Triumph (TR), Tynaugh (TY), Rammelsberg (RM), Meggen (MG), Mirgalimsai (MR), and Tekeli (TK).

(Large, in press), the Irish basin (Sevastopulos, 1981) and the central Siberian basin (Smirnov, 1977) occur along the margins of the Laurasian and Kazakhstan continental blocks (Fig. 1.1). The distribution of stratiform Pb-Zn deposits of Proterozoic age, combined with the Proterozoic continental reconstruction of Piper (1983), indicates that stratiform deposits formed both along the margins of the Proterozoic supercontinent (e.g., Broken Hill, Ducktown, Aberfeldy) as well as within intracontinental rift zones (e.g., Sullivan, MacArthur River, Zawar) (Fig. 1.2).

Within the stratigraphic sequence of a miogeoclinal or intracontinental rift, stratiform Pb-Zn deposits occur in marine strata that postdate the early redbed-basalt-evaporite stage of rift basin formation (Large, 1986). Stratigraphic evidence, such as locally derived sedimentary breccia (Williams, 1978; Turner, 1985) and abrupt changes in facies or thickness of sediment (Krebs, 1981; Hannak, 1981) within the strata hosting the stratiform deposits, suggests association with active synsedimentary faults. Faults are interpreted to reflect a rift tectonic setting (Russell, 1978; Large, 1981) or a transcurrent tectonic setting (Eisbacher, 1983; Smith, 1983;). Extensional tectonism and associated stratiform Pb-Zn deposits postdate the age of initial rift formation of the basin or continental margin by tens to several hundred million years. The oldest sediments in the Selwyn basin, for example, were deposited during a Late Proterozoic rift event (750 to 650 my), yet the major stratiform deposits are related to extensional or transform faulting events of Lower Cambrian (~ 550 my), Lower Silurian (~ 430 my) and Late Devonian (~ 375 my) ages (Abbott, in press).

Age

Stratiform Pb-Zn deposits occur in strata ranging in age from Early Proterozoic (2500 my) to Mississippian (320 my) (Table 1.1, Fig. 1.3) and are conspicuously absent from strata of latest Paleozoic, Mesozoic and Cenozoic age. The absence of stratiform Pb-Zn deposits in the Archean has been attributed to the absence of stabilized cratons and hence the absence of continental rift environments (Sawkins, 1983), the lack of a crustal lead source (Sangster, 1972) and the lack of a sulfur source for non-volcanogenic hydrothermal systems (Meyer,

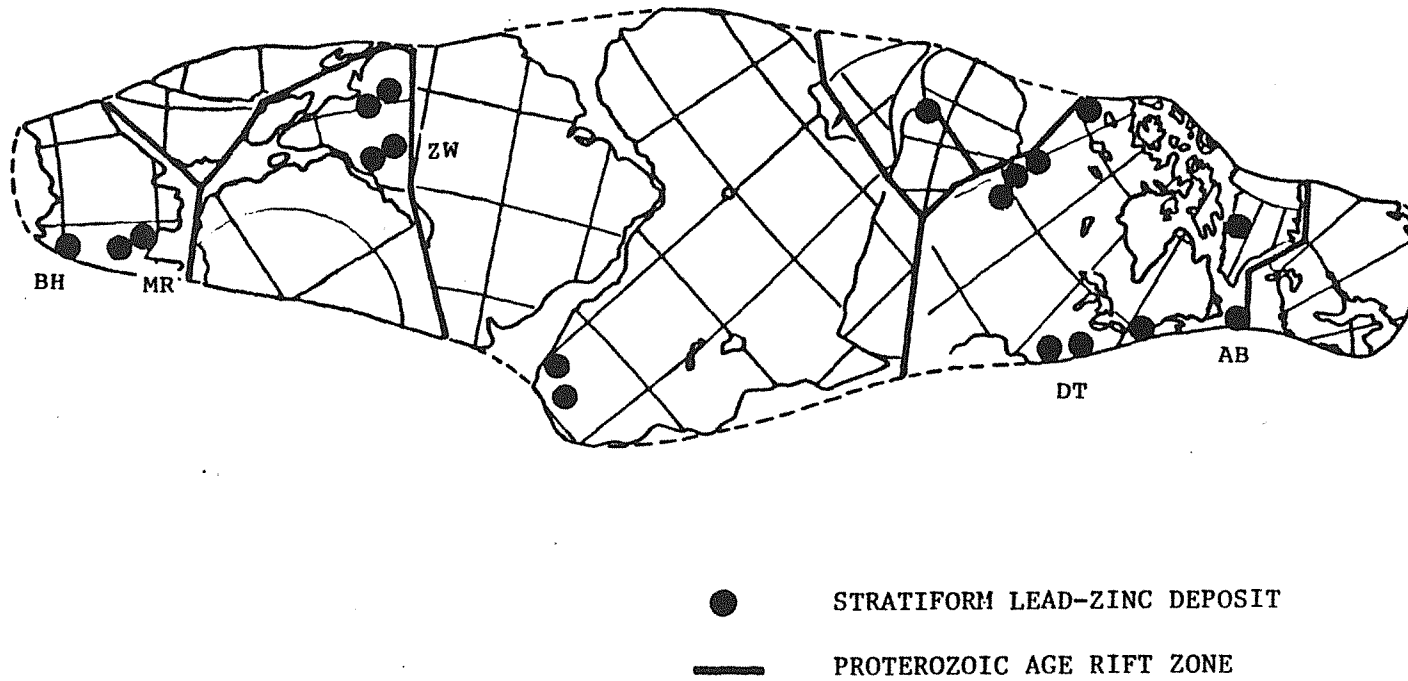


Figure 1.2 The distribution of stratiform Pb-Zn deposits of Proterozoic and Lower Cambrian age plotted on the Proterozoic supercontinent of Piper (1983). The perimeter of the continental mass is interpreted as a continental margin environment. Selected Proterozoic age deposits are labeled: Broken Hill (BH), McArthur River (MR), Zawar (ZW), Sullivan (SL), Ducktown (DT) and Aberfeldy (AB).

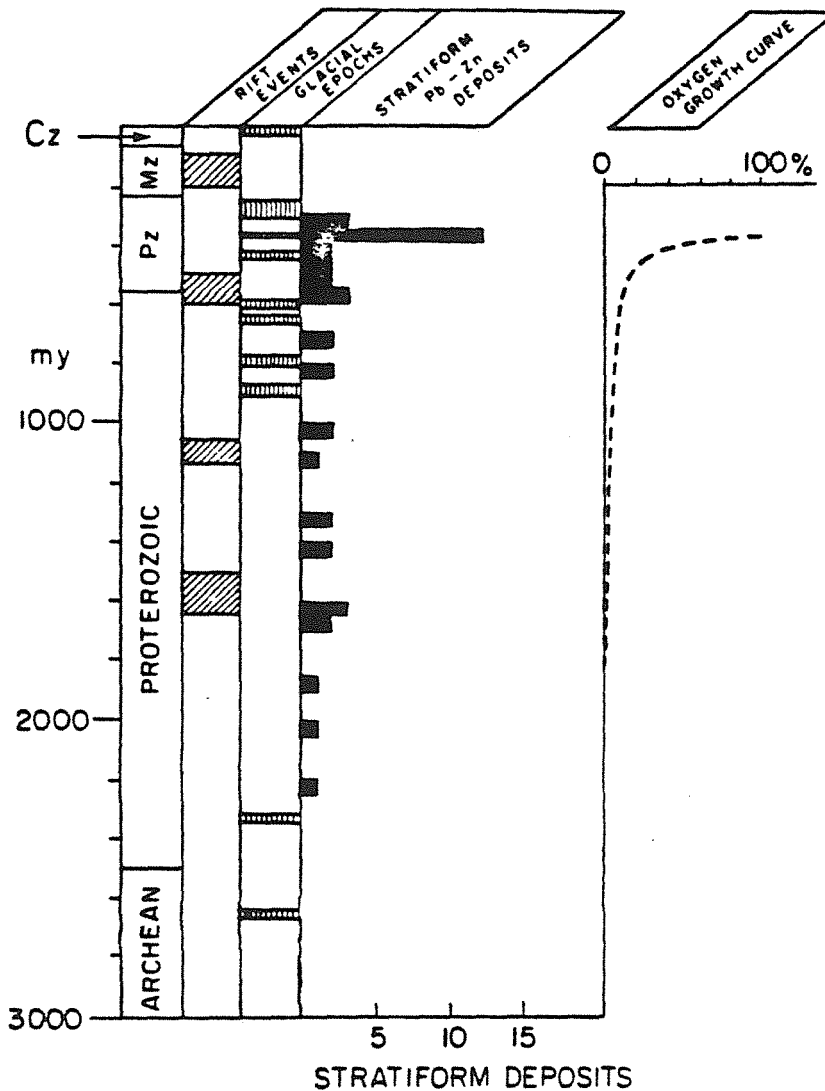


Figure 1.3 The distribution of stratiform Pb-Zn deposits with respect to geologic time based on Table 1. Also plotted are major periods of rifting after Baer (1983) and Piper (1983); glacial epochs after Harland (1983) and Crowell (1983); and the atmospheric oxygen growth curve of Cloud (1978) showing atmospheric oxygen content as a percentage of present atmospheric oxygen content.

1981).

The absence of stratiform Pb-Zn deposits in post-Mississippian strata may be attributable to several possible causes. These are: (1) the lack of the appropriate tectonic setting for the formation of stratiform Pb-Zn deposits during post-Mississippian time, (2) the present lack of exposure of sedimentary strata that might host post-Mississippian stratiform Pb-Zn deposits and/or (3) the absence of the necessary physiochemical conditions for the formation of stratiform Pb-Zn deposits in post-Mississippian time. Each of these possibilities is discussed below.

Tectonic settings favorable for the formation of stratiform Pb-Zn mineralization have been repeated throughout post-Mississippian times. Many examples of continental margin sedimentary rocks of late Paleozoic, Mesozoic and Cenozoic age are interpreted to have formed within an extensional or wrench tectonic setting. For example, rift basins of Pennsylvanian age occur in the western United States and evidence for Late Paleozoic submarine transform faulting in southern Europe and northern Africa has been presented by Arthaud and Matte (1977). In neither case are stratiform Pb-Zn deposits known to occur. The rifting of the Pangean super-continent from the Triassic to the Holocene established major continental margins on all the present continental masses (Windley, 1977). Although there are Pb-Zn deposits that formed in association with Jurassic rifting of the Alpine-Mediterranean region, Cretaceous rifting in the Benue trough, Africa and late Tertiary rifting in the Red Sea area (Windley, 1977), these deposits are epigenetic in character, rather than syngenetic stratiform deposits.

Sawkins (1983) suggests that rift-related strata of Mesozoic or Cenozoic age that might host stratiform Pb-Zn deposits are deeply buried under modern continental margin sequences. While this is true for present-day Atlantic-type margins, Mesozoic and Cenozoic sediments deposited along rifted margins of Pangean continental fragments are exposed within the Alpine orogenic belt over a strike length of almost 4000 km (Windley, 1984). Late Paleozoic to Cenozoic continental margin sedimentary rocks are exposed along a strike length of over

5000 km in the Himalayan orogenic belt (Gansser, 1964). Continental margin sequences are also exposed along the rifted margins of the Red Sea (Cochrane, 1983) and the Gulf of California. None of strata is known to host stratiform sediment-hosted Pb-Zn deposits. Neither an absence of the appropriate tectonic setting nor a lack of exposure of host sedimentary rocks appears adequate to explain the absence of stratiform deposits in post-Mississippian time. The implication is that the occurrence of the necessary physiochemical environment for stratiform sulfide deposition, particularly reduced ocean water masses, was much less common in post-Devonian times.

SUBOXIC AND ANOXIC MARINE ENVIRONMENTS

Demaison and Moore (1980) define anoxic environments in the modern ocean as settings where the concentration of dissolved oxygen in the ambient ocean water is less than 0.5 ml/l. Where these waters impinge on the ocean floor, the extremely low oxygen values limit biologic activity and enhance the capacity of sea floor muds to preserve organic matter which is generally enriched in these environments. Indeed, Rhodes and Morse (1971) formulated a now widely applied model relating decreasing dissolved oxygen values to decreasing biologic activity and bioturbation of sediment involving (1) homogenized-well bioturbated sediments and normal megafaunal associations at dissolved oxygen values of 1.0 ml/l or higher, representing oxic (e.g. aerobic) settings, (2) reduced megafaunal activity and bioturbation at dissolved oxygen values between 1.0 and 0.3 ml/l representing suboxic (e.g. dysaerobic) conditions, and (3) elimination of megafaunal activity and preservation of laminated depositional structure when dissolved oxygen values are less than 0.1 ml/l representing fully anoxic (e.g. anaerobic) environments. Such oxygen concentrations correspond to Eh values of -0.3 to -0.4 volts. This model has recently been updated by Thompson et al., (1985) based upon observations at sites where the so-called oxygen minimum zone (OMZ) or layer impinges against the continental margin off central California. These workers report biologically homogenized sediment at dissolved oxygen values as low as 0.5 ml/l. In short,

anoxic marine environments leave a clear sedimentary imprint both in terms of laminated structure and greater preservation of organic matter leading to organic-rich and laminated sedimentary rocks (Demaison and Moore, 1980).

Anoxic and near-anoxic conditions on the sea floor commonly occur where the biochemical oxygen demand exceeds the supply of dissolved oxygen in the ambient ocean water. The distribution of dissolved oxygen in the modern ocean is a function of surface air/sea mixing, temperature and salinity induced stratification of ocean waters, the origin of the discrete water masses, vigor of vertical circulation, rate of biologic productivity in surface waters, rate of advection of intermediate water, and bathymetric control of intermediate and deep water circulation. Because advective processes are important in deeper water the "age" of a given water mass also can have a bearing on its dissolved oxygen content as the water travels at depth below the surface layer.

Significantly, a distinct oxygen minimum zone (OMZ) or layer characterizes the intermediate water masses of the modern ocean at depths between 200 and 1000 m (Wystki, 1962; Kennet, 1982). This feature is especially well developed beneath areas of vigorous upwelling and consequent high biologic productivity. In fact, the degree of anoxia within the OMZ is related to the rate of biologic productivity in the overlying surface layer and to the rate of advection of the intermediate waters. The OMZ in the modern ocean is most strongly developed beneath equatorial areas and the eastern sides of ocean basins, regions characterized by vigorous upwelling and high primary productivity. The well developed OMZ in these areas reflects the relatively large amounts of biologic debris descending to intermediate depths, the extraction of dissolved oxygen via the combustion of the material, and the fact that oxygen cannot be replenished at these depths. The OMZ is often most intensely developed in areas of coastal upwelling (Calvert and Price, 1971) and in marginal seas such as the Gulf of California (Roden, 1964) where complex bottom topography restricts circulation and flushing of deep basin waters. Patterns of dissolved oxygen in the array of marginal basins developed in the borderland off southern California clearly illustrate the role

of basin topography and sill depth in the creation of anoxic and suboxic basin slope and floor settings characterized by laminated and highly organic sediments (Savrda, Bottjer, and Gorsline, 1984).

Sedimentation in anoxic environments

The total organic carbon content of a rock reflects the competing effects of biologic productivity, degree of preservation of the organic matter, and the rate of clastic sedimentation which dilutes the organic component. Mudrock deposited under anoxic conditions is commonly rich in organic matter (Fischer and Arthur, 1977; Didyk et al., 1978; Demaison and Moore, 1980). Although organic productivity is sometimes low in waters overlying stratified anoxic waters (Broecker, 1977), anoxic environments strongly favor the preservation of organic matter, largely because of the lack of oxygen. The benthic fauna common under oxic conditions consume organic matter and facilitate oxidation of sediment by their burrowing activity (Demaison and Moore, 1980). Mudrock deposited under anoxic conditions commonly has a finely laminated texture because of the exclusion of a benthic infauna when dissolved oxygen is less than 0.2 ml/l (Calvert, 1964; Rhodes and Morse, 1971; Soutar et al., 1977).

ANOXIC PROTEROZOIC AND PALEOZOIC GLOBAL OCEAN

Lower Paleozoic Ocean

Geological evidence indicates that the Lower Paleozoic ocean was characterized by a much expanded and more intensely developed oxygen minimum zone (OMZ) within the intermediate water layer than is present in the modern oceans (Berry and Wilde, 1978). The widespread distribution of organic-rich, non-bioturbated shales of Middle Cambrian to Early Devonian age indicates widespread anoxic conditions existed along continental margins during this period (Berry and Wilde, 1978). The distribution of pre-Middle Devonian organic-rich rocks, in contrast to younger Paleozoic strata, is not consistent with the inferred locations of paleo-upwelling zones suggesting that anoxic environments were not limited to

upwelling zones (Parrish, 1982). The low carbon to sulfur ratios of Cambrian to Devonian strata suggest deposition during anoxic conditions (Berner and Raiswell, 1983). Models of the sulfur and carbon flux through Earth history imply a low burial rate of organic carbon during the Lower Paleozoic and a low organic productivity which is typical of stratified ocean conditions (Berner and Raiswell, 1983).

There is evidence that this intensified oxygen minimum zone was overturned and dissipated in Devonian times. Evaporites of Late Devonian age worldwide record a sharp increase in $\delta^{34}\text{S}$ that suggests a sudden overturn of very anoxic seawater (Holser, 1977; Claypool et al., 1980). The virtual extinction of graptolites and the initial proliferation of fishes during the Middle Devonian (Berry and Wilde, 1978) may be explained by this proposed toxic overturn event and subsequent expansion of hospitable environments for nectic and planktonic life.

Proterozoic Ocean

The paleo-chemistry of waters below the surface mixing zone in the Early and Middle Proterozoic ocean is poorly known. Because benthic fauna did not evolve until the Late Proterozoic (Cloud, 1978), finely laminated sediment of Proterozoic age is not necessarily diagnostic of formation under anoxic conditions. The paucity of sulfate deposits and the poor biostratigraphic age control provide few constraints on the sulfur isotope variation of the Proterozoic ocean water through time (Claypool et al., 1980). However, several lines of evidence suggest that the Proterozoic oceans may have been less oxygenated than the modern ocean. The late Early Proterozoic and Middle Proterozoic are distinctive by the absence of glaciation events (Harland, 1983). Globally equable climates with weak latitudinal thermal gradients result in sluggish oceanic circulation and the consequent expansion of the oxygen minimum zone. Colder glacial epochs are characterized by increased oceanic circulation, more efficient oxygenation of the oceans and the contraction of the oxygen minimum zone (Fischer and Arthur, 1977). Therefore, this period from 2000 my to 1000 my likely was typified by sluggish oceanic circulation, a setting that favors oceanic stratification. However,

it must be noted that stratiform deposits do not appear to be more abundant during this non-glacial period than the following Late Proterozoic period which was punctuated by major glacial events. The low levels of atmospheric oxygen during the Proterozoic would also have favored a poorly oxygenated hydrosphere. Cloud (1978) argues that even by the end of the Proterozoic, the oxygen concentration in the atmosphere had only reached ten percent of the present atmospheric oxygen level, although this assertion has been challenged by several authors (e.g., Windley et al., 1984). The low carbon to sulfur ratios in Precambrian strata (Berner, 1984) also support the presence of a anoxic ocean.

Causes of Anoxia and Ventilation

Berry and Wilde (1978) suggest that an anoxic deep water mass, inherited from the Archean, persisted through the Proterozoic and Lower Paleozoic and that oxygenation of the deep oceans lagged behind that of the shallow oceans and atmosphere. Several major periods of glaciation occurred during the Late Proterozoic between 900 and 600 my (Harland, 1983). The major Late Carboniferous glaciation in Gondwanaland persisted from mid-Carboniferous to mid-Permian (Crowell, 1983). Less significant glacial periods also occurred during the Late Ordovician and Middle Devonian (Crowell, 1983). Berry and Wilde (1978) argue that these successive glaciations during the late Precambrian and Paleozoic caused a progressive expansion of the deep, oxygenated waters of the oceans and a simultaneous contraction of the residual oxygen minimum zone. The Middle Devonian and major mid-Carboniferous to mid-Permian glaciations completed this oxygenation process. Holland (1983) notes that this proposed oxygenation of the oceans does coincide with a major increase in atmospheric oxygen concentration levels associated with the Devonian invasion of the continents by higher land plants as proposed by McLean (1978).

Variations in Degree of Anoxia in Lower Paleozoic Ocean

Temporal variations may have existed in the redox state of anoxic Lower Paleozoic oceans. Four periods of extreme basin water stagnation have been interpreted from evidence

in Lower Cambrian to Late Devonian strata in the Selwyn basin, Yukon (Goodfellow and Jonasson, 1984). More oxygenated periods of the stratified oceans were likely related to periods of expansion of the polar ice cap (Berry and Wilde, 1978).

In addition to these temporal variations, spatial variations in oceanic redox conditions due to upwelling and basin restriction likely caused the local development of extremely reduced waters within the anoxic global ocean. Parrish (1982) predicts the locations of upwelling during the Paleozoic era using paleogeographic reconstructions and modeled atmospheric circulation. Demaison and Moore (1980) indicate that throughout geologic time, the Coriolis effect has focused deep circulation on the western side of ocean basins, causing a tendency for relatively sluggish circulation to occur on the eastern sides of oceanic basins. Claypool et al. (1980) recognize that during interpreted periods of overturn of stratified waters, the sharp rise in the general worldwide levels of $\delta^{34}S$ is accompanied by even higher values of $\delta^{34}S$ within particular regions. These very high values are interpreted by the authors to reflect the overturn of locally developed very anoxic basins.

ASSOCIATION OF STRATIFORM Pb-Zn DEPOSITS AND ANOXIC CONDITIONS

Textural and Stratigraphic evidence

Of the 44 stratiform Pb-Zn deposits listed in Table 1.1, 30 are hosted by strata rich in organic carbon. An anoxic depositional environment is inferred from the finely laminated carbonaceous strata associated with most unmetamorphosed stratiform Pb-Zn deposits. Of the remaining deposits, eight are hosted by micritic carbonate sediments. As the rate of carbonate mud sedimentation is characteristically high (Bathurst, 1978), the low organic carbon content of these deposits may reflect dilution by high carbonate sedimentation rates. Five of the deposits have undergone medium to high grade metamorphism that may have caused the oxidation of organic matter (Nesbitt and Kelly, 1980). The Sullivan deposit is hosted by siltstone turbidites which reflect deposition in a site with a high rate of terrigenous sedimentation (Hamilton et al., 1983).

Four paleo-anoxic settings are recognized for the carbonaceous, non-bioturbated mudrocks that host stratiform sulfide deposits:

(1) Regionally extensive, non-bioturbated carbonaceous shale and chert: these strata are interpreted to reflect very starved, anoxic, deep marine basin conditions. Such stratigraphic units host the Howards Pass stratiform deposit, Selwyn Basin. The very heavy sulfur isotope content of pyrite, non-bioturbated carbonaceous sediment, graded beds of pyrite framboids, anomalously high sulfur-to-carbon ratios in the sediment and the absence of ostracods and deep-water conodonts suggest a stratified, very anoxic water column in the Selwyn Basin during the formation of the Howards Pass deposit (Goodfellow and Jonasson, in press). Other examples of stratiform deposits in similar depositional settings are the Cirque and Driftpile Creek deposits (Table 1.1). At the Red Dog deposit, the change from anoxic to oxidizing conditions within the local water column during the Mississippian to Permian coincides with the disappearance of sulfide mineralization in the strata (Moore et al., in press).

(2) Regionally extensive non-bioturbated carbonaceous shale with interbedded coarser turbidite sediments: these sedimentary rocks are interpreted to reflect fluctuations between very low and high rates of sedimentation in anoxic deep marine basin environments. The non-bioturbated carbonaceous chert and siltstone, characterized by isotopically very heavy pyrite and very high V/Cr ratios and interbedded with coarse-grained turbidites and debris flows that host the Jason and Tom deposits are suggestive of a very reducing bottom water environment (Large, 1981; Turner, 1984; Goodfellow and Jonasson, 1984). Other deposits in similar sedimentary settings are Rammelsberg and Triumph (Table 1.1).

(3) Locally developed non-bioturbated carbonaceous shales adjacent to coeval non-carbonaceous facies: these sedimentary rocks are interpreted to reflect locally developed anoxic marine environments adjacent to shallower marine oxygenated environments. A close spatial relationship exists between sulfide lenses and graphitic schist and isotopically very heavy pyrite in the Anvil district (Shanks et al., in press). Other deposits in similar settings are Meggen and Gamsberg (Table 1.1).

(4) Locally developed, finely laminated lacustrine carbonaceous shales adjacent to coeval non-carbonaceous strata. At the McArthur River deposit, the carbonaceous strata hosting sulfide mineralization are interpreted by Muir (1983) to reflect a shallow-water, anoxic lacustrine environment adjacent to oxic lacustrine and subaerial environments.

Settings 1 and 2 suggest formation of stratiform deposits within large, deepwater anoxic basins. Settings 3 and 4 suggest formation of stratiform deposits within anoxic waters close to an interface with shallower oxic waters. Each of the groups illustrates the close association of stratiform sulfide deposits and anoxic depositional environments.

Temporal Association

As argued above, a stratified global ocean with a much expanded oxygen minimum zone existed during Proterozoic and Lower Paleozoic times. This stagnant state may have been disrupted during the Devonian and Mississippian (Fig. 1.3). Stratiform Pb-Zn deposits occur throughout the Proterozoic and Lower Paleozoic but are absent in rocks younger than Mississippian age. The exclusive formation of stratiform Pb-Zn deposits during the existence of a very stratified global ocean strongly suggests that a genetic link exists between anoxic conditions and the formation and/or preservation of stratiform Pb-Zn mineralization.

Paleo-latitudinal Control

In all cases, stratiform Pb-Zn deposits formed at paleolatitudes less than 45 degrees and that over 75 percent formed at a paleolatitude of less than 30 degrees (Fig. 1.4). This latitudinal control is interpreted to reflect the greater tendency of highly anoxic conditions to form at low latitudes. Oxygen is less soluble in the warmer waters of tropical latitudes (Weiss, 1970). Tropical areas are at a maximum distance from the polar source areas of oxygenated deep waters and, hence, deep oxygenated waters may be consumed prior to reaching low latitudes during periods of sluggish circulation (Berry and Wilde, 1978). Upwelling, the major cause of anoxia in the modern ocean, is most commonly developed at latitudes less than 40 degrees (Ziegler et al., 1979).

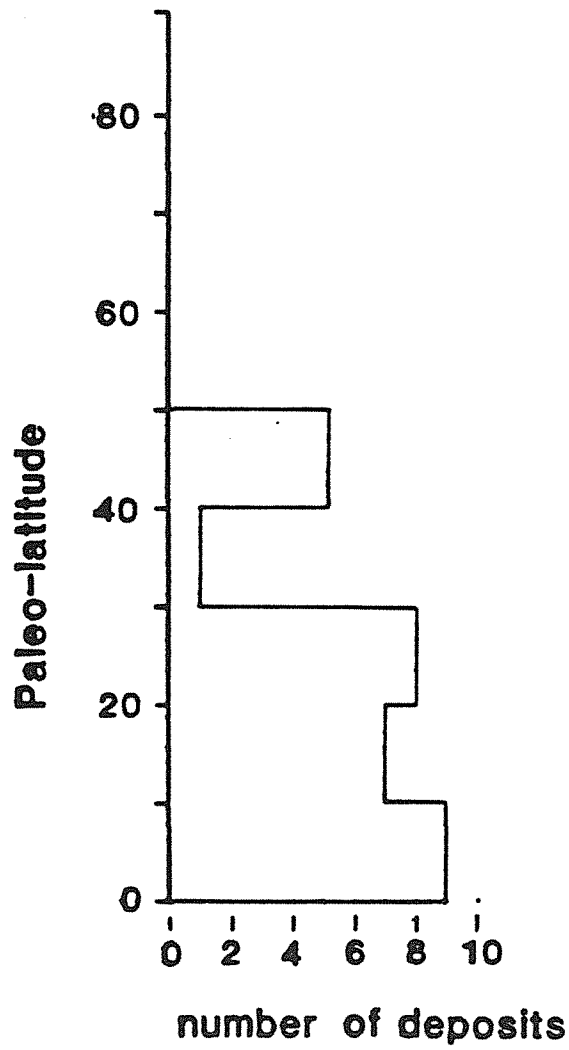


Figure 1.4 The relationship of paleo-latitude and the occurrence of stratiform Pb-Zn deposits of Paleozoic age (based on data from Irving, 1977; Piper, 1973 and Scotese, 1984).

Selwyn Basin

Within this low latitude belt of stratiform Pb-Zn deposit occurrences, more local factors may have been important in creating environments of extreme anoxia. The $\delta^{34}S$ of Late Devonian evaporites in the Alberta basin of Canada suggest that they formed adjacent to an anomalously anoxic marine basin (Claypool et al, 1980). The source of these very anoxic waters was, at least in part, the Selwyn basin, a Lower Paleozoic marginal sea on the west coast of Paleozoic North America (Abbott, in press). Goodfellow and Jonasson (1984) and Shanks et al (in press) suggest that the formation of stratiform Pb-Zn deposits in the Selwyn basin coincided with periods of extreme basin stagnation. Based on the $\delta^{34}S$ values for basinal diagenetic pyrite from Lower Paleozoic strata, these authors conclude that stratiform deposits of Lower Cambrian, Lower Silurian and Late Devonian age formed during basin-wide stagnation events in which most or all the seawater sulfur was in a reduced state. The extreme anoxia in the waters of the "Selwyn Sea" likely reflects the combined effects of upwelling (Figs. 5, 7, 8, 9, in Parrish, 1982), restriction of basinal waters (Goodfellow, 1984), the regional stagnation of ocean waters on the eastern side of the proto-Pacific ocean (Demaison and Moore, 1980) and the anoxic state of the global oceans. This evidence is suggestive that stratiform Pb-Zn deposits preferentially formed in extremely reduced environments within the globally stratified Proterozoic and Paleozoic oceans.

ANOXIA, SULFUR SOURCE AND STRATIFORM DEPOSITS

The association of anoxic conditions and stratiform deposits may reflect two different but related factors: (1) the availability of reduced sulfur for metal sulfide formation and (2) the post-depositional preservation of the metal sulfide sediment. The possible major sources of sulfur for sulfides in sediments are the mantle and seawater or evaporite sulfate. Isotopic evidence suggests that seawater sulfate has been a major source of sulfide in sediment-hosted deposits during the Phanerozoic (Sangster, 1968, 1976) and as far back as the Archean (Monster et al., 1979; Schidlowski, 1979). The reduction of seawater sulfate to sulfide may result from several processes. Low-temperature ($T < 70^\circ C$) biogenic reduction by sulfate-

reducing bacteria that use sulfate for anaerobic oxidation of organic matter can occur in anoxic seawater (Brewer and Spencer, 1974) and shallowly buried reducing sediments (Trudinger, 1976). The non-biogenic reduction of sulfate by organic matter at higher temperatures ($T > 80^{\circ} \text{C}$) has been suggested to explain isotopic patterns in sulfur species associated with the maturation of hydrocarbons in sedimentary basins (Orr, 1974). As well, high temperature ($T > 250^{\circ} \text{C}$) inorganic reduction of sulfate by ferrous iron has been established experimentally by several workers (e.g., Hajash, 1975). Unfortunately, there are no unequivocal criteria for distinguishing whether the sulfide in a sediment-hosted ore deposit is biogenically reduced sulfate or non biogenically reduced sulfate (Trudinger, 1976). Sulfur isotope data, the most commonly used criteria, can be ambiguous because both bacteriogenic exchange reactions and high-temperature inorganic exchange reactions between sulfide and sulfate can produce similar isotopic patterns (Ohmoto and Rye, 1979).

Several lines of evidence, however, favor bacterially-reduced seawater sulfate as a major sulfur source during the formation of stratiform sediment-hosted Pb-Zn deposits. Mathematical modeling of sulfide production in organic-rich sediments (Trudinger et al., 1972; Rickard, 1973), as well as kinetic studies of the rates of sulfate reduction in modern anoxic marine sediments (Trudinger, 1981) suggest that bacteriogenic sulfide production is sufficient to produce sulfide accumulations equivalent in mass to stratiform ore deposits. The results of sulfur isotopic studies of individual stratiform Pb-Zn deposits have also been used to argue that a major source of sulfur was the biogenic reduction of seawater sulfate. Such deposits include Silvermines (Coomer and Robinson, 1976); Sullivan (Campbell et al., 1978); Jason (Gardner and Hutcheon, 1985); Howards Pass (Goodfellow and Jonasson, in press) and Anvil (Shanks et al., in press). Sulphur isotope data from the Meggen deposit (Buschendorf et al., 1963); the Rammelsberg deposit (Anger et al., 1966) and Tom deposit (Large, 1981) is compatible with a biogenically-reduced seawater sulfate source, although the authors of the particular studies favored different sources of sulfur or different mechanisms of sulfate reduction. Goodfellow and Jonasson (1984, in press) and Shanks et al., (in press) suggest that

the sulfur in metal sulfides in the Howards Pass, Tom, Jason and Anvil stratiform Pb-Zn deposits of the Selwyn basin was derived from very stratified, basin waters where quantitative bacteriogenic reduction of sulfate to sulfide had created a sulfidic water mass.

The association of stratiform Pb-Zn deposits and anoxic depositional environments may also reflect the high preservation potential of metal sulfides in anoxic waters and reduced sediments. The typical occurrence of stratiform deposits in mudrocks suggests that these deposits form in environments of very low sedimentation rates. Stratiform Pb-Zn deposits have been interpreted by Sawkins (1984a, 1984b) to result from episodic mineralization events that may span several million years. Goodfellow and Jonasson (in press) interpret paleontological data at the Howards Pass deposit, Yukon, to indicate that mineralization spanned 3 to 5 million years. The Jason deposit may have formed over a period of 150,000 years (Chapter 3). Preservation of sedimentary sulfides from post-depositional oxidation in conditions where rapid burial by sediment does not occur requires a reduced bottom water. In modern sediments, most biogenically produced sulfide is rapidly reoxidized to sulfate (Trudinger, 1981). Rapid oxidation of massive sulfides in the oxygenated conditions of the modern oceans has been documented at hydrothermal sites on ocean ridges (Francheteau et al., 1979). Only environments that are insulated from the oxygenated modern ocean allow the preservation of stratiform sulfide, such as the brine pool of the Atlantis II deep, Red Sea (Zierenberg, 1984).

CONCLUSIONS

Modern metal transporting geothermal systems are sulfur-deficient, and the factor limiting the formation of base-metal sulfides is the availability of reduced sulfur (White, 1981). Bacterial reduction of seawater sulfate is widespread in anoxic basins and reducing sediments, and formation of metal sulfide is limited only by the availability of metal (Trudinger et al., 1972; Rickard, 1973). Therefore, the coincidence of a exhalative metal-bearing geothermal system and a reduced watermass is very favorable for the formation of stratiform sulfide mineralization.

The distribution of anoxic ocean waters in time and space is proposed as a first-order control on the occurrence of stratiform Pb-Zn deposits. The modern ocean, characterized by vigorous circulation, is predominantly oxygenated, and anoxic conditions are commonly associated with upwelling and development of an intense oxygen minimum zone along the eastern sides of major ocean basins (Demaison and Moore, 1980). During the Mesozoic and Cenozoic eras, periods of regional oceanic stagnation occurred for timespans of only 20 million years or less (Arthur and Fischer, 1978). In contrast, anoxic oceanic conditions likely persisted throughout much of Lower Paleozoic time, a period of over 240 my. It is likely that the Proterozoic ocean was anoxic for much of its history as well. The occurrence of stratiform Pb-Zn deposits throughout the Proterozoic and Lower Paleozoic and the disappearance of these deposits from the rock record coincident with the period of oxygenation of the world ocean strongly supports the contention that anoxic ocean waters were prerequisite for the formation and preservation of stratiform Pb-Zn deposits.

REFERENCES

- Abbott, J.G., S.P. Gordey, and D.J. Templeman-Kluit, Regional setting of Paleozoic sediment-hosted stratiform lead-zinc deposits in Yukon and northeastern British Columbia, *Mineral deposits of the Northern Cordillera: Canadian Inst. Mining Metall., Spec. Vol.*, in press .
- Anger, G., H. Nielsen, H. Puchelt, and W. Rieke, Sulfur isotopes in the Rammelsberg ore deposit (Germany), *Econ. Geol.*, *61*, 511-536, 1966.
- Anhaeusser, C. R., and A. Button, A review of southern African stratiform ore deposits - their position in time and space, in *Handbook of stratiform and stratiform ore deposits*, edited by K. H. Wolf, pp. 257-319, Elsevier, Vol. 5, Amsterdam, 1976.
- Arthaud, F., and P. Matte, Late Paleozoic strike-slip faulting in southern Europe and northern Africa: result of right-lateral shear zone between the Appalachians and the Urals, *Geol. Soc. Amer. Bull.*, *88*, 1305-1320, 1977.
- Badham, J. P. N., Shale-hosted Pb-Zn deposits: products of exhalation of formation waters?, *Trans. Instn. Min. Metall.*, *90*, B70-B76, 1981.
- Bathurst, R. G. C., *Carbonate sediments and their diagenesis*, 658 pp., Elsevier, Amsterdam, 1975.
- Berner, R. A., Sedimentary pyrite formation: An update, *Geochim. Cosmochim. Acta*, *4*, 605-615, 1984.
- Berner, R. A., and R. Raiswell, Burial of organic carbon and pyrite sulfur in sediments over Phanerozoic time: a new theory, *Geochim. Cosmochim. Acta*, *47*, 855-862, 1983.
- Berry, W. B. N., and P. Wilde, Progressive ventilation of the oceans, *Amer. Jour. Sci.*, *278*, 257-275, 1978.
- Brewer, P. G., and D. W. Spencer, Distribution of some trace elements in Black Sea and their flux between dissolved and particulate load, in *The Black Sea - geology, chemistry and biology*, edited by E. T. Degens and D. H. Ross, pp. 137-143, American Assoc. Petrol. Geologists, Memoir 20, 1974.
- Broecker, W. S., *Chemical oceanography*, 214 pp., Harcourt, Brace, Jovanovich, New York, 1974.

- Burke, K., and F.J. Sawkins, Were the Rammelsberg, Meggen, Rio Tinto and related deposits formed in a Devonian rifting event? [abs.], *Econ. Geol.*, **73**, 308, 1978.
- Buschendorf, Fr., H. Neilsen, H. Puchelt, and W. Ricke, Schwefel-Isotopen-Untersuchungen am Pyrite-Sphalerit-Baryt-Lager Meggen/Lenne (Deutschland) und am verschiedenen Devon-Evaporiten, *Contr. Mineralogy Petrology*, **27**, 501-523, 1983.
- Calvert, S. E., and N. B. Price, Upwelling and nutrient regeneration in the Benguela Current; October 1968, *Deep-Sea Research*, **18**, 505-523, 1971.
- Campbell, F. A., V. G. Ethier, H. R. Krouse, and R. A. Both, Isotopic composition of sulfur in the Sullivan orebody, British Columbia, *Econ. Geol.*, **73**, 246-268, 1978.
- Carne, R.C., Geological setting and stratiform lead-zinc-barite mineralization, Tom Claims, Yukon Territory, *Open File Rept. EGS 1979-4*, 30p, 1979.
- Carr, G. R., and J. W. Smith, A comparative isotopic study of the Lady Loretta zinc-lead-silver deposit, *Mineral. Deposita*, **12**, 105-110, 1977.
- Claypool, C. E., W. T. Holser, I. R. Sakai, and I. Zak, The age curves for sulfur and oxygen isotopes in marine sulphate and their mutual interpretation, *Chem. Geol.*, **28**, 199-260, 1980.
- Cloud, P., *Cosmos, earth and man*, 372 pp., Yale University Press, New Haven, 1978.
- Coats, J. S., C. G. Smith, N. J. Fortney, M. J. Gallagher, F. May, and W. J. McCourt, Strata-bound barium-zinc mineralization in Dalradian schist near Aberfeldy, Scotland, *Inst. Mining Metallurgy Trans.*, **89**, 110-122, 1980.
- Cochran, J.R., A model for the development of Red Sea, *Amer. Assoc. Petrol. Geol. Bull.*, **67**, 41-69, 1983.
- Coomer, P. G., and B. W. Robinson, Sulphur and sulphate-oxygen isotopes and the origin of the Silvermines deposits, Ireland, *Mineralium Deposita*, **11**, 155-169, 1976.
- Crowell, J. C., The recognition of ancient glaciations, in *Proterozoic geology: Selected papers from an international Proterozoic symposium*, edited by L. G. Medaris, Jr., C. W. Byers, D. M. Michelson and W. C. Shanks, pp. 289-297, Geological Society of America Memoir 161, 1983.

- Deb, M., and A. K. Bhattacharya, Geological setting and conditions of metamorphism of Rajpura-Dariba polymetallic ore deposit, Rajasthan, India, *Proceedings of the Fifth IAGOD symposium*, pp. 679-697, E. Schweizerbart'sche Verlagsbuchhandlung, Vol. 1, Stuttgart, 1980.
- Degens, E. T., and P. Stofers, Stratified waters as a key to the past, *Nature*, 263, 22-27, 1976.
- Dejonghe, L., Discovery of a sedimentary Ba(Fe,Zn,Pb) ore body of Frasnian age at Chaudfontaine, Province of Liege, Belgium, *Mineral. Deposita*, 14, 15-20, 1979.
- Demaison, G. J., and G. T. Moore, Anoxic environments and oil source bed genesis, *American Assoc. Petrol. Geologists Bull.*, 8, 1179-1209, 1980.
- Didyk, B. M., Simoneit, B. R. T., Brassell, S., and Eglington, G., Organic geochemical indicators of paleoenvironmental conditions of sedimentation, *Nature*, 272, 216-222, 1978.
- Eisbacher, G. H., Devonian-Mississippian sinistral transcurrent faulting along the cratonic margin of western North America: A hypothesis, *Geology*, 11, 7-10, 1983.
- Emery, K. O. and Hulesmann, J., The relationships of sediments, life, and water in a marine basin, *Deep-sea Research*, v. 8, 165-180 1965.
- Fiess, P. G., and S. A. Hauck, Tectonic setting of massive sulphide deposits in the southern Appalachians, in *Proceedings of the Fifth IAGOD Symposium*, edited by J.D. Ridge, pp. 567-580, E. Schweizerbart'sche Verlagsbuchhandlung, Vol. 1, Stuttgart, 1980.
- Fischer, A. G., and M. A. Arthur, Secular variations in the pelagic realm, *S.E.P.M. Spec. Pub.*, 25, 19-50, 1977.
- Forrest, K., Geological and isotopic studies of the Lik deposit and the surrounding mineral district, DeLong Mountains, western Brooks Range, Alaska, Ph.D thesis, University of Minnesota, Minneapolis, 161p, 1983.
- Francheteau, J., H. D. Needham, P. Choukroune, T. Juteau, M. Seguret, R. D. Ballard, P. J. Fox, W. Normark, A. Carranza, D. Cordoba, J. Guerrero, C. Rangin, H. Bougalt, P. Cambon, and R. Hekinian, Massive deep-sea sulphide ore deposits discovered on the East Pacific Rise, *Nature*, 277, 523-528, 1979.
- Gansser, A., *Geology of the Himalayas*, 289 pages, Interscience Publishers, London, 1964.

- Gardner, H. G., and I. Hutcheon, Geochemistry, mineralogy and geology of the Jason Pb-Zn deposits, Macmillan Pass, Yukon, Canada, *Econ. Geol.*, 5, 1257-1276, 1985.
- Goodfellow, W., Geochemistry unveils 'blind' deposits, *GEOS*, 17-20, 1985.
- Goodfellow, W.D., and I.R. Jonasson, Ocean stagnation and ventilation defined by 34S secular trends in pyrite and barite, Selwyn Basin, Yukon, *Geology*, 12, 583-586, 1984.
- Goodfellow, W. D., and I. R. Jonasson, Environment of formation of the Howards Pass (XY) Zn-Pb deposit, Selwyn Basin, Yukon, *Mineral deposits of the Northern Cordillera: Canadian Inst. Mining Metall., Spec. Vol.*, in press.
- Gustafson, L. B., and N. Williams, Sediment-hosted stratiform deposits of copper, lead and zinc, *Econ. Geol. 75th Anniv. Vol.*, pp. 139-178, 1981.
- Hajash, A., Hydrothermal processes along mid-ocean ridges: an experimental investigation, *Contributions to Mineralogy and Petrology*, 53, 205-226, 1975.
- Hamilton, J. M., D. T. Bishop, H. C. Morris, and O. E. Owens, Geology of the Sullivan orebody, Kimberley, B.C., Canada, *Geol. Assoc. Canada Special Paper 25*, 597-625, 1982.
- Hannak, W., Genesis of the Rammelsberg ore deposit near Goslar, Upper Harz, Federal Republic of Germany, in *Handbook of strata-bound and stratiform ore deposits*, edited by K. H. Wolf, pp. 551-642, Elsevier, Vol. 9, Amsterdam, 1981.
- Harland, W. B., The Proterozoic glacial record, in *Proterozoic geology: Selected papers from an international Proterozoic symposium, Geological Society of America Memoir 161*, edited by L. G. Medaris, Jr., C. W. Byers, D. M. Michelson and W. C. Shanks, pp. 279-288, 1983.
- Holland, H. D., *The chemical evolution of the atmosphere and ocean*, 582 pp., Princeton University Press, Princeton, 1984.
- Holser, W.T., Catastrophic chemical events in the history of the ocean, *Nature*, 267, 403-408, 1977.
- Hoy, T., Stratigraphic and structural setting of stratabound lead-zinc deposits in southeastern B.C., *Can. Inst. Mining Metall. Bull.*, 75, 114-134, 1982.
- Irving, E., Paleopoles and paleolatitudes of North America and speculations about displaced ter-

- rains, *Can. J. Earth Sci.*, 16, 669-694, 1979.
- Jefferson, C. W., D. B. Kilby, L. C. Pigage, and W. J. Roberts, The Cirque barite-zinc-lead deposits, northeastern British Columbia, *Mineral. Assoc. Canada, Short Course Handbook, Vol. 9*, 121-140, 1983.
- Jennings, D. S., and G. A. Jilson, Geology and sulphide deposits of Anvil Range, Yukon Territory, in *Mineral deposits of the Northern Cordillera: Canadian Inst. Mining Metall., Spec. Vol.*, edited by J. Morin, in press.
- Johnson, I. R., and G. C. Klingner, The Broken Hill ore deposit and its environment, in *Economic geology of Australia*, edited by C. L. Knight, pp. 476-491, Australasian Institute of Mining and Metallurgy, Mon. 5, Vol. 1, 1975.
- Jonasson, I. R., and W. D. Goodfellow, Sedimentary and diagenetic textures, and deformation structures within the sulphide zone of the Howards Pass (XY) Zn-Pb Deposit, Yukon and Northwest Territories, in *Mineral Deposits of the Northern Cordillera: Canadian Inst. Mining Metall., Spec. Vol.*, edited by J. Morin, in press.
- Kennett, J. P., *Marine geology*, 813 pp., Prentice-Hall, Inc., Englewood Cliffs, N.J., 1983.
- Kiilsgaard, T. H., The geology and ore deposits of the Triumph-Parker mineral belt, *Idaho Bur. Mines Geol., Pamphlet 90*, pp. 39-62, 1950.
- Krebs, W., The geology of the Meggen ore deposit, in *Handbook of strata-bound and stratiform ore deposits*, edited by K. H. Wolf, pp. 509-549, Elsevier, Vol. 9, Amsterdam, 1981.
- Lambert, I. B., The McArthur zinc-lead-silver deposit: Features, metallogenesis and comparisons with some other stratiform ores, in *Handbook of stratabound and stratiform ore deposits*, edited by K. H. Wolf, pp. 535-585, Elsevier, Vol. 6, Amsterdam, 1976.
- Large, D. E., Sediment-hosted submarine exhalative lead-zinc deposits - a review of their geological characteristics and genesis, in *Handbook of strata-bound and stratiform ore deposits*, edited by K. H. Wolf, pp. 469-507, Elsevier, Vol. 9, Amsterdam, 1981.
- Large, D. E., On the geology, geochemistry and genesis of the Tom Pb-Zn-barite deposit, Yukon Territory, Canada, Ph.D thesis, University of Braunschweig, 152 pp., 1981a.

- Large, D. E., Sediment-hosted massive sulphide lead-zinc deposits: and empirical model, in *Sediment-hosted stratiform lead-zinc deposits*, edited by D.F. Sangster, pp. 1-29, Mineral. Assoc. Canada, Short Course Handbook, Vol. 9, 1983.
- Large, D. E., The paleotectonic setting of Rammelsberg and Meggen, Germany - A basin analysis study, in *The genesis of stratiform sediment-hosted lead and zinc deposits -- Conference proceedings*, edited by Turner, R. J. W. and M. T. Einaudi, pp. 109-113, Stanford Univ. Pubs., Geol. Sci., v. XX. , 1986 .
- Laznicka, P., Data on the worldwide distribution of stratiform and stratabound ore deposits, in *Handbook of stratabound and stratiform ore deposits*, edited by K. H. Wolf, pp. 79-576, Elsevier, Vol. 9, Amsterdam, 1981.
- Lea, E. R., and D. B. Dill, Zinc deposits of the Balmat-Edwards district, New York, *AIME Gratton - Sales Vol. 1*, pp. 20-48, 1968.
- Loudon, A. G., M. K. Lee, J. F. Dowling, and R. Bourn, Lady Loretta silver-lead-zinc deposit, in *Economic geology of Australia and Papua, New Guinea*, edited by C. L. Knight, pp. 377-382, Australasian Inst. Mining Metall., Mon. 5, Vol. 1, 1975.
- Lydon, J.W., Chemical parameters controlling the origin and deposition of sediment-hosted stratiform lead-zinc deposits, in *Sediment-hosted lead-zinc deposits*, edited by D. F. Sangster, pp. 175-250, Mineral. Assoc. Canada, Short Course Handbook, Vol. 9, 1983.
- MacIntyre, D. G., Geology and stratiform barite-sulphide deposits of the Gataga district, northeast British Columbia, in *Sediment-hosted stratiform lead-zinc deposits*, edited by D. F. Sangster, pp. 85-120, Mineral. Assoc. Canada, Short Course Handbook, Vol.9, 1983.
- Mathias, B. V., and G. J. Clark, Mount Isa copper and silver-lead-zinc orebodies - Isa and Hilton mines, in *Economic geology of Australia*, edited by C. L. Knight, pp. 351-376, Australasian Institute of Mining and Metallurgy, Mon. 5, Vol. 1, 1975.
- McLean, D. M., Land floras: The major late Paleozoic atmospheric carbon dioxide/oxygen control, *Science*, 200, 1060-1062, 1978.
- Meyer, C., Ore-forming processes in geological history, *Econ. Geol. 75th Anniv. Vol.*, 6-41, 1981.

- Miller, D., and J. Wright, Mel barite-zinc-lead deposit, *Mineral deposits of the Northern Cordillera, Abstracts, Joint Canadian Geological Association of Canada Meeting, Whitehorse, December, 1983*, p.18, 1983.
- Monster, J., P. W. U. Appel, H. G. Thode, M. Schidlowski, C. M. Carmichael, and D. Bridgewater, Sulfur isotope studies in early Archean sediments from Isua, West Greenland: implications from the antiquity of bacterial sulfate reduction, *Geochimica et Cosmochimica Acta*, **43**, 403-413, 1979.
- Moore, D. W., L. E. Young, J. S. Modene, and J. T. Plahuta, Geologic setting and genesis of the Red Dog zinc-lead-silver deposit, Western Brooks Range, Alaska, in *The genesis of stratiform sediment-hosted lead and zinc deposits - Conference proceedings*, edited by Turner, R. J. W. and M. T. Einaudi, pp. 104-108, Stanford Univ. Pubs., Geol. Sci., v. XX., in press.
- Muir, M. D., N. G. K. Nair, and A. Ray, Syndepositional and diagenetic features in pyrite ores of Amjhore, Bihar, India, *Miner. Deposita*, **12**, 151-154, 1977.
- Mukherjee, A. D., and R. N. Sen, Geochemical Implications in the genesis of Zawar lead-zinc deposit, Rajasthan, India, in *Proceedings of the Fifth IAGOD Symposium*, edited by J. D. Ridge, pp. 709-718, E. Schweizerbart'sche Verlagbuchhandlung, Vol. 1, Stuttgart, 1980.
- Nesbitt, B. E., and W. C. Kelly, Metamorphic zonation of sulfides, oxides and graphite in and around the orebodies at Ducktown, Tennessee, *Econ. Geol.*, **75**, 1010-1021, 1980.
- Nockelberg, W. J., and G. R. Winkler, Stratiform zinc-lead deposits in the Drenchwater Creek area, Howard Pass quadrangle, northwestern Brooks Range, Alaska, *United States Geological Survey Prof. Paper 1209*, **22**, 1982.
- Ohmoto, H., and R. O. Rye, Isotopes of sulphur and carbon, in *Geochemistry of hydrothermal ore deposits*, edited by H. L. Barnes, pp. 509-567, John Wiley and Sons, New York, 1979.
- Page, D.C., and M.D. Watson, The Pb-Zn deposit of Rosh Pinah mine, South West Africa, *Econ. Geol.*, **71**, 306-327, 1976.
- Parrish, J. T., Upwelling and petroleum source beds with reference to the Paleozoic, *Amer. Assoc. Petrol. Geologists Bull.*, **6**, 750-774, 1982.

- Pederson, F. D., Remobilization of the massive sulphide ore of the Black Angel mine, central west Greenland, *Econ. Geol.*, 75, 1022-1041, 1980.
- Piper, J. D. A., Dynamics of the continental crust in Proterozoic times, *Geol. Soc. America Memoir 161*, 11-34, 1983.
- Rhodes, D. C. and Morse, J. W., Evolutionary and ecologic significance of oxygen-deficient marine basins, *Lethia*, v. 4 413-428, 1971.
- Rickard, D. T., Limiting conditions for synsedimentary sulfide ore formation, *Econ. Geol.*, 68, 605-617, 1973.
- Roden, G. I., Oceanographic aspects of Gulf of California, *Amer. Assoc. Petrol. Geologists Memoir 161*, 30-58, 1964.
- Rozendaal, A., The Gamsberg zinc deposit, South Africa: a banded stratiform basemetal sulfide ore deposit, in *Proceedings of the Fifth IAGOD symposium*, edited by J. D. Ridge, pp. 619-633, E. Schweizerbart'sche Verlagbuchhandlung, Vol. 1, Stuttgart, 1980.
- Russell, M.J., Downward-excavating hydrothermal cells and Irish-type ore deposits: importance of an underlying thick Caledonian prism, *Inst. Mining Metall. Trans.*, 87, B168-B171, 1978.
- Ryan, W. B. F., and M. B. Cita, Ignorance concerning episodes of ocean-wide stagnation, *Marine Geology*, 23, 197-215, 1977.
- Sangster, D. F., Relative sulphur isotope abundances of ancient seas and stratabound sulphide deposits, *Geological Association of Canada, Proceedings 19*, pp. 79-91, 1968.
- Sangster, D.F., Precambrian volcanogenic massive sulphide deposits in Canada: a review, *Geol. Surv. Can. Pap. 72-22*, 44p., 1972.
- Sangster, D. F., Sulphur and lead isotopes in stratabound deposits, in *Handbook of stratabound and stratiform ore deposits*, edited by K. H. Wolf, pp. 219-266, Elsevier, Vol. 2, Amsterdam, 1976.
- Sarkar, S. C., Sulphide mineralization at Sargipali, Orissa, India, *Econ. Geol.*, 69, 206-217, 1974.
- Savrda, C. E., Bottjer, D. J., and Gorsline, D. S., 1984, Towards development of a comprehensive euxinic biofacies model; evidence from Santa Monica, San Pedro, and Santa Barbara Basins,

- California, *Amer. Assoc. Petroleum Geologists Bulletin*, v. 68, 1179-1192, 1984.
- Sawkins, F. J., Tectonic controls of the time-space distribution of some Proterozoic metal deposits, in *Proterozoic Geology: Selected papers from an International Proterozoic Symposium*, edited by L. G. Medaris, Jr., C. W. Byers, D.M. Michelson and W. C. Shanks, pp. 179-189, Geol. Soc. America Memoir 161, 1983.
- Sawkins, F. J., *Metal deposits in relation to plate tectonics*, p. 325, Springer-Verlag, Berlin, 1984a.
- Sawkins, F. J., Ore genesis by episodic dewatering of sedimentary basins: Application to giant Proterozoic lead-zinc deposits, *Geology*, 12, 451-454, 1984b.
- Schidlowski, M., Antiquity and evolutionary status of bacterial sulfate reduction: sulfur isotope evidence, *Origins of Life*, 9, 299-311, 1979.
- Scotese, C. R., An introduction to this volume: Paleozoic paleomagnetism and the assembly of Pangea, in *Plate reconstruction from the Paleozoic paleomagnetism*, edited by R. Van der Voo, C. R. Scotese and N. Bonhommet, pp. 1-10, American Geophysical Union, Geodynamic Series, Vol. 12, 1984.
- Sevestopulo, G. D., Lower Carboniferous, in *A geology of Ireland*, edited by C. H. Holland, pp. 147-171, John Wiley and Sons, New York, 1981.
- Shanks, W. C., III, L. G. Woodruff, G. A. Jilson, D. S. Jennings, J. S. Modene, and B. D. Ryan, Sulfur and lead isotope studies of stratiform Zn-Pb-Ag deposits, Anvil Range, Yukon: Basinal brine exhalation and anoxic bottom-water mixing, in *The genesis of stratiform sediment-hosted lead and zinc deposits - Conference proceedings*; edited by Turner, R. J. W. and M. T. Einaudi, pp. 94-98, Stanford Univ. Pubs., Geol. Sci., v. XX., in press.
- Smirnov, V. I., and D. I. Gorzhersky, Deposits of lead and zinc, in *Ore deposits of the USSR*, edited by V. I. Smirnov, pp. 182-256, Pitman, Vol. 2, London, 1977.
- Smith, C.L., Sediment-hosted stratiform lead-zinc-silver deposits, in *Revolution in the Earth Sciences- advances in the past half-century, proceeding of a symposium held at Carleton College, Northfield, Minnesota*, edited by S.J. Boardman, pp. 281-300, Kendall Hunt Publishing Company, Dubuque, Iowa, 1983.

- Soutar, A., Kling, S. A., Crill, P. A., Duffrin, E., and Bruland, W., Monitoring the marine environment through sedimentation, *Nature*, v. 266, 136-139, 1977.
- Taylor, S., Structural and paleotopographic controls of lead-zinc mineralization in the Silvermines orebodies, Republic of Ireland, *Econ. Geol.*, 79, 529-548, 1984.
- Thompson, J. B., Mullins, H. T., Newton, C. R., and Vercoutere, T. L., Alternative biofacies model for dysaerobic communities, *Lethia*, v. 18, 167-179, 1985.
- Thorson, J. P., Suggested revisions of the lower Belt Supergroup stratigraphy of the Highland Mountains, southwestern Montana [abs.], in *The Belt - Abstracts with summaries, Belt Sym. II, 1983*, edited by S. W. Hobbs, pp. 10-12, Montana Bur. Mines and Geol., Spec. Pub. 90, 1984.
- Trudinger, P. A., Microbiological processes in relation to ore genesis, in *Handbook of stratabound and stratiform ore deposits*, edited by K. H. Wolf, pp. 135-190, Elsevier, Vol. 2, Amsterdam, 1976.
- Trudinger, P. A., Origins of sulphide in sediments, *BMR Journal of Australian Geology and Geophysics*, 6, 279-285, 1981.
- Trudinger, P. A., I. B. Lambert, and G. W. Skyring, Biogenic sulfide ores: a feasibility study, *Econ. Geol.*, 67, 1114-1127, 1972.
- Turner, R.J., Geology of the South Zone deposits, Jason property, Macmillan Pass area, Yukon, *Yukon Exploration and Geology 1983*, 105-114, 1984.
- Turner, R. J., A Late Devonian stratiform Pb-Zn and stratiform barite metallogenic event in the North American cordillera: Margin-long extension and implications for the Antler orogeny, *Geol. Soc. America Abstracts with Progs.*, Vol. 16, p. 414, 1985.
- Vaughan, D. J., Sedimentary geochemistry and the mineralogy of the sulfides of lead, zinc, copper and iron and their occurrence in sedimentary ore deposits, in *Handbook of strata-bound and stratiform ore deposits*, edited by K.H. Wolf, pp. 317-363, Elsevier, Vol. 2, Amsterdam, 1976.
- Weiss, R. F., The solubility of nitrogen, oxygen, and argon in water and seawater, *Deep Sea Research*, 17, 721-735, 1970.

- Whitcher, I. G., Dugald River zinc-lead lode, in *Economic geology of Australia and Papua New Guinea*, edited by C. L. Knight, pp. 372-376, Australasian Institute of Mining and Metallurgy, Mon. 5, Vol. 1, 1975.
- White, D. E., Active geothermal systems and hydrothermal ore deposits, *Econ. Geol. 75th Anniv. Vol.*, 392-423, 1981.
- Williams, N., Studies of the base-metal sulfide deposits at McArthur River, Northern Territory, Australia I: The Cooley and Ridge deposits, *Econ. Geol.*, 73, 1005-1056, 1978a.
- Williams, N., and R. G. Logan, Geology and evolution of the H.Y.C. stratiform Pb-Zn orebodies, Australia, *Geological Sciences Series*, 11, in press.
- Windley, B. E., *The evolving continents*, 385 pp., John Wiley and Sons, 1977.
- Windley, B. F., P. R. Simpson, and M. D. Muir, The role of atmospheric evolution in Precambrian metallogenesis, *Fortschritte der Mineralogie*, 2, 253-267,
- Wyrski, K., The oxygen minimum in relation to ocean circulation, *Deep-sea Research*, v. 9, 11-23, 1962.
- Ziegler, A. M., J. T. Parrish, and R. G. Humphreville, Paleogeography, upwelling and phosphorites [abs.], *Proterozoic and Cambrian phosphorites*, p. 21, Proc., 1st Mtg. Internat. Geol. Correlation Project 156, 1979.
- Zierenberg, R. A., The Mattagami Lake mine Archean Zn-Cu sulphide deposit, Quebec: Hydrothermal coprecipitation of talc and sulfides in a sea-floor brine pool - evidence from geochemistry, 180/160, and mineral chemistry - a discussion, *Econ. Geol.*, 79, 1951-1952, 1984.

CHAPTER 2

SYNSEDIMENTARY FAULT CONTROL OF LATE DEVONIAN AGE SEDIMENTARY BRECCIAS AND STRATIFORM LEAD-ZINC DEPOSITS, JASON PROPERTY, MACMILLAN PASS, YUKON

INTRODUCTION

Stratiform sediment-hosted lead-zinc deposits are sheet-like bodies of zinc, lead and iron sulfides interbedded concordantly with fine-grained sedimentary strata. These deposits are up to tens of meters in thickness, up to thousands of meters in lateral dimension and include some of the largest accumulations of sulfide minerals known. Numerous authors have presented stratigraphic and textural evidence to support the theory that stratiform lead-zinc deposits form by the submarine discharge of metal-rich hydrothermal fluids along active faults during periods of rifting or wrench faulting of intracratonic or continental margin sedimentary basins (Carne, 1979; Large, 1981; Hannak, 1981). The source of the metalliferous hydrothermal fluids are thought to be sedimentary basin brines (Badham, 1981; Lydon, 1983) or heated waters convected through continental crust during extensional faulting (Russell, 1983).

Though much regional and deposit scale stratigraphic evidence suggests that the formation of stratiform mineralization is associated with extensional faults (Sampson and Russell, 1983; Krebs, 1981; Hoy, 1982; Walker et al., 1977), only studies of the Silvermines lead-zinc deposits (Taylor and Andrew, 1978; Taylor, 1984; Andrew, 1986) have identified specific synsedimentary faults that acted as a fluid conduit for hydrothermal fluids. The present study of the stratigraphic and structural setting of the Jason deposit provides additional evidence for the genetic link between synsedimentary faulting and stratiform lead-zinc mineralization.

Stratiform lead-zinc sulfides interbedded with marine carbonaceous shale and turbidites were discovered on the Jason property near Macmillan Pass, Yukon (Fig. 2.1) in 1976. Smith (1978) first recognized a link between Devonian age synsedimentary faults and stratiform mineralization in this area. Later workers have presented data on the stratigraphic setting (Teal and Teal, 1979; Winn et al., 1981; Turner, 1985; Bailes et al., in press) and the character of the stratiform mineralization (Gardner, 1983; 1985; Turner, 1985). Turner (1985) documented a synsedimentary fault, here termed the Jason fault, immediately adjacent to the stratiform sulfide body that he interpreted as a conduit for exhalative hydrothermal fluids. The present paper documents in greater detail the lithologies of the sedimentary deposits adjacent to the Jason fault, the nature of the fault itself and the mineralization and alteration that is in proximity to it. These data are combined to yield an integrated model for the sedimentation of mass flow deposits adjacent to the submarine scarp, and the flow of hydrothermal fluids that moved up the fault and both infiltrated laterally into shallow sediments and discharged onto the seafloor.

The principal method of investigation was the study of over 10,000 m of drill core; key intercepts were logged at a scale of 1 cm = 1 m. Selected samples were studied in thin section and by X-ray diffraction and electron microprobe to confirm hand lens mineral identification and determine mineral compositions. Five stratigraphic sections were measured on surface to augment existing geological maps by company geologists.

GEOLOGICAL SETTING OF THE MACMILLAN PASS AREA

The oldest rocks exposed in the Macmillan Pass area are shale, limestone and sandstone of late Proterozoic to Cambrian age (Fig. 2.2) deposited along the northwestern continental margin of North America. These units are overlain by Road River Group carbonaceous shale, chert, silty carbonate and volcanic rocks of Ordovician to Early Devonian age, interpreted as slope to basin floor sediments of the Selwyn Basin, a deep water embayment into the carbonate shelf margin (Cecile, 1982). The Road River Group is overlain with local unconformity by the Lower Earn Group, a sequence of coarse-grained turbidite and

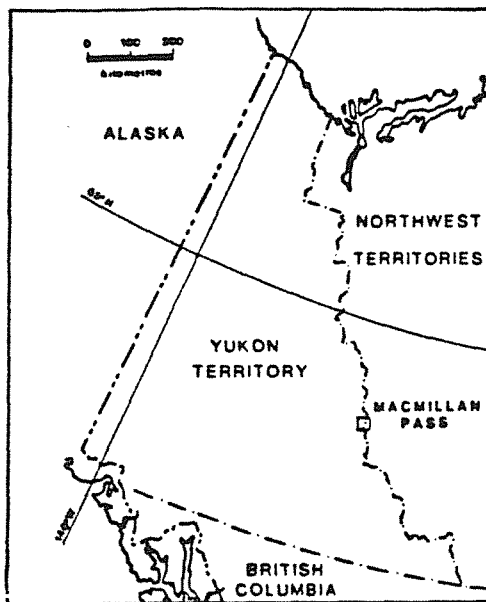


Figure 2.1 Location of Macmillan Pass area in Yukon, Canada (from Gardner and Hutcheon, 1985).

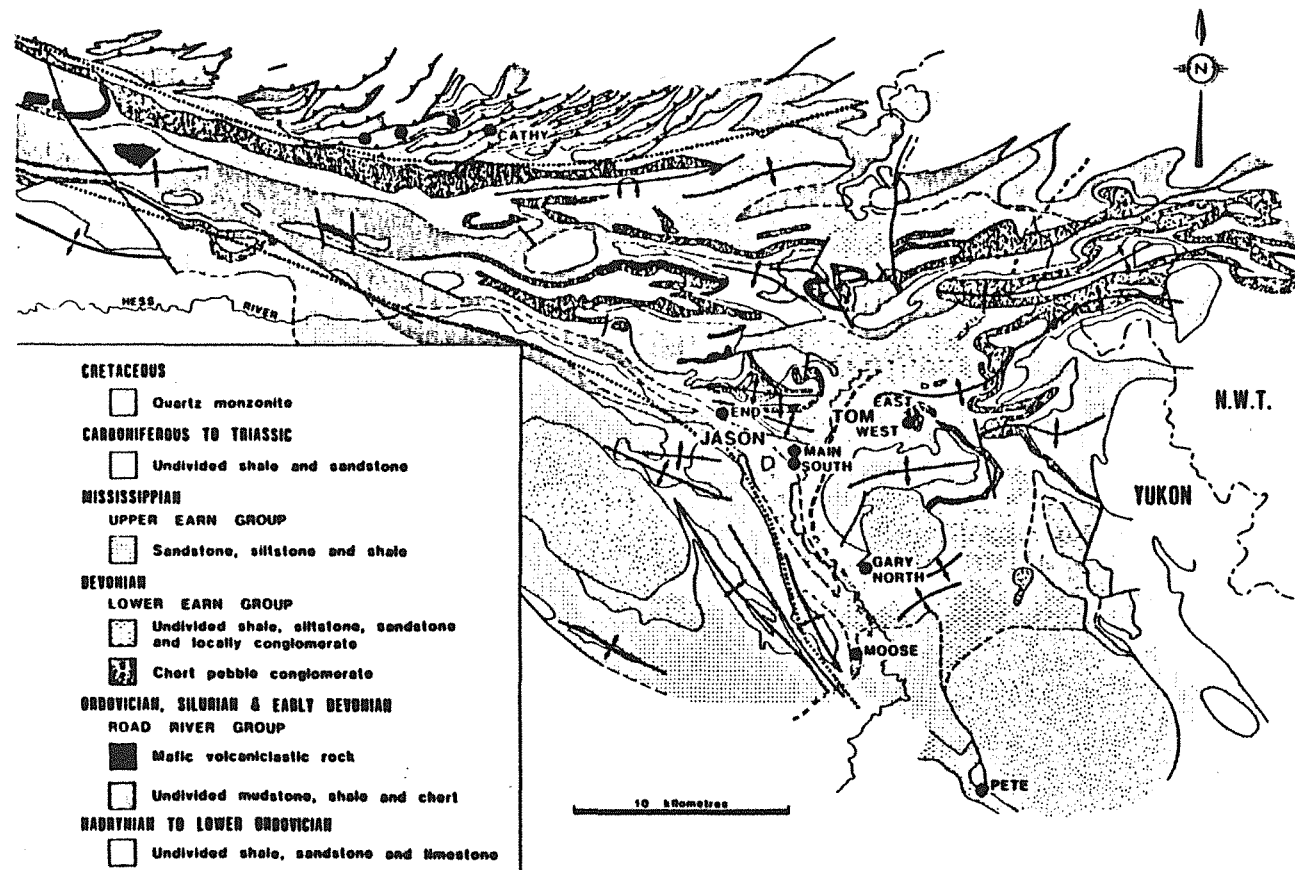


Figure 2.2 Geological map of the Macmillan Pass area (from Bailes et al., in press and modified after Abbott, 1982).

carbonaceous siliceous shale of Middle to Late Devonian age (Gordey et al., 1982). The Lower Earn Group is unconformably overlain by quartz sandstone, siltstone and shale of the Upper Earn Group of latest Devonian to early Mississippian age. The Paleozoic miogeoclinal strata are deformed into a west-trending set of open to isoclinal folds, high angle reverse faults and north-dipping thrust faults (Fig. 2.2) known as the Macmillan fold belt (Abbott, 1982). These structures appear to be related to regional Jura-Cretaceous deformation and are cut by quartz monzonite to granite stocks of Late Cretaceous age (Abbott, 1982). The regional metamorphic grade of the miogeoclinal strata is sub-greenschist facies.

The Earn Group, and equivalent strata exposed throughout northeastern British Columbia and central Yukon are characterized by local coarse-grained turbidite fan complexes, abrupt changes in facies and sediment thickness, locally developed unconformities, and evidence for synsedimentary faulting (Lenz, 1972; Winn et al., 1981; Gordey, 1981; Gordey et al., 1982). These features have been attributed to rifting or wrench faulting of the outer continental margin during Middle Devonian to early Mississippian time (Tempelman-Kluit, 1979; Eisbacher, 1983; Abbott, 1983; Turner, 1985b). Stratiform sediment-hosted sulfide and stratiform barite deposits of Late Devonian age present throughout northeastern British Columbia and the Yukon are thought to reflect submarine geothermal activity associated with this extensional faulting (Carne, 1979; Cathro and Carne, 1982; MacIntyre, 1983; Turner, 1985a,b).

The lithologic characteristics of the Lower Earn Group suggest deposition in a euxinic, deep-water setting. This evidence includes the organic-rich nature of carbonaceous siliceous shale, the absence of evidence for benthic faunal activity or of wave reworking, and the deposition of all coarse clastic sediments by mass flow. In addition, Goodfellow and Jonnason (1984) interpret sulfur isotope ratios from diagenetic pyrite with the Lower Earn Group strata to reflect deposition below a very stagnant water mass in which much of the seawater sulfate had been reduced to sulfide.

The occurrence of a cluster of stratiform lead-zinc deposits and stratiform barite

deposits within the Lower Earn Group in the Macmillan Pass area (Fig. 2.2) has made this area the focus of several stratigraphic and structural studies (Smith, 1978; Carne, 1979; Lydon et al, 1981; Winn et al., 1981; Abbott, 1982, 1983). There is evidence for two sets of Devonian age faults in the Macmillan Pass area; a northwest trending set with strikelengths greater than 10 km, and a northeast trending set with much shorter strikelengths. Regional mapping by Abbott (1982,1983b) defined two major northwest-trending structural zones, the Hess and Macmillan faults, that separate the region into three domains possessing contrasting structural styles and differing lower Paleozoic stratigraphies. Abbott (1983a) interprets the Hess and Macmillan faults to have been zones of normal or strike-slip displacement during mid-Paleozoic time; younger Mesozoic deformation was influenced by these faults. Abbott (1985) interprets a discontinuity in the level of erosion beneath the sub-Lower Earn Group unconformity trending northwest from the Tom stratiform Pb-Zn deposit (Fig. 2.3) as evidence of a Devonian age fault. Evidence for northeast trending faults of Devonian age include (Fig. 2.3): (1) restoration of the Jason fault (see below) to its Devonian orientation indicates a east-northeast trend; (2) outcrops of sedimentary breccias within the Lower Earn Group trend to the northeast from the End zone stratiform Pb-Zn mineralization (Fig. 2.4); (3) the change in the level of erosion below the sub-Lower Earn Group unconformity across two north trending faults (Abbott, 1983a) that are 5 km to the north and 10 km to the northwest of the Jason deposit; and (4) a northeast trend of sedimentary breccias and interbedded mafic flows within the Lower Earn Group (D. Rhodes, pers. comm. 1983) 15 km to the northwest of the Jason deposit. The distribution of Devonian age northeast-trending faults is limited to the northeast and southwest by Devonian age northwest trending faults; these faults define a rectangular domain of Devonian age extension. Palinspastic reconstruction of Jura-Cretaceous age regional shortening would lengthen the pull-apart basin in the northeast direction; it also is likely that some degree of rotation of the trend of faults has occurred during this compressional event. None-the-less, this geometry of coeval faults is suggestive of the geometry of a pullapart basin associated with strike slip fault zones (see

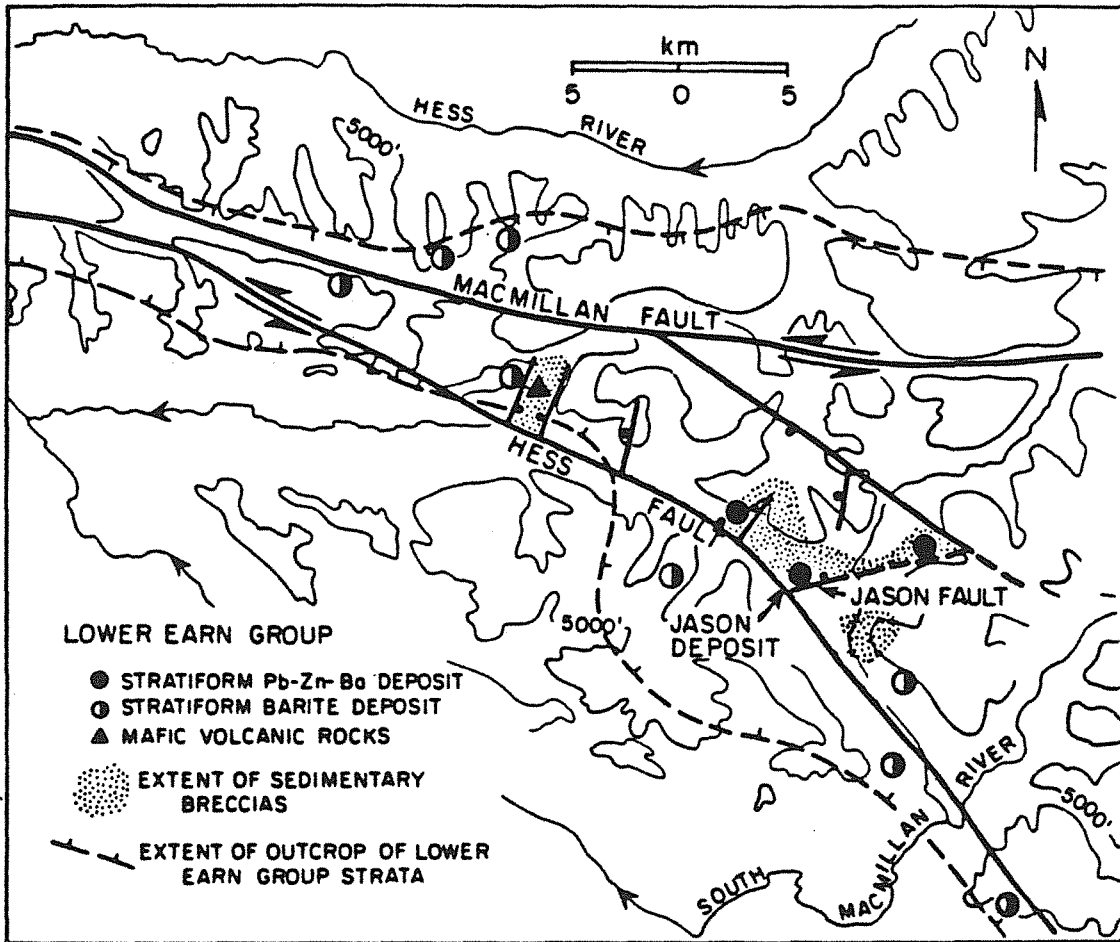


Figure 2.3 Distribution of Late Devonian age faults, sedimentary breccias, stratiform Pb-Zn-Ba deposits and, stratiform barite deposits in the Macmillan Pass area.

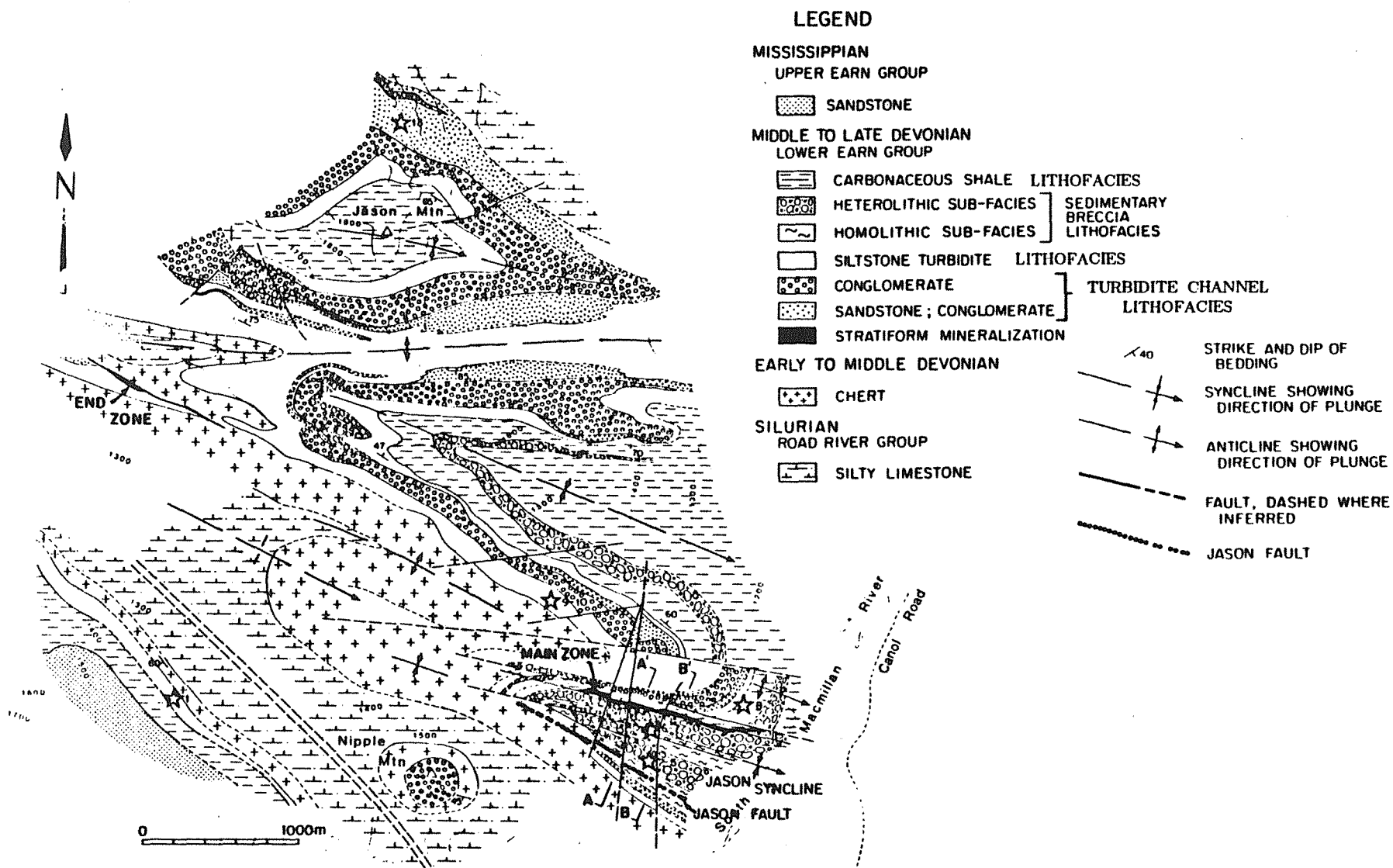


Figure 2.4 Geological map of the area near the Jason stratiform deposits (modified after unpublished company map, Cordilleran Engineering). The location of stratigraphic sections in Figure 2.7 are indicated by a star symbol. The location of cross-section A-A' and B-B' (Figures 2.5, 2.6) are indicated.

Crowell, 1974; Rogers, 1980). Late Devonian age stratiform lead-zinc deposits and mafic volcanic rocks are localized at the intersection of northeast trending and northwest trending faults. Stratiform barite deposits hosted by Lower Earn Group strata occur adjacent to the Hess and Macmillan Faults peripheral to the pull-apart basin.

GEOLOGY OF THE JASON SYNCLINE AREA

The Jason stratiform Zn-Pb-Ba mineralization occurs on the north limb (Main zone) and south limb (South zone) of a southeasterly plunging, tightly folded syncline of Mesozoic age immediately north of the Hess fault (Figs. 2.4, 2.5, 2.6). The stratiform bodies are dominantly planar but locally deformed into small scale tight folds. West-trending cleavage axial to the Jason syncline occurs in the host argillaceous strata and is defined by oriented clay and fine-grained muscovite grains; within the sulfide horizons associated with locally developed small-scale folds the cleavage is defined by oriented growth of barite and sulfide minerals. The syncline, here referred to as the Jason syncline, is cut by steeply dipping, east-southeasterly trending faults that are parallel or oblique to the axial plane of the syncline (Fig. 2.4). Younger north-trending high angle faults offset all other structures with small displacement.

Previous workers have divided the Lower Earn Group in the Macmillan Pass area into a vertical succession of informal stratigraphic units (Teal and Teal, 1978; Carne, 1979; Abbott, 1983a). However, because of the informal nature of these terms, and the abrupt facies changes of the Lower Earn stratigraphy near the Jason fault, these terminologies will not be used here. Instead, the stratigraphy of the Lower Earn Group is divided into four lithofacies of local extent that are tentatively correlated with the stratigraphy elsewhere in the Macmillan Pass area (Figs. 2.4, 2.5, 2.6, 2.7). These lithofacies are: (1) siltstone turbidite lithofacies; (2) channel complex lithofacies; (3) sedimentary breccia lithofacies and (4) carbonaceous shale lithofacies.

Abbott (1983a) considers a carbonaceous chert unit of Lower Devonian age as the lowermost part of the Lower Earn Group. However, in the Jason area an unconformity separates this chert unit from the rest of the Lower Earn Group (Fig. 2.7). As this chert lacks

SSW

NNE

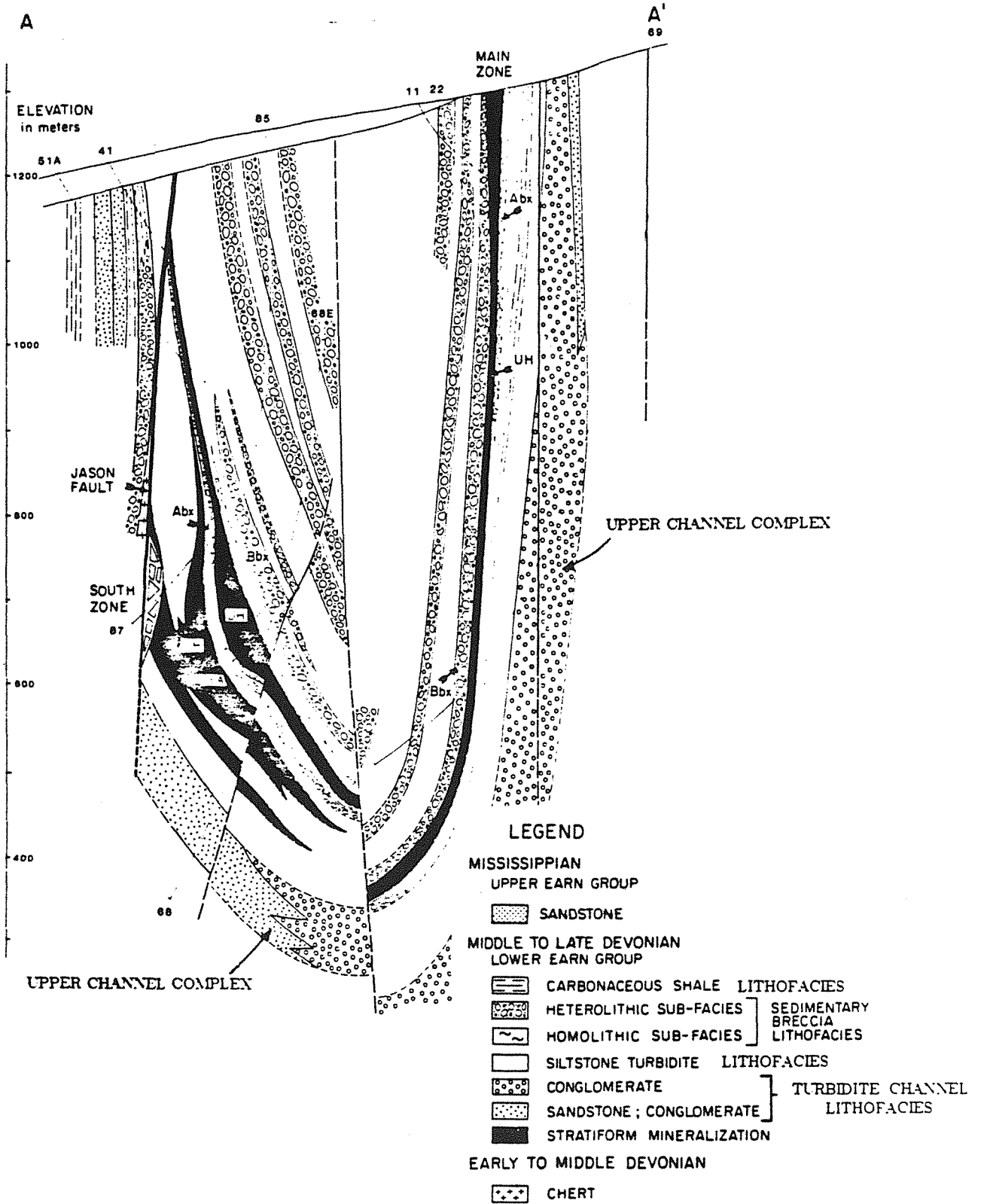


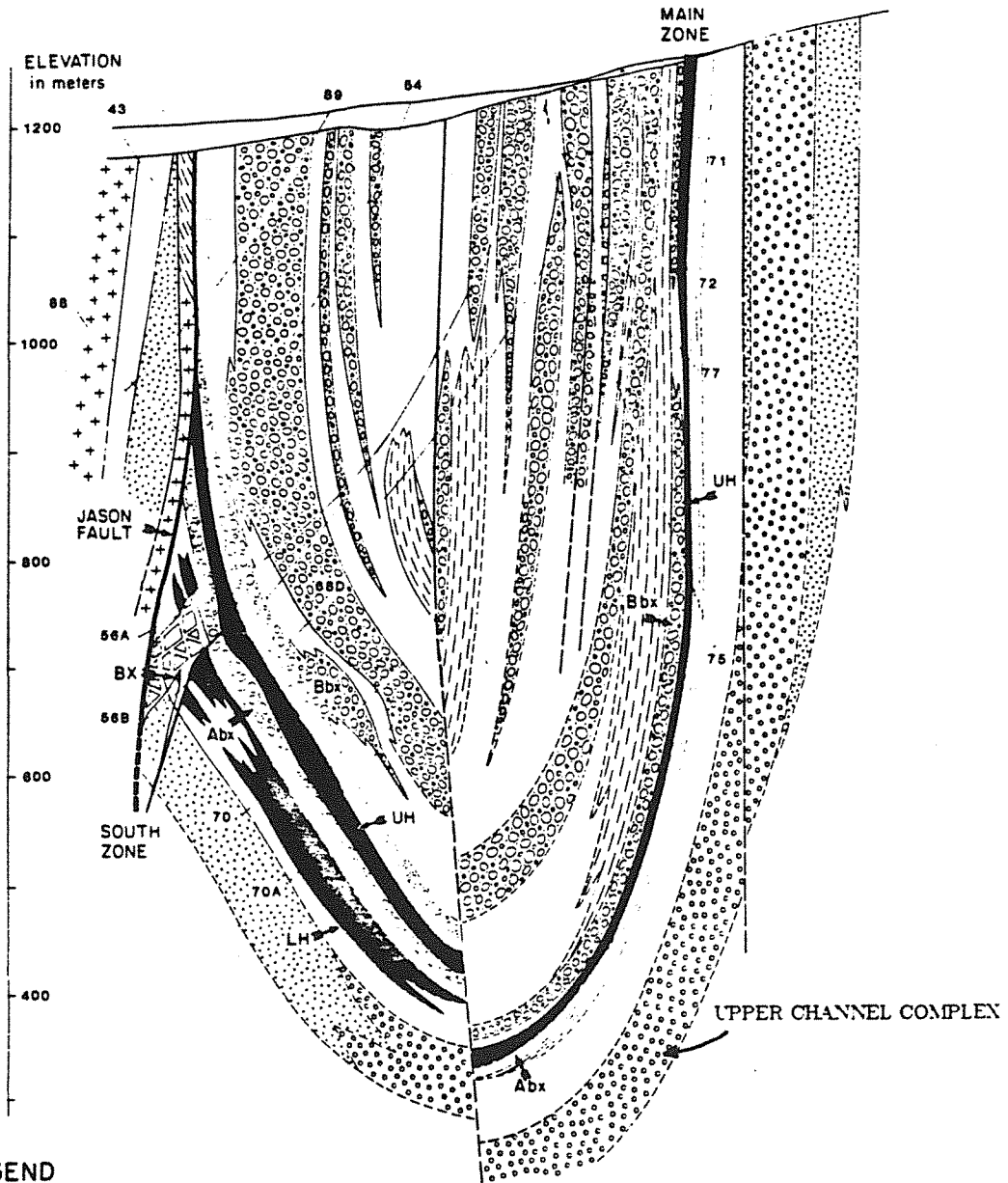
Figure 2.5 Geological cross-section A-A' (looking west) of the Jason Syncline. The upper horizon (UH), lower horizon (LH), A sedimentary breccia unit (Abx), and B sedimentary breccia unit (Bbx) are indicated.

SSW

NNE

B

B'



LEGEND

MISSISSIPPIAN
UPPER EARN GROUP

SANDSTONE

MIDDLE TO LATE DEVONIAN
LOWER EARN GROUP

CARBONACEOUS SHALE LITHOFACIES

HETEROLITHIC SUB-FACIES } SEDIMENTARY BRECCIA LITHOFACIES

HOMOLITHIC SUB-FACIES }

SILTSTONE TURBIDITE LITHOFACIES

CONGLOMERATE

SANDSTONE ; CONGLOMERATE } TURBIDITE CHANNEL LITHOFACIES

STRATIFORM MINERALIZATION

EARLY TO MIDDLE DEVONIAN

CHERT

Figure 2.6 Geological cross-section B-B' (looking west) of the Jason Syncline. The upper horizon (UH), lower horizon (LH), breccia body (BX), A sedimentary breccia unit (Abx), and B sedimentary breccia unit (Bbx) are indicated.

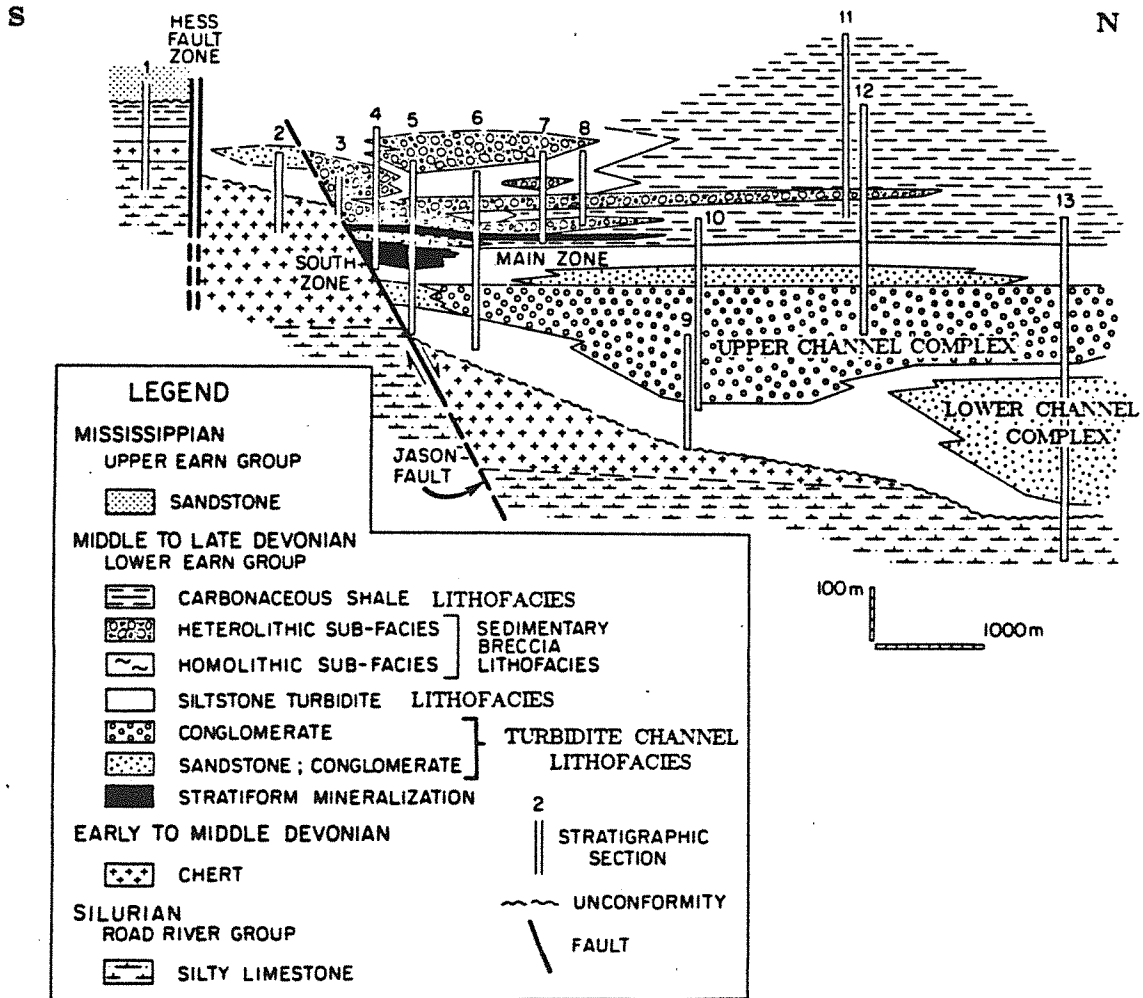


Figure 2.7 Restored stratigraphic cross-section of Lower Earn Group in the Jason area. Horizontal scale is approximate. Stratigraphic sections are both from drill hole data (2,3,4,5,6,7,8,11,12) and surface data (1,9,10,13). Location of stratigraphic sections is shown on Figure 2.4 .

evidence of deposition during the tectonism characteristic of the Lower Earn Group, it is not considered here as a part of the Lower Earn Group.

Lithofacies

Siltstone Turbidite Lithofacies

A monotonous sequence of thin siltstone beds, carbonaceous argillite and minor thin sandstone beds up to 300 m thick unconformably overlies Ordovician to Lower Devonian strata in the Jason area. This siltstone turbidite lithofacies is comprised of thin-bedded siltstone T_{ce} , T_{de} turbidites (after Bouma, 1962) up to 4 cm thick with parallel and cross-lamination that are interbedded with laminae and beds of carbonaceous mudstone. Where the siltstone turbidite lithofacies occurs lateral to the lower channel complex and overlies the upper channel complex, it is interbedded with up to 15 percent discontinuous, cross-laminated sandstone beds (T_{ce}) to 5 cm in thickness interpreted as starved-ripple trains, and 1 to 5 percent sandstone beds up to 30 cm thick comprised of T_{be} and T_{ce} turbidite divisions. Beds of the siltstone turbidite lithofacies are interpreted as basin plain deposition; the more sand-rich portions of this lithofacies adjacent to channel complexes (see below) likely reflect channel lateral or levee facies deposition (Mutti, 1977).

Turbidite Channel Lithofacies

Massive to graded thick-bedded conglomerate, pebbly sandstone and sandstone comprise two lenticular bodies in excess of 100's of feet thick referred to as the lower and upper channel complexes. These channel complexes occur within and at the top of the siltstone turbidite lithofacies.

The lower channel complex is a composite of lenticular channel-like bodies of thick-bedded massive conglomerate, pebbly sandstone and massive sandstone that form thinning and fining upward sequences 5 to 20 m thick. Conglomeratic units vary from massive disorganized beds (see Walker, 1970) to organized beds with horizontal and inclined stratification; the latter suggests deposition on gravel bars within a braided complex of

turbidite channels (Winn et al. 1981). Isopachs of the lower channel complex indicate it is comprised of two southeast trending lobes (Hubecheck, 1981). The more southwesterly lobe (Fig. 2.7) unconformably overlies Road River strata and exceeds 250 m in thickness. To the southeast and southwest, the lower channel complex thins abruptly and is transitional into siltstone turbidite lithofacies.

The upper channel complex is comprised of amalgamated beds, 1 to 20 m thick, of massive chert pebble conglomerate that lack sedimentary structures. Towards the Jason fault, the upper channel complex thins markedly and becomes sand-rich adjacent to the Jason fault (Fig. 2.7). The upper channel complex is more laterally extensive than the lower channel complex and occurs throughout much of the Macmillan Pass area north of the Hess fault. It is correlative with unit muDcg of Abbott (1983a).

Sedimentary Breccia Lithofacies

The stratigraphy of the Jason area is characterized by a thick sequence of sedimentary breccias. Thick-bedded sedimentary breccia units interbedded with beds of siltstone turbidite and carbonaceous mudstone comprise a northward thinning lithofacies that near the Jason fault exceeds 280 m in thickness. This facies is described separately in the next section.

Carbonaceous Shale Lithofacies

A sequence of carbonaceous siliceous shale and minor chert 200 to 500 m thick (unit muDpt of Abbott, 1983a) occurs at the top of the Lower Earn Group in the Jason area. Beds of carbonaceous siliceous shale are composed of 60 to 80 per cent fine-grained quartz, 5 to 30 percent opaque carbonaceous matter and less than 10 percent fine-grained clays. Sparsely preserved radiolaria suggest a biogenic origin for the silica. Towards the Jason fault, the carbonaceous mudstone lithofacies interfingers with the sedimentary breccia lithofacies.

The sharp transition between the carbonaceous shale lithofacies and the underlying turbidite channel complex indicates a rapid cessation of turbidite deposition. Stratiform sulfides occur at the stratigraphic level of this transition zone adjacent to the Jason Fault

(Fig. 2.7). Ages determined from conodonts collected within the carbonaceous siliceous shale are Frasnian in age (M. Orchard, pers. comm. 1986). The carbonaceous shale lithofacies is interpreted to represent organic- and silica-rich hemipelagic deposition.

The Jason fault is a steeply dipping, northwest trending structure that offsets strata on the south limb of the Jason syncline (Figs. 2.4, 2.5, 2.6). The Jason fault juxtaposes Road River Group strata and the overlying lower part of the Lower Earn Group on the south side against siltstone, sedimentary breccia and stratiform sulfide deposits of the middle and upper part of the Lower Earn Group on the north. Minimum stratigraphic offset across the fault is between 80 and 250 m. Fifteen drill holes provide data on the nature of the fault over an area of 400 m along dip and 300 m along strike. Structural reconstruction that involves unfolding the host syncline indicates that the trend of the Jason fault during Devonian time was N 60 E. The Jason fault appears to have formed normal to the trend of the nearby major southeast-trending structural zone of Devonian age, the Hess fault. The Jason fault cuts strata at about 40 degrees; by comparison with the surface expression of most normal faults (Wallace, 1978), this dip is strikingly shallow and may be due to compactional drape of the lithifying sediments adjacent to the fault zone as noted at the Tynaugh lead-zinc deposit (McM. Moore, 1975). In the paragraphs that follow, all references to the hangingwall (north side) and footwall (south side) of the Jason fault apply to the orientation of the fault during Devonian time.

STRATIGRAPHY OF THE SEDIMENTARY BRECCIA LITHOFACIES

Because of the special significance of the sedimentary breccia lithofacies with regard to interpretation of the synsedimentary faulting and debris flows, and because of the spatial coincidence of this unit and sulfide strata, special emphasis is placed here on describing the rock types, their facies relations, and the morphology of breccia lobes.

At least 280 m of interbedded sedimentary breccia, thick-bedded conglomerate and sandstone, thin-bedded siltstone turbidite and carbonaceous mudstone of the sedimentary breccia lithofacies overlie the upper turbidite channel complex adjacent to the Jason fault

(Figs. 2.5, 2.6, 2.7). Sedimentary breccias have been divided into two lithotypes termed heterolithic breccia and homolithic breccia (Bailes et al., in press). Heterolithic breccia is characterized by heterolithic mixture of clasts and a high matrix to clast ratio. Homolithic breccia is monolithic and has a lower matrix to clast ratio.

Lithologies

Fine-Grained Sedimentary Rocks

The most common fine-grained sedimentary rocks interbedded with the sedimentary breccia units in the South zone area and with sedimentary breccia in the upper part of the sedimentary breccia lithofacies are thin siltstone beds, thin lenticular cross-laminated sandstone beds and organic-rich mudstone laminae similar to the strata of the underlying siltstone turbidite lithofacies (Fig. 2.8a). Thin siltstone beds vary in thickness from 1 to 3 cm, are ungraded, have sharp upper and basal contacts and are composed predominantly of silt sized grains of chert, with minor clay and quartz sand grains. Thin laminae at the base of the siltstone beds are lenticular and cross laminated or normally graded with load cast bases. The beds can be classified as T_{c-e} or T_{d-e} beds (Bouma, 1962) or T_{0-4} beds (Stow and Shanmugan, 1980) and reflect suspension load deposition from muddy turbidity flows with periods of tractional movement during deposition of the coarser fraction. Such siltstone beds compose 60 to 90 percent of the stratigraphic section above the stratiform deposits. Lenticular, cross-laminated beds of chert-quartz sandstone up to 10 cm thick compose up to 25 percent of the strata. These sandstone beds have sharp contacts suggesting deposition from the tractional movement of sand turbidity flows. Minor normally graded chert-quartz sandstone beds, 5 to 20 cm thick, also occur. Hemipelagic laminae and beds up to 2 cm thick of organic-rich mudstone and chert are interbedded with the siltstone and sandstone.

Carbonaceous siliceous mudstone is the dominant lithology interbedded with sedimentary breccia in the lower part of the sedimentary breccia lithofacies in the Main zone area (Fig. 2.7), but also occurs throughout the sedimentary breccia lithofacies unit. Carbonaceous siliceous mudstones are massive, have a high organic carbon content (3-10%)

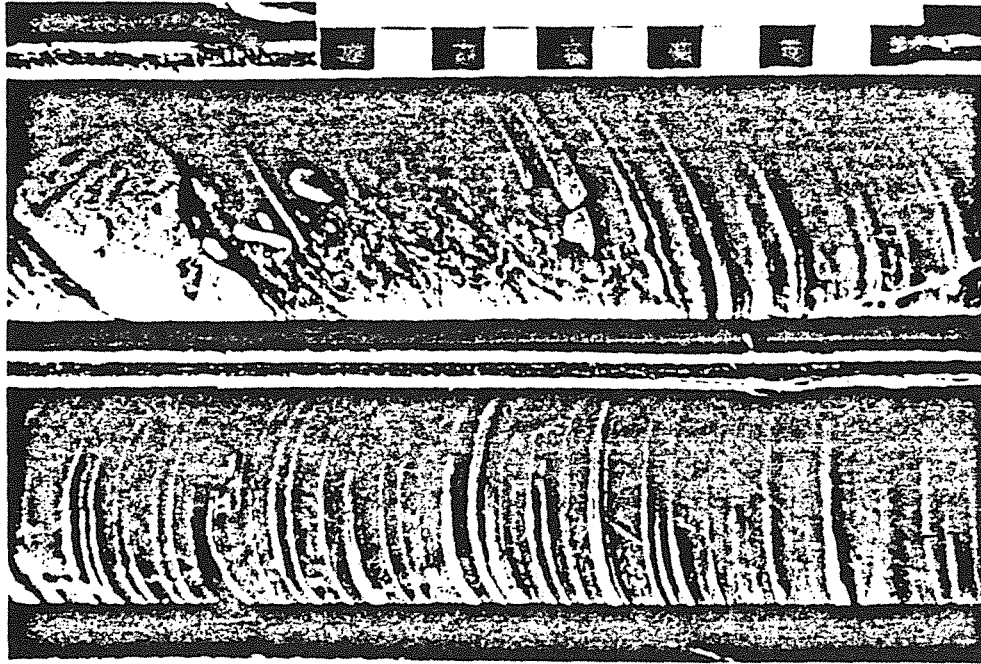


Figure 2.8a Thin-bedded siltstone beds cut by a disrupted zone of homolithic breccia. Scale in centimeters.

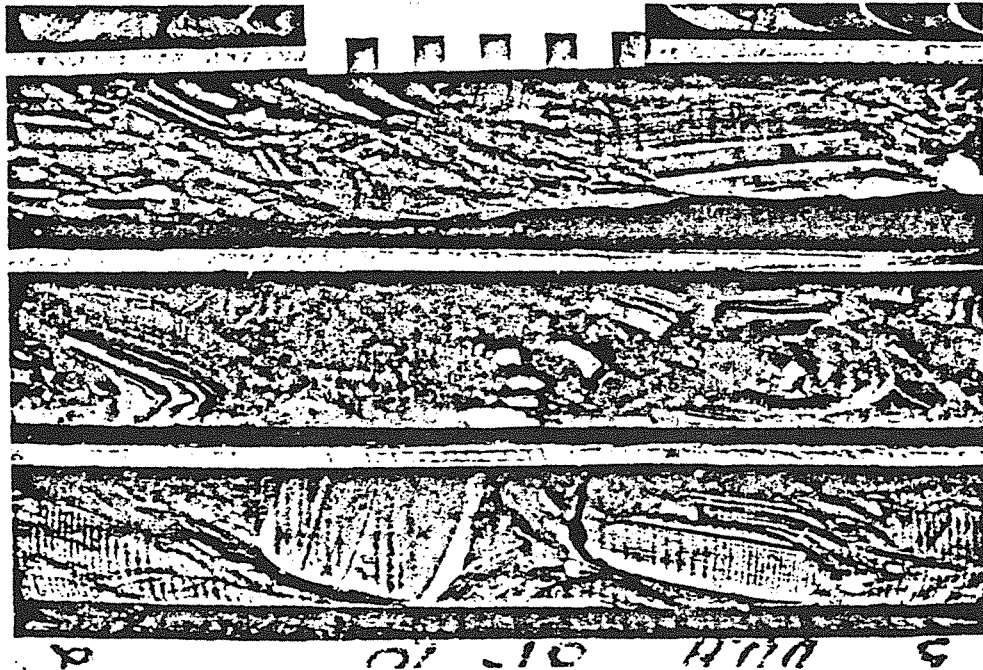


Figure 2.8b Heterolithic breccia containing fragments of sandbanded argillite, siltstone, argillite and chert pebbles in a silty mudstone matrix. Scale is in centimeters.

and a very high silica content ($> 80\%$). The ratio of carbonaceous mudstone to siltstone increases to the north within the syncline. North of the syncline, the sedimentary breccia lithofacies unit correlates with a thick carbonaceous mudstone sequence containing thin sedimentary breccia units and lacking thin-bedded siltstone (Fig. 2.6).

Homolithic Breccia

Homolithic breccia (Bailes et al, in press) is monomictic, clast supported, and contains siltstone or mudstone intraclasts (Fig. 2.8a). Chert pebbles are not present. Individual intraclasts range in diameter up to 1 or 2 meters, but average 0.1 to 0.3 meter in diameter, and commonly comprise 60 to 95 percent of the breccia. The matrix of homolithic breccia is silty mudstone or mudstone. In the Jason syncline, a continuum appears to exist between homolithic breccia, contorted and faulted strata and undisturbed strata (Winn et al., 1981). Stratigraphic correlations suggest that homolithic siltstone breccia correlate laterally over distances of less than 50 to 100 m with undisturbed siltstone. Homolithic breccia units have only been recognized in the sedimentary breccia lithofacies even though siltstone turbidite comprises the bulk of the siltstone turbidite lithofacies.

Heterolithic Breccia

Heterolithic breccia units in the Jason area are poorly sorted, matrix to clast supported, heterogeneous mixtures of mud, intraclasts, chert pebbles and sand (Figs. 2.8b,c,d,e). They range from intraclast breccia to intraclast-rich pebbly mudstone and pebbly or sandy mudstones (Fig. 2.9). Individual breccia units range up to 90 m in thickness (Fig. 2.6) and are characterized by lateral changes in the range of clast size, clast compositions and clast to matrix ratio. Heterolithic breccia units are intimately interbedded with medium- to thick-bedded, massive to stratified chert pebble conglomerate and sandstone beds (Fig. 2.10).

Intraclasts in the heterolithic breccia are subangular to subrounded, and consist of thin-bedded siltstone, carbonaceous mudstone and more rarely, chert pebble conglomerate, sandstone and sulfide fragments. Intraclasts range up to several meters in diameter but average 10 to 30 cm and constitute up to 60 percent of the heterogeneous breccia. The

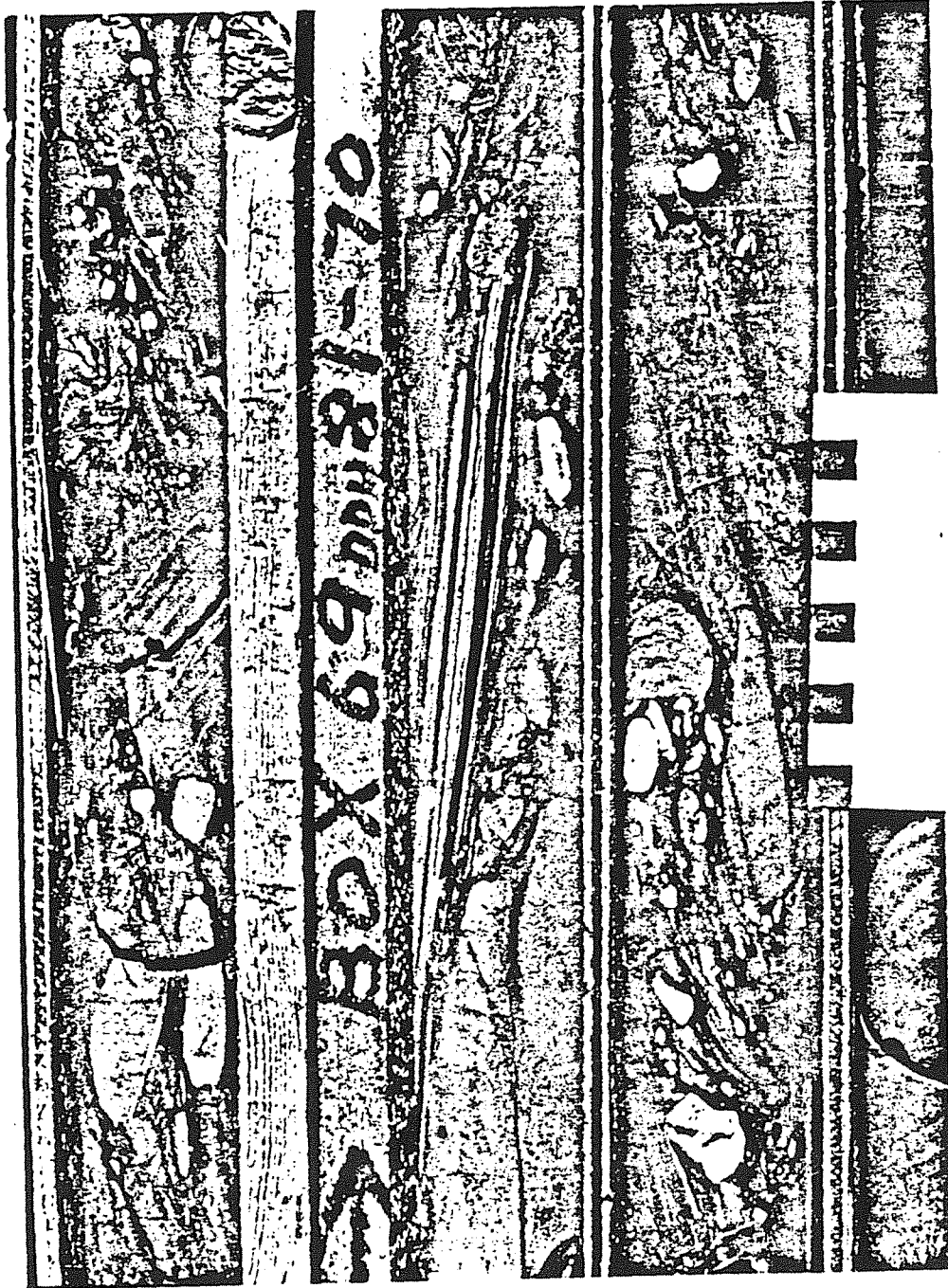


Figure 2.8c Core samples of heterolithic breccia. Field of view is 50 cm.

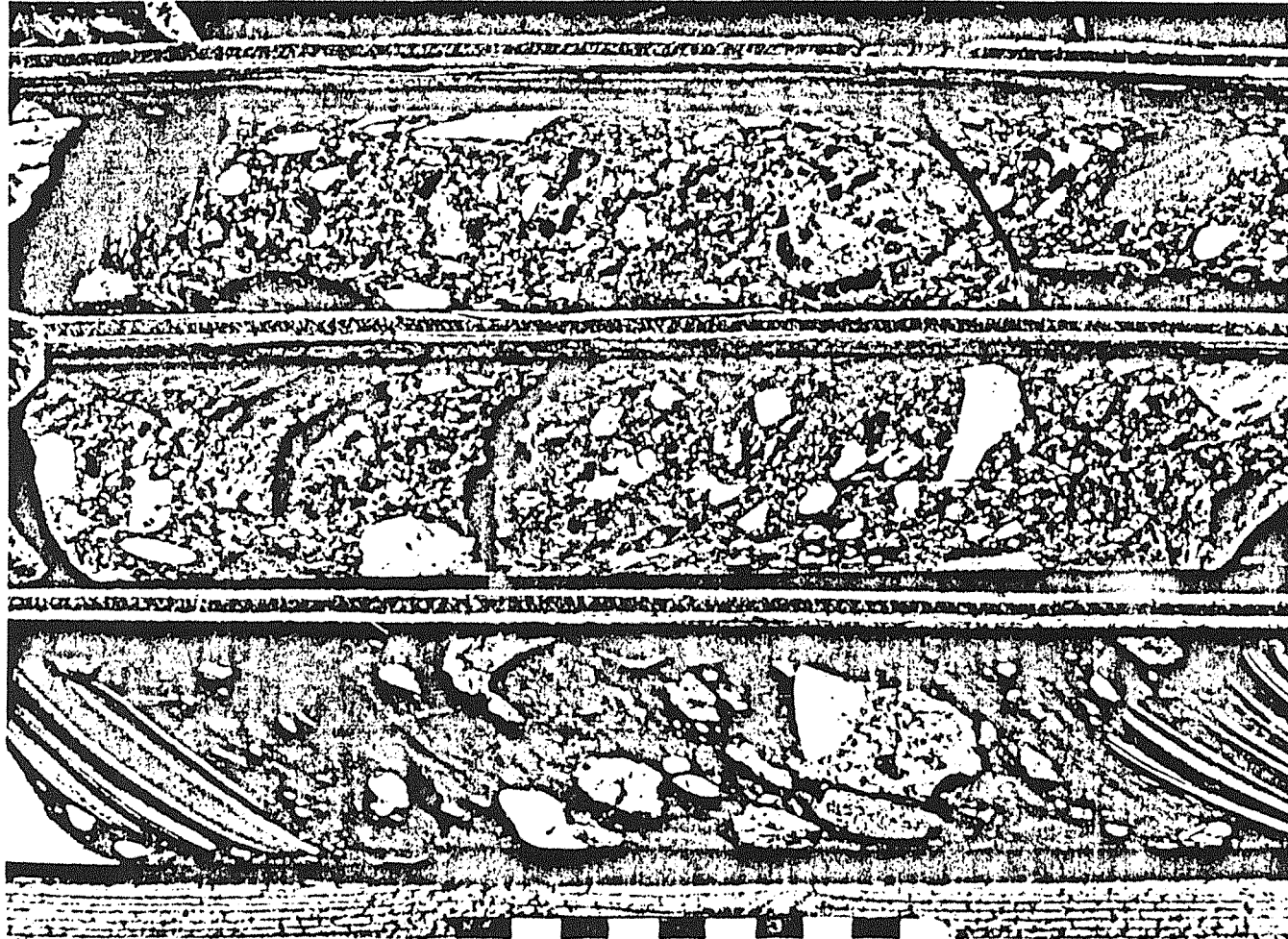


Figure 2.8d Core samples of heterolithic breccia bed and sandy conglomerate bed. Within the heterolithic breccia bed is a clast of conglomerate cemented by pyrite and siderite (A); within the sandy conglomerate bed is a coarse-grained siderite fragment (B) similar in mineralogy and texture to parts of the Jason fault. Scale in centimeters.

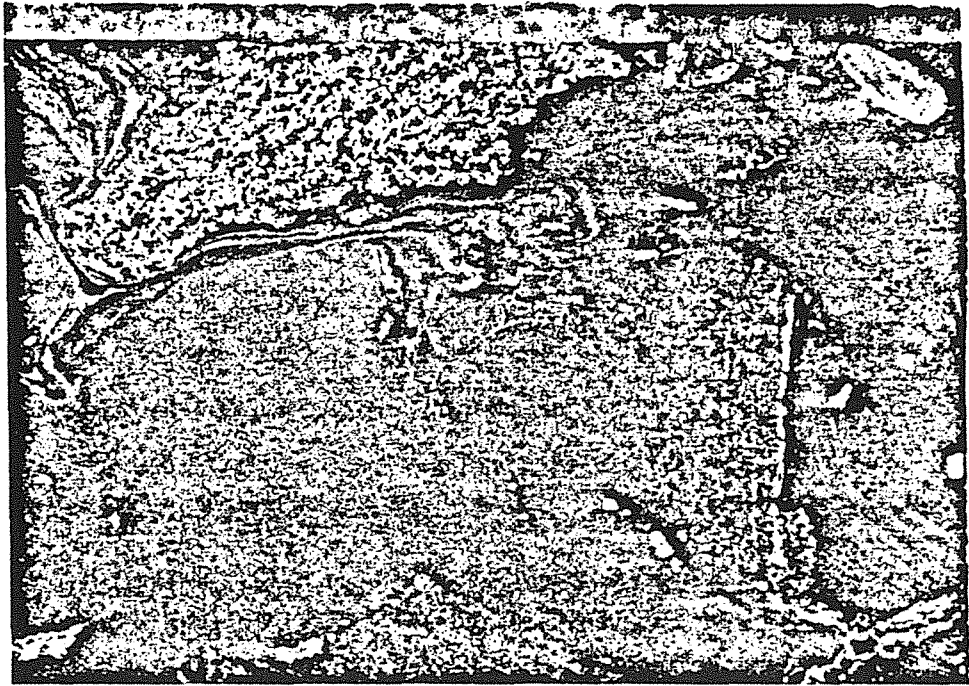


Figure 2.8e Clast of massive galena-sphalerite and laminated pyrite-chert within a sedimentary breccia. Scale in centimeters.

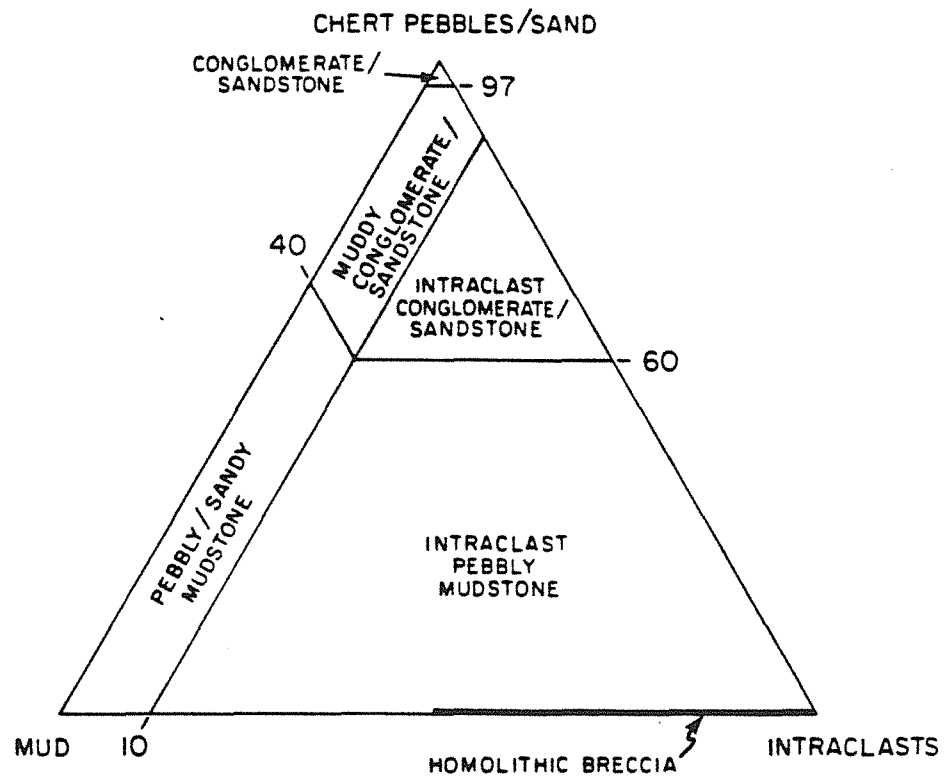


Figure 2.9 Ternary classification diagram used for coarse-grained sediments in the Jason syncline.

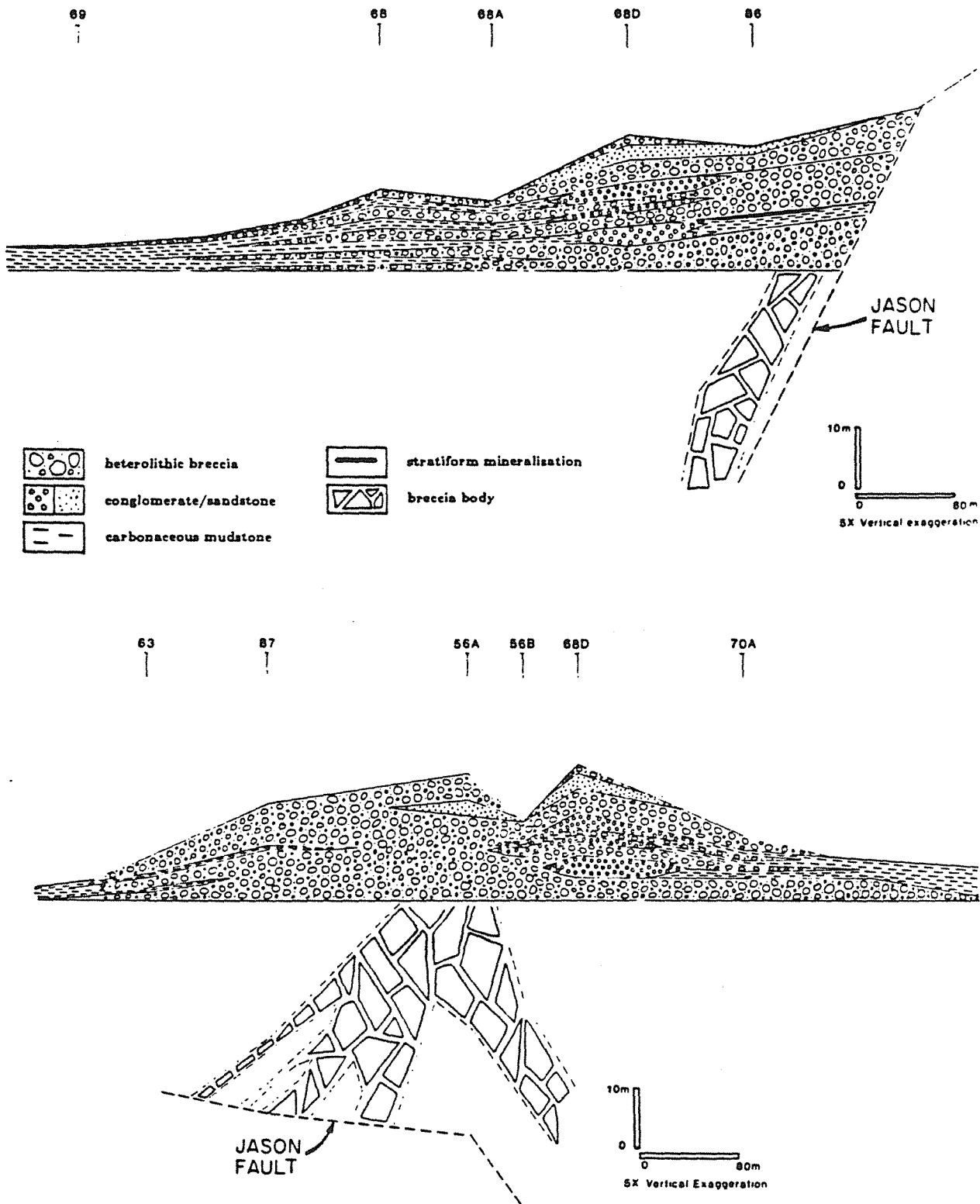


Figure 2.10 Restored stratigraphic cross-section of the A1 breccia unit parallel to the axis of the lobe and perpendicular to the Jason Fault (upper), and transverse to the axis of the breccia lobe and parallel to the trace of the Jason Fault (lower). The positions of drill holes indicated at the top of each figure penetrate the section shown.

composition of the intraclasts is identical to that of underlying Lower Earn Group bedded siltstone, mudstone, conglomerate and sandstone. Conglomerate fragments are characterized by a cement of quartz, siderite or ankerite and up to 10 percent pyrite (Fig. 2.8d). Sulfide fragments occur in sedimentary breccia immediately overlying the stratiform mineralization (Fig. 2.8e).

Chert pebbles to 3 cm in diameter commonly comprise 5 to 20 percent of the heterolithic breccia in the Jason syncline. Chert pebbles typically display replacement rims or disseminations of pyrite and more rarely minor sphalerite and galena. The total sulfide content of chert pebbles is much greater than that of associated intraclasts within the same sedimentary breccia. Chert pebbles are similar in character to chert pebbles within conglomerate intraclasts, interbedded conglomerate and the upper channel complex (Winn et al, 1981).

The matrix of heterogeneous breccia ranges from carbonaceous mudstone to silty or sandy mudstone and it commonly makes up 30 to 50 percent of the breccia unit. The matrix is typically less carbonaceous than interbedded carbonaceous mudstone.

Thick-Bedded Conglomerate and Sandstone

Studies of drill core at the Jason reveal a variety of chert-pebble-rich and sand-rich beds. The terminology describing conglomeratic rocks is that of Walker (1975); other finer-grained turbidites are described using the terminology of Bouma (1962). Beds of disorganized chert-pebble conglomerate up to 10 m in thickness, beds of organized sandy conglomerate and pebbly sandstone up to 5 m thick (Fig. 2.8f), and massive beds of sandstone (T_{abc}) 0.5 to 3 m thick with faint parallel lamination are interbedded with beds of heterolithic breccia. All three types of conglomerate and sandstone vary in mud content, and a continuum exists between well-sorted conglomerate and sandstone to muddy conglomerate and sandstone to pebbly or sandy mudstone (Fig. 2.9). Conglomerates also vary in intraclast content; siltstone and mudstone intraclasts can compose up to 40 percent of a conglomerate and a continuum exists between conglomerate, intraclast-rich conglomerate and intraclast-rich pebbly

mudstone.

Lithologic Sub-Facies

The sedimentary breccia lithofacies can be divided into sub-facies based on distinctive lithological associations that form correlatable stratigraphic units. These are the homolithic sub-facies composed of siltstone turbidite and homolithic breccia, and the heterolithic sub-facies composed of heterolithic breccia, conglomerate and sandstone.

Homolithic Sub-Facies

Though thin-bedded siltstone turbidite and carbonaceous mudstone occur in other stratigraphic units, homolithic breccia has been recognized only in the sedimentary breccia lithofacies. Laterally equivalent homolithic siltstone breccia and bedded siltstone occur together as stratigraphic units 5 to 50 m thick and are referred to here as the homolithic facies (Figs. 2.4, 2.5, 2.6). The homolithic facies are interbedded with units of heterolithic breccia and conglomerate-sandstone units overlying the stratiform ores.

Heterolithic Sub-Facies

Stratigraphic intervals of interbedded heterolithic sedimentary breccia, conglomerate and sandstone are referred to here as the heterolithic facies. The heterolithic sub-facies units interbedded with the stratiform ores are named, in ascending stratigraphic order, the A, B and C breccia units (Figs. 2.5 and 2.6). Isopachs of the A and B breccia units based on 50 drill hole intersections over an area 1200 m by 1200 m indicate that during the Devonian period, northwest trending lobes of heterolithic facies were deposited adjacent to the Jason fault (Fig. 2.11). Individual lobes exceed 800 m in length, vary from 200 to 600 m in width and range up to 90 m in thickness. All but one of the breccia lobes thicken markedly to the southeast in restored plan view. In the South zone area, lobes thicken up to the Jason fault.

Though considerable variation exists in the distribution of sedimentary breccia, conglomerate, sandstone and siltstone within individual breccia lobes, a general facies pattern does exist. Breccia lobes are wedge-shaped in longitudinal profile and show a thinning and

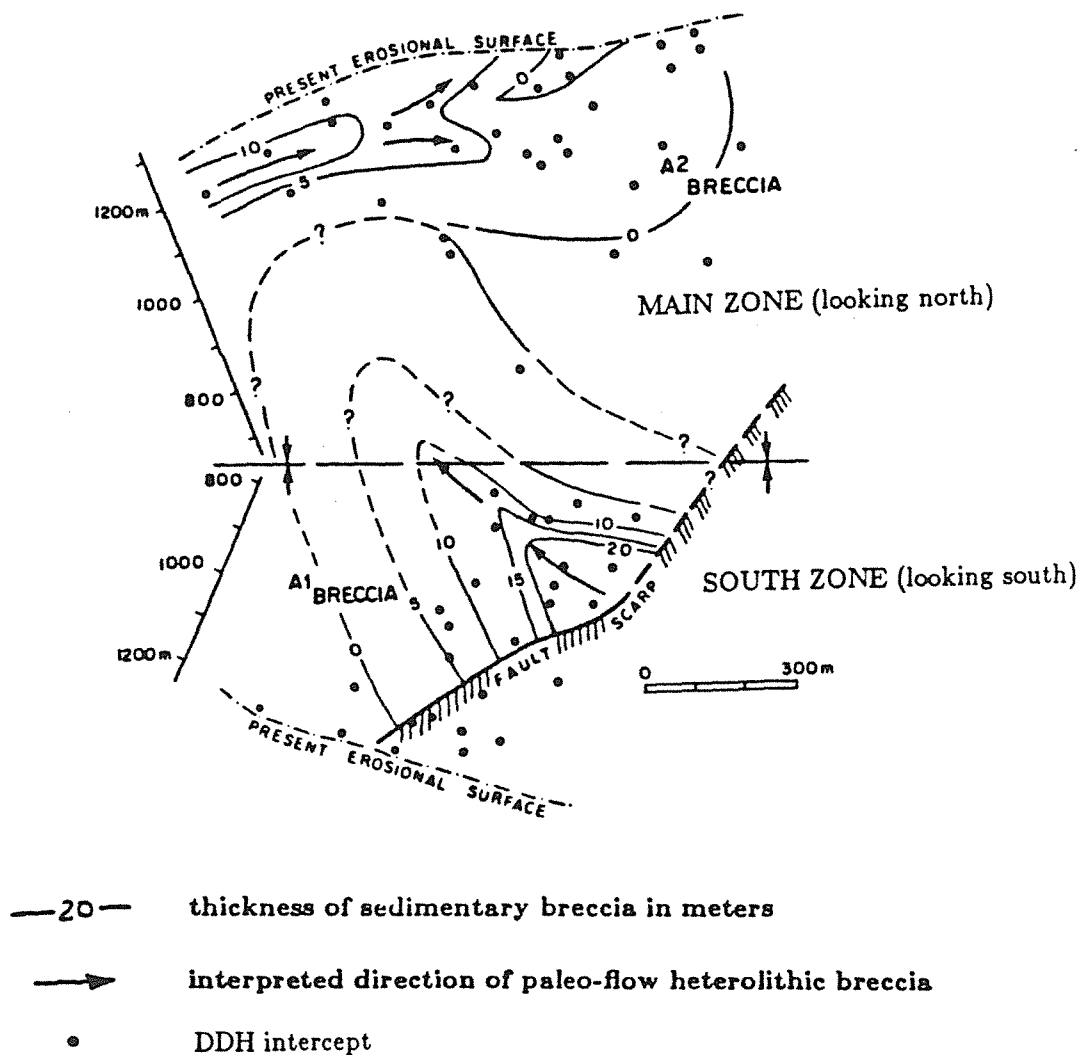
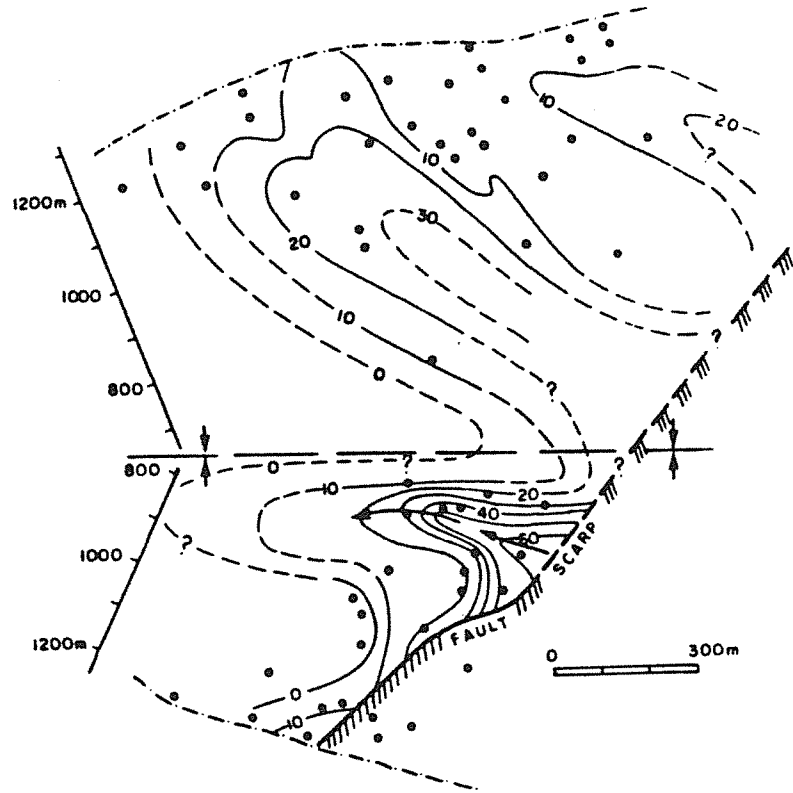
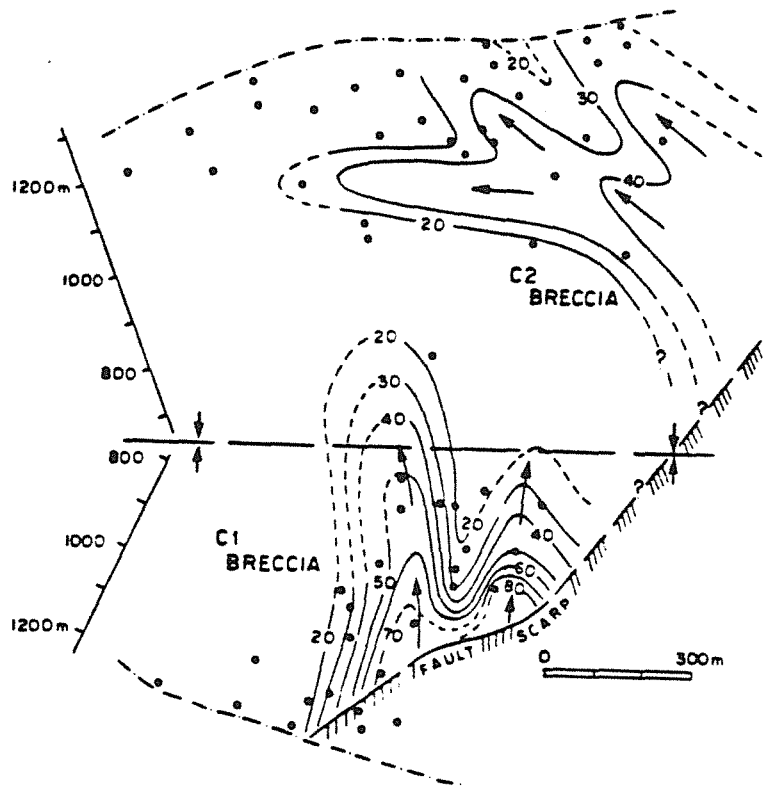


Figure 2.11a Isopach of the thickness of the A sedimentary breccias in a restored plan view at the stratigraphic level of the A sedimentary breccias. Strata on the north and south limbs of the syncline have been unfolded about the southeast plunging fold axis. The area to the southeast of the intersection of the Jason Fault and the stratigraphic level of the A sedimentary breccia units was the scarp area of the Jason fault at the time of deposition of the A sedimentary breccia.



- 20 — thickness of sedimentary breccia in meters
- interpreted direction of paleo-flow heterolithic breccia
- DDH intercept

Figure 2.11b Isopach of the thickness of the B sedimentary breccias in a restored plan view at the stratigraphic level of the B sedimentary breccias. Strata on the north and south limbs of the syncline have been unfolded about the southeast plunging fold axis. The area to the southeast of the intersection of the Jason Fault and the stratigraphic level of the B sedimentary breccia units was the scarp area of the Jason fault at the time of deposition of the B sedimentary breccia.



- 20— thickness of sedimentary breccia in meters
- interpreted direction of paleo-flow heterolithic breccia
- DDH intercept

Figure 2.11c Isopach of the thickness of the C sedimentary breccias in a restored plan view at the stratigraphic level of the C sedimentary breccias. Strata on the north and south limbs of the syncline have been unfolded about the southeast plunging fold axis. The area to the southeast of the intersection of the Jason Fault and the stratigraphic level of the C sedimentary breccia units was the scarp area of the Jason fault at the time of deposition of the C sedimentary breccia.

fining of units away from the Jason fault (Fig. 2.10). The thickest part of the lobe is dominated by intraclast-rich pebbly mudstone. Close to the fault individual breccia beds are amalgamated as a massive breccia deposit. Away from the fault sedimentary breccia units become thinner, the entrained clasts become smaller and sedimentary breccia beds are interbedded with mudstone or siltstone beds. Individual cycles 2 to 4 m thick of underlying clast supported conglomerate overlain by intraclast-rich conglomerate or sedimentary breccia are characteristic in the distal portions of the sedimentary breccia lobes. Transverse to the axis of the lobe, sedimentary breccia beds thin and interfinger with mudstone or siltstone beds (Fig. 2.10). Massive to bedded conglomerate, sandy conglomerate, intraclast rich conglomerate and sandstone occur as lenticular, channel-like bodies trending parallel to the axis of the breccia lobe, predominantly in the intermediate to distal parts of the breccia lobes. Conglomerate lenses correlate laterally with carbonaceous mudstone beds in the proximal parts of lobes but correlate laterally with thin-bedded siltstone in the distal parts of lobes.

The A2 breccia (Fig. 2.11a) is anomalous with respect to other sedimentary breccia units. The trend of the A2 breccia is parallel to the Jason fault, and the breccia unit is thinner and finer grained than the northwest trending breccia lobes. It is composed of a central massive sandy conglomerate flanked by heterolithic breccia. The A2 breccia thickens towards the southwest and thins towards the east where it broadens and passes into siltstone beds.

Origin of Sedimentary Breccias

The following discussion of the origin of the sedimentary breccia lithofacies utilizes theoretical models of mass flow transport developed in studies by Hampton (1972), Middleton and Hampton (1976) and Lowe (1982). Subaqueous sliding or slumping from a scarp commonly gives rise to debris flows via the entrainment of water which breaks up the coherence of the sediment. Clasts within a debris flow are supported during transport by the cohesive strength of the matrix, and to a lesser extent, by buoyancy, dispersive pressure and turbulence. The mud-rich nature and poorly sorted character of the heterolithic breccia at

turbulence. The mud-rich nature and poorly sorted character of the heterolithic breccia at Jason suggest that they represent deposition by cohesive freezing from mud-rich debris flows (cf., Lowe, 1982). Muddy conglomerate and muddy sandstone also may also reflect debris flow transport (cf., Hampton, 1972). Beds with a basal conglomerate overlain by sedimentary breccia occur in the distal parts of the sedimentary breccia lobes (Fig. 12). These reflect deposition from a turbulent debris flow likely evolved from debris flows via incorporation of water during flow. The lower conglomerate reflects suspension sedimentation of gravel from the lower part of a turbulent mud flow followed by the cohesive freezing of the upper part of the mud flow.

The massive, unstratified and clast-supported character of the conglomerate units suggests that the conglomerate and intraclast-rich conglomerate represent deposition by frictional freezing from a traction carpet at the base of high density gravel-rich turbidity currents or grain flows (Lowe, 1982). The conclusion that sandy conglomerate were deposited by frictional freezing of lower density sandy turbidity flows is based on the presence of horizontal stratification and grading in the beds. Graded sandstone beds likely represent deposition from the residual downslope ends of these high density turbidity flows; this strong lateral separation of sand and gravel reflects the differing transport processes of pebbles (i. e. dispersive pressure) versus sand (i. e. flow turbulence).

The thickening and coarsening of individual heterolithic facies lobes towards the Jason fault indicates that the Jason fault scarp was the source of the sedimentary breccia. Siltstone and mudstone intraclasts, chert pebbles and chert and quartz sand that make up the heterogeneous facies appear to be derived from the turbidite channel sequence of the Lower Earn Group that was uplifted along the Jason fault. That cohesive but unlithified mud and silt beds were eroded from the fault scarp is supported by the presence of deformation of the margins of intraclasts (Winn et al., 1981). Gravels exposed on the fault scarp were largely uncemented yielding a high ratio of chert pebbles to conglomerate clasts. The anomalous A2 breccia (Fig. 2.11a) is interpreted to be the distal end of a breccia lobe sourced from the Jason

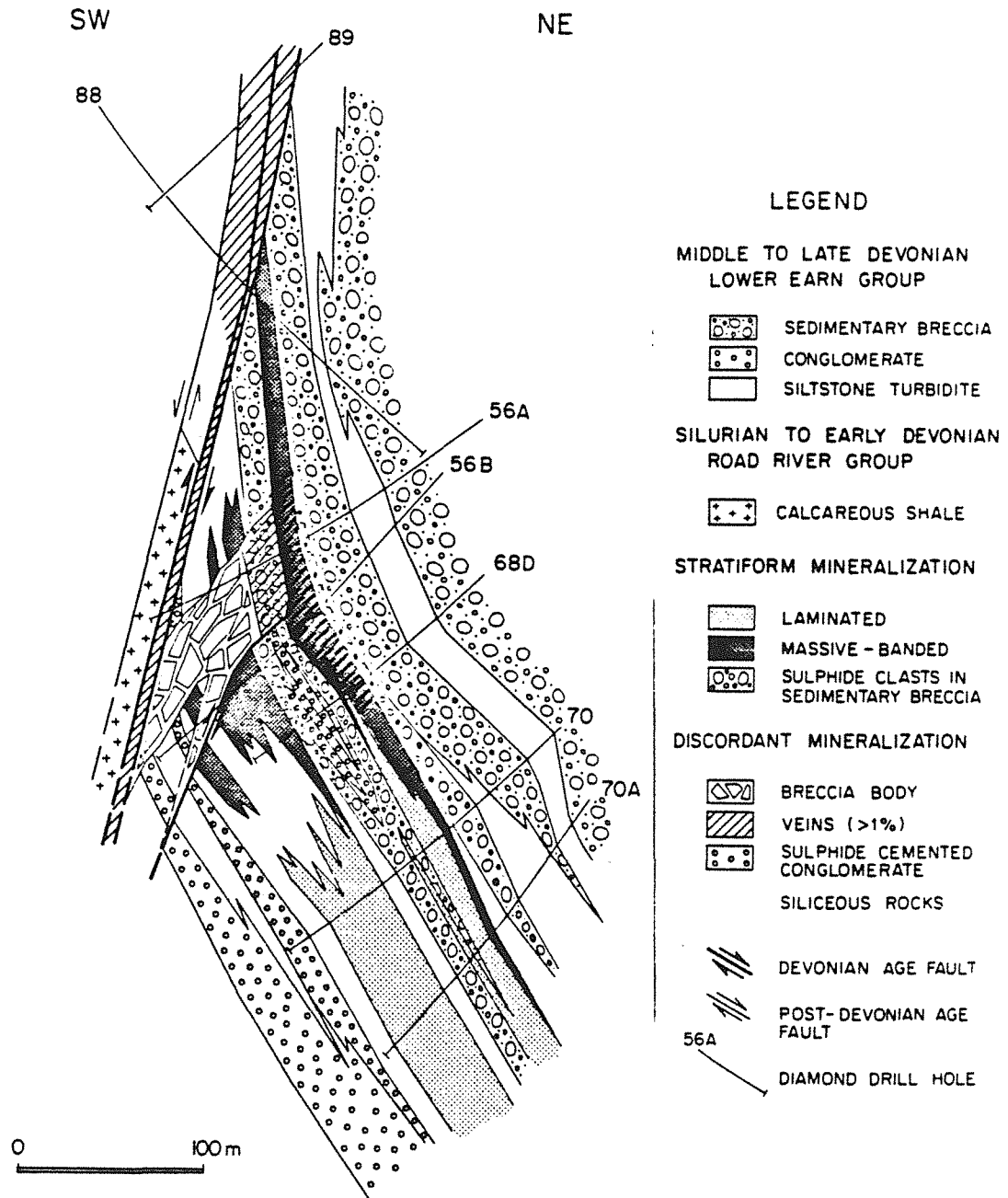


Figure 2.12 Structural cross-section (looking northwest) of stratiform and discordant ores adjacent to the Jason Fault in the South Zone area.

fault along strike to the west because of its lesser thickness, predominance of sandstone and conglomerate versus sedimentary breccia and trend parallel to the Jason fault scarp.

Each heterolithic facies lobe represents the amalgamation of mixed sediment derived from a heterogeneous scarp area of bedded silts, muds, gravels and sands. Slumped interbeds of mixed silts, muds and gravels evolved to debris flows. The slumping of massive gravel beds created high density turbidity flows or grain flows. The predominance of conglomerate and sandstone in the more distal parts of individual sedimentary lobes suggests that turbidity flows travelled further from the scarp than debris flows. Collectively, the heterolithic facies lobes can be described as a debris apron or fault scarp apron using the terminology of Pickering (1982).

In contrast, homolithic breccia units, with their lack of mixed clasts, low percentage of matrix and continuity with undeformed adjacent sediments represent short travelled slides frozen prior to or during transformation to a debris flow (Winn et al., 1981). They also may reflect *in situ* thixotropic disruption of sedimentary beds by seismic activity or elevated fluid pressures. It is likely that homolithic breccias represent partial slumping or *in situ* disruption of silts and muds deposited below the fault scarp rather than resedimentation of sediments uplifted on the fault scarp. The interfingering of thin-bedded siltstone with carbonaceous shale away from the Jason fault suggests the siltstone turbidites also are derived from the Jason fault and reflect dilute muddy silt turbidity flows whose sources were minor slumps along the Jason fault.

JASON HYDROTHERMAL SYSTEM

Associated with sedimentary breccias along the Jason fault are large deposits of stratiform Pb-Zn-Ba minerals; these are associated with hydrothermal veins of the Jason fault (Fig. 2.12) which indicates that the fault was a flow path for the hydrothermal fluids that formed the stratiform bodies. Based on texture and distribution, the hydrothermal deposit is divided into: (1) veins and disseminations associated with the Jason fault; (2) breccias in the immediate hangingwall of the Jason fault; (3) massive and laminated stratiform ores; (4)

sulfide cemented conglomerates adjacent to the Jason fault;

Previous workers (Winn et al, 1981; Gordey et al., 1982; Gardner, 1985) interpret the stratigraphic position of the South zone stratiform horizon to lie below that of the Main zone. However, this study indicates that both the South and Main zone stratiform horizons occur at the base of the sedimentary breccia lithofacies above the upper turbidite channel sequence (Fig. 2.5, 2.6, 2.7). Individual heterolithic breccia units, A and B, interbedded with the stratiform ores can be correlated from the South to the Main zone. The occurrence of Road River strata immediately below parts of the South zone deposit is a result of structural juxtaposition by the Jason fault; it does not indicate that the South zone ores occurs in the lower part of the Lower Earn Group as suggested by Gardner (1985). In addition, the systematic changes of mineralogy and metal ratios as well as variations in thickness of the stratiform ores imply that the South and Main zones are parts of a single zoned stratiform body with a paleovent zone in the South zone area (Figs. 2.13, 2.14).

Jason Fault

The Jason fault is a single or bifurcating zone of pebble breccia to pebbly mudstone up to 3 m in thickness (Figs. 2.5, 2.6, 2.12) that has been intercepted over a dip distance of 400 m. It forms the footwall to mineralization; no stratiform sulfide or barite occur in its footwall. Rounded to subangular clasts of siderite +/- chalcopyrite, pyrrhotite, sphalerite, galena veins, mudstone clasts veined by siderite-sulfide, and mudstone and siltstone clasts occur in a matrix of clay and variable amounts of fine-grained quartz, siderite and barian muscovite (Figs. 2.15a,b,c). The deepest part of the fault intersected has a very siliceous matrix with disseminated pyrite, pyrrhotite, sphalerite and galena (Fig. 2.15c). At shallower levels, the argillaceous matrix of the Jason fault is variably altered and mineralized to fine-grained barian muscovite and massive fine-grained siderite; some siderite veins have a tube-like shape with narrow selvages of muscovite (Fig. 2.15d). In the uppermost levels of the fault, the matrix is unaltered mudstone. Disseminated fine-grained pyrite is common throughout the Jason fault, and exceeds 3 to 5 percent in the uppermost part of the fault.

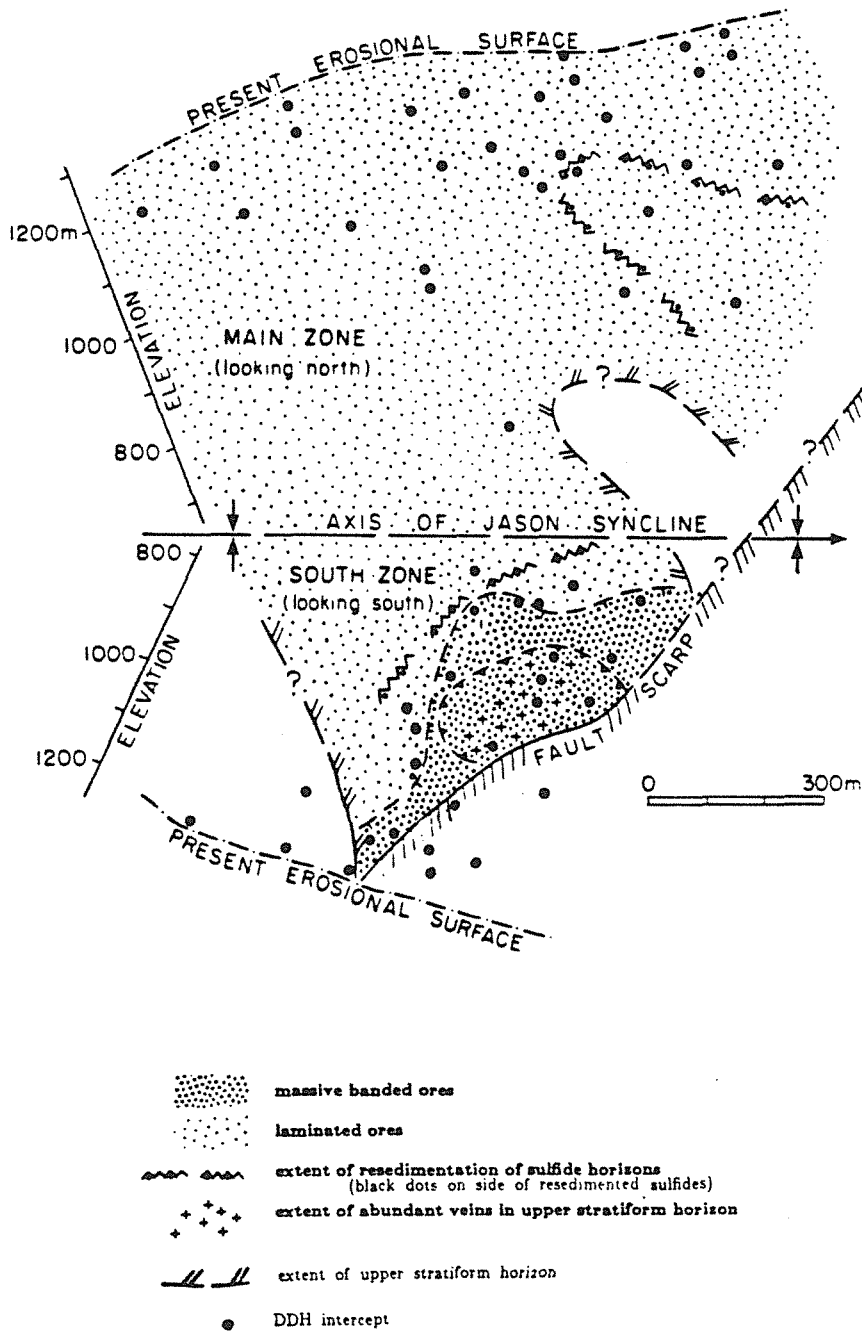


Figure 2.13 Restored plan view at the stratigraphic level of the upper stratiform horizon illustrating the distribution of textural facies within the upper stratiform horizons. Strata on the north and south limbs of the syncline have been unfolded about the southeast plunging fold axis. The area to the southeast of the intersection of the Jason Fault and the stratigraphic level of the upper stratiform horizon reflects the fault scarp area at the time of upper stratiform horizon deposition.

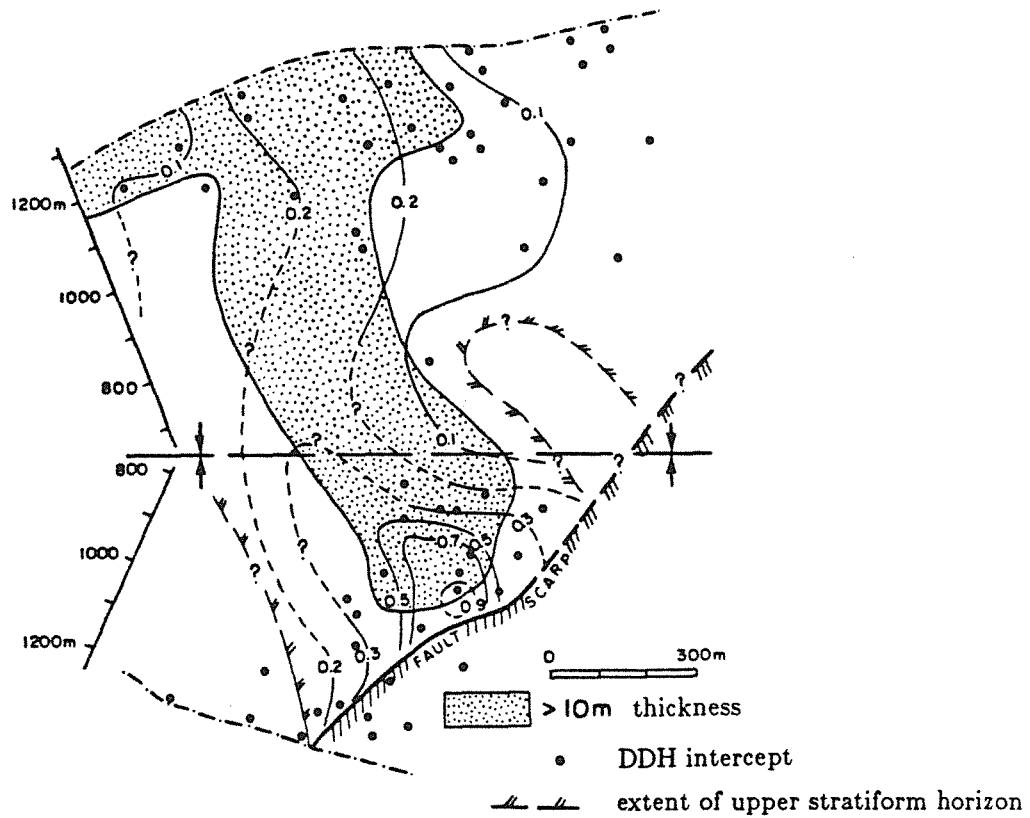


Figure 2.14 Restored plan view at the stratigraphic level of the upper stratiform horizon illustrating contours of lead/lead + zinc ratio within the the upper stratiform horizon. The extent of stratiform ore in excess of 10 m thick is indicated. Strata on the north and south limbs of the syncline have been unfolded about the southeast plunging fold axis.

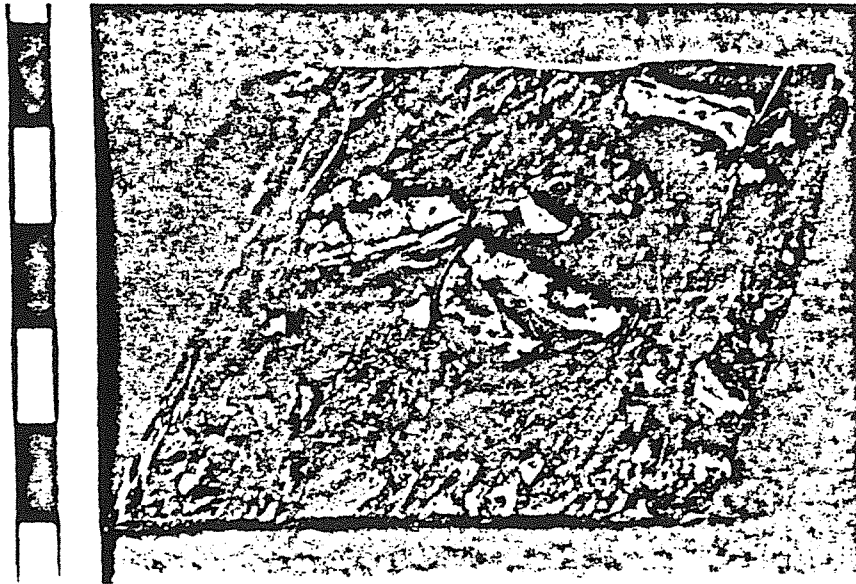


Figure 2.15a Jason fault. Angular to rounded clasts of argillite with siderite veins in an argillaceous mud matrix. Scale is in centimeters.

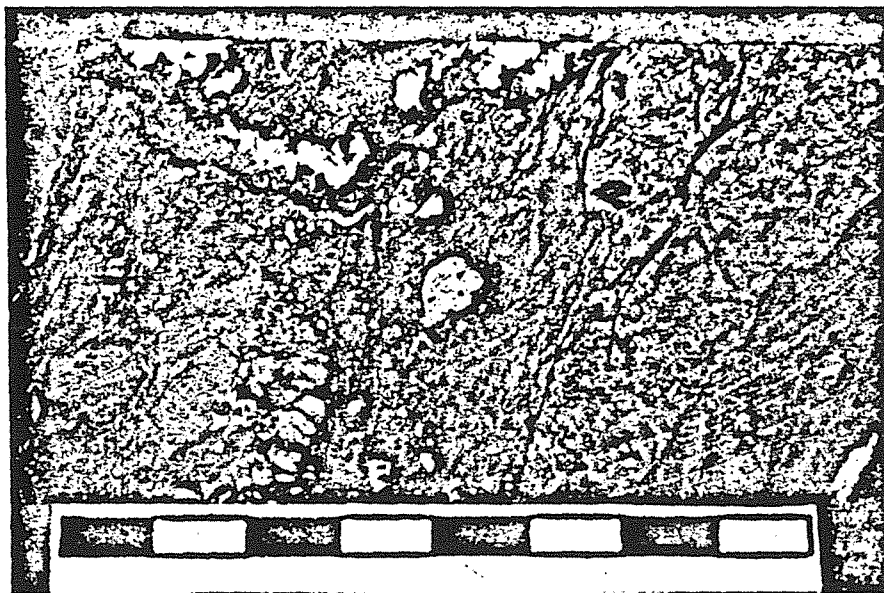


Figure 2.15b Jason fault. Irregular clasts of coarse-grained siderite (white), fine-grained massive quartz-siderite-pyrite (grey) and silicified argillite (dark grey) in silicified argillaceous matrix cut by a late sphalerite-quartz vein. Deep portion of Jason fault, DDH 87.

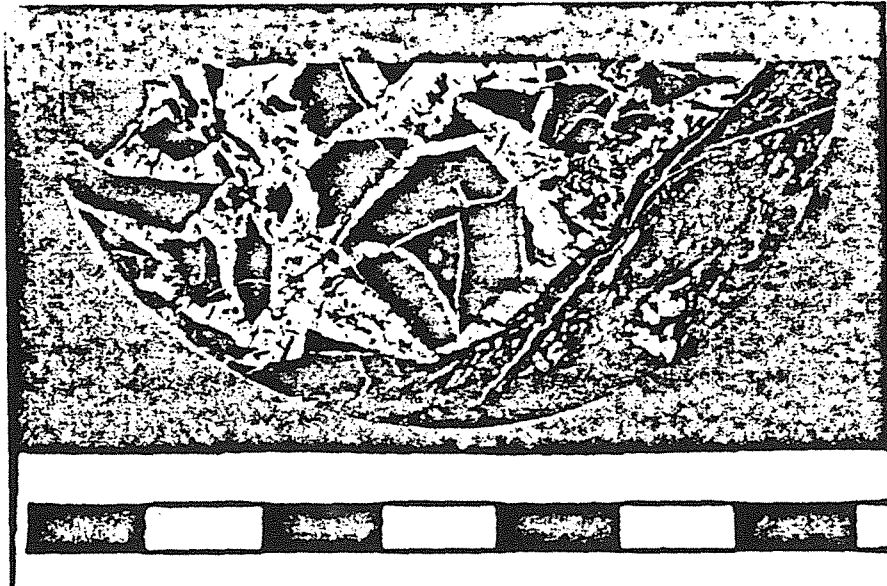


Figure 2.15c Jason fault. Breccia clast within sericitized fault matrix. Silicified argillite fragments in a siderite matrix comprise the breccia clast. Scale is in centimeters.

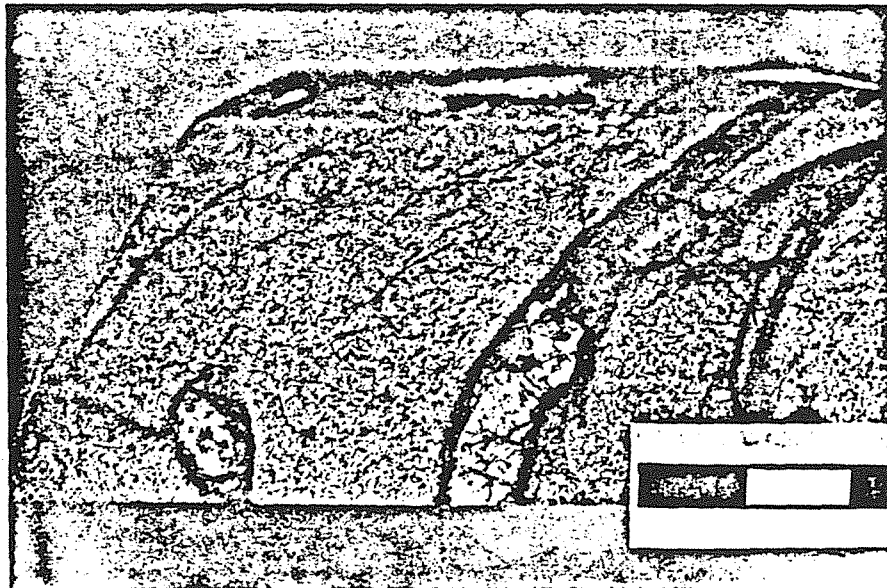


Figure 2.15d Jason fault. Tube-shaped vein with dark selvage of barian muscovite cuts muscovite-quartz-rich clastic fault matrix.

Sphalerite and galena occur as fine-grained disseminations throughout and locally as coarse-grained pods. Clasts of siderite-rich fault mineralization occurs within heterolithic breccia overlying the stratiform mineralization (Fig. 2.8d).

At depth, the Jason fault is a sharp-walled zone of milled rock adjacent to silicified rock in both the hangingwall and footwall. At the shallowest levels drilled, the fault is a narrow zone of pebble breccia bracketed by a broad, 10 m wide zone of unaltered and ductilely strained siltstone and sandstone (Fig. 2.16a). Both of these textural styles of the Jason fault are distinct from the foliated graphitic and chloritic gouge typical of other faults in the Jason area.

Irregular and discontinuous veins (Fig. 2.16b) and breccia veins (Fig. 2.16c) of siderite-ankerite-muscovite-chalcopyrite-pyrite compose 1 to 3 percent of the footwall strata adjacent to the Jason fault. These footwall veins lack alteration selvages and are similar to, but more chalcopyrite-rich, than fragmented veins within the Jason fault. Minor siderite veins occur within the ductilely deformed hangingwall strata adjacent to the upper part of the fault. These veins are pyrite-rich; veins that cut bedding at high angles show both compactional folding (Fig. 2.16d) and normal offset of strata across the vein.

There is widespread silicification of sedimentary strata adjacent to the Jason fault. Silicification occurs within footwall mudstone and siltstone adjacent to the Jason fault, within the fault matrix at deep to intermediate depths, and in the deepest levels of the hangingwall adjacent to the breccia body. A single silicification front within siltstone was noted in core (Fig. 2.17a). This silicification front is sharp and at high angles to bedding and siltstone beds display greater compaction beyond the silicified zone than within in it.

The character of the rocks in the footwall of the shallow parts of the fault contrast with that of the hangingwall rocks. The footwall is characterized by silicified and nonsilicified siltstone, the absence of ductile strain and an abundance of siderite veins. The hangingwall is silicified only adjacent to the breccia body, evidence of ductile strain is abundant and veins are minor.

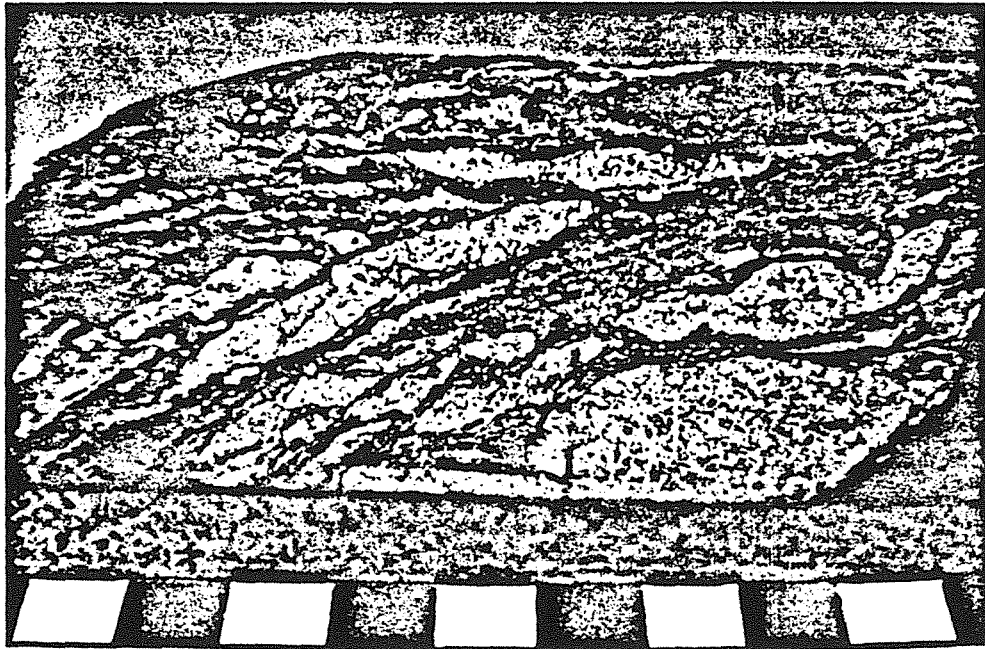


Figure 2.16a Sheared sandstone adjacent to the upper part of the Jason Fault. The ductile style of boudinage in these sub-greenschist rocks suggests deformation must have predated the lithification of the sediments. Scale in centimeters.

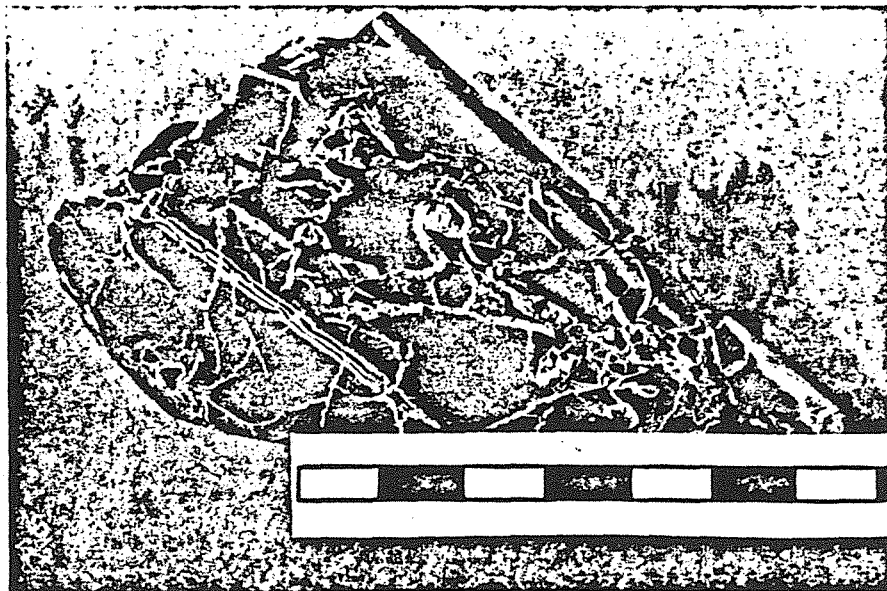


Figure 2.16b Crackle breccia with siderite-pyrite matrix in silicified argillite; footwall of the Jason fault. Scale is in centimeters.

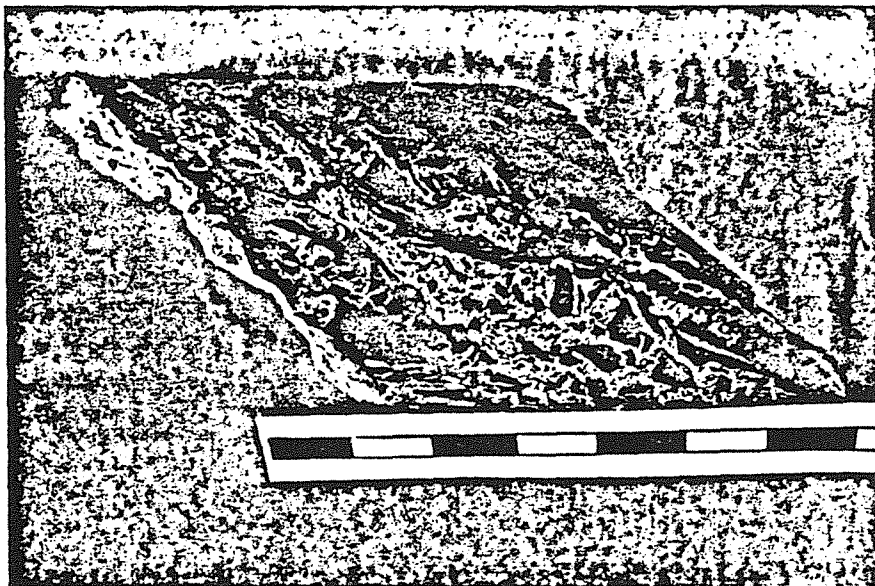


Figure 2.16c Breccia vein of ankerite-quartz-galena in silicified argillite; footwall of the Jason fault. Scale is in centimeters.

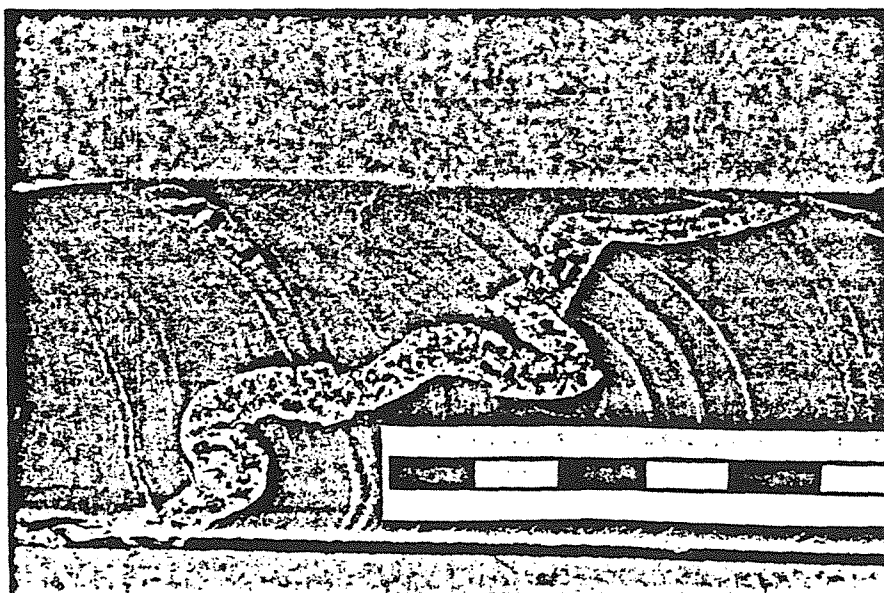


Figure 2.16d Folded siderite-pyrite vein cuts thin-bedded siltstone in the hangingwall of the upper portion of the Jason fault. Some post-lithification stylolitic dissolution adjacent to the fold hinges of the vein has exaggerated the fold amplitudes.

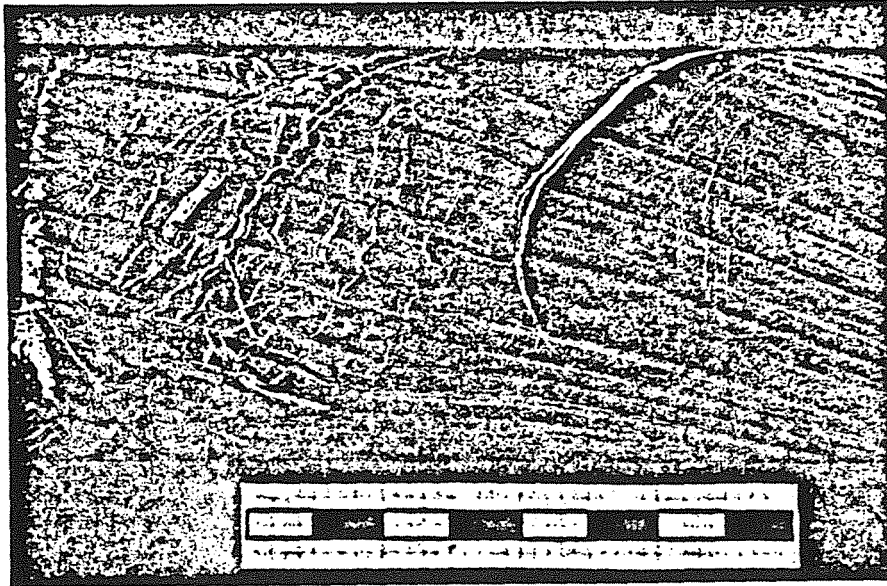


Figure 2.17a Thinning of siltstone beds across silicification front indicates that the timing of silicification predated full compaction of the siltstone. The silicification is spatially associated with the extent of siderite veinlets. Scale is in centimeters.

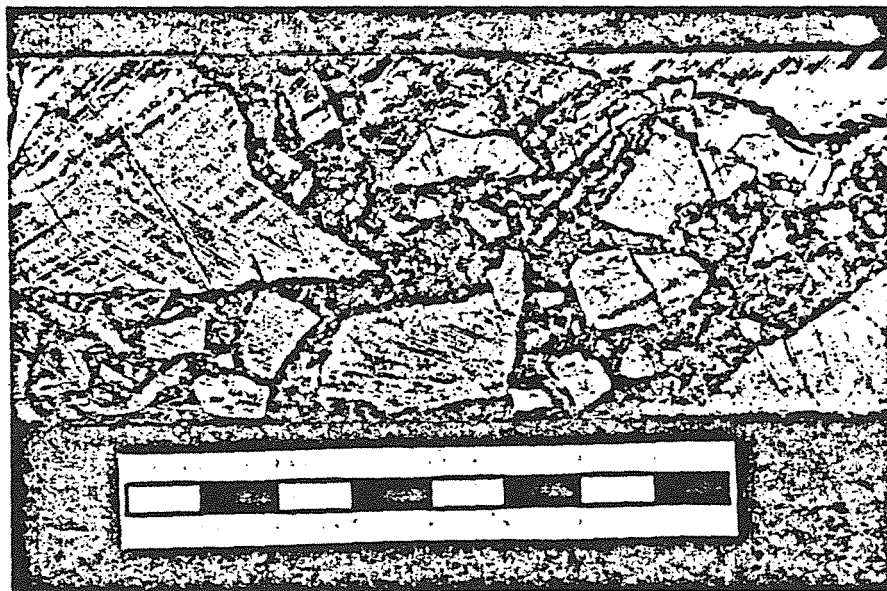


Figure 2.17b Angular fragments of silicified siltstone in a matrix of siderite, ankerite, quartz, pyrrhotite and barian muscovite within the breccia body. Scale is in centimeters.

Breccia Body

A steeply dipping, 300 m long podlike body of brecciated rock, trending subparallel to the Jason fault (Figs. 2.6, 2.13) cuts across the thin-bedded siltstone turbidite unit, merges with the Jason fault at depth, and extends up to the base of the A heterolithic breccia unit. This breccia body is characterized by angular fragments of silicified siltstone turbidite up to 10 cm in diameter in a matrix of pyrite, pyrrhotite, ankerite, siderite and lesser quartz, sphalerite, chalcopyrite and barian muscovite (Fig. 2.17b). The angular nature of fragments within the breccia body and the high fragment to matrix ratio suggests that there was little vertical movement and milling of fragments. Discrete faults can be recognized within zones of brecciated rock and the breccia body may be an amalgamation of several fault breccia zones.

Veins occur immediately adjacent to the breccia body. Where the A heterolithic breccia unit overlies the breccia body, it is cut by pyrrhotite veinlets with patchy and irregular selvages of disseminated siderite and/or pyrite. These veinlets are likely time equivalent to similar pyrrhotite-rich veinlets within the overlying stratiform mineralization (see below).

Sulfide Cemented Conglomerate

The uppermost conglomerate beds of the upper channel complex are completely cemented by pyrite for distances up to 100 m from the Jason fault (Fig. 2.12). Regionally, quartz is the dominant cement in the conglomerate. Thin conglomerate beds interbedded with the A breccia unit adjacent to the Jason fault are cemented by galena, pyrite and ankerite.

Stratiform Ore Horizons

Two stacked stratiform bodies, referred to as the upper horizon and the lower horizon occur adjacent to the Jason fault. The lower horizon is a tabular-shaped body 300 m by 400 m and up to 40 m thick (Fig. 2.5, 2.6) lying within the uppermost part of the siltstone turbidite lithofacies above the upper channel complex. Thirty percent of the stratigraphic

interval of the lower horizon is comprised of thin siltstone turbidites 1 to 2 cm thick (Fig. 2.17c). The upper horizon is thinner but more extensive body that is continuous for over 1200 m from the Jason fault to where it is truncated by the present erosional surface in the Main zone area (Figs. 2.5, 2.6). The upper horizon is separated from the lower horizon by the A breccia unit and is interbedded with minor beds of siliceous mudstone and sedimentary breccia of the basal sedimentary breccia lithofacies; it is directly overlain by the B sedimentary breccia unit.

Textures, mineralogy and metal ratios within both stratiform horizons are zoned with respect to the Jason fault. The proximal (used here with reference to distance from the Jason fault) part of the stratiform bodies is composed of beds of massive pyrite and massive to banded siderite-ankerite-galena (Fig. 2.17d). In the upper horizon, these proximal beds are interbedded with beds of massive galena-pyrite and banded galena-sphalerite and are cut by an abundance of irregular veinlets and nodules of iron carbonate (Fig. 2.17d), and veinlets of iron carbonate-muscovite, pyrrhotite +/- sphalerite, +/- galena, +/- chalcopyrite +/- pyrite; and ankerite-quartz-galena (Fig. 2.18c). Away from the Jason fault, ore is characterized by laminated barite-quartz-sphalerite-galena-pyrite interbedded with siliceous terrigenous interbeds (Fig. 2.18a). This laminated mineralization is comprised of fine-grained (0.005 to 0.04 mm), anhedral minerals within finely bedded laminae 0.01 to 5 mm thick. Laminae are characterized by sharp boundaries and an absence of terrigenous component. Laminae dominantly composed of one mineral (e.g. barite, sphalerite, galena or quartz) and polymineralic laminae (e.g. quartz-sphalerite, sphalerite-galena) occur. No sequential paragenesis exists among laminated minerals suggesting the synchronous deposition of barite, sphalerite, galena and quartz. Laminae are in sharp contact with the interbeds of siltstone and mudstone. Coarse-grained, euhedral, disseminated pyrite, barian feldspars, barian carbonates and iron carbonates are present in the laminated ores.

The upper horizon adjacent to the Jason fault has a narrow, northeast trending trough-like shape (Fig. 2.14); further away from the fault it is more extensive laterally. Lead to zinc

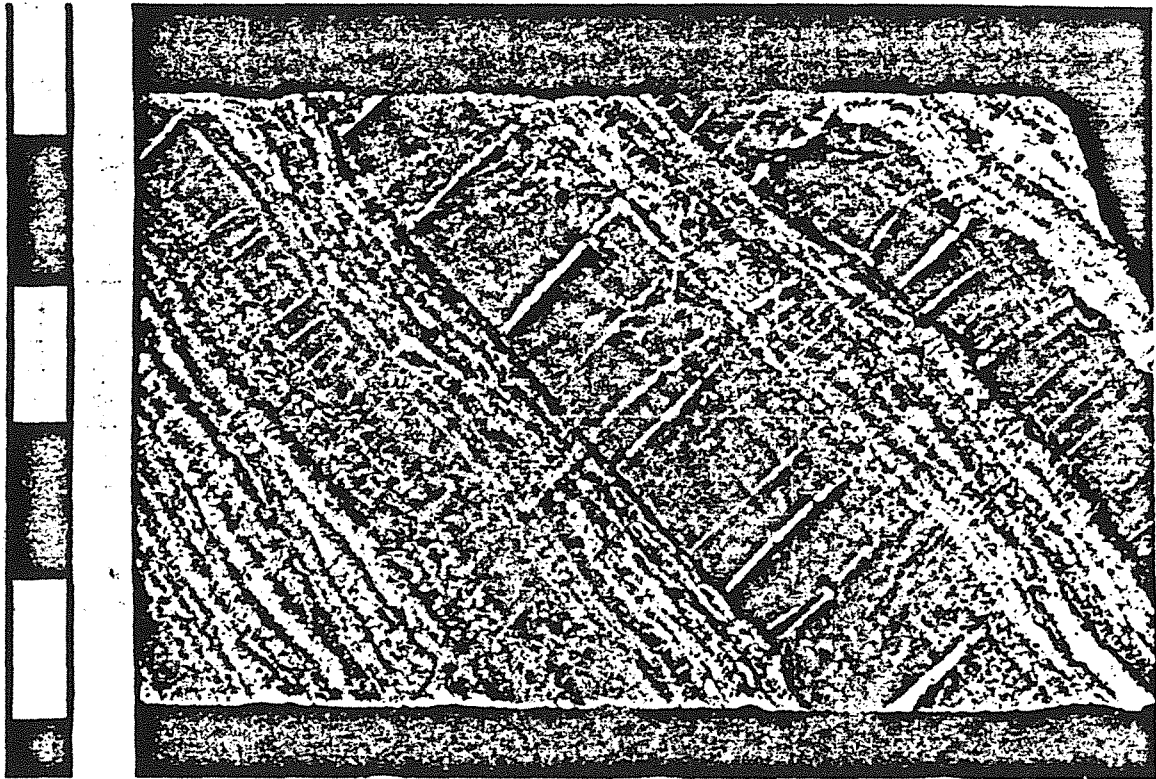


Figure 2.17c Laminae of barite, sphalerite, quartz interbedded with silicified siltstone beds in the distal laminated body. Thin quartz-filled tension gashes with siliceous siltstone beds are related to Mesozoic deformation. Scale is in centimeters.



Figure 2.17d Irregular ankerite veins crosscut massive ankerite-galena within massive-banded facies, upper stratiform horizon. Scale is in centimeters.

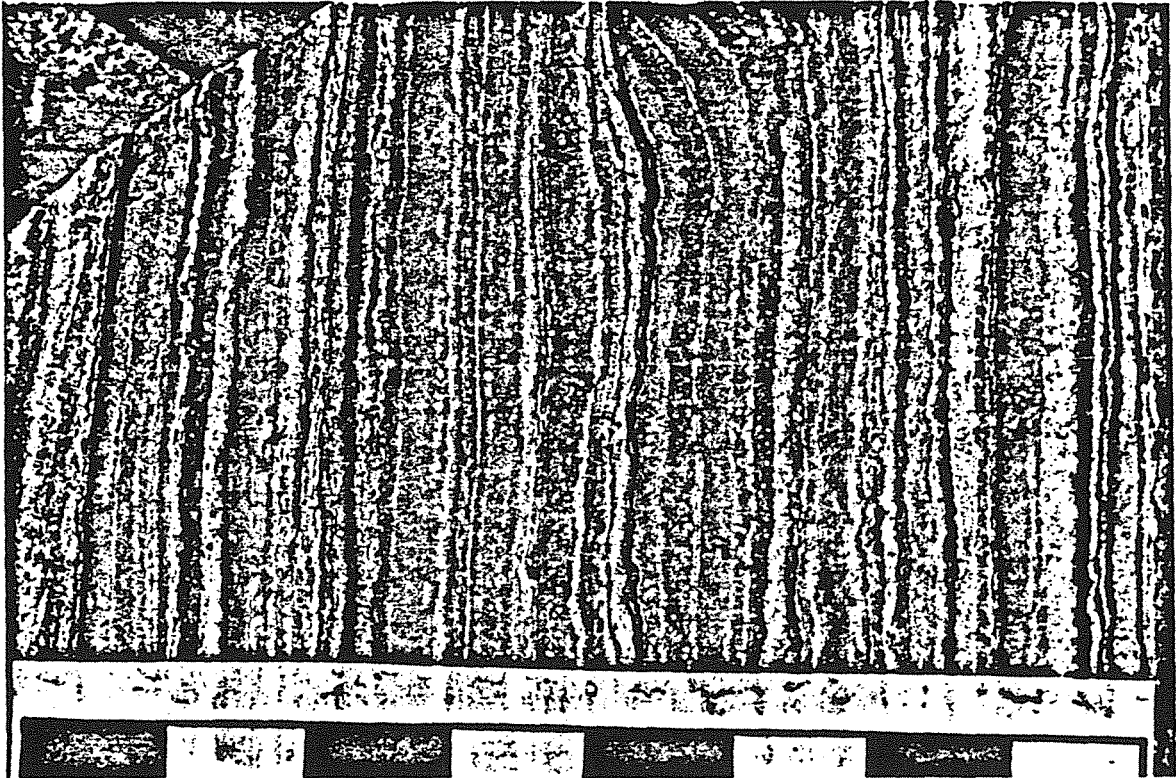


Figure 2.18a Laminae of barite (grey), chert (dark grey) and sphalerite (pink to creamy buff) within the laminated stratiform mineralization of the upper horizon. Late barian carbonate stained red (medium dark brown in photo) occurs as disseminations and discordant bands.

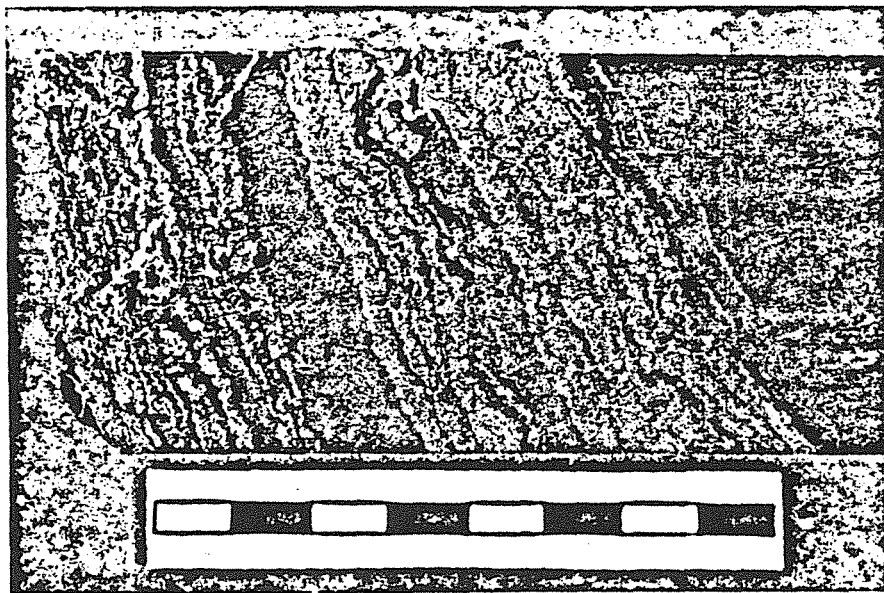


Figure 2.18b Remobilization of pyrite beds and the replacement of interbedded thin-bedded siltstone adjacent to the breccia body. Siltstones are silicified and bleached. Scale is in centimeters.



Figure 2.18c Ankerite-galena-quartz vein parallel to bedding within the banded zone. Cockscomb ankerite crystals grow inwards from the walls of the vein and galena-quartz compose the vein center. Siderite band with disseminated pyrrhotite interbanded with silicified and sericitized (barian muscovite) argillaceous siltstone beds. Scale is in centimeters.

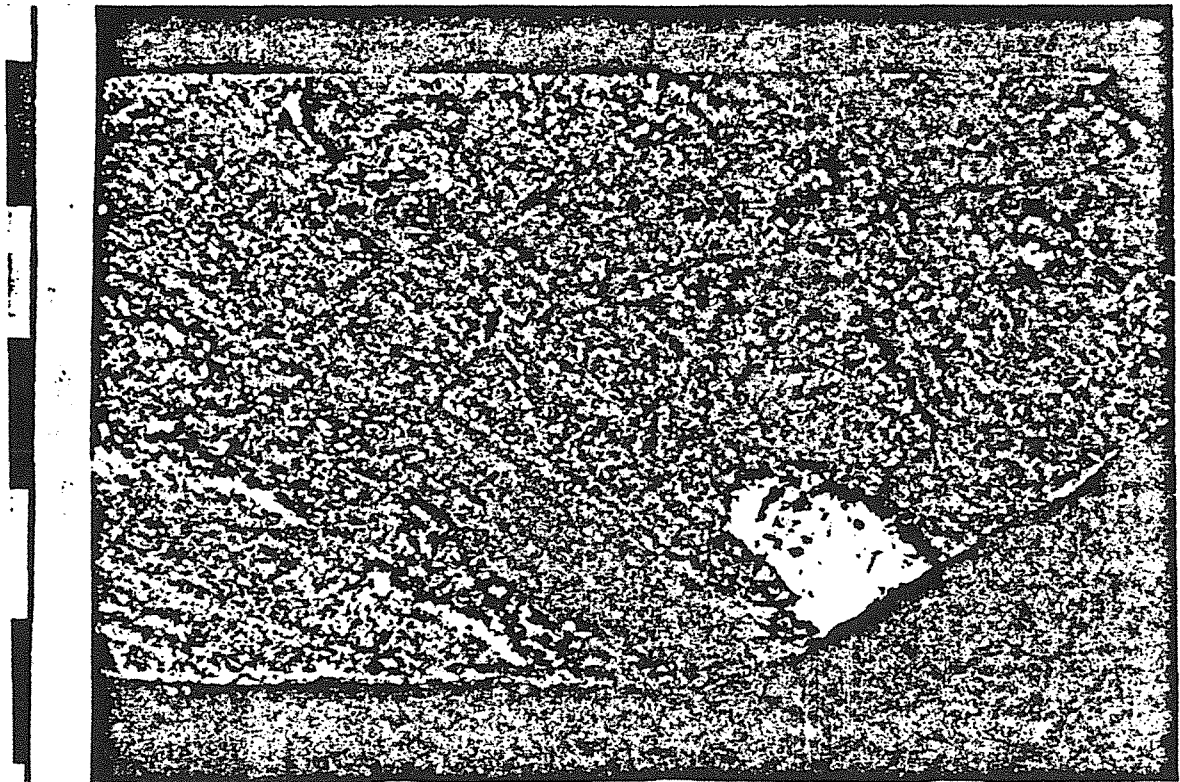


Figure 2.18d Banded massive sulphide at the top of the upper stratiform horizon overlain unconformably by sedimentary breccia. Massive sphalerite-ankerite bands are truncated by the erosional surface. Scale is in centimeters. Grains of sphalerite (SL), ankerite (ANK) and pyrite (PY) are indicated.

ratios in the upper horizon decrease away from the Jason fault. The maximum Pb/Pb+Zn values occur as a node adjacent to the Jason fault and coincide with the area of abundant epigenetic veinlets that is underlain by the breccia body (Fig. 2.14). An elongate zone of higher Pb/Pb+Zn values trends normal to the fault trend away from the maxima and coincides with the elongate zone of thickening of the upper horizon. Pb/Pb+Zn values also decrease away from the Jason fault within the lower horizon.

The breccia body cuts the proximal part of the lower horizon. Adjacent to the breccia body, pyrite beds and siderite beds are generally concordant but locally replace siltstone interbeds (Fig. 2.18b). Interbedded mudstone beds are altered to massive fine-grained muscovite. Within the siderite beds a consistent paragenesis exists; siderite grains are replaced by fine-grained disseminations of pyrrhotite along cleavage planes or by irregular pyrrhotite veinlets that cut the siderite bands. The siderite layers and pyrrhotite veinlets are cut by ankerite-galena veinlets with cockscomb-textured ankerite crystals growing from the veinlet walls (Fig. 2.18c). The ankerite-galena veinlets are parallel to bedding.

The uppermost part of the upper horizon locally contains rounded chert clasts within massive beds of sphalerite, quartz, galena and ankerite. Similar chert pebbles occur within massive pyrite beds within the lower horizon. Bedded sulfide beds at the top of the upper stratiform horizon are locally truncated by the overlying B heterolithic breccia unit (Fig. 2.18d); the basal part of the B breccia unit contains clasts of banded galena-sphalerite (Fig. 2.8e), similar in character to rocks of the proximal part of the upper horizon.

DISCUSSION

Temporal Link Between Fault Movement, Sedimentation and Hydrothermal Activity

The spatial relationships of the stratiform mineralization, breccia body and heterolithic sedimentary breccia lobes have been described above; the establishment of the temporal relationships between these features is critical for a model of sedimentation and hydrothermal

activity controlled by a submarine synsedimentary fault.

Age of the Jason Fault Relative to Sedimentation

The interpretation that the heterolithic breccias were derived from the submarine scarp of the Jason fault is based on the thinning and fining of heterolithic sedimentary breccia lobes away from the Jason fault (Figs. 2.10, 2.11). This interpretation is supported by the composition of clasts within the heterolithic breccia which are similar to the upper turbidite channel complex that was uplifted along the Jason fault. The occurrence of clasts similar in composition and texture to the mineralized portions of the Jason fault within these heterolithic breccia lobes indicates erosion of the fault during sedimentation of the sedimentary breccia.

Faults in the Jason area are characterized by poorly consolidated zones of graphitic or chloritic gouge. These faults are both axial and perpendicular to the Jason syncline and offset the folded strata. For these reasons they are interpreted to be of Mesozoic or younger age. The Jason fault is unlike these faults because of its indurated nature and massive, non-foliate matrix. It is offset by these younger faults (Fig. 2.4) and appears to pre-date Mesozoic deformation.

At depth, the Jason fault is sharp-walled; upwards it broadens into a broad zone of ductile strain with veins that show post-depositional compaction folding. This ductile strain zone is not associated with other local faults; as the rocks are of low metamorphic grade (sub-greenschist) the ductile style of deformation of the rock suggests it deformed prior to lithification. The more brittle deformational style of the footwall block with respect to the hangingwall block and the change in deformational style with depth within the observed part of the fault is compatible with the the juxtaposition of sediments in different states of lithification by a fault cutting a sedimentary sequence undergoing compaction and lithification. Therefore, both the character of the sedimentary breccia lobes and that of the fault point to the active movement on the Jason fault during the deposition of the Lower Earn Group sediments. Furthermore, the lack of gouge, slickensides or fault polish that cuts

the massive clastic texture within the Jason fault argues that the Jason fault has not been reactivated since the Devonian and hence the 80 to 200 m of apparent normal displacement occurred during the time of Lower Earn Group deposition.

Age of Stratiform Mineralization Relative to Sedimentation

Stratiform Pb-Zn ores hosted by marine clastic strata are widely interpreted to be a product of sulfide deposition from metal-rich hydrothermal fluids that discharged onto the seafloor (Large, 1981) or infiltrated into shallowly buried unlithified sediments (Williams, 1979a,b). The occurrence of sulfide clasts within heterolithic sedimentary breccia immediately overlying the upper horizon, and the truncation of banded-massive sulfide beds at the top of the upper horizon by overlying sedimentary breccia indicates that stratiform mineralization was resedimented on the seafloor via incorporation within slumps from the fault scarp. The absence of any terrigenous component within sulfide-barite laminae or beds (except in the massive-banded ores of the lower horizon discussed below), the sharp contact between mineral laminae or beds and interbedded terrigenous sediment, and the absence of significant barite, galena and sphalerite within the interbedded terrigenous sediments is compatible with the formation of the bands and laminae as sediments on the seafloor. The textural evidence of local replacement of siltstone beds by siderite and pyrite beds in the lower horizon near the breccia body is interpreted to reflect the lateral infiltration of hydrothermal fluids from the breccia body following the formation of the lower horizon. The sericitization of interbedded siltstones and the pyrrhotite and ankerite-galena veinlets may be related to this later event.

Age of Breccia Body Relative to Faulting and Stratiform Mineralization

Several lines of evidence can be used to constrain the age of the breccia body relative to faulting and stratiform mineralization. The breccia body is spatially associated with the Jason fault and merges with it at depth; the breccia is located at a change in strike of the fault which could have been a dilatant zone. Both of these observations are compatible with the hypothesis that hydrothermal fluids rose along and were focussed by the Jason fault. Above the breccia body are irregular veins and nodules of sulfide, carbonate and other

minerals that are interpreted to have formed within unlithified carbonate-rich muds. Furthermore, the stratiform ores display an abrupt increase in thickness in the area overlying the breccia body, suggesting movement on faults in the breccia coincided with deposition of the stratiform ores.

Age of Veins Relative to Faulting and Sedimentation

The occurrence of veins within sedimentary clasts within heterolithic breccia units and the compactional folding of veins is evidence for vein formation within the shallow sediments. Given the synsedimentary Devonian age of movement on the Jason fault and a lack of younger reactivation, brecciated and milled veins within the Jason fault must be of Devonian age.

The timing of siderite-ankerite-muscovite-chalcopyrite veins in the footwall of the Jason fault is more equivocal. However, the close spatial association of these veins with the Jason fault and the common occurrence of brecciated fragments of wallrock within the veins argues that they formed during the movement on the Jason fault. The compositional similarity of these veins in to the matrix of the breccia body (siderite-ankerite-muscovite-sulfide) suggests both formed during the same hydrothermal event. Because they have been uplifted on the Jason fault, the footwall veins represent the deepest epigenetic mineralization associated with the Devonian hydrothermal event. The copper-rich character of the veins is compatible with a high temperature of formation relative to Pb-Zn mineralization (Lydon, 1983).

Age of Infiltration Relative to the Formation of the Breccia Body and Stratiform Mineralization

The widespread cementing of conglomerate and sandstone beds by pyrite, galena, ankerite and galena suggest hydrothermal fluids moved laterally from the fault and breccia body through these permeable horizons. Furthermore, compactional drape of siltstone beds across a silicification front suggests that infiltration and mineralization occurred during compaction. The widespread occurrence of barian muscovite with veins and breccia matrix suggests that sericitic alteration of siltstones adjacent to the breccia body also is related to

such infiltration.

Age of Hydrothermal Activity Relative to Fault Movement

Assuming an exhalative mode of formation, stratigraphic evidence argues that the deposition of stratiform mineralization coincides with the earliest part of an accelerated period of movement on the Jason fault. The upper turbidite channel complex thins and fines abruptly near the Jason fault suggesting that the fault did influence deposition of the unit. Southeast trending paleocurrent indicators in strata at the top of the upper turbidite channel complex (Teal and Teal, 1978) are at high angle to the restored east-northeast trace of the Jason fault during the Devonian. Debris flows are absent in strata stratigraphically below the level of the stratiform mineralization (Fig. 2.7). Minor, thin (<1 m thick) sedimentary breccias occur at the stratigraphic level of the lower horizon and thick sedimentary breccias underlie and overlie the upper horizon. Therefore it is probable that minor movement occurred synchronously with the development of the upper turbidite channel complex and that accelerated movement started synchronously with the deposition of the lower horizon and continued during and after the deposition of the upper horizon.

This coincidence of fault movement with hydrothermal activity suggests that seismic pumping may have aided hydrothermal discharge during fault activity. Sibson et al. (1975) argue that fracture dilation during the strain build-up prior to movement on a fault and subsequent release during fault slip creates pressure gradients that first cause fluids to accumulate adjacent to the fault at depth prior to failure and after failure forces fluids up the fault. This model for fluid flow is supported by observed surface discharge of hydrothermal waters from the surface traces of fault zones following shallow earthquakes (Briggs and Troxell, 1955; Yoshioka et al., 1970). The very hot, saline character of the hydrothermal fluids that formed the Jason deposit (Gardner, 1985) is compatible with derivation from heated basinal fluids that were tapped by the Jason fault.

Sedimentological Environment of Deposition of Stratiform Ores

The upper horizon near the Jason fault is an elongate, northwest-trending lobe (with respect to restored Devonian orientation). This orientation is parallel to the orientation of the underlying A1 breccia lobe which near the fault exceeds 20 m in thickness. Coincident with the thinning of the underlying heterolithic breccia lobes away from the Jason fault, the upper horizon becomes more laterally extensive. Near the Jason fault thickening of the upper horizon coincides with the thinning of the underlying A heterolithic breccia unit (Fig. 2.13); abrupt lateral changes in thickness of the stratiform bodies occur in the vicinity of the Jason fault. Thus, hydrothermal deposition near the Jason fault appears to have occurred in bathymetric lows between sedimentary breccia lobes. Coincident with the decrease in the bathymetric relief of the lobes away from the fault, the upper stratiform horizon becomes more sheet-like and extensive consistent with deposition from a bottom hugging, dense fluid (Sato, 1972).

The localization of heterolithic breccia near the Jason fault of thick stratiform ores immediately adjacent to the active fault, particularly the lower horizon, argues for the existence of a large-scale depression adjacent to the Jason fault. Such topographic lows are commonly noted immediately adjacent to active normal faults (Wallace, 1978).

The area of abundant veinlets within the upper horizon adjacent to the Jason fault is interpreted to represent the area of hydrothermal fluid venting. Fluid inclusion data for quartz, siderite and ankerite veinlets indicate that fluid temperatures in the immediate subsurface averaged 250° C (Gardner, 1985). The veinlets cut massive to banded stratiform ore. The massive nature of this ore is suggestive of rapid sedimentation, and their high lead to zinc ratios is similar to the massive ores of other stratiform lead-zinc deposits that are thought to have been deposited in vent areas (Campbell and Ethier, 1984; Carne, 1979; Taylor and Andrew, 1978).

The thin siltstone turbidite beds interbedded with the lower horizon suggest a higher rate of terrigenous sedimentation than during the deposition of the upper horizon. The lower

horizon is not interbedded with sedimentary breccia deposits and interestingly appears to lack an elongate trough-like form. It has an oval shaped plan view that likely reflects hydrothermal sedimentation within a shallow depression created by fault related subsidence on a featureless ocean floor covered by thin-bedded turbidite deposits. This stratigraphic evidence suggests the fault scarp was only weakly active during the deposition of the lower horizon.

Hydrothermal Infiltration of Sediments

The occurrence near the Jason fault and breccia body of local veinlets and irregular masses of siderite and pyrite along the margins of beds of similar composition, of silicified and sericitic siltstones and mudstone, and conglomerate beds cemented by pyrite, ankerite and galena indicates that significant infiltration of the shallow sediments by hydrothermal fluids occurred.

Relationships between different paragenetic stages of the epigenetic mineralization yield insights about the physical processes of formation. A progressive induration of the siltstone turbidites during successive infiltrational events is suggested by the textural evolution of successive paragenetic stages (Fig. 2.18c). Silicification is the most widespread alteration, is cut by all other mineralization events, and is interpreted to be the earliest alteration event. Siderite is confined to irregular pods and disseminated grains in the silicified siltstone. Pyrrhotite occurs as pods, irregular veinlets and disseminations cutting siderite and silicified siltstone. Planar bedding-parallel veins of ankerite-galena cut all other assemblages. This textural progression of alteration style with time from pervasive to disseminated or pod-like to irregular veinlet to planar veinlet suggests that during the sequential alteration of the originally permeable sediment, the flow path of hydrothermal fluids changed from pervasive to specific permeable beds to non-brittle fractures to brittle fractures.

Silicification is the most widely developed type of alteration. The solubility of quartz and amorphous silica is strongly temperature dependent and silicification of shallow level rock is common in modern geothermal systems (White, 1981) as well as ancient submarine massive

sulfide deposits (Henley and Thornley, 1979). Silica precipitation below the seabottom in the Jason system likely occurred where hydrothermal fluids mixed with cooler connate waters. The distribution of hydrothermal quartz adjacent to the Jason fault suggests this mixing occurred in the lower part of the Jason fault, in the breccia body and within the sediments during infiltration. Such early silicification likely created an impermeable cap on the hydrothermal system; the breccia body may reflect rupture of this indurated cap by subsequent fault movement.

The cause of infiltration may have been fluid overpressures adjacent to the Jason fault. The presence of fluid overpressures at very shallow levels below the Devonian seafloor is suggested by the presence of bedding parallel veins in the massive-banded zone of the lower horizon adjacent to the breccia body. Similar 'jack-up' veins at the Silvermines stratiform deposit have been used to suggest that hydrostatic fluid pressures exceeded lithostatic pressure during the formation of the stratiform mineralization (M. Russell, pers. comm. 1983). Such fluid overpressures must have coincided with periods when the exhalative discharge of hydrothermal fluids was plugged, possibly due to self sealing of the hydrothermal discharge as described by Henley and Thornley (1979) or due to the physical capping of the hydrothermal system by the rapid sedimentation of the thick B sedimentary breccia overlying the stratiform mineralization. If the later was the case, the timing of the infiltration that formed the massive-banded zone of the lower horizon would slightly postdate the formation of the upper horizon.

The area of the breccia zone and veined stratiform mineralization coincides with the area of active slumping during A, B and C breccia times (Fig. 2.10). This suggests the possibility that rising hydrothermal fluids may have destabilized the fault scarp sediments and caused mass flow. The abundance of sulfide mineralization of chert clasts and the presence of gravels cemented by hydrothermal siderite, ankerite and quartz within the sedimentary breccia indicate that the gravel beds adjacent to the Jason fault were very permeable to hydrothermal fluids. As well, the distribution of altered sediment adjacent to

the breccia body suggests hydrothermal fluids flowed laterally through adjacent silts for distances up to 100 m. The infiltration of permeable beds adjacent to the Jason fault by hydrothermal fluids may have increased the sediment pore pressure and decreased the stability of the unlithified sediments. Alternatively, it is possible that the fluid discharge coincided with the zone of maximum throw on the fault; this area would likely be the most unstable part of the scarp. A modern analogue can be found in the Matsushiro fault zone, where subaerial landslides were triggered by fluid discharge during a period of microseismicity in 1966 (Morimoto et al., 1967; Yoshioka et al., 1970).

Tectonic Setting of the Jason Fault

Movement on the Jason fault coincides with regionally extensive normal faulting that disrupted the outer continental margin of northwestern North America during the Middle Devonian to early Mississippian. The depositional and tectonic setting of the Lower Earn Group strata suggests analogy to the Late Cenozoic to Recent borderland basins of Southern California which represent a submarine component of the broad San Andreas wrench tectonic regime (Blake et al., 1978). There, a broad array of faults have resulted in a seabottom of ridges and basins undergoing very rapid vertical strain. Narrow debris aprons occur along the fault bound margins of the basins (Nardin et al., 1979); baritic sinters formed by the venting of hydrothermal fluids have been discovered along such faults (Lonsdale, 1979).

Euxinic conditions during deposition of the Lower Earn Group strata likely reflect the superposed effects of the general anoxic nature of the Lower Paleozoic oceans (Berry and Wilde, 1978), upwelling along the margin of northwestern North America (Parrish, 1982, 1983), and basinal restriction due to the ridge and basin bathymetry associated with faulting (Goodfellow, 1985).

A linear east to southeast trending belt of coarse-grained chert-rich detritus was deposited in the Macmillan Pass area during Lower Earn Group time. The southeast trend of isopachs of the lower and upper channel complexes (Hubecheck, 1981), the occurrence of southeasterly oriented solemarks in sandstone beds overlying the upper channel complex (Teal

and Teal, 1978) and the depositional pinchout of the channel complexes to the southeast (Teal and Teal, 1978; Abbott, 1982) argues for a westerly source of the chert-rich detritus (Winn et al., 1981). Devonian age erosion of basinal Road River cherts and Proterozoic strata has been documented 120 km to the west of the Macmillan Pass (S. Gordey, pers. comm. 1984). Channelized turbidite systems of similar regional magnitude have been described elsewhere (Winn and Dott, 1979; Hein and Walker, 1982). The unconformable deposition of the turbidite channel complexes on the Road River Group suggests transport within a submarine canyon setting (Winn et al., 1981) or fault-bound graben where submarine erosion of strata accompanied channelized deposition (see Clifton, 1981). The thinning and fining of the upper channel complex towards the Jason fault suggest that the fault was at least weakly active during deposition of these channelized turbidites. Thinner bedded siltstone and sandstone strata likely reflect deposition on levees and overbank areas lateral to the channel area.

Accelerated movement on the Jason fault coincided with the shut off of the coarse-grained turbidites that were transported from the west along the tectonic grain of the strike-slip faults. This coincidence indicates that the cut off of this sediment supply was related to faulting to the west that was synchronous with activity on the Jason fault; such faulting may have disrupted the sediment transport path of the submarine canyon or caused subsidence of the source area. Subsequent sedimentation in the Macmillan Pass area is distinctive for the absence of terrigenous material and was dominated by the deposition of siliceous and organic rich hemipelagic muds. The high silica content of the carbonaceous mudstone suggests elevated concentrations of silica in the bottom waters; such conditions have been inferred to develop in stratified water masses due to continued input of biogenic silica from overlying waters and the lack of recycling of this silica to shallower waters via upwelling (Fisher and Arthur, 1977, pg. 42).

The Jason fault is one of a set of northeast trending normal faults within a pull-apart basin bound by northwest trending Devonian age strike-slip (?) faults. Devonian age strike-slip

movement is suggested by a map-scale north-trending fold and an axial plane cleavage present in the Lower Earn Group that is absent in younger strata (McClay, 1983; pers. comm. by K. McClay to G. Abbott cited in Abbott, 1985). Synchronous extensional faulting and compression is suggestive of a transtensional-transpressive tectonic regime (Aydin and Page, 1984) rather than a purely extensional setting. Eisbacher (1983) has proposed that left-lateral strike-slip faulting occurred during Late Devonian to Early Mississippian time along the continental margin of North America. Strike-slip movement on the northwest trending fault set may have resulted in a local zone of dilation expressed by the northeast trending fault set.

Submarine geothermal activity and minor volcanism was focused at the intersections of the northeast and northwest trending faults within the pull-apart basin. The general association of brine pools with the intersection of transform faults and spreading axes in the Red Sea was noted by Bignell (1975). The Jason and Tom stratiform Pb-Zn deposits reflect the submarine discharge of hydrothermal fluids at temperatures near 250 C (Gardner, 1983; Ansdell, 1985). The saline nature of these fluids (9-10 weight percent NaCl equivalent; Gardner, 1985; Ansdell, 1985) is compatible with a heated basinal brine source. Stratiform barite deposits hosted by the Lower Earn Group strata occur adjacent to the Hess and Macmillan faults peripheral to the pull-apart basin and are not associated with active fault scarps (Turner, 1984). Stratiform barite deposition reflects the submarine discharge of warm, hydrothermal fluids at temperatures of less than 100 C from shallowly penetrating faults (Lydon et al., 1985).

CONCLUSIONS

Uplift on the Jason fault caused slope failure and slumping of shallowly buried bedded silts, muds, gravels and sands that accumulated as debris lobes at the base of the fault scarp. Slump debris accumulated in lobe-like deposits that extended over 1000 m from the submarine fault; the thickness of these accumulations varied from 20 to 60 m thick near the fault to less than 10 m a kilometer away. Slumped interbedded silts, muds and gravels were transported as intraclast-rich debris flows that in some cases evolved into turbulent debris

flow due to the incorporation of water during flow. Failure of uncemented gravel and sand beds caused high density turbidity flows or grain flows that deposited by frictional freezing. The concentration of gravel deposition near the scarp and sand deposition further out reflects the differing transport processes of pebbles (i.e. dispersive pressure) versus sand (ie. flow turbulence). Thin-bedded siltstone turbidites sequences were deposited with the heterolithic debris lobes near to the Jason fault scarp. Further from the fault the siltstone beds interfinger with carbonaceous mudstones. The well sorted character of these turbidites argues for a considerable transport distance; the lack of thickening towards the Jason fault suggests it is unlikely that they were derived from the adjacent Jason fault scarp. These siltstones are indistinguishable from siltstones in the underlying siltstone turbidite lithofacies and may reflect the waning flow of the westerly derived turbidite channel deposition that was focused along the bathymetric low adjacent to the Jason fault. Such deposition corresponds to the southeastward shift of the axis of turbidite deposition with time (Fig. 6); such a shift would be expected during continuing subsidence within a half-graben adjacent to the Jason fault. These siltstone turbidite sequences were prone to partial disaggregation due *in situ* thixotropic disruption by seismic activity or elevated fluid pressures and dewatering due to infiltration of hydrothermal fluids from the fault area.

Initiation of accelerated movement on the Jason fault allowed heated saline basinal fluids to rise to the seafloor where they deposited hydrothermal sediments in a sag zone adjacent to the Jason fault. Coincident with deposition of the lower stratiform horizon was the episodic deposition of thin silt turbidites reflecting the retrograde distal deposition of the westerly derived turbidite detritus and minor, thin sedimentary breccia immediately adjacent to the Jason fault.

Reactivation of movement on the Jason fault coincided with cessation of silty turbidite deposition and resulted in slumping of the fault scarp and the deposition of the A sedimentary breccia lobe. Immediately adjacent to the fault, lobes of mass flows created a hummocky seabottom and hydrothermal sedimentation was favored in the intra-lobe lows.

Massive thick-bedded pyrite, ankerite, galena and sphalerite were deposited rapidly during initial mixing of hydrothermal fluids with seawater; laminated sulfide-rich hydrothermal sediments were deposited more slowly from the mixed discharge after it spread laterally away from the vent area.

Fluid flow on the Jason fault was accommodated by fracture permeability, and the fractures also were the site of deposition of siderite and sulfides. Renewed movement on the fault brecciated the old siderite filled fractures and created new ones that accommodated the next pulse of hydrothermal discharge. Fracturing also took place in indurated wall rocks adjacent to the fault and fault movement brecciated the hydrothermal sediments interbedded with silicified sediments in the vent area of the lower horizon, resulting in a breccia body adjacent to the Jason fault and immediately below the seabottom. This early induration and subsequent brittle failure of these early sediments created a high permeability zone that focused subsequent discharge, allowing the formation of a massive sulfide deposit.

The precipitation of carbonates, sulfides and quartz in the breccia body likely caused the episodic plugging of fluid flow through the upper breccia body. Fluid overpressures that developed during periods of retarded discharge due to mineral precipitation in fractures caused hydrothermal fluids to infiltrate sediments adjacent to the breccia body and resulted in the alteration of sediment. Subsequent overpressures ruptured these indurated and mineralized sediments forming bedding parallel veins that accommodated lateral fluid flow.

Hydrothermal sedimentation was interrupted by renewed movement on the Jason Fault, scarp failure, and deposition of at least 80 m of mud-rich debris flows and gravel rich high density turbidity flows (B sedimentary breccia) over the vent area of the upper horizon. Resedimentation of the uppermost hydrothermal sediments coincided with the onset of slope failure. It is likely that this rapid physical capping of the hydrothermal system also caused continued lateral infiltration after the cessation of exhalative activity.

REFERENCES

- Abbott, G., Structure and stratigraphy of the MacMillan fold belt: evidence for Devonian faulting, *Dept. Ind. Affairs Northern Development, Open File Rept., 16 p., 16, 1982.*
- Abbott, J.G., Possible Mid-Paleozoic faults near barite and metaliferous barite deposits, MacMillan Pass, Yukon, *Geological Association of Canada Annual Meeting, Program with Abstracts, 1983.*
- Abbott, J. G., Geology of the MacMillan Fold Belt 105 O - S.E. and parts of 105 P - S.W. (3 maps 1:50,000 and legend), *Open File , 1983.*
- Abbott, J. G., Devonian extension and wrench tectonics near Macmillan Pass, Yukon Territory, Canada, in *The genesis of stratiform sediment-hosted lead and zinc deposits - Conference proceedings*, edited by R. J. W. Turner and M. T. Einaudi, pp. 85-89, Stanford Univ. Pubs., Geol. Sci., v. XX, 1986.
- Abbott, J. G., S. P. Gordey, and D. J. Tempelman-Kluit, Setting of stratiform sediment-hosted lead-zinc deposits in Yukobn and northeastern British Columbia, *C. I. M. M., Spec. Vol., Mineral Deposits of the Northern Cordillera*, in press.
- Ansdell, K. M., Fluid inclusion and stable isotope study of the Tom Ba-Pb-Zn deposit, Yukon Territory, M. Sc. Thesis, University of Alberta, Edmonton, 123 p., 1985.
- Aydin, A., and B. Page, Diverse Pliocene-Quaternary tectonics in a transform enviroment, San Francisco Bay region, California, *Geol. Soc. America Bull., 95, 1303-1317, 1984.*
- Badham, J. P. N., Shale-hosted Pb-Zn deposits: products of exhalation of formation waters?, *Trans. Instn. Min. Metall., 90, B70-B76, 1981.*
- Bailes, R. J., B. W. Smee, D. W. Blackadar, and H. D. Gardner, Geology of the Jason lead-zinc-silver deposits, Macmillan Pass, Yukon Territory, in *Mineral Deposits of the Northern Cordillera: Canadian Inst. Mining Metall., Spec. Vol.*, edited by J. Morin, in press.
- Bischoff, J. L., Red Sea geothermal brine deposits: their mineralogy, chemistry, and genesis, in *Hot Brines and Recent Heavy Metal Deposits in the Red Sea*, edited by E. T. Degens and D. A. Ross, pp. 368-401, Springer, 1969.

- Blake, M. C., M. C. Blake, Jr., R. H. Campbell, T. W. Dibble, Jr., D. G. Howell, T. H. Nilsen, W. R. Normark, J. C. Vedder, and E. A. Silver, Neogene basin formation in relation to plate-tectonic evolution of the San Andreas fault system, California, *Amer. Assoc. Petroleum Geologists Bull.*, 62, 344-372, 1978.
- Bouma, A. H., *Sedimentology of Some Flych Deposits*, 168 p., Elsevier, Amsterdam, 1962.
- Briggs, R. C., and H. C. Troxell, Effect of Arvin-Techapi earthquake on spring and stream flow, *Calif. Div. Mines Bull.* 171,, 81-98, 1955.
- Campbell, I. H., T. J. McDougall, and J. S. Turner, A note on fluid dynamic processes which can influence the deposition of massive sulphides, *Econ. Geol.*, 79, 1905-1913, 1984.
- Carne, R.C., Geological setting and stratiform lead-zinc-barite mineralization, Tom Claims, Yukon Territory, *Open File Rept. EGS 1979-4*, 30, 1979.
- Carne, R. C., and R. J. Cathro, Sediment exhalative (sedex) zinc-lead-silver deposits, northern Canadian cordillera, *Canadian Mining Metall. Bull.*,, 75, 66-78, 1982.
- Cecile, M.P., The lower Paleozoic Misty Creek Embayment, Selwyn Basin, Yukon and Northwest Territories, *Geological Survey of Canada Bulletin* 78, 78, 1982.
- Cecile, M.P., Evidence against large-scale strike-slip separation of Paleozoic strata along the Richardson-Hess fault system, northern Canadian Cordillera, *Geology*, 12, 403-407, 1984.
- Clifton, H. E., Submarine canyon deposits, Point Lobos, California, *Society of Economic Paleontologists and Mineralogists Field trip Guidebook*, 72-92, 1981.
- Craig, H., Geochemistry and origin of Red Sea brines, in *Hot Brines and Recent Heavy Metal Deposits in the Red Sea*, edited by E. T. Degens and D. A. Ross, pp. 208-242, Springer, 1969.
- Crowell, J. C., Origin of late Cenozoic basins in Southern California, *Spec. Publ. Soc. econ. Paleont. Miner.*, 22, 190-204, 1974.
- Dawson, K.M., and M.J. Orchard, Regional metallogeny of the northern cordillera: Biostratigraphy, correlation and metallogenic significance of bedded barite occurrences in eastern Yukon and western District of Mackenzie, *Current Research, Part C, Geological Survey of Canada, Paper 82 - 1C*, pp. 31-38, 1982.

- Demaison, G. J., and G. T. Moore, Anoxic environments and oil source bed genesis, *American Assoc. Petrol. Geologists Bull.*, *8*, 1179-1209, 1980.
- Eisbacher, G., Devonian-Mississippian sinistral transcurrent faulting along the cratonic margin of western North America: a hypothesis, *Geology*, *11*, 7-10, 1983.
- Facca, G., and F. Tonani, The self-sealing geothermal field, *Bull. Volcanol.*, *30*, 271-273, 1967.
- Fischer, A. G., and M. A. Arthur, Secular variations in the pelagic realm, *S.E.P.M. Spec. Pub.*, *25*, 19-50, 1977.
- Gardner, H. D., Petrologic and geochemical constraints on genesis of the Jason Pb-Zn deposits, Yukon Territory, M.S. Thesis, , University of Calgary, 1983.
- Gardner, H. D., and I. Hutcheon, Geochemistry, mineralogy and geology of the Jason Pb-Zn deposits, Macmillan Pass, Yukon, Canada, *Econ. Geol.*, *80*, 1257-1276, 1985.
- Goodfellow, W. D., and I. R. Jonasson, Ocean stagnation and ventilation defined by 34S secular trends in pyrite and barite, Selwyn Basin, Yukon, *Geology*, *12*, 583-586, 1984.
- Gordey, S.P., Stratigraphy of southeastern Selwyn Basin in the Summit Lake area, Yukon Territory and Northwest Territories, Current Research, Part A, , pp. 13-16, 1979.
- Gordey, S.P., Stratigraphy, structure and tectonic evolution of southern Pelly Mountains in the Indigo Lake area, Yukon Territory, *Bulletin 318*, *44*, 1981.
- Gordey, S.P., J.G. Abbott, and M.J. Orchard, Devonian-Mississippian (Earn Group) and younger strata in east-central Yukon, *Geol. Surv. Canada, Paper 82-1B*, 93-100, 1982.
- Hamilton, J. M., D. T. Bishop, H. C. Morris, and O. E. Owens, Geology of the Sullivan orebody, Kimberley, B. C., Canada, in *Precambrian sulfide deposits (H. S. Robinson Memorial Volume)*, edited by R. W. Hutchinson, C. D. Spence and J. M. Franklin, pp. 597-625, Geol. Assoc. Canada Special Paper 25, 1982.
- Hampton, M. A., The role of subaqueous debris flow in generating turbidity currents, *Jour. Sed. Petrology*, *42*, 775-793, 1972.
- Hein, F. J., and R. G. Walker, The Cambro-Ordovician Cap Enrage Formation, Quebec: conglomeratic deposits of a braided submarine channel with terraces, *Sedimentology*, *29*, 309-

329, 1982.

Henley, R. W., and P. Thornley, Some geothermal aspects of polymetallic massive sulphide formation, *Econ. Geol.*, v. 74, p. 1600-1612, 1979.

Henley, R. W., and P. Thornley, Some geothermal aspects of polymetallic massive sulfide formation, *Econ. Geol.*, 1600-1612, 1600-1612, 1979.

Hoy, T., The Purcell Supergroup in southeastern British Columbia; sedimentation, tectonics and stratiform lead-zinc deposits, *Geol. Assoc. Canada Special Paper 25*, 127-148, 1982.

Kanasewich, E. R., Precambrian rift; genesis of stratiform ore deposits, *Science*, 161, 1002-1005, 1968.

Large, D. E., Sediment-hosted submarine exhalative lead-zinc deposits - a review of their geological characteristics and genesis, in *Handbook of strata-bound and stratiform ore deposits, 9, Regional studies and*, edited by K. H. Wolf, pp. 469-507, Elsevier, Amsterdam, 1981.

Lenz, A. C., Ordovician to Devonian history of northern Yukon and adjacent District of Mackenzie, *Bulletin of Canadian Petroleum Geology*, 2, 321-361, 1972.

Link, M. H., and T. H. Nilsen, The Rocks Sandstone, an Eocene sand-rich deep-sea fan deposit, northern Santa Lucia Range, California, *Jour. Sed. Petrology*, 50, 583-602, 1980.

Lonsdale, P., A deep-sea hydrothermal site on a strike-slip fault, *Nature*, 281, 531-534, 1979.

Lowe, D. R., Sediment gravity flows: II. Depositional models with special reference to the deposits of high-density turbidity currents, *Jour. Sed. Petrol.*, 1, 279-297, 1982.

Lydon, J.W., Chemical parameters controlling the origin and deposition of sediment-hosted stratiform lead-zinc deposits, in *Short Course on sediment-hosted lead-zinc deposits*, edited by D. F. Sangster, pp. 175-250, Mineral. Assoc. Canada, 1983.

Lydon, J.W., R.D. Lancaster, and P. Karkkainen, Genetic controls of Selwyn Basin stratiform barite/sphalerite/galena deposits: an investigation of the dominant barium mineralogy of the Tea deposit, Yukon, *Current Research, Part B, Geological Survey of Canada, Paper 79-1B*, 223-229, 1979.

Lydon, J. W., W. D. Goodfellow, and I. R. Jonasson, A general genetic model for stratiform bari-

- tic deposits of the Selwyn Basin, Yukon Territory and District of Mackenzie, *Current Research, Part A, Geological Survey of Canada, Paper 85-1A*, pp. 651-660, 1985.
- MacIntyre, D., Geology and stratiform barite-sulphide deposits of the Gataga District, northeastern British Columbia, in *Short Course on sediment-hosted lead-zinc deposits*, edited by D.F. Sangster, pp. 85-119, 1983.
- McClay, K.R., and G.E. Bidwell, *Abstracts with Programmes, C.I.M. Symposium on Mineral deposits of the northern Cordillera, Whitehorse*, 16 pp., 1983.
- McDougall, T. J., Fluid dynamic implications for massive sulphide deposits of hot saline fluid flowing into a submarine depression from below, *Deep Sea Research*, 2, 145-170, 1984.
- McDougall, T. J., Convective processes caused by a dense, hot saline source flowing into a submarine depression from above, *Deep Sea research*, 11, 1287-1309, 1984b.
- McLean, D. M., R. Revelle, and K.O. Emery, Barite concretions from the ocean floor, *Geol. Soc. America Bull.*, 62, 707-724, 1951.
- Middleton, G. V., and M. A. Hampton, Sediment gravity flows: mechanics of flow and deposition, *Turbidites and Deep-Water Sedimentation*, pp. 1-38, Pacific Section Short Course Lecture Notes, 1973.
- Middleton, G. V., and M. A. Hampton, Subaqueous sediment transport and deposition by sediment gravity flows, in *Marine Sediment Transport and Environmental Management*, edited by D. J. Stanley and D. J. P. Swift, pp. 197-218, Wiley, New York, 1976.
- Moore, J. McM., Fault tectonics at Tynaugh mine, Ireland, *Trans. Inst. Mining Metallurgy*, B84, B1-6, 1975.
- Morimoto, R., K. Nakamura, Y. Tsuneishi, J. Osaka, and N. Tsunoda, Landslides in the epicentral area of the Matsushiro earthquake swarm - Their relationship to the earthquake fault, *Bull, Earthq. Res. Inst.*, 45, 241-263, 1967.
- Mutti, E., Distinctive thin-bedded turbidite facies and related depositional environments in the Eocene Hecho Group (South-central Pyrenees, Spain), *Sedimentology*, 24, 107-131, 1977.
- Nardin, T. R., B. D. Edwards, and D. S. Gorsline, Santa Cruz Basin, California Borderland: dom-

- inance of slope processes in basin sedimentation, *S. E. P. M. Special Publication No. 27*, pp. 209-221, 1979.
- Pickering, K. T., The shape of deep-water siliciclastic systems: a discussion, *Geo-Marine Letters*, *2*, 41-46, 1982.
- Rogers, D. A., Analysis of pull-apart basin development produced by en echelon strike-slip faults, *Spec. pub. Int. Assoc. Sediment.*, *4*, 27-41, 1980.
- Russell, M. J., Structural controls of base metal mineralization in Ireland in relation to continental drift, *Trans. Instn. Min. Metall. (sect. B: Appl. earth sci.)*, *77*, B117-128, 1968.
- Russell, M.J., Major sediment-hosted exhalative zinc and lead deposits: formation from hydrothermal convection cells that deepen during crustal extension, *Mineral. Assoc. Canada, Short Course, Sediment-hosted stratiform lead-zinc deposits, Victoria*, pp. 251-282, 1983.
- Samson, I. M., and M. J. Russell, Fluid inclusion data from Silvermines base-metal-baryte deposits, Ireland, *Inst. Mining Metallurgy Trans.*, *92, sec. B.*, B67-71, 1983.
- Sato, T., Behaviors of ore-forming solutions in seawater, *Mining Geology*, *22*, 31-42, 1972.
- Schoell, M., and M. Hartmann, Detailed temperature structure of the hot brines in the Atlantis II deep area (Red Sea), *Marine Geology*, *14*, 1-14, 1973.
- Scotese, C. R., An introduction to this volume: Paleozoic paleomagnetism and the assembly of Pangea, *Geodynamic Series*, *12*, 1-10, 1984.
- Scotese, C. R., and et al., Paleozoic base maps, *Jour. Geol.*, *87*, 217-277, 1979.
- Sevestapulo, G. D., Lower Carboniferous, in *A geology of Ireland*, edited by C. H. Holland, pp. 147-171, John Wiley and Sons, New York, 1981.
- Shanks, W. C., III, and J. L. Bischoff, Ore transport and deposition in the Red Sea geothermal system: a geochemical model, *Geochim. Cosmochim. Acta*, *41*, 1507-1519, 1977.
- Shaw, D. R., Wall-rock alteration at the Sullivan Mine, Kimberley, B. C., in *The genesis of stratiform sediment-hosted lead and zinc deposits - Conference proceedings*, edited by R. J. W. Turner and M. T. Einaudi, pp. 13-21, Stanford Univ. Pubs., Geol. Sci., v. XX, in press.
- Sibson, R.H., J. McM. Moore, and A.H. Rankin, Seismic pumping--a hydrothermal fluid transport

- mechanism, *Geol. Soc. London Jour.*, 191, 653-659, 1975.
- Smirnov, V. I., Geological setting of Jason and Tom deposits, Macmillan Pass area, Eastern Yukon, *Summary of presentation, Whitehorse Geoscience Forum 1978*, 6, 1977.
- Smith, C.L., Sediment-hosted stratiform lead-zinc-silver deposits, in *Revolution in the Earth Sciences- advances in the past half-century, proceeding of a symposium held at Carleton College, Northfield, Minnesota*, edited by S.J. Boardman, Kendall Hunt Publishing Company, Dubuque, Iowa, 1983.
- Stow, D. A. V., and G. Shanmugam, Sequence of structures in fine-grained turbidites: comparison of Recent deep sea and ancient flysh sediments, *Sedimentary Geology*, 25, 23-42, 1980.
- Surlyk, F., Submarine fan sedimentation along fault scarps on tilted fault blocks (Jurassic/Cretaceous boundary, East Greenland), *Bull. Gronlands Geologiske Undersogelse*, 128, 108pp., 1978.
- Taylor, S., Structural and paleotopographic controls of lead-zinc mineralization in the Silvermines orebodies, Republic of Ireland, *Econ. Geol.*, 79, 529-548, 1984.
- Taylor, S., and C.J. Andrew, Silvermines orebodies, Co. Tipperary, Ireland, *Inst. Mining Metallurgy Trans.*, 87, sec. B, 111-124, 1978.
- Teal, P. R., and S. E. Teal, *Geology and sedimentary interpretation of the Macmillan Pass area (Jason and Tom properties), Yukon territory, unpublished company report*, 35 p., 1978.
- Templeman-Kluit, D. J., Transported cataclasite, ophiolite and granodiorite in Yukon: evidence of arc-continent collision, *Geological Survey of Canada Paper 79-14*, 27p, 1979.
- Turner, J. S., and L. B. Gustafson, The flow of hot saline solution from vents in the sea floor -- some implications for exhalative massive sulphide and other ore deposits, *Econ. Geol.*, 73, 1082-1100, 1978.
- Turner, R.J., Geology of the South Zone deposits, Jason property, Macmillan Pass area, Yukon, *Yukon Exploration and Geology 1983*, 105-114, 1984.
- Turner, R. J. W., A Late Devonian stratiform Pb-Zn and stratiform barite metallogenic event in the North American cordillera: margin-long extension and implication for the Antler Oro-

- geny, *Geol. Soc. America Abstr. Prog.*, 1985b.
- Walker, R. G., Generalized facies models for resedimented conglomerates of turbidite association, *Geol. Soc. America Bull.*, 86, 737-748, 1975.
- Walker, R. N., R. G. Logan, and J. G. Binnekamp, Recent geological advances concerning the H. Y. C. and associated deposits, McArthur River, N. T., *Geol. Soc. Australia Jour.*, 24, 365-380, 1977.
- Wallace, R. E., Geometry and rates of change of ault generated range fronts, north-central Nevada, *U. S. Geological Survey, Journal of Research*, 6, 637-649, 1978.
- White, D. E., Active geothermal systems and hydrothermal ore deposits, *Econ. Geol.*, 75th Anniv. Vol., pp. 392-423, 1981.
- Williams, N., Studies of the base-metal sulfide deposits at McArthur River, Northern Territory, Australia I: The Cooley and Ridge deposits, *Econ. Geol.*, 73, 1005-1056, 1978a.
- Winn, R. D., Jr., and R. H. Dott, Jr., Deep-water fan-channel conglomerates of Later Cretaceous age, southern Chile, *Sedimentology*, 26, 203-228, 1979.
- Winn, R.D., R.J. Bailes, and K.I. Lu, Debris flows, turbidites and lead-zinc sulfides along a Devonian submarine fault scarp, Jason prospect, Yukon Territory, in *Deep-water clastic sediments, a core workshop*, edited by C.T. Seimers, R.W. Tillman and C.R. Williamson, pp. 396-416, Soc. Econ. Paleontologists Mineralogists, 1981.
- Yoshioka, R., O. Setsuo, and Y. Kitano, Calcium chloride type water discharge from Tatsushiro area in connection with swarm earthquakes, *Geochemical Journal*, 4, 61-74, 1970.
- Zierenberg, R. A., and W. C. Shanks, III, Mineralogy and geochemistry of epigenetic features in metalliferous sediment, Atlantis II deep, Red Sea, *Econ. Geol.*, 78, 57-72, 1984.

CHAPTER 3

DEPOSITIONAL PROCESSES IN STRATIFORM SEDIMENT-HOSTED Pb-Zn DEPOSITS; EVIDENCE FROM THE JASON DEPOSIT, MACMILLAN PASS, YUKON

INTRODUCTION

Review articles by Large (1980) and Smith (1983) have recognized sediment-hosted stratiform lead-zinc deposits as a distinct class of ore deposit. Stratiform lead-zinc deposits are concordant bodies of laminated to bedded lead, zinc and iron sulfides hosted by fine-grained sedimentary strata. The depositional processes that form these deposits are poorly understood. A widely held view is that most stratiform lead-zinc deposits form as hydrothermal sediments in submarine or sub-lacustrine environments (Large, 1980). This view is based largely on the general characteristics of stratiform deposits, such as the sediment-like character of laminated to bedded sulfides, great lateral extent at a single stratigraphic horizon, commonly massive character, and in some cases association with altered footwall rocks. However, fundamental questions remain concerning the genesis of stratiform deposits. (1) What is the timing of sulfide deposition relative to the deposition of the host sediments? Textural and isotopic studies at the McArthur River stratiform Pb-Zn deposit have lead workers to conflicting conclusions as to the timing of the stratiform deposition; both exhalative sedimentary (Lambert, 1979) and a diagenetic infiltrational (Williams, 1979) models have been proposed. (2) What are the dominant processes that deposit the hydrothermal minerals? Within the exhalative model it might be expected that a stratiform body might reflect a complex history that could include hydrothermal sedimentation, resedimentation of previously formed hydrothermal material, metasomatic processes in vent areas and recrystallization and remobilization during diagenesis. (3) What is the depositional environment of sulfide accumulation? Two possible submarine exhalative environments that

are recognized in today's ocean provide possible modern analogues (Zierenberg, 1983); deposition from hydrothermal fluids that mix directly with seawater (e.g. mid-ocean ridge vent areas) and deposition from warm bodies of hydrothermal fluid ponded on the seafloor (e.g. Red Sea brine pools). The importance of these two exhalative analogues to stratiform sediment-hosted deposits has yet to be established.

The characteristics of the Jason stratiform lead-zinc deposit make it an attractive study area to tackle such questions about processes of formation of stratiform deposits. At the Jason deposit, stratiform ore was deposited adjacent to an active synsedimentary fault (Chapter 2) and some of the ore body was resedimented. This provides critical evidence towards a sedimentary origin. The occurrence of massive, veined stratiform ore near the synsedimentary fault and finely laminated ore distal to the fault suggest that a range of depositional processes formed the stratiform body. Mineral assemblages in veins and breccias within and underlying the stratiform body place constraints on the composition of the hydrothermal fluids prior to deposition of minerals in the stratiform deposit. Recent studies by Eldridge et al. (1983) have underscored the value of detailed petrographic studies in elucidating the genetic processes that formed the Kuroko volcanogenic massive sulfide deposits. The present study has integrated deposit scale stratigraphic analysis of the Jason stratiform deposit with petrographic analysis of an extensive suite of selected samples. X-ray diffraction and electron microprobe analysis were used to determine mineral compositions. Strontium isotope analysis of selected samples provide constraints on the degree of mixing of hydrothermal fluid and seawater during deposition of the hydrothermal minerals.

GEOLOGICAL SETTING

The Jason deposit is located at MacMillan Pass, in the eastern Yukon Territory, Canada (Fig. 3.1). The Paleozoic miogeoclinal strata in the MacMillan Pass area are deformed into a west-trending set of open to tight folds and high angle reverse faults of Mesozoic age and metamorphosed to a sub-greenschist grade (Abbott, 1982). Cretaceous age granite stocks locally intrude these deformed strata.

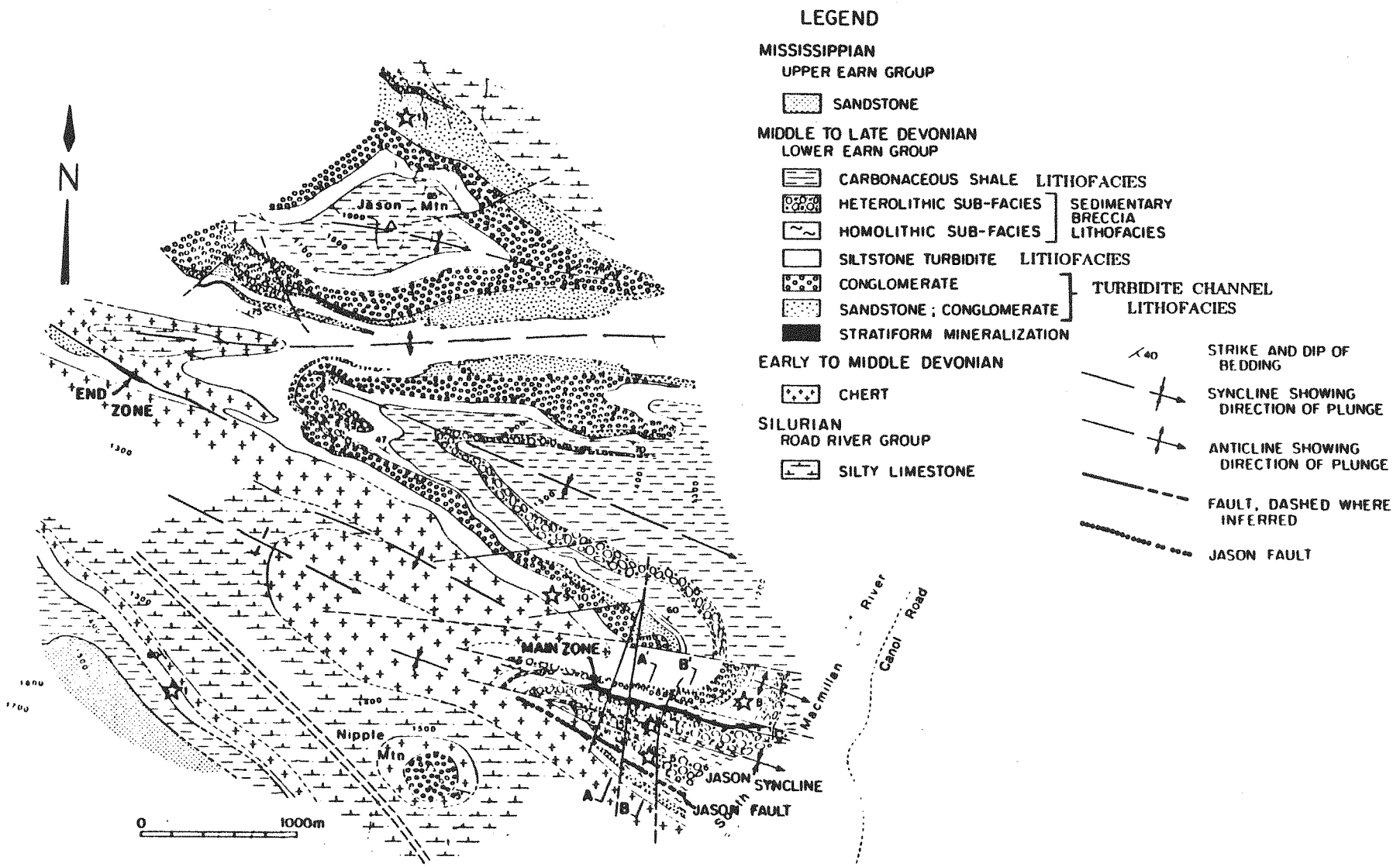


Figure 3.1 Geological map of the area near the Jason stratiform deposits (modified after unpublished company map, Cordilleran Engineering) with location of cross-section B-B' (Figure 3.2).

The Jason stratiform mineralization is hosted by carbonaceous siliceous shale and siltstone turbidite of the Lower Earn Group of Middle to Late Devonian age (Abbott, 1983). Throughout the Yukon and northeastern British Columbia, the Lower Earn Group, and correlative strata are characterized by small coarse-grained turbidite fan complexes, abrupt changes in facies and sediment thickness, locally developed unconformities, and evidence for synsedimentary faulting (Lenz, 1972; Winn et al., 1981; Gordey, 1981; Gordey et al., 1982). These features have been attributed to rifting or wrench faulting of the outer continental margin of North America during Middle Devonian to early Mississippian time (Templeman-Kluit, 1979; Eisbacher, 1983; Abbott, 1983). Stratiform sediment-hosted sulfide and stratiform barite deposits of Late Devonian age present throughout northeastern British Columbia and the Yukon are thought to reflect submarine geothermal activity associated with this extensional faulting (Cathro and Carne, 1982).

In the MacMillan Pass area, the absence of evidence of wave reworking and the deposition of the coarser clastic sediments by mass flow transport in the Lower Earn Group strata indicates a deep-water setting. Very heavy sulfur isotope ratios of diagenetic pyrite (Goodfellow and Jonnason, 1984), the absence of evidence of benthic faunas and high organic carbon content within the Lower Earn Group suggests that the marine conditions were anoxic. Such stagnant conditions may reflect several factors that include anoxic nature of the global Lower Paleozoic oceans (Berry and Wilde, 1978), coastal upwelling (Parrish, 1982, 1983) and restricted seawater circulation within the irregular topography of this faulted continental margin.

The depositional and tectonic setting of the Lower Earn Group strata may be analogous to the Late Cenozoic to Recent age borderland basins of Southern California. The borderland represents a submarine component of the broad San Andreas wrench fault regime (Blake et al., 1978). This seafloor of ridges and basins is undergoing very rapid vertical strain and narrow debris aprons occur along the fault bounded margins of the basins (Nardin et al., 1979). Basin depths range from 500 to 2000 m in depth. Baritic sinters and nodules formed

from the venting of hydrothermal fluids have been discovered along basin bounding strike-slip faults (Revelle and Emery, 1951; Lonsdale, 1979).

STRATIFORM MINERALIZATION

Stratiform Pb-Zn-barite ores on the Jason property occur on the north limb (Main zone) and south limb (South zone) of a southeasterly plunging, tightly folded syncline known as the Jason syncline (Figs. 3.1, 3.2). Based on stratigraphic correlations and the match of metal ratios and mineralogical trends, the South and Main zones are interpreted to be parts of one stratiform body (Chap. 2). Steep, southeast-trending faults are parallel to the axial plane of the syncline and locally cut the Main zone. Younger north-trending high angle faults offset all other structures and the stratiform ores with small displacement.

The Jason stratiform Pb-Zn-barite deposit is characterized by its small tonnage, high Pb+Zn grade, high Ag content, strong textural and mineralogical zoning, high Pb/(Pb+Zn) ratio, high barite content and the active tectonic setting of its depositional environment. Reserves are estimated at 15.5 million tons averaging 7.1% Pb, 6.6% Zn and 2.3 oz/ton Ag (Bailes et al., 1984). Previous studies of the Jason deposits include Winn et al.(1981), Gardner (1983), Turner (1984), Gardner and Hutcheon (1985) and Bailes et al. (in press).

The stratiform ore occurs adjacent to the synsedimentary Jason fault (Chapter 2) and is interstratified with sedimentary breccias, organic-rich siliceous shale and thin-bedded siltstone turbidite (Fig. 3.2). There are two stacked stratiform bodies comprising the Jason deposit, referred to as the upper horizon and the lower horizon. The lower horizon is interbedded with a sequence of thin-bedded siltstone turbidites; the upper horizon is interbedded with siliceous shale and lesser sedimentary breccia units and siltstone turbidite. Both stratiform horizons are mineralogically and texturally zoned away from the Jason fault. A steeply dipping body of brecciated and mineralized rock adjacent to the Jason fault underlies the upper horizon and cuts the lower horizon. The proximal part (used here with reference to the distance from the Jason fault) of both the upper and the lower stratiform bodies is composed of beds of massive pyrite and massive to banded siderite-ankerite-galena cut by abundant veins. In the

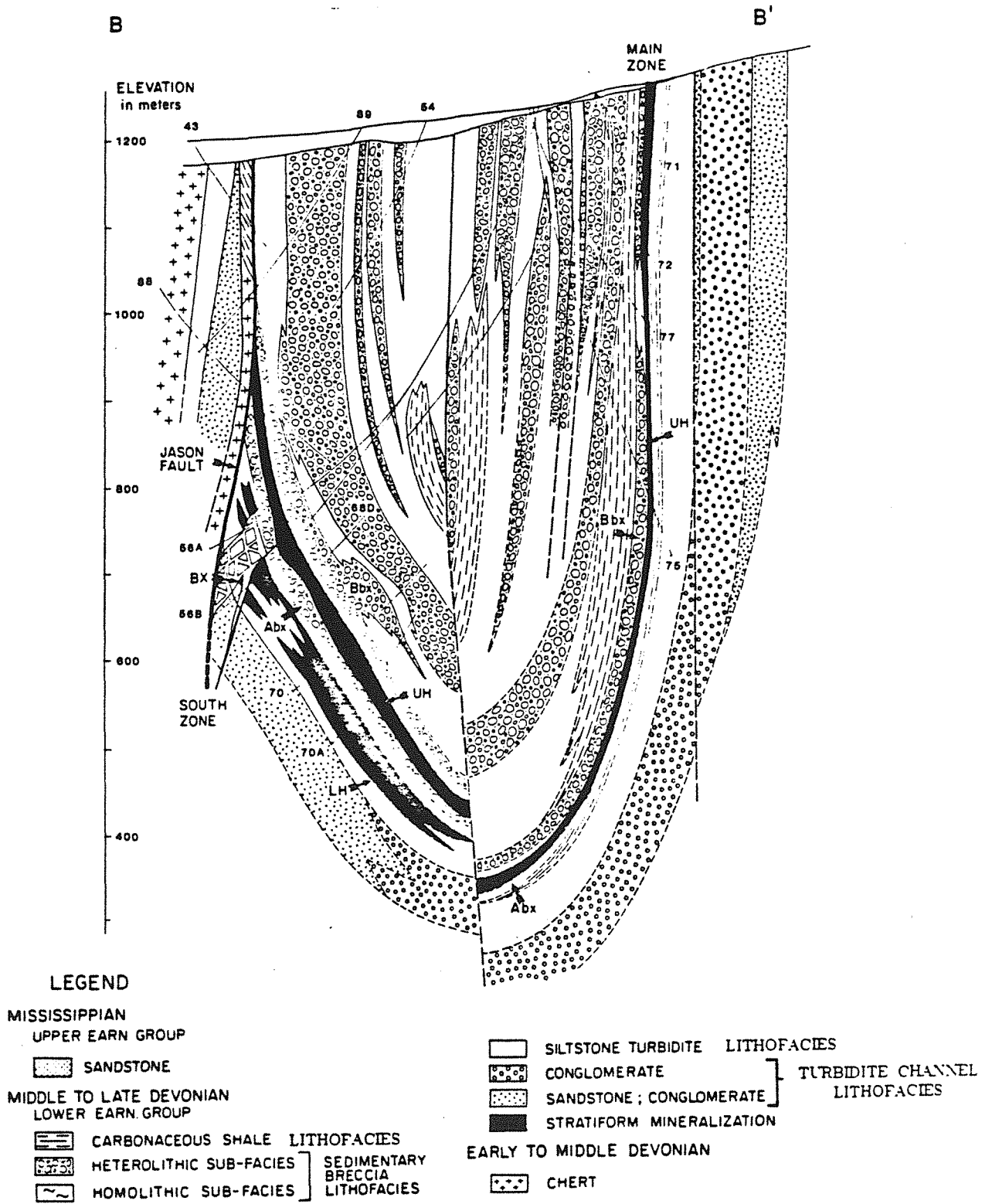


Figure 3.2 Geological cross-section B-B' of the Jason syncline (looking west). The upper horizon (UH), lower horizon (LH), breccia body (BX), A sedimentary breccia unit (Abx) and B sedimentary breccia unit (Bbx) and drill holes are indicated.

upper horizon, these beds also are interbedded with banded galena-pyrite and banded galena-sphalerite-pyrite. Distal to the synsedimentary fault, ore in both horizons is characterized by laminated barite-quartz-sphalerite-galena-pyrite and interbedded siliceous sediment. Siliceous sediment forms an envelope around the distal stratiform bodies.

The structure of stratiform bodies is generally planar. Locally strata are deformed into small-scale (1-2 m amplitudes) tight folds. A west-trending cleavage axial to the Jason syncline is developed in argillaceous strata and is defined by oriented clays and fine-grained muscovite. Where sulfide horizons are deformed into small scale folds a cleavage is defined by oriented growth of barite and sulfide minerals. Extension veins are abundant within siliceous beds within and adjacent to the stratiform bodies. Faults sub-parallel to bedding occur in the eastern portion of the Main Zone and have caused brecciation and displacement of the strata.

STRATAL TYPES IN STRATIFORM ORES

The term stratiform is used here to describe textures of discrete, sharply bounded, monominerallic or polyminerallic, concordant beds typically composed of fine-grained anhedral minerals between 0.005 and 0.05 mm in diameter. Disseminated mineral grains whose distribution is sharply defined by stratum contacts (ie. galena in sphalerite laminae) are included in the stratiform textural category. Minerals of non-stratiform distribution are generally coarser grained (0.1 to 1.5 mm) and occur as disseminated subhedral grains (eg. celsian, pyrite), discontinuous concordant lenses (e.g. quartz-celsian), discordant veinlets or nodules (e.g. quartz), and veins and breccias (e. g. ankerite in Jason fault and breccia body). The distinction between stratiform and non-stratiform textures is easily made in the distal parts of the stratiform bodies; however, it often is ambiguous in the massive proximal facies.

Terms for grain size are modified from the Wentworth scale (Wentworth, 1922): very fine-grained (<0.0039 mm), fine-grained (.0039 to 0.0625 mm), medium grained (0.0625 to 0.5 mm), coarse-grained (0.5 to 2.0 mm) and very coarse-grained (>2.0 mm). The terminology used to describe bed thickness here is modified after Ingram (1954): micro-laminated (<0.1

	LAMINAE/ BED THICKNESS	MINERAL ABUNDANCE (%) RANGE OF GRAIN SIZE (mm)											
		GM	SL	PY	PO	CP	QT	BA	SD	AK	JLL	RADS	CO
CARBONACEOUS QUARTZ- PYRITE	0.1 mm - 1 m	tr.	(3	3-30	--	--	50-80	--	--	--	1-4	0-1	3-20
		--	.005-.02	.003-1.0	--	--	<.005	--	--	--	.006-.00	--	<.001
QUARTZ- SPHALERITE	0.05 mm - 1 m	(3	5-50	tr.	--	--	50-95	--	--	--	--	0-1	--
		.005-1	.005-.06	.003-.1	--	--	.005-.01	--	--	--	--	--	--
SPHALERITE	0.05 mm - 2 mm	0-5	50-100	0-2	--	tr.	0-50	--	--	0-5	--	--	--
		.01-.1	.005-.1	.003-.2	--	--	.005-.01	--	--	.1-.6	--	--	--
SPHALERITE -SALENA	0.1 mm - 5 mm	5-80	20-80	1-5	--	tr.	0-10	tr.	--	0-10	--	--	--
		.01-.3	.01-.1	.01-1.0	--	--	.05-.5	--	--	.1-.6	--	--	--
SALENA	0.05 mm - 15 mm	80	0-20	1-5	--	--	tr.	--	--	.5	--	--	--
		.01-.1	.005-.1	.01-1.0	--	--	--	--	--	.1-.6	--	--	--
SALENA- PYRITE	0.1 mm - 10 cm	40-70	1-5	10-40	--	tr.	1-3	--	--	3-30	--	--	--
		.05-.4	.05-.2	.002-.5	--	.002-.02	.06-.6	--	--	.1-.6	--	--	--
PYRITE	4 cm - 4 m	0-10	tr.	70-100	--	--	0-3	--	--	0-30	--	--	--
		.005-.01	--	.005-.3	--	--	.005-.01	--	--	.01-.06	--	--	--
SIDERITE	1 mm - 50 cm	0-3	--	--	--	--	--	--	95-100	0-2	--	--	--
		.05-.4	--	--	--	--	--	--	.01-.5	.1-.5	--	--	--
ANKERITE	3 mm - 2 m	1-15	tr.	--	tr.	--	0-2	--	0-30	70-99	--	--	--
		.05-.4	--	--	--	--	.1-1.0	--	.05-.6	.03-.6	--	--	--
BARITE	1 mm - 10 mm	0-10	0-3	0-3	--	--	2-5	97-98	--	--	--	--	--
		.01-.10	.005-.1	.005-.2	--	--	.008-.01	.02-.2	--	--	--	--	--
Siltstone	1 mm - 3 cm	--	--	1-10	--	--	.80.	--	0-5	0-5	2-5	--	1-2
		--	--	.005-1.0	--	--	.005-.01	--	.01-.1	.02-.2	--	--	<.001

Table 3.1 Abundance and grain size of mineral constituents in strata types.

mm), very finely laminated (0.1 to 1 mm), finely laminated (<3 mm), thickly laminated (3 to 10 mm) and bedded (>10 mm).

Stratiform ore can be divided into commonly occurring and distinctive mineral assemblages referred to here as stratal types (Table 3.1). Stratiform facies, discussed later, are defined as commonly occurring associations of stratal types that comprise mappable portions of the stratiform horizons (Fig. 3.3).

Siltstone Strata

Thin siltstone beds, 1 to 3 cm thick, comprise about 40 % of the lower horizon and 5% of the upper horizon (Fig. 3.4, 3.5). They are T_{cde} , T_{de} or T_{ce} turbidites using the terminology of Bouma (1962). Silt-size quartz and chert grains comprise the beds, clays are a minor component. These siltstone beds differ from bedded siltstone beds overlying and underlying the stratiform horizons by their lighter color (light grey), absence of organic matter and more siliceous nature. Beyond the stratiform deposit, siltstone beds are dark grey to black in color and composed largely of quartz silt with minor floating quartz or chert sand grains, clay minerals and carbonaceous opaque matter. Siltstone turbidites interbedded with some siderite beds near the breccia body contain up to 20 % fine-grained massive barian muscovite (Fig. 3.5).

Carbonaceous Quartz-Pyrite Strata

Carbonaceous quartz-pyrite strata are characterized by the predominance of very fine-grained quartz and the presence of submicroscopic carbonaceous matter and disseminated pyrite (Table 1). These strata comprise a major portion of the distal fringe of the stratiform horizon. Carbonaceous quartz-pyrite beds can be divided petrographically into two types: finely laminated and massive. Finely laminated beds are clay poor and are composed of organic-rich and quartz-rich microlaminae (0.005 to 0.01mm) (Fig. 3.6) with up to 1% radiolaria. Pyrite commonly occurs as coarser subhedral grains 0.004 to 1.0 mm in diameter, or less commonly as 0.005 mm framboidal spheres, clusters and atolls concentrated

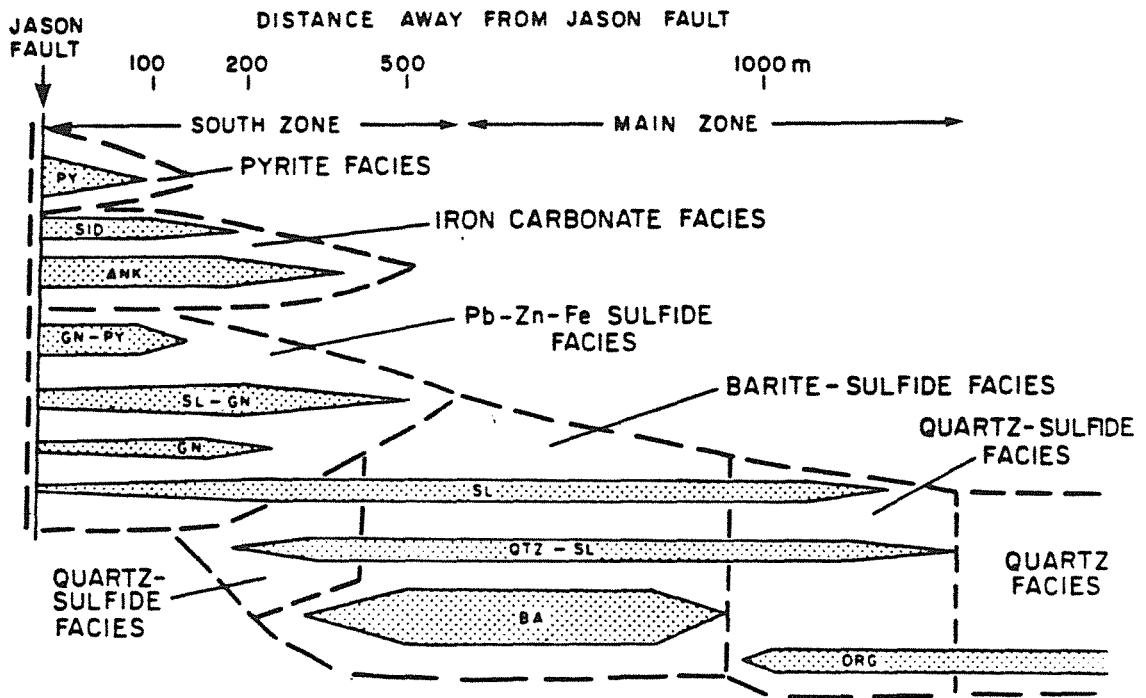


Figure 3.3 Spatial distribution of laminae types within the stratiform horizons with respect to distance from the Jason fault. Dotted lines include the laminae that comprise each stratiform facies.

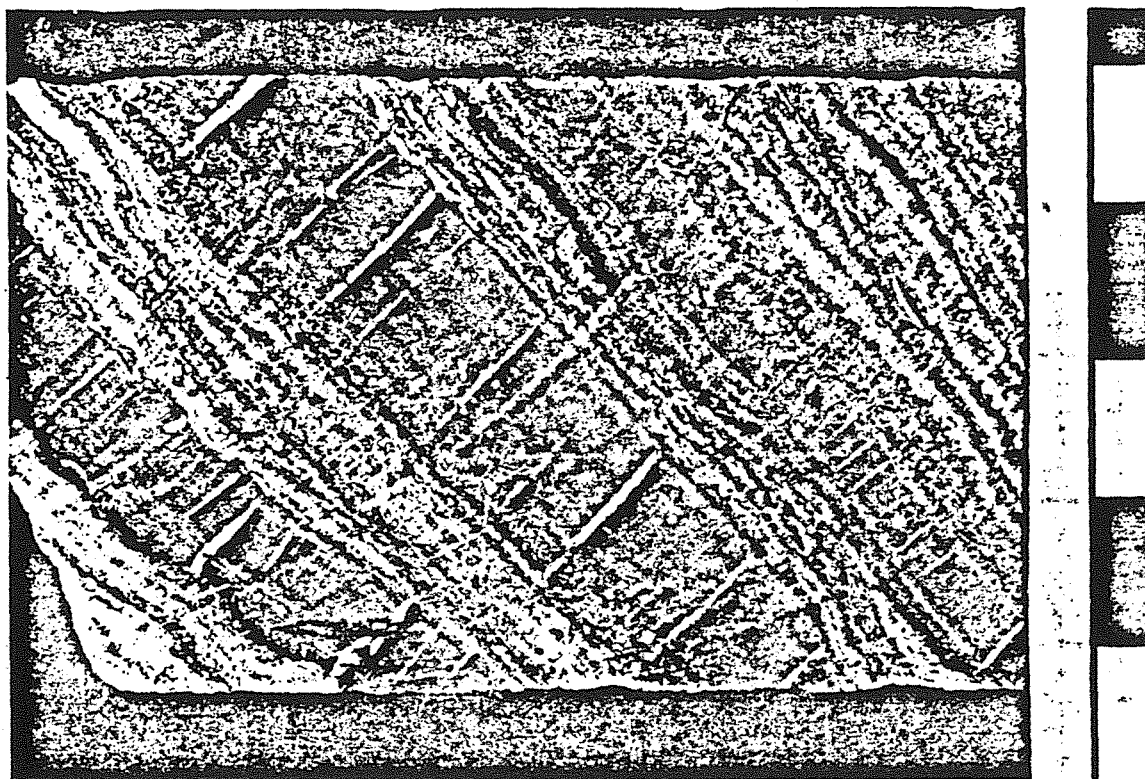


Figure 3.4 Barite facies: Laminae of barite (white) and sphalerite (yellowish brown) interbedded with silicified and bleached T_{bd} (Bouma, 1962) siltstone turbidites (medium olive brown) in the lower stratiform horizon. Stratigraphic tops to right. Disseminated ankerite grains occur in the siltstone beds. White quartz extension veinlets cut siltstone beds are related to deformation of Mesozoic age. Scale is in centimeters. Lower stratiform horizon, DDH 68A.



Figure 3.5 Iron carbonate facies: Siderite beds (brown) with galena (silver) and silicified, bleached and sericitized, thin-bedded siltstone turbidite beds (pale grey) cut by quartz-ankerite (blue) vein and ankerite breccia (blue). Blue colour due to staining with potassium ferricyanide. Field of view is 8 cm. Lower horizon, DDH 56B.

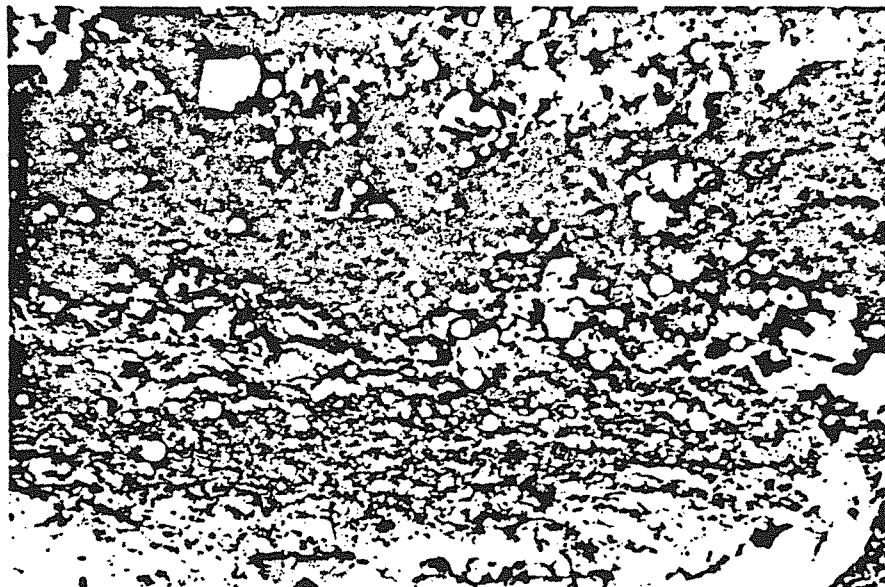


Figure 3.6 Quartz-sulfide facies: Very-finely laminated massive sphalerite laminae (grey) 0.2 mm thick underlying carbonaceous chert (dark grey). Framboidal pyrite (white) are abundant in both the sphalerite laminae and the organic-rich chert. Transmitted and reflected light. Field of view is 0.7 mm. Upper horizon, DDH 24.



Figure 3.7 Quartz-sulfide facies: Quartz-celsian band (QCB) within light colored quartz-sphalerite and sphalerite laminae (SL) are interbedded with carbonaceous quartz-pyrite (black) laminae of both the microlaminated subtype (thin laminae) and massive subtype (thick bed). Ripple-like laminae set have resulted from the compactional drape of laminae on irregularities of the quartz-celsian band. Field of view is 6 cm. Upper horizon, DDH 69.

along bedding planes (Fig. 3.7). Very fine-grained sphalerite may occur as disseminated anhedral grains where carbonaceous quartz-pyrite laminae are interbedded with sphalerite laminae. Sphalerite rims on pyrite framboids occur locally.

The massive type of carbonaceous quartz pyrite beds are commonly 1 to 5 cm thick but may exceed a meter in thickness. They lack internal lamination, are clay rich (2 to 4 % illite) and have 1 to 4 % floating silt-sized grains of quartz and chert (Fig. 3.7). The content of organic matter in these massive beds decreases towards the Jason fault resulting in an increasingly paler grey color. Irregular domains of black 'chert' within these grey 'chert' beds, as well as grey selvages along fractures that cut carbonaceous quartz-pyrite beds indicate that there was post-depositional destruction of the organic matter.

Compared to laterally equivalent shales beyond the stratiform bodies, carbonaceous quartz-pyrite beds are similar in texture and carbon content but differ by a greater abundance of quartz and pyrite.

Quartz-Sphalerite Strata

Quartz-sphalerite laminae are defined by greater than 95 % sphalerite + quartz, between 5 and 50 % sphalerite and an absence of carbonaceous matter and framboidal pyrite (Table 3.1). Pale-colored sphalerite occurs as fine-grained anhedral grains within a mosaic of very fine- to fine-grained quartz. Galena is a minor component, with darker colored sphalerite associated with increasing galena content. Pyrite content is very low. Radiolarian tests are common. Quartz-sphalerite strata are divided into two subtypes; laminated and massive thick-bedded.

Laminated quartz-sphalerite strata are 0.1 to 1.5 mm thick and show faint micro-laminae (0.01 to 0.1mm) that suggest that the bed is an amalgamation of very fine-scale depositional events (Fig. 3.8). The massive thick-bedded subtype of quartz-sphalerite beds are thick-bedded (2cm to 1m) and massive in nature lacking internal lamination. The common association of massive quartz-sphalerite beds with sedimentary breccia beds and the

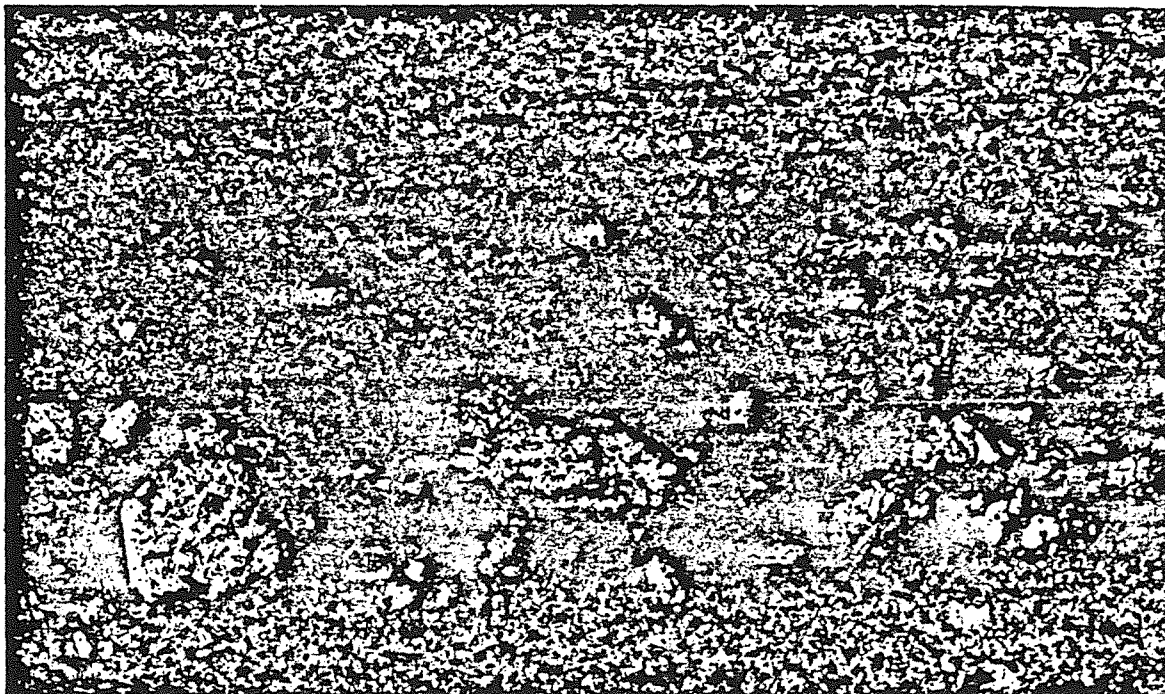


Figure 3.8 Quartz-sulfide facies: Quartz-sphalerite graded unit. Asymmetric upward thinning set of micro-laminae of sphalerite-rich (dark) and chert-rich (light) quartz-sphalerite. Stratigraphic tops up. Thick basal laminae with a sharp base is overlain by thin sphalerite-rich and chert-rich quartz-sphalerite laminae. The quartz-sphalerite graded unit is interbedded with quartz-rich beds with minor disseminated sphalerite. Anhedral to subhedral celsian (white) occur in both the quartz-sphalerite laminae and the quartz beds. Field of view is 3 mm. Non-polarized transmitted and reflected light. Upper horizon, DDH 68.



Figure 3.9 Clast of laminated chert-sphalerite within conglomeratic sandstone bed immediately overlying the upper stratiform horizon in the Main Zone area. The irregular boundary of the laminated chert-sphalerite clast suggests that the clast was only partly lithified when eroded. The sphalerite-rich laminae (sl) in this eroded clast are thicker and more diffuse than is typical of non-eroded laminae of similar composition. As the laminae orientation within the clast was at high angle to bedding during compaction, these laminae underwent less compaction and hence more closely reflect the character of the laminae at the time of sedimentation. Late quartz veins (white) cut both the clast and conglomeratic sandstone bed. Field of view is 7 cm. DDH 23-121.7m

similarity of the composition and texture of these beds to the matrix of bedded breccias rich in fragments of quartz-sphalerite beds suggests that these beds represented resedimented quartz-sphalerite strata.

Clasts of laminated quartz-sphalerite occur within conglomerate lens channels immediately overlying the upper stratiform horizon (Fig. 3.9); clasts of both massive and laminated quartz-sphalerite occur within beds of fine-grained massive quartz-sphalerite (Fig. 3.10) in distal portions of the upper horizon.

Sphalerite Strata

Sphalerite laminae are defined by greater than 50 % anhedral very fine- to fine-grained sphalerite (Fig. 3.11, 3.12, 3.13) and less than 5% galena; they commonly contain greater than 95% sphalerite. Quartz, and to a lesser extent, galena and ankerite are the most common accessory phases (Table 3.1). Quartz and ankerite commonly occur as grain aggregates; galena occurs as fine to medium-grained patches interstitial to anhedral sphalerite grains. Pyrite content typically is very low. Laminae typically are massive and where sphalerite is fine-grained contacts are commonly sharp and planar (Fig. 3.13); medium-grained sphalerite laminae have more irregular contacts that follow grain boundaries (Fig. 3.6). A compositional continuum exists between sphalerite laminae and quartz-sphalerite laminae, and sphalerite laminae and sphalerite-galena laminae (Fig. 3.11, 3.12). Sphalerite laminae are the most widespread stratal type within the stratiform horizons and occur interbedded with all other stratal types except siderite and pyrite beds (Figs. 3.11, 3.12, 3.13, 3.14, 3.15). Sphalerite laminae typically are 0.1 to 1.0 mm thick where interbedded with carbonaceous chert-pyrite-sphalerite, chert and barite laminae and up to 10 mm where interbedded with galena and galena-sphalerite laminae. There is a textural and mineralogical zoning of the sphalerite laminae within the stratiform bodies; away from the Jason fault laminae decrease in thickness, grain size, galena content, chalcopyrite content and darkness of color. The color of sphalerite laminae ranges systematically from dark red-brown near the Jason fault to

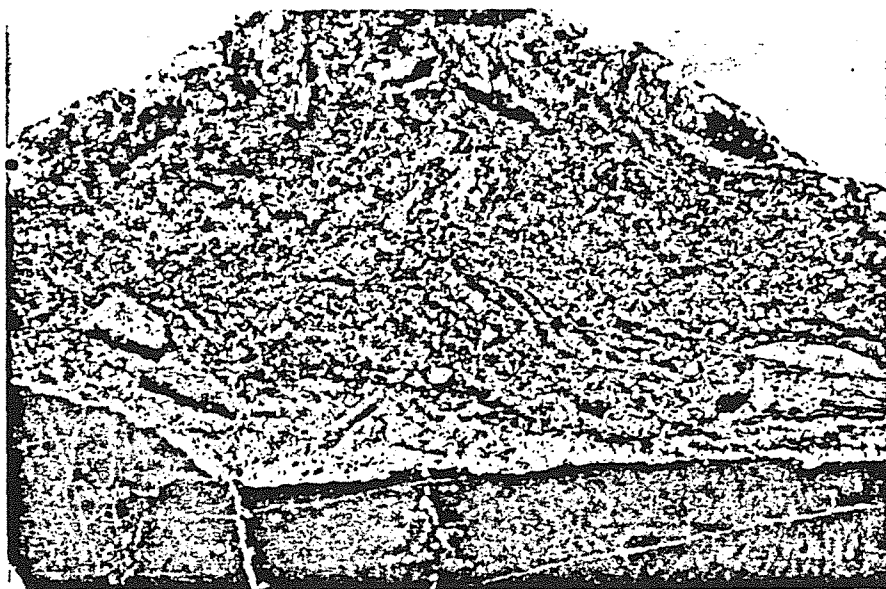


Figure 3.10 Sedimentary sulfide breccia: Sedimentary contact of sulfide-quartz breccia with underlying siliceous argillite. Clasts of quartz-sphalerite, sphalerite and carbonaceous quartz-pyrite occur in quartz-sphalerite matrix. Thin quartz veinlets (white) cut the siliceous argillite.

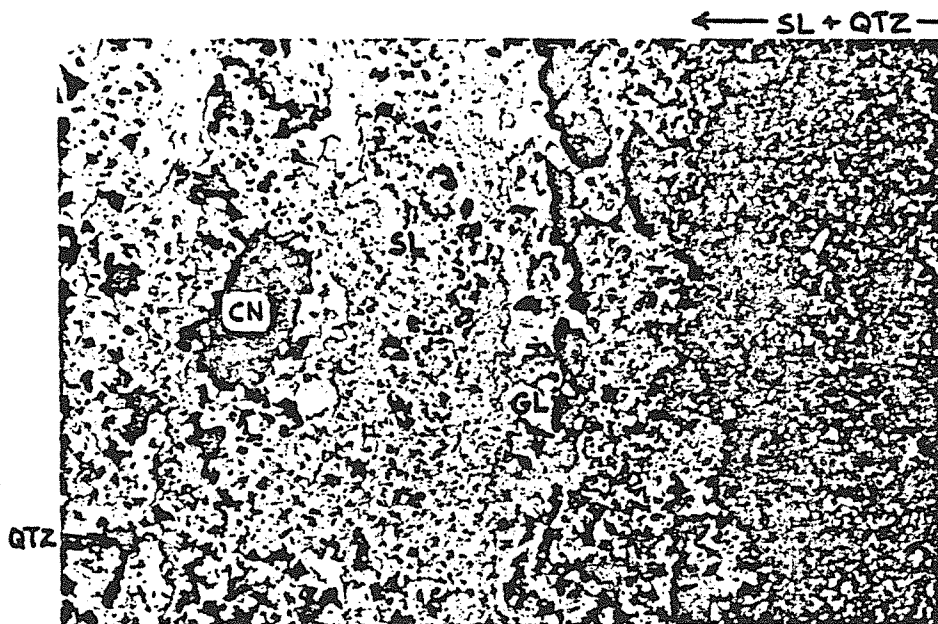


Figure 3.11 Pb-Zn-Fe sulfide facies: Contact between a bed (left) containing laminae 0.4 mm thick of sphalerite (light grey) and quartz (dark grey) and sphalerite-galena (white)-quartz laminae (0.2 mm thick), and a quartz-sphalerite bed (right). Subhedral celsian (CN) occur in quartz-rich sphalerite laminae. Field of view is 3 mm. Cross polarized transmitted and reflected light. Upper horizon, DDH 63B.

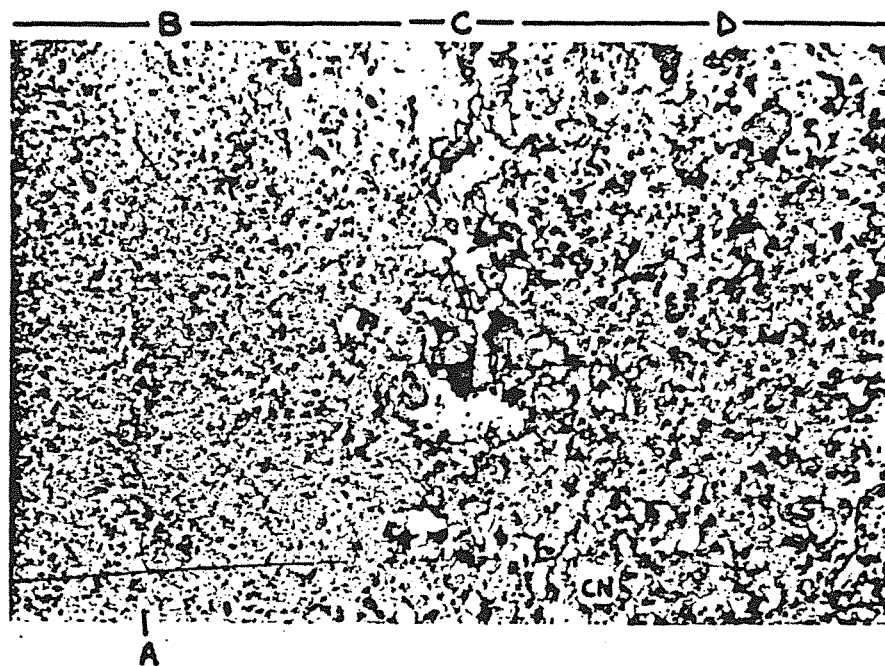


Figure 3.12 Pb-Zn-Fe sulfide facies: Laminae of A) fine-grained (0.01 mm) sphalerite-galena; within B) fine-grained sphalerite-quartz; C) medium to coarse-grained galena-rich sphalerite-galena-quartz; and D) sphalerite-rich sphalerite-galena-quartz laminae. Coarse-grained subhedral celsian (CN) is partly altered to kaolinite. Field of view is 3mm. Cross polarized transmitted and reflected light. Upper horizon, DDH 63B.



Figure 3.13 Pb-Zn-Fe sulfide facies: Sharp bedding contact between a massive sphalerite-quartz (right) bed and underlying galena-pyrite-quartz (left) bed. Within the galena-pyrite bed, pyrite (py) occurs as subhedral to euhedral grains or amalgamated clusters of grains within a massive galena (gl) matrix. Quartz occurs as coarse-grained pods. Very fine grained massive sphalerite forms the overlying bed. Field of view is 3.5 mm. Reflected light. B82-124

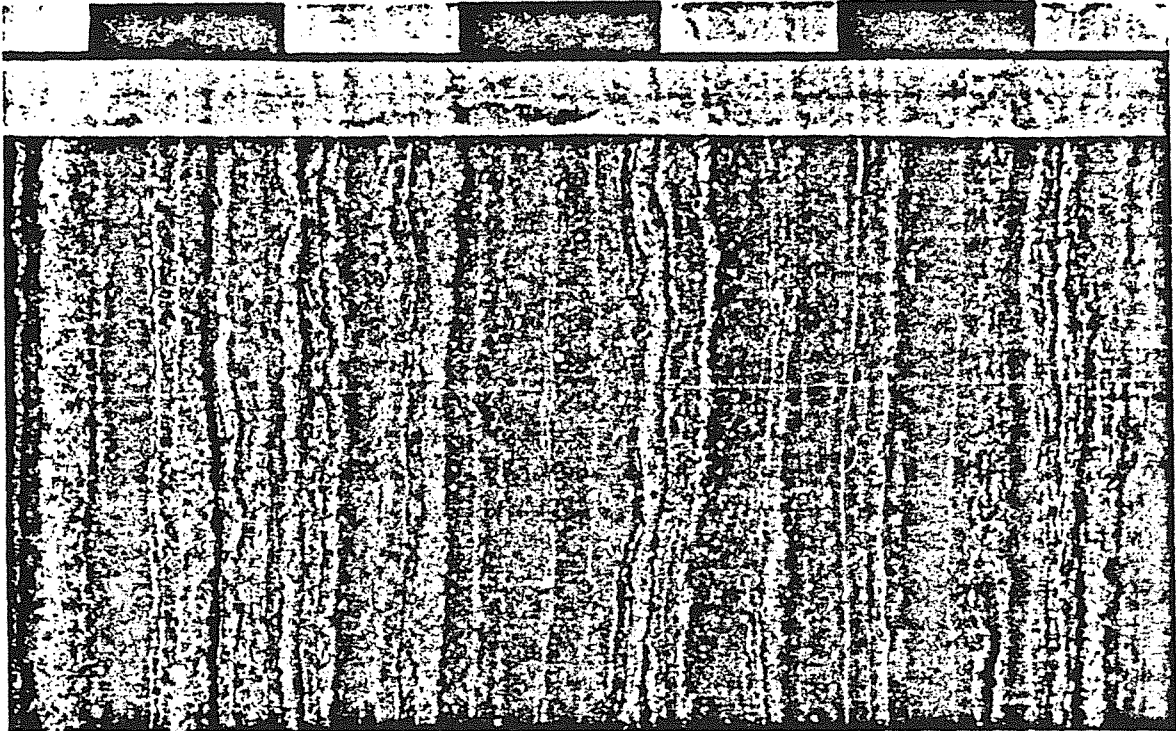


Figure 3.14 Barite facies: Finely laminated character of the distal stratiform mineralization (barite facies). Interbedded massive carbonaceous-quartz-pyrite beds (dark grey) with barite laminae (light grey), and sphalerite laminae (buff). Barium carbonates are stained red using Alizaran Red S (brown in photo). Disseminated pyrite (light yellow) is concentrated within carbonaceous-quartz-pyrite beds. Scale in centimeters.

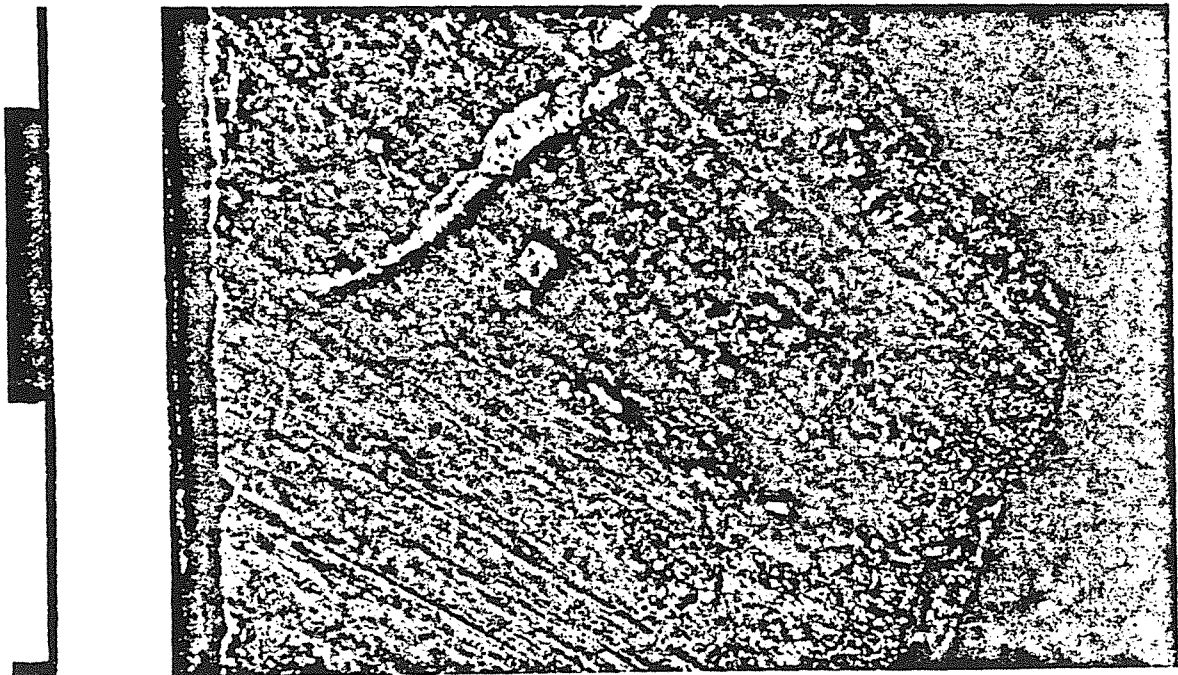


Figure 3.15 Iron carbonate and Pb-Zn-Fe sulfide facies: Very sharp contact between very finely laminated quartz-sphalerite (brown) and underlying banded ankerite stained with potassium ferricyanide (blue). Sphalerite bands (brown) within the ankerite are stylolitic surfaces parallel to the Mesozoic cleavage. Quartz vein (white) cuts carbonate. Scale is in centimeters. Upper horizon, DDH 86A.

pink and yellow, to buff and white in the most distal parts of the deposit.

Sphalerite-Galena Strata

Sphalerite-galena laminae are polyminerallic laminae defined by greater than 60% sphalerite+galena and greater than 5% galena; they are intermediate in composition between sphalerite laminae and galena laminae (Table 3.1). Medium-grained anhedral brown to dark red brown sphalerite and medium-grained galena occur in subequal proportions (Fig. 3.11, 3.12). In sphalerite-rich beds, galena occurs within the interstices of anhedral sphalerite grains; within galena-rich layers the sphalerite occurs as scattered anhedral grains within a coarse-grained matrix of galena. Medium to coarse-grained anhedral ankerite and quartz grains may comprise 5 to 20 % of the bed. Disseminated subhedral to euhedral pyrite grains 0.1 to 1 mm in diameter comprise less than 5 percent of the laminae. Galena-rich laminae tend to be quartz-poor, whereas sphalerite-rich laminae are more quartz-rich (Fig. 3.11). Sphalerite-galena strata are typically associated with sphalerite, galena and galena-pyrite laminae (Fig. 3.16) and range in thickness to 20 mm. Sphalerite-rich and galena-rich microlaminae comprise some laminae. Rounded clasts of massive fine-grained pyrite or growth banded pyrite up to 1 cm in diameter occur in some thicker, massive beds (Fig. 3.16). Clasts of massive sphalerite-galena beds occur intercalated with the upper horizon and within sedimentary breccia beds overlying the upper stratiform horizon (Fig. 3.17).

Galena Strata

Galena laminae are composed of greater than 80 % galena, with sphalerite more abundant than pyrite. The abundance of sphalerite distinguishes this stratal type from galena-pyrite laminae. Ankerite is a common accessory mineral, quartz is very minor (Table 3.1). Galena laminae rarely exceed 1 mm in thickness and are much less widespread and abundant than the sphalerite laminae with which they commonly are interbedded. Galena laminae typically are discontinuous and occur as irregular elongate patches along bedding (Fig. 3.11, 3.12).



Figure 3.16 Pb-Zn-Fe sulfide facies: Massive bed composed of laminae of sphalerite-galena (dark grey) and galena (light grey) containing rounded and broken clast of fine grained pyrite (PY). Pods of coarse-grained quartz (white) of diagenetic origin occur within bed. Field of view is 4 cm. Upper horizon, DDH 88.

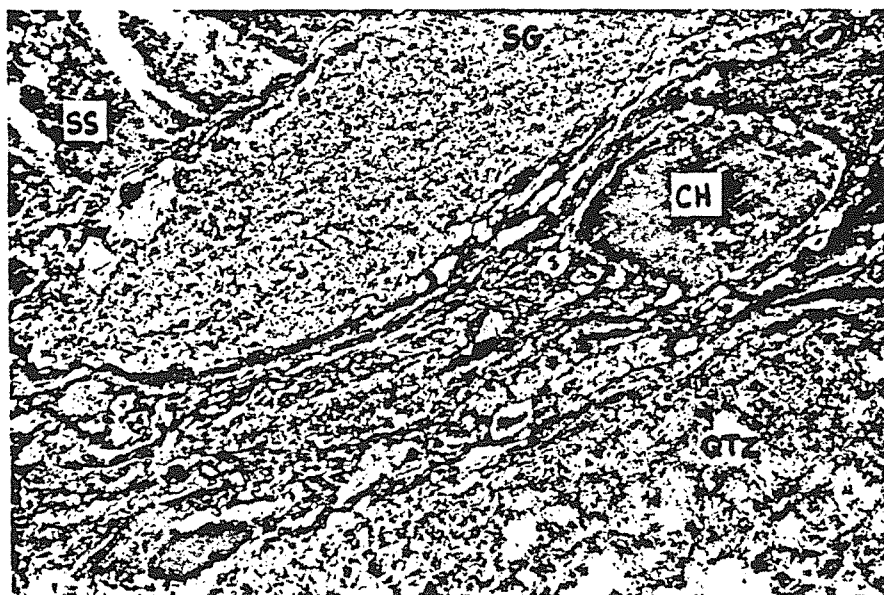


Figure 3.17 Pb-Zn-Fe sulfide facies: Sedimentary breccia with clasts of sphalerite-galena bed (SG), coarse-grained quartz with interstitial galena (QTZ), quartz veined sandstone (SS) and chert (CH) in sphalerite-rich argillaceous matrix. Field of view is 7 cm. Upper horizon, DDH 51A.

Galena-Pyrite Strata

Galena-pyrite laminae occur exclusively in the upper stratiform horizon near to the Jason Fault (Fig. 3.3). These laminae, ranging in thickness from 0.1 to 10 cm, are characterized by subequal amounts of medium- to coarse-grained galena and pyrite and less than 5 percent sphalerite (Table 3.1). Ankerite and minor quartz are accessory phases. Galena occurs as massive medium-grained aggregates. Pyrite occurs in two textural styles within the galena matrix: very fine-grained aggregates and medium-grained subhedral disseminations. Such very fine-grained pyrite aggregates may be massive or growth-banded and comprise 3 to 10 percent of the beds. Massive fine-grained aggregates are commonly rounded in shape, or highly irregular and surrounded by an archipelago of very fine-grained pyrite islands (Fig. 3.18). Very fine-grained rounded aggregates up to 1 mm in diameter commonly display fine scale planar or concentric growth banding of pyrite and intergrown pyrite-galena (Fig. 3.19, 3.20). Truncated growth bands occur at the margin of some pyrite aggregates suggesting that the aggregates are detrital clasts (Fig. 3.19). Pyrite also occurs as disseminated subhedral to euhedral grains to 0.5 mm which may comprise up to 30 percent of the galena-pyrite beds (Fig. 3.19).

Medium- to coarse-grained ankerite or quartz form irregular pods up to 5 mm in diameter within the galena matrix (Fig. 3.13). These pods locally cut bed contacts or colliform pyrite-galena (Fig. 20) indicating that they grew insitu within the galena-pyrite bed. Euhedral pyrite grains locally cross the margins of ankerite and quartz pods (Fig. 3.20).

Pyrite Strata

Pyrite beds are thick-bedded and composed of greater than 80% pyrite content. Galena and ankerite occur as minor phases. Pyrite beds occur immediately adjacent to the Jason fault (Fig. 3.3). Two pyrite bed subtypes exist: fine-grained growth banded pyrite and medium-grained massive pyrite.

(1) Growth banded pyrite: very fine-grained pyrite and lessor galena in textures similar to

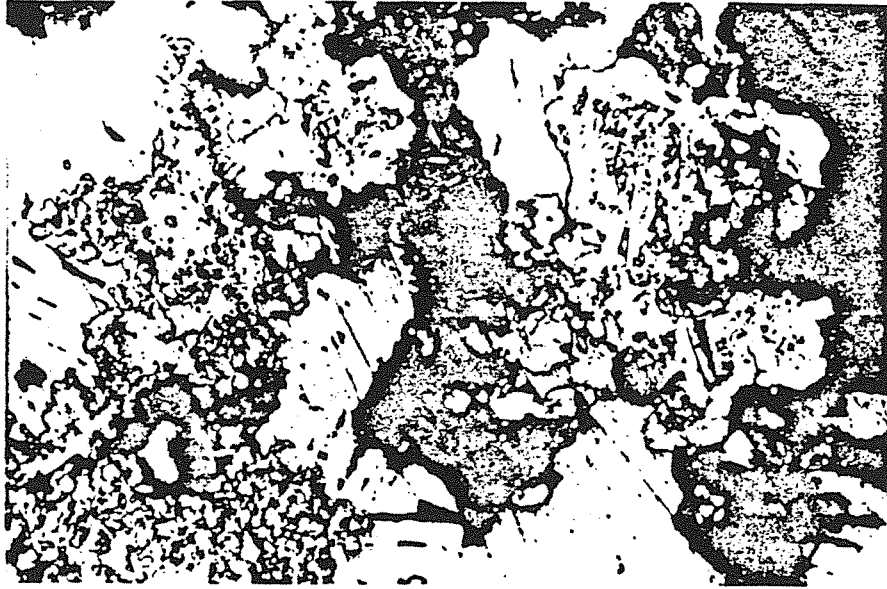


Figure 3.18 Pb-Zn-Fe sulfide facies: Galena-pyrite (+ sphalerite) bed. Archipelago of fine pyrite (white) grains surrounding embayed pyrite grain within matrix of galena (gray) and sphalerite (dark gray) suggesting replacement of the pyrite by galena and sphalerite. Sphalerite and quartz (black) occur as anhedral grains within galena matrix. Reflected light; field of view is 0.7 mm. Upper horizon, DDH 88.

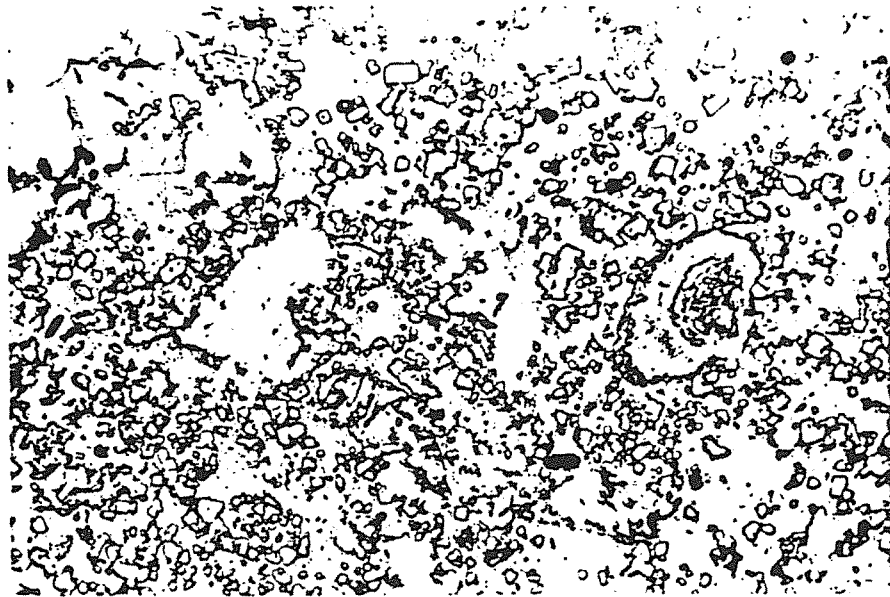


Figure 3.19 Pb-Zn-Fe sulfide facies: Galena-pyrite bed. Clot (clast?) of colliform banded pyrite-galena, irregular clots of quartz and ankerite (white), and disseminated anhedral and subhedral pyrite (light grey) within a galena matrix (medium grey). Reflected light. Field of view is 3.5 mm. Upper horizon, DDH 56B.



Figure 3.20 Pb-Zn-Fe sulfide facies: Galena-pyrite bed paragenesis. Colliform pyrite (white) in matrix of galena (medium grey) is replaced by ankerite (dark grey); late pyrite (white) replaces both colliform pyrite and ankerite. Field of view is 0.7 mm; reflected light. Base of upper horizon, DDH 56B.

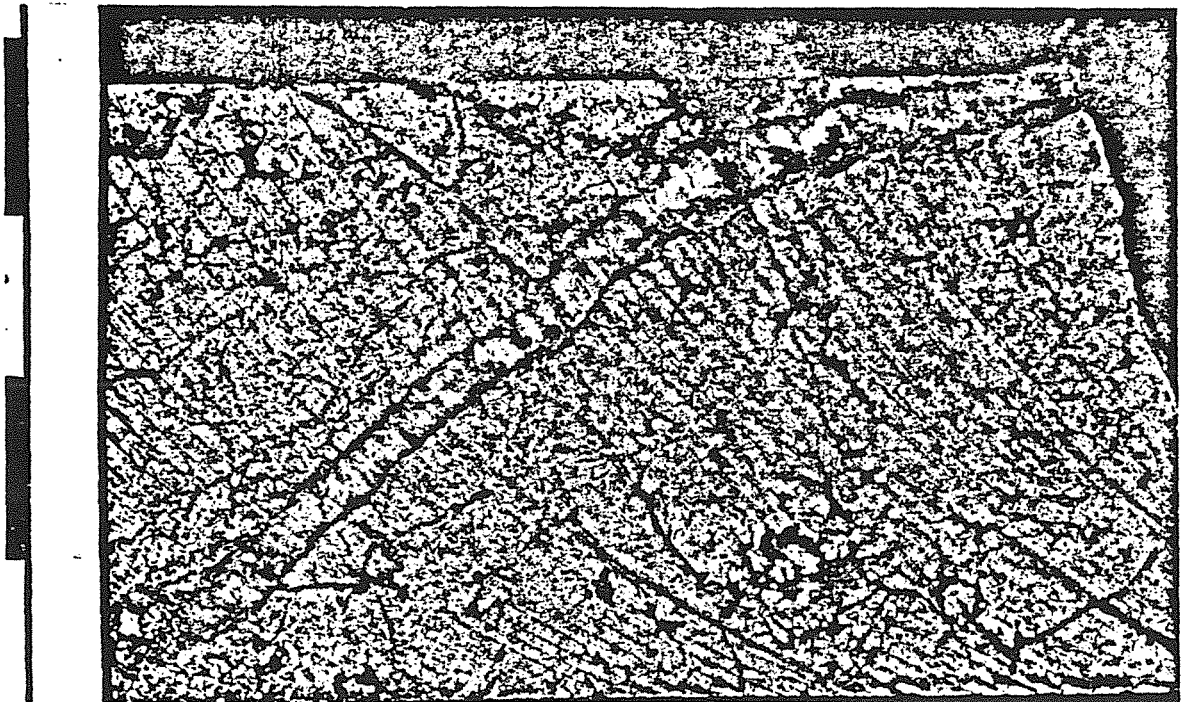


Figure 3.21 Pyrite facies: Massive, medium-grained pyrite bed (buff colored) cut by irregular veinlets of sphalerite (dark brown; see Fig. 3.41) and quartz-chalcopyrite vein. Scale in centimeters. Upper horizon, DDH 88.

those in galena-pyrite beds form undulatory growth bands or colliform spherulites aligned in irregular layers subparallel to bedding. Individual bands range from 0.01 to 0.05 mm in thickness and are composed of either very fine-grained pyrite or finely intergrown pyrite and galena. Growth banded aggregates form a bed up to a meter thick at the base of the stratiform horizon.

(2) Massive pyrite: Massive, monominerallic beds of medium-grained pyrite range up to 0.8 m in thickness. In the upper horizon, massive beds 30 to 80 cm thick cut by abundant quartz-sulfide veinlets (Fig. 3.21) are interbedded along sharp contacts with sedimentary breccia, galena-pyrite and ankerite beds. Massive pyrite beds in the lower horizon range in thickness from mm scale to 30 cm; contacts with interbedded siltstone beds are generally concordant but near the breccia body discordant contacts are common (Fig. 3.22). Locally, chert pebbles float within these massive pyrite beds (Fig. 3.23).

Barite Strata

Barite laminae are commonly composed of greater than 90% fine to medium-grained equigranular barite. Minor disseminated quartz, galena, pyrite and sphalerite occur as accessory minerals. Barite laminae range in thickness from 1 to 10 mm and typically have sharp contacts with adjacent laminae (Figs. 3.4, 3.24). Barite laminae are the most abundant stratal type in the deposit and occur throughout much of the distal part of the stratiform horizons (Fig. 3.3).

Barite laminae are interbedded with sphalerite, quartz-sphalerite, quartz and galena-sphalerite laminae in both the upper and lower stratiform horizons (Fig. 3.4). Near the Jason fault, barite laminae tend to be coarse-grained, thicker and contain more sulfide (Fig. 3.25). In such galena and sphalerite-rich strata, sets of sphalerite-galena laminae are successively overlain by sphalerite-galena-barite laminae and barite laminae forming asymmetric sulfide-sulfate cycles (Fig. 3.26). The ratio of galena to sphalerite within barite laminae is commonly high.



Figure 3.22 Pyrite facies: Generally concordant contacts of pyrite laminae (light gray) with interbedded silicified and bleached siltstone beds (dark grey) adjacent to the breccia body. Discordant pods and veinlets of pyrite are interpreted to represent post-depositional mobilization of pyrite due to hydrothermal fluid infiltration in the vent complex area. Scale in centimeters. Lower stratiform horizon, DDH 56B.



Figure 3.23 Pyrite facies: Angular chert fragments floating within a massive pyrite bed. Field of view is 8 cm. Lower horizon, DDH 56B.

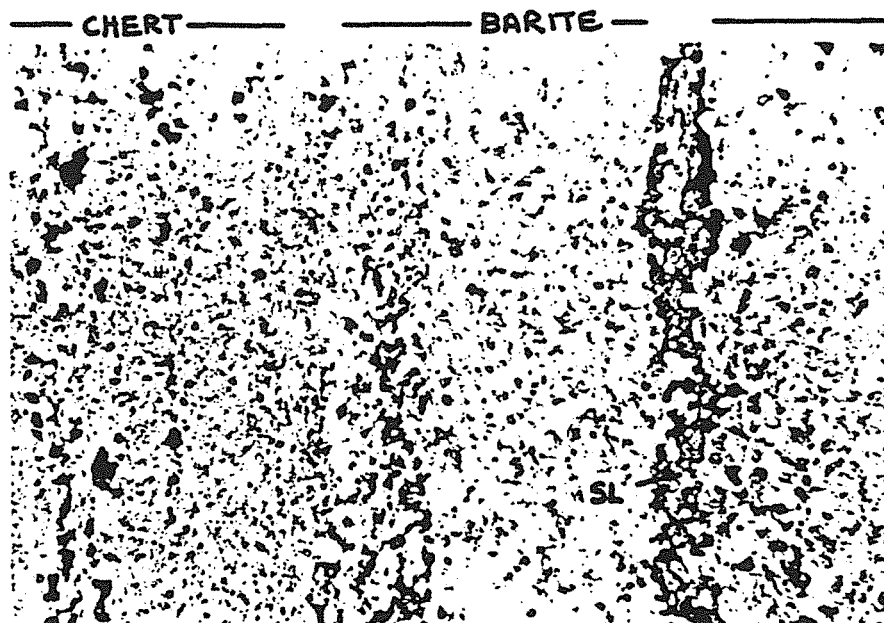


Figure 3.24 Barite-sulfide facies: Contact between chert bed (light grey, on left) and barite bed (white, on right). Thin sphalerite-rich bands (SL) occur in both the barite bed and chert beds. Disseminated pyrite (black) occurs preferentially with the sphalerite-rich laminae in the chert bed. Plane transmitted light. Field of view is 3.5 mm. Lower horizon, DDH 68A.

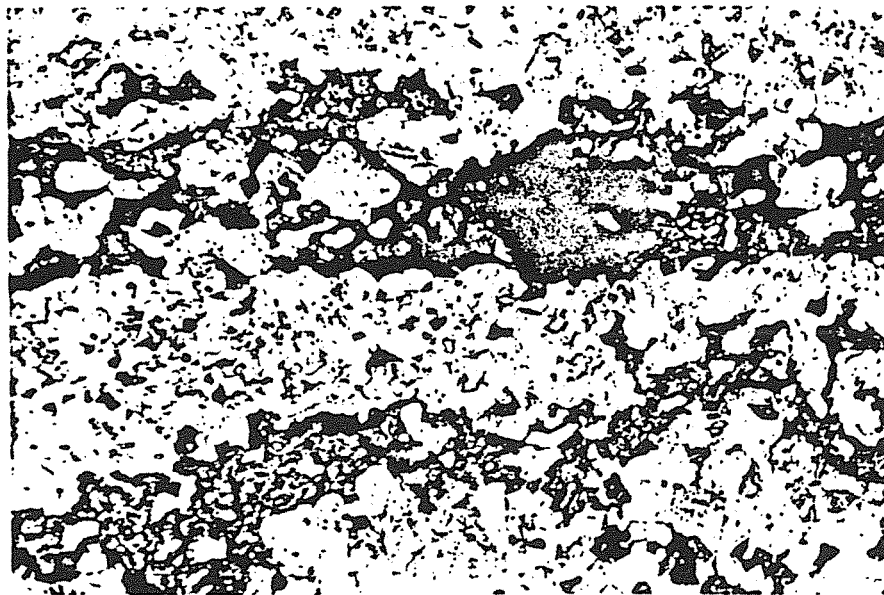


Figure 3.25 Barite facies: Barite-rich sphalerite-galena laminae interbedded with barite (+ quartz) laminae. Barite (grey), quartz (white), sphalerite (dark grey), galena (black). Near stratigraphic contact of Pb-Zn-Fe sulfide facies with barite facies. Field of view is 3.5 mm. Transmitted light. Upper horizon, DDH 68D.

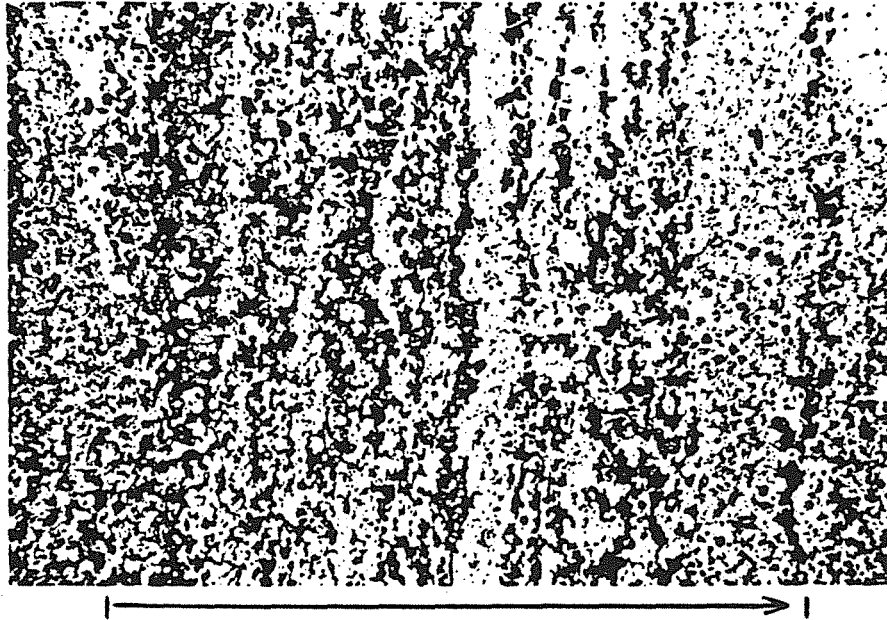


Figure 3.26 Transition zone from Pb-Zn-Fe sulfide facies to barite-sulfide facies: Sphalerite-galena laminae is overlain successively by sphalerite-galena rich barite laminae and by barite laminae. Stratigraphic tops to right. This succession (indicated by extent of arrow) represents cyclic deposition of sulfide and barite. Sphalerite (grey), galena (black), and barite (white). Field of view is 15 mm; transmitted light. Upper horizon, DDH 68D.

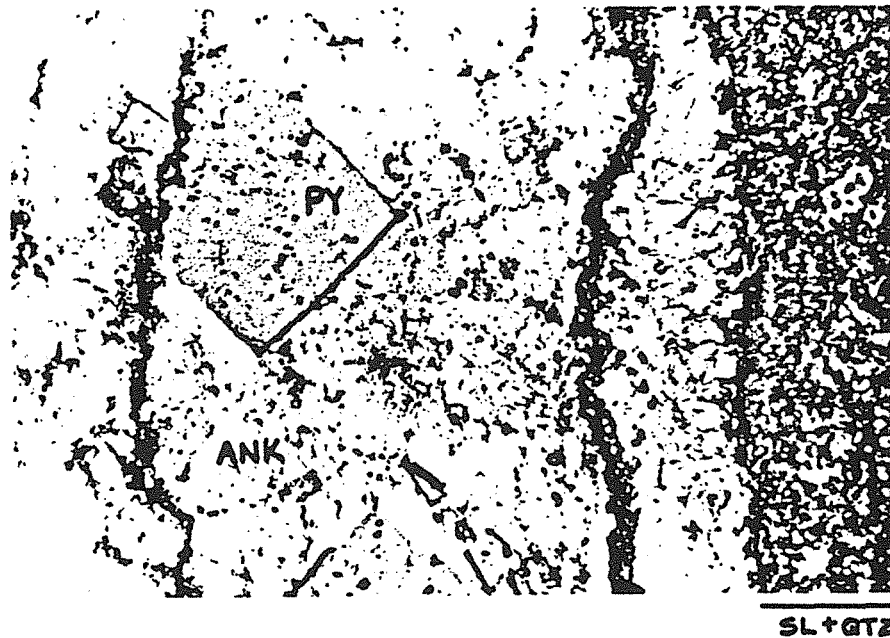


Figure 3.27 Iron carbonate facies: Sharp contact between banded ankerite beds (ANK) and bed of sphalerite and quartz bed (SL + QTZ). The sphalerite-rich bands within the ankerite are sulfide-rich stylolitic surfaces; note the truncation of the pyrite euhedra along the stylolite surface. Field of view is 3.5 mm. Plane transmitted and reflected light. Upper horizon, DDH 86A.

Siderite Strata

Siderite beds commonly consist of fine- to coarse-grained siderite (Table 3.1) and range in thickness from 1 to 50 cm. However, medium-grained galena intergrown with siderite locally may comprise up to 15 % of the beds. Siderite beds occur only in the lower horizon near the Jason fault (Fig.3.3) interbedded with silicified and bleached siltstone beds and sericitized argillite beds (Fig. 3.5). Bedding contacts of siderite with interbedded siltstone are sharp though disseminated euhedra of siderite commonly occur within adjacent siltstone beds. Near the breccia body, siderite beds are cut by irregular veins and disseminated grains of pyrrhotite; associated with such areas of pyrrhotite replacement, siderite aggregates replace adjacent siltstone beds.

Ankerite Strata

Ankerite beds are composed of greater than 60 percent medium to coarse-grained ankerite with lessor galena, siderite, pyrrhotite, pyrite and sphalerite. Ankerite beds occur in both the upper and lower horizons adjacent to the Jason fault (Fig. 3.3). There are two subtypes: ankerite-rich beds and ankerite-galena beds. The latter commonly contain 5 to 20 % galena interstitial to anhedral ankerite grains. Ankerite-rich beds typically contain minor galena and pyrrhotite, range in thickness from millimeter to meter scale and are most thick-bedded near the Jason Fault. Further from the Jason Fault ankerite beds are interbedded with other laminated mineralization and range from 3 to 10 mm thick (Fig. 3.15). Contacts of thick-bedded ankerite beds with other strata are typically sharp (Fig. 3.15, 3.27) though ankerite may replace quartz, barite and sphalerite where ankerite beds are interbedded with quartz-sphalerite, quartz, and barite laminae (Fig. 4a).

SUMMARY OF MINERAL TEXTURES IN STRATA TYPES

Distal, Laminated Horizons

Strata in the distal laminated portion of the stratiform horizons are characterized by aggregates of anhedral, subequant grains. Barite occurs as xenomorphic granular aggregates

similar to foam textures described by Stanton (1972). Sphalerite and quartz in sphalerite-quartz aggregates are also mosaics of anhedral, subequant grains with planar grain contacts. Where sphalerite is the minor phase in sphalerite galena aggregates, it forms rounded grains with high dihedral angles within galena aggregates, whereas minor galena in sphalerite dominant aggregates occurs as interstitial, cusped patches. The idiomorphic texture of pyrite is distinct among the sulfides; such grains locally embody relicts of pyrite framboids and suggest diagenetic growth.

Locally, the stratiform horizon is tightly folded and insoluble carbonaceous matter and sulfides are concentrated on bedding parallel stylolitic surfaces. In such areas, barite is recrystallized into slightly elongate, grains parallel to cleavage and pyrite grains are microfractured.

Proximal, Thick-Bedded Horizons

Mineral textures in the proximal stratiform bodies are more diverse than those in distal areas. Grain size is typically coarser. Based on descriptions given above, a complex array of replacement reactions occur within strata and include the replacement of carbonate by carbonate (ankerite after siderite), the replacement of carbonate by sulfide (pyrrhotite and galena after siderite and ankerite) and the replacement of sulfide by sulfide (chalcopyrite after iron-rich sphalerite, galena and sphalerite after early pyrite, late pyrite after pyrrhotite). Chalcopyrite occurs as very fine-grained rounded disseminations within iron-rich sphalerite grains.

NON-STRATIFORM TEXTURES IN STRATIFORM HORIZONS

Distal Horizons

Non-stratiform textures within the distal laminated portions of the stratiform horizons include disseminated grains, irregular aggregates of grains, conformable lenses and bands, and discordant veinlets (Fig. 3.28).

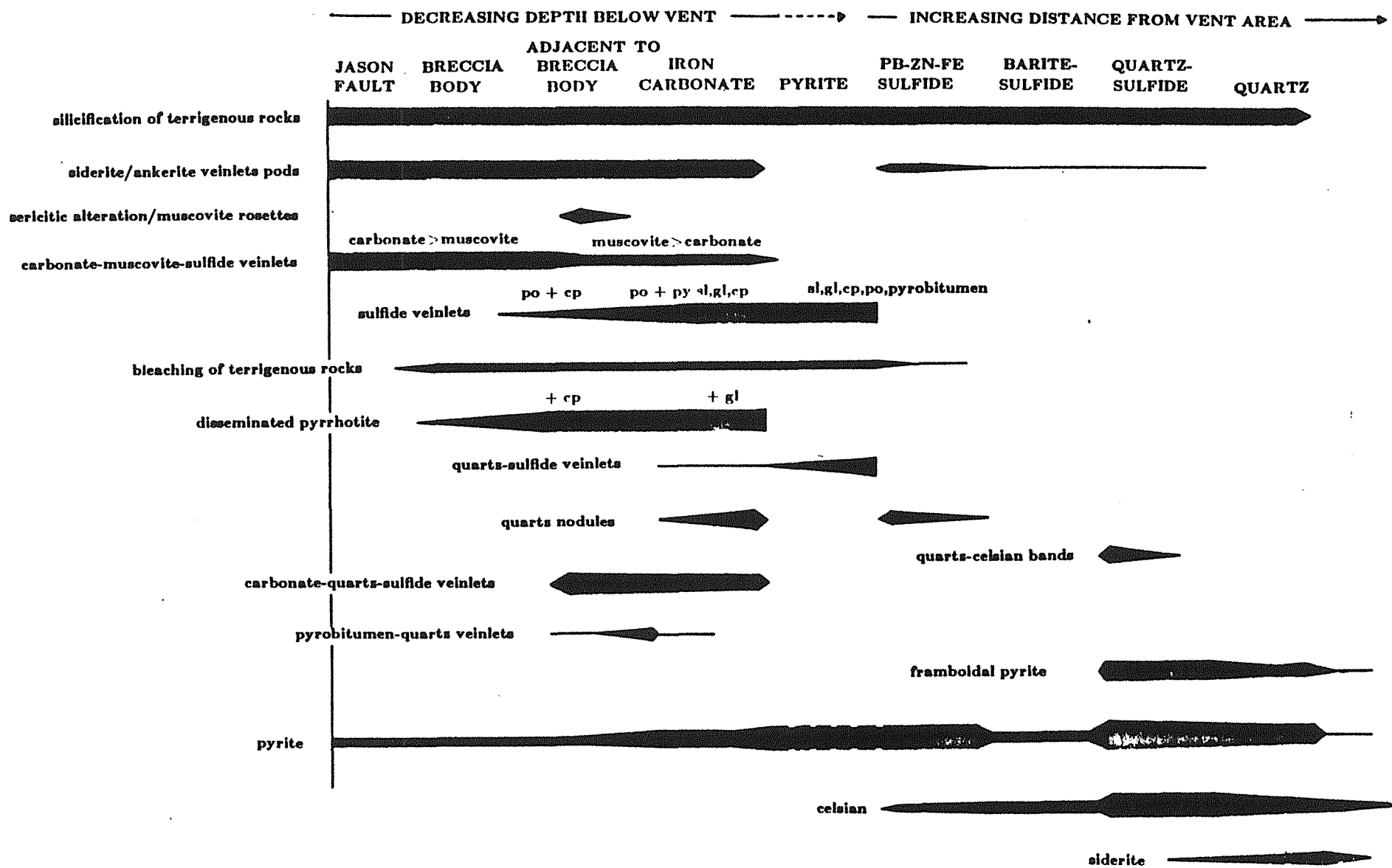


Figure 3.28 Schematic distribution of discordant and non-stratiform mineral assemblages associated with the stratiform ores. Changes in thickness of bars indicates changes in the abundance of the mineral assemblages.

Disseminated and Banded Celsian/Hyalophane

Medium to coarse-grained euhedral to anhedral grains of barian feldspars are widespread within all lamina/bed types except pyrite and siderite beds (Figs. 3.8, 3.11, 3.29) and are most abundant on the periphery of the barite facies (see below)(Fig 3.28). Where barian feldspars exceed 20 % of the rock, they commonly form along bedding and coalesce to form irregular, discontinuous bands with quartz (Fig. 3.30). Feldspar compositions range from celsian ($BaAlSi_3O_8$) to hyalophane ($(K,Ba)AlSi_3O_8$). The Ba/K ratio of the feldspar tends to reflect the host lithology; celsian is common within strata that include barite laminae; hyalophane dominates within clay-rich strata at the periphery of the stratiform horizons. Barian feldspars also occur within sedimentary breccias, siltstone and shale above and below the stratiform horizons. The concentration of barium within sedimentary breccias and siltstone overlying the upper horizon where barian feldspars are the dominant barium phase shows a logarithmic decrease for 60 m above the upper stratiform horizon (Bailes et al., in press). Barian feldspars commonly are replaced by minor barian carbonates along cleavage (Fig. 3.29); these carbonates have been identified as witherite, norsethite and barytocalcite by Gardner (1983, 1985). Partial or complete alteration of barian feldspars to kaolinite is widespread and is best developed adjacent to post-Devonian faults that cut the stratiform bodies, suggesting kaolinite may be related to supergene alteration.

Quartz-Celsian Bands

Medium- to coarse-grained anhedral quartz and subhedral celsian form concordant but discontinuous bands up to 8mm thick within sequences of siliceous shales and carbonaceous quartz-pyrite beds at the base and top to the stratiform body. Closely spaced sets of bands 1 to 5 cm thick commonly are associated with disseminated medium-grained sphalerite (Fig. 3.30). Shale beds display compactional drape over the irregular surface of quartz-celsian bands (Fig. 3.7) and the bands locally are truncated by erosional surfaces near the Jason fault (Fig. 3.31).

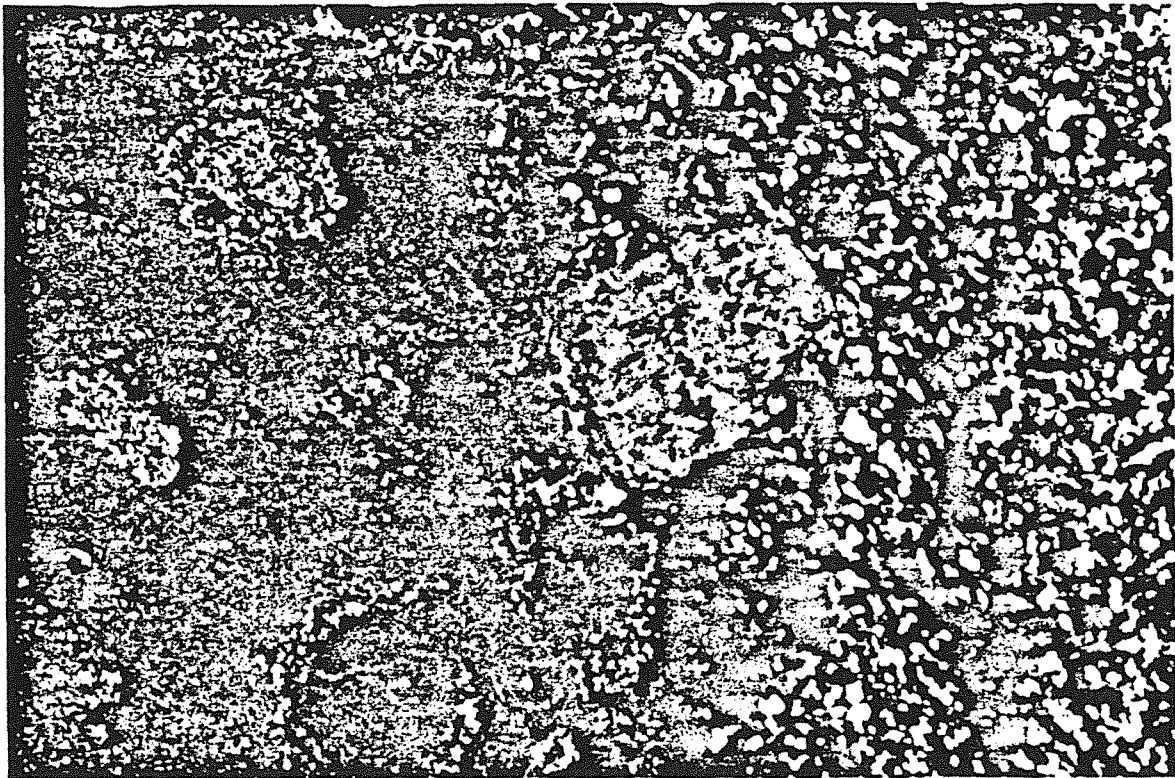


Figure 3.29 Barite facies: Celsian grain (c) at contact between laminae of fine-grained equigranular barite (b) and a silicified siltstone bed (s). Medium-grained subhedral grains of ankerite (a) occur within the siltstone bed; barian carbonate replaces celsian along cleavage. Field of view is 1 mm; cross nichols, transmitted light. Lower horizon, 68A.



Figure 3.30 Quartz-sulfide facies: Rock slab of sets of bands of quartz-celsian (white) bracketed by disseminated dark sphalerite (grey) grains and interbedded with massive subtype carbonaceous quartz-pyrite beds (black). Field of view is 6 cm. Upper horizon, DDH 70.

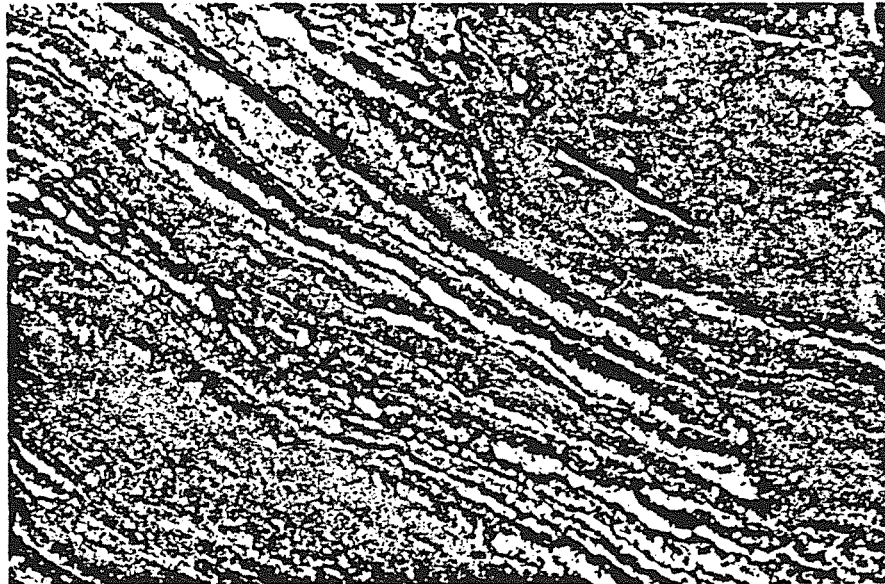


Figure 3.31 Quartz-sulfide facies: Sets of quartz-celsian (white) bands interbedded with sandy siltstones truncated by disconformable base of overlying sedimentary breccia containing quartz-celsian bands within clasts. Field of view is 6 cm. Upper horizon, DDH 51A.

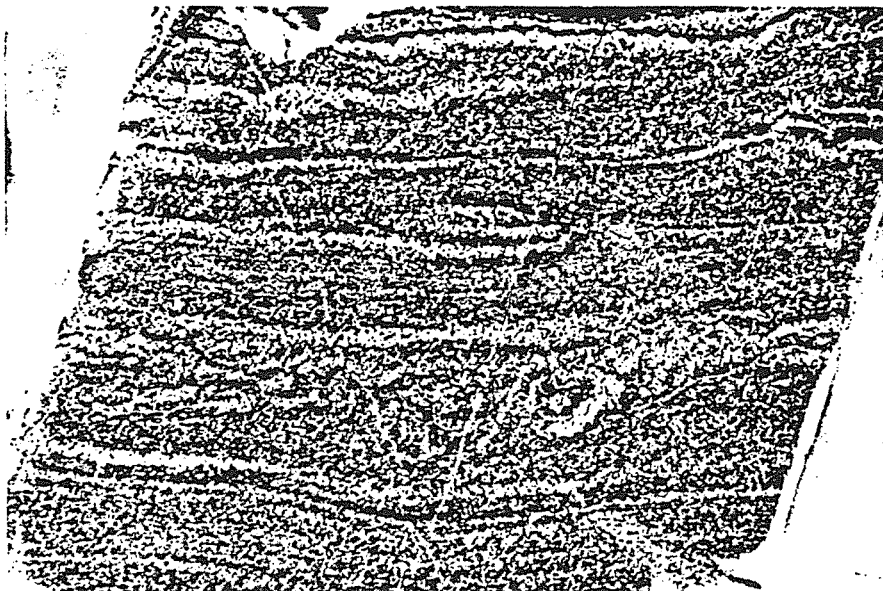


Figure 3.32 Quartz facies: Disseminated pyrite-rich carbonaceous quartz-pyrite beds and laminae. Pyrite occurs preferentially along bedding and in nodular forms. Field of view is 6 cm. Upper horizon, DDH 39.

Quartz Veins

Planar fractures filled by fibrous quartz oriented perpendicular to vein walls occur within siliceous siltstone beds interbedded with barite laminae (Fig. 3.4). Quartz veins are localized in siliceous beds and are absent in adjacent, ductily deformed barite-rich beds.

Disseminated Pyrite

Disseminated pyrite is ubiquitous throughout the stratiform horizons where it typically comprises 1 to 3 % of the rock. It is most abundant on the margins of the stratiform horizons (Fig. 3.28, 3.32), within carbonaceous strata. Pyrite predominantly occurs as fine- to coarse-grained subhedral to euhedral grains; fine-grained framboidal pyrite occurs with subhedral pyrite within organic-rich carbonaceous quartz-pyrite laminae. Beds drape around nodular patches of disseminated pyrite (Fig. 3.33).

Disseminated Iron Carbonate

Medium-grained euhedral ankerite grains are widespread within terrigenous sediments interbedded with carbonaceous quartz-pyrite beds (Fig. 3.29); anhedral siderite grains are common within terrigenous strata on the periphery of the stratiform body and commonly have corroded outlines.

Irregular Veinlets of Sphalerite, Galena, Quartz and Celsian

Minor irregular veinlets of medium-grained anhedral sphalerite, galena, quartz and subhedral celsian grains cut stratiform bodies with similar sulfide-quartz mineralogy. Veinlet margins are transitional with adjacent sediments, interdigitate along laminae, and commonly are sinuous to ptygmatically folded (Fig. 3.34).

Proximal Stratiform Body

Non-stratiform textures are much more common in the proximal than in the distal part of the deposit; and adjacent to the Jason fault non-stratiform textures locally characterize the bulk of the stratiform body. Non-stratiform textures are classified as disseminated, nodular, irregular veinlet, or veinlet.

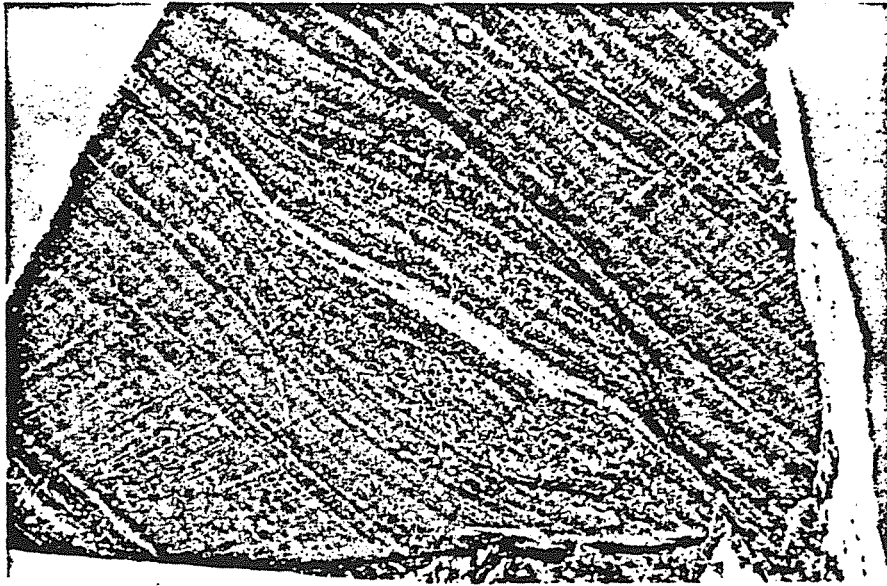


Figure 3.33 Quartz facies: Differential compaction of siltstone strata around nodule of disseminated pyrite indicates pyrite growth during compaction. Field of view is 6 cm. Upper horizon, DDH 86.



Figure 3.34 Quartz-sulfide facies: Irregular sphalerite-galena-celsian-quartz veinlet cutting quartz-sphalerite (galena) lamina. The galena to sphalerite ratio and sulfide to quartz ratio is higher in the veinlet than in the host laminated sulfide-quartz. Veinlet has a sinuous galena-rich center that may reflect folding due to compaction. Margins of the veinlet are irregular and merge laterally with sulfide-rich laminae. Cross polarized transmitted and reflected light. Field of view is 3 mm. Sphalerite (SL), galena (GN), celsian (CN), and quartz (QTZ). Upper horizon, DDH 63B.

Quartz Nodules

Irregular nodules of coarse-grained quartz 0.5 to 10 cm in diameter occur within ankerite beds (Fig. 3.35); similar but much smaller nodules are common within sulfide-rich beds of galena-pyrite, sphalerite-galena, galena and sphalerite laminae (Figs. 3.13, 3.16). Clasts of coarse-grained quartz pods occur within sedimentary breccias immediately overlying the upper stratiform horizon (Fig. 3.17)

Ankerite Nodules:

Nodules texturally similar to quartz nodules occur within ankerite beds and sulfide-rich laminae. In ankerite beds, the coarse-grained ankerite occurs in both a nodular and irregular vein-like form (Fig. DG) and are cut by all other non stratiform textural types. In sulfide-rich beds, ankerite nodules 0.2 to 1.0 cm in diameters cut bed and laminae contacts and sulfide clast margins (Fig. 3.13, 3.20). Ankerite nodules may comprise up to 30% of ankerite or sulfide-rich beds.

Disseminated Barian Muscovite

Barian muscovite occurs as fine-grained concordant beds interbedded with siltstones and siderite and pyrite beds in the lower horizon (Fig. 3.5). Barian muscovite also occurs as coarse-grained rosettes adjacent to the deeper parts of the breccia body (Fig. 3.28); rosettes are commonly replaced by pyrrhotite (Fig. 3.37). The thinning of some siltstone beds adjacent to rosettes suggests formation of the latter during sediment compaction.

Disseminated Pyrrhotite

Fine-grained pyrrhotite occurs as irregular disseminated grains within ankerite-sulfide and siderite beds. Pyrrhotite replaces siderite and ankerite along cleavage and grain boundaries (Fig. 3.38).

Pyrite

Medium- to coarse-grained subhedral to euhedral pyrite occurs throughout the proximal portion of the deposit (Fig. 3.28) as disseminated grains and aggregates of grains (Figs. 3.15,

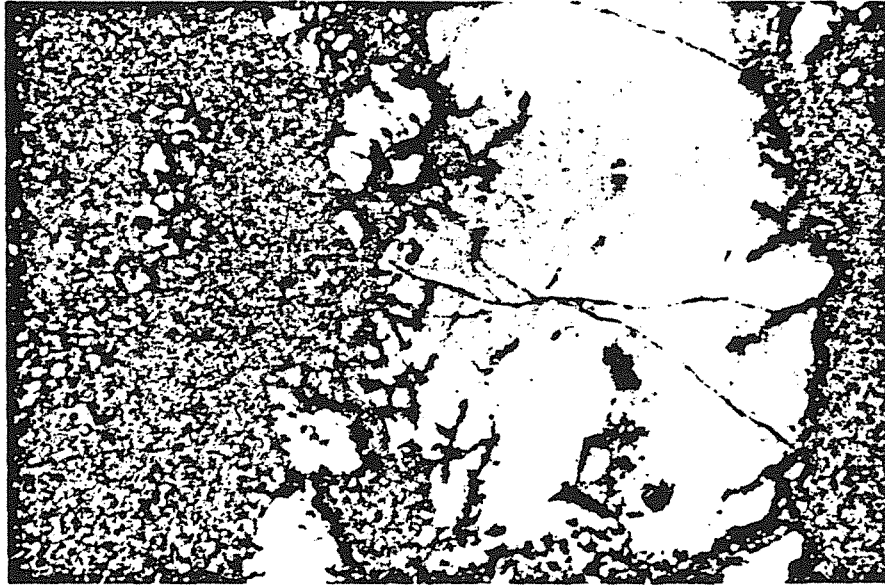


Figure 3.35 Iron carbonate facies: Irregular quartz nodules (white) within galena-ankerite bed (grey). Field of view is 4 cm. Upper horizon, DDH 56A.

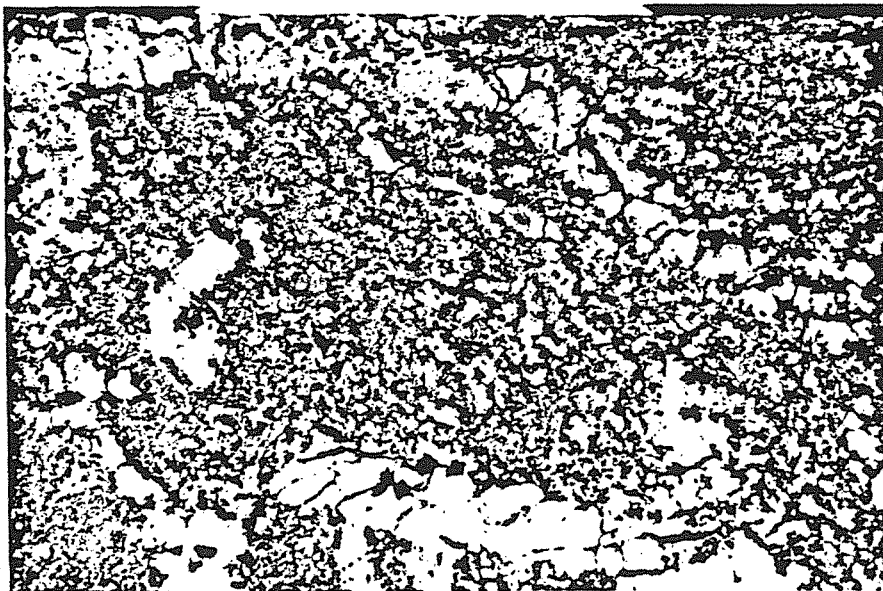


Figure 3.36 Iron carbonate facies: Irregular veins of coarse-grained ankerite cutting medium-grained ankerite-galena bed. Field of view is 3 cm. Upper horizon, DDH 56A.



Figure 3.37 Pyrite facies: Rosette of coarse-grained barian muscovite (black) within siltstone bed. Muscovite is partially replaced by pyrrhotite (white). Reflected light. Field of view is 2.5 cm. Lower horizon, DDH 86.



Figure 3.38 Iron carbonate facies: Replacement of siderite bed (grey) by pyrrhotite (black) along cleavage and grain boundaries. Transmitted light. Field of view is 5 mm. Lower zone, DDH 56B.

3.19, 3.27, 3.39). Pyrite grains grow across all other non-stratiform mineralization except quartz veins.

Siderite-ankerite veinlets and breccia matrix

In the upper horizon, irregular coarse-grained ankerite veinlets (Fig. 3.36) are cut by younger carbonate-muscovite-sulfide veins.

Carbonate-muscovite-sulfide veinlets

Massive fine-grained barian muscovite occurs with coarser ankerite and sphalerite as irregular veinlets and pods (Fig. 3.4) that cut siderite and ankerite beds of the upper and lower horizon (Fig. 3.28). Siderite crystals lining the pods are corroded and mantled by coarser barian muscovite. These veins are likely associated with the siderite-muscovite-sulfide matrix of the breccia body (see below) and siderite-muscovite-sulfide veins within and adjacent to the Jason fault.

Sulfide veinlets

Sulfide veinlets composed of pyrrhotite +/- sphalerite, galena, chalcopryrite and pyrite occur within the upper horizon, the underlying sedimentary breccia unit and the lower horizon adjacent to the breccia body and Jason fault. Sulfide veinlets are discontinuous and irregular in shape. They are spatially associated with replacement of iron carbonate by disseminated pyrrhotite (Fig. 3.41). Within this vein set there is a vertical zoning from pyrrhotite+/-chalcopryrite veins in the lower horizon to pyrrhotite+/-sphalerite, galena, chalcopryrite or pyrrhotite+pyrite in the upper horizon. A steeply dipping pyrrhotite+pyrite vein in the upper horizon was noted to merge into an overlying massive pyrite bed suggesting that the vein was a conduit for fluids that formed the pyrite bed. Sulfide veinlets are locally cut by carbonate-quartz-sulfide and quartz-sulfide veinlets.

Sphalerite, galena and pyrobitumen occur within irregular net-like veinlets rimmed by euhedral pyrite (Figs. 3.21, 3.41) within pyrite beds of the upper horizon adjacent to the Jason fault.

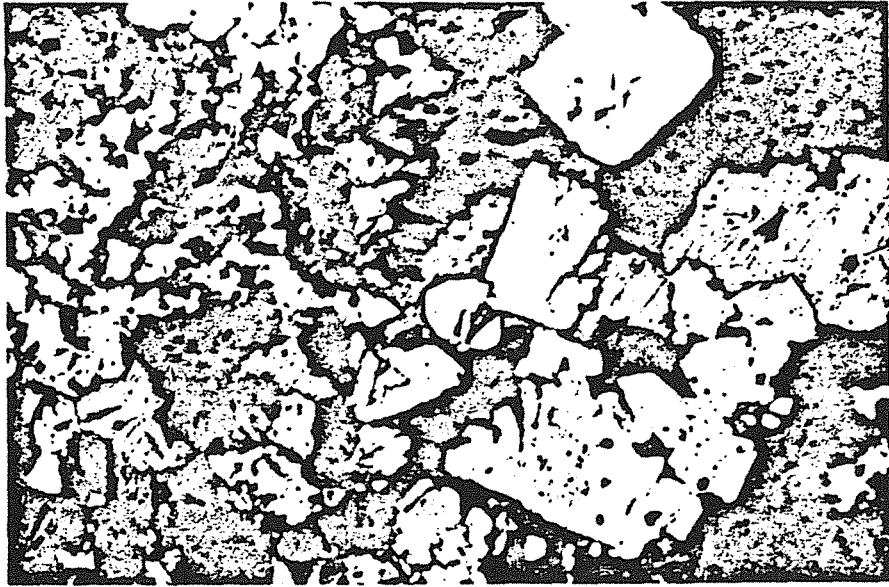


Figure 3.39 Iron carbonate facies: Disseminated galena (gl) and pyrrhotite (po) intergrown with or replacing ankerite (ank); euhedral pyrite (py) cuts both sulfide and carbonate. Field of view is 5 mm. Upper horizon, DDH 56A.



Figure 3.40 Iron carbonate facies: Coarse zoned ankerite crystals surround an irregular pod of fine-grained barian muscovite (white) and coarse sphalerite (black). Growth bands in ankerite are truncated by corroded margin of ankerite crystal. Transmitted light. Field of view is 15 mm. Lower horizon, DDH 56B.

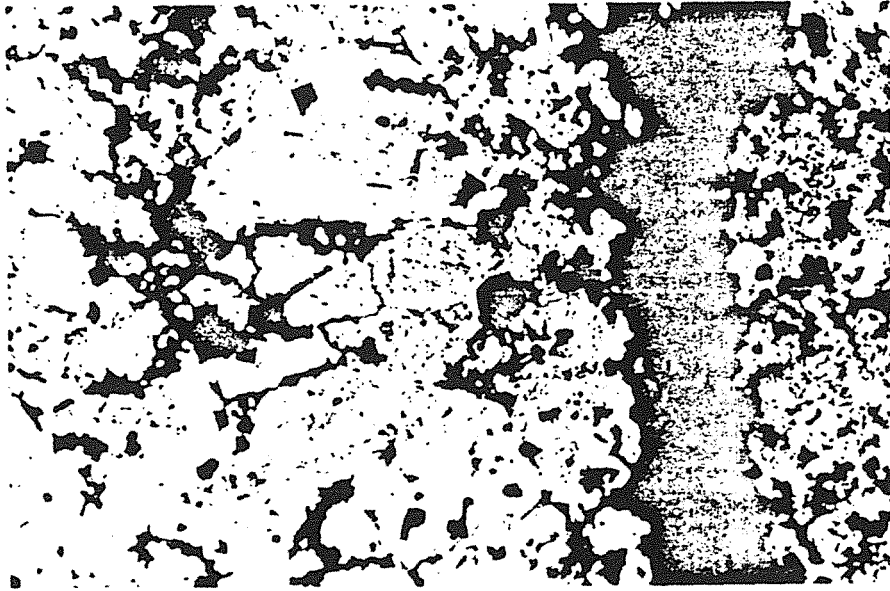


Figure 3.41 Iron carbonate facies: Pyrrhotite-galena-sphalerite veinlet (black) cuts medium-grained ankerite bed; degree of replacement of ankerite by disseminated pyrrhotite and galena (black) increases towards veinlet. Transmitted light. Field of view is 10 mm. Upper horizon, DDH 56B.

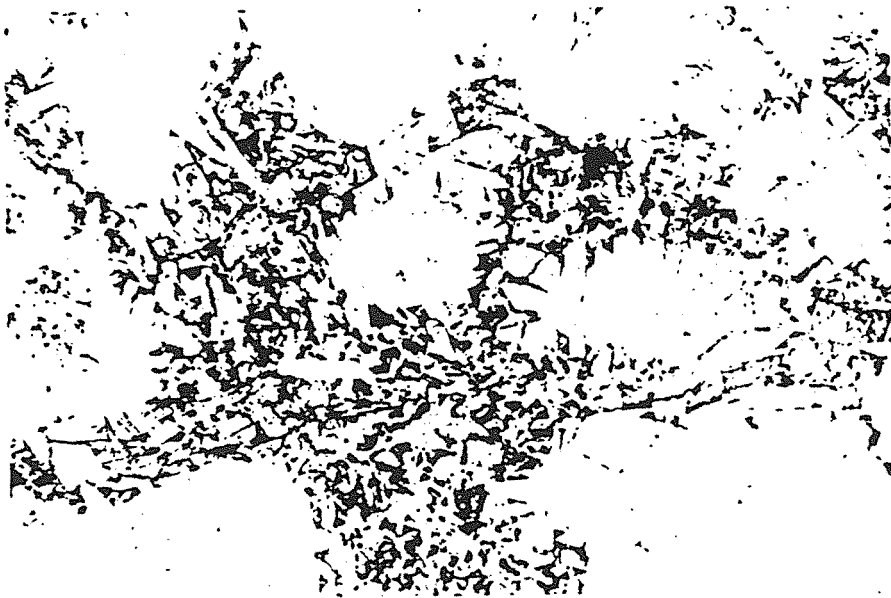


Figure 3.42 Pyrite facies: Pyrite (white) pseudomorphs of marcasite crystals line a sphalerite-filled (dark grey) cavity within a massive pyrite bed. Field of view is 10 mm. Reflected light. Upper horizon, DDH 88.

Quartz-Sulfide Veinlets

Medium-grained quartz+/-sphalerite, galena, chalcopyrite, pyrrhotite and pyrobitumen occur within irregular and planar veinlets cutting pyrite beds adjacent to the Jason fault (Fig. 3.21, 3.43).

Carbonate-Quartz-Sulfide Veinlets

Coarse-grained ankerite-quartz-galena veins form planar to irregular veinlets that cut ankerite-sulfide beds and siderite beds of the upper and lower horizons (Fig. 3.5). Veins are commonly zoned, with ankerite-galena centers bordered by quartz, and are commonly concordant to siderite bedding within the lower horizon. Crosscutting relationships suggest that the formation of the carbonate-quartz-sulfide veinlets in the lower and upper horizons postdate the formation of the sulfide veinlets (Fig. 3.21).

Pyrobitumen Veinlets

Pyrobitumen-quartz veins concordant to bedding locally comprise 1 to 5 % of siderite beds at the fringe of the iron carbonate facies in the lower horizon.

Quartz Veins

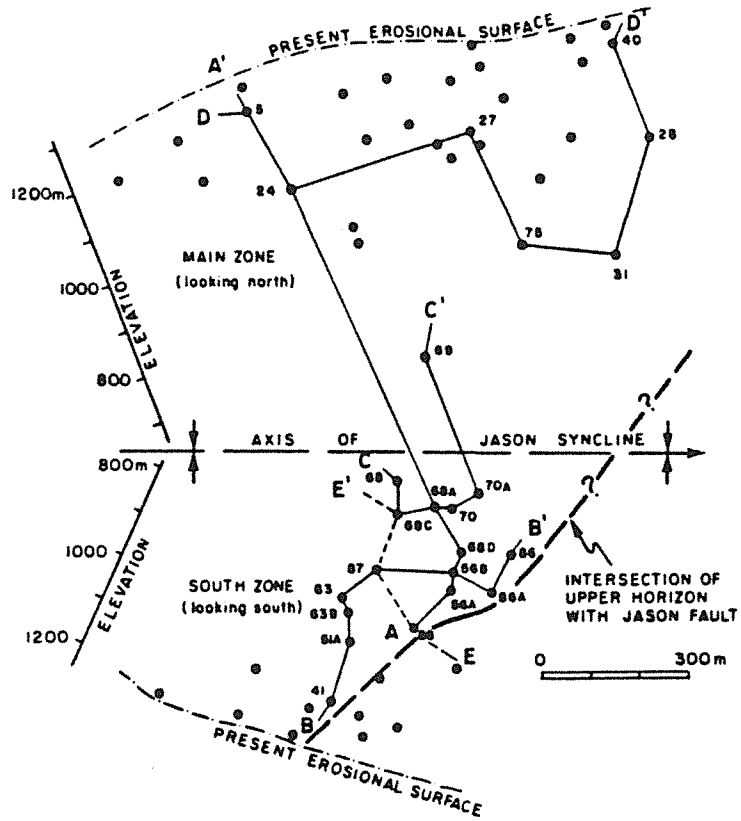
Planar quartz veins similar to those within the distal stratiform body occur within siliceous strata. Quartz veins cut all other mineralization types. Elongate grains of quartz perpendicular to vein walls in quartz veins is distinct from quartz in quartz-rich sulfide veinlets and breccia matrix in the pyrite facies.

Breccia Body

The term "breccia body" is used to describe the volume of rock adjacent to the Jason fault cut by narrow zones of breccia up to 3 m thick. In plan view this aggregate of breccia zones is elongate parallel to the Jason fault (Fig. 3.44b) and dips steeply to the north (Devonian orientation), merging at depth with the more shallowly dipping Jason fault (Figs. 3.45, 3.46). Where the upper horizon overlies the breccia body, it is cut by abundant veinlets (Fig. 3.47). The breccia body also cuts the siliceous siltstones and interbedded pyrite and iron



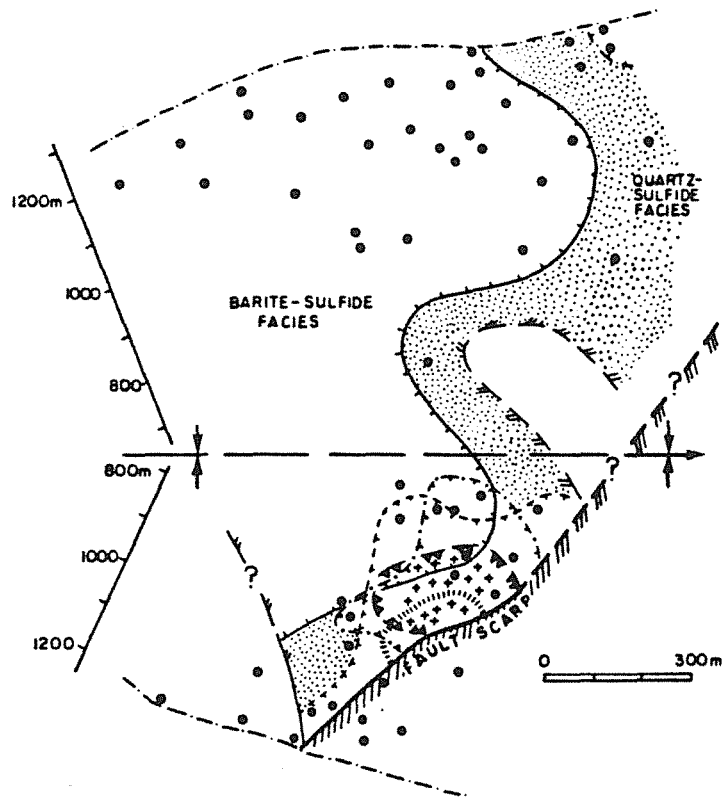
Figure 3.43 Pyrite facies: Quartz-sulfide vein cutting massive pyrite bed. Quartz (q), galena (g), sphalerite (s), chalcopyrite (c), pyrite (p). Reflected light. Field of view is 3mm. Upper horizon, DDH 88.



LEGEND

- intersection of drill hole with top of upper horizon
- A ——— A' line of stratigraphic section (Figs. 7-12)
- E - - - - E' line of stratigraphic section (Fig. 13)

Figure 3.44a Plan view map of the upper stratiform horizon unfolded about the axis of the Jason syncline. Location of stratigraphic cross-sections A-A' (Fig. 7), B-B' (Fig. 8), C-C' (Fig. 9) and D-D' (Fig. 10).



LEGEND


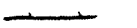
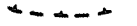

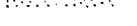




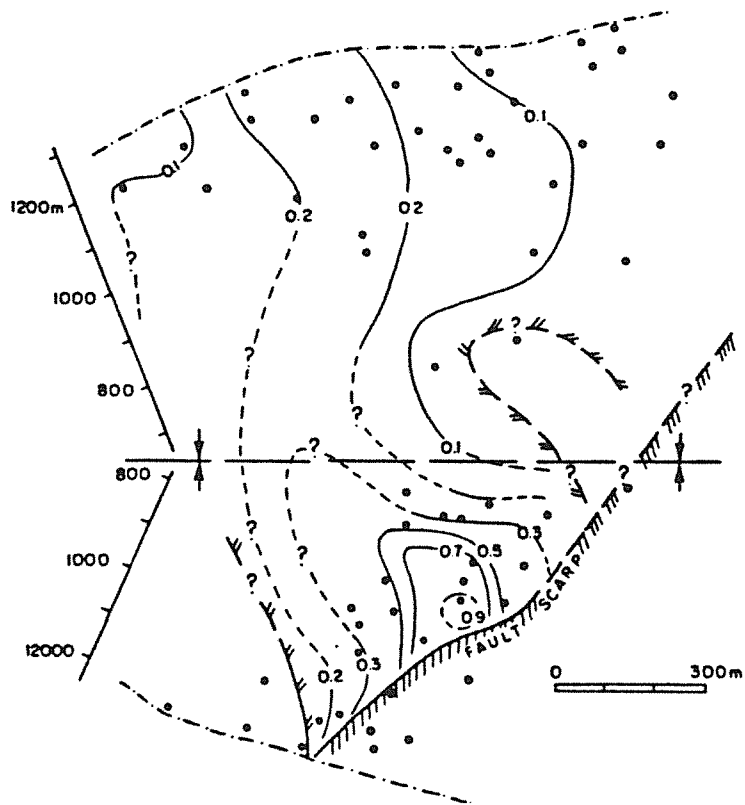
-  extent of stratiform horizon (known, inferred)
-  extent of barite-sulfide facies
-  extent of Pb-Zn-Fe facies
-  extent of pyrite facies
-  extent of predominance of quartz-sulphide facies
-  inferred scarp area of Jason fault during Late Devonian
-  extent of iron carbonate facies
-  extent of breccia body
-  extent of abundant veining

Figure 3.44b Distribution of stratiform facies in the upper horizon.



LEGEND


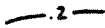


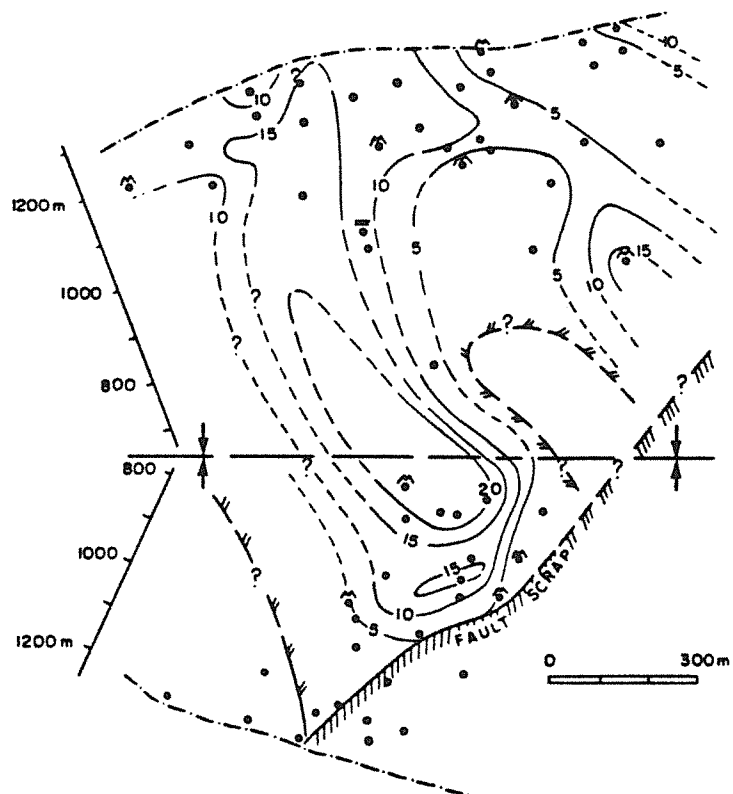
-  extent of stratiform horizon (known, inferred)
-  .2 Pb/Pb+Zn ratio of stratiform horizon based on averaged drill intercepts
-  intersection of drill hole with top of upper horizon
-  inferred scarp area of Jason fault during Late Devonian

Figure 3.44c Contour map of averaged Pb/Pb+Zn values for drill hole intersections of upper horizon.



LEGEND




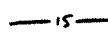

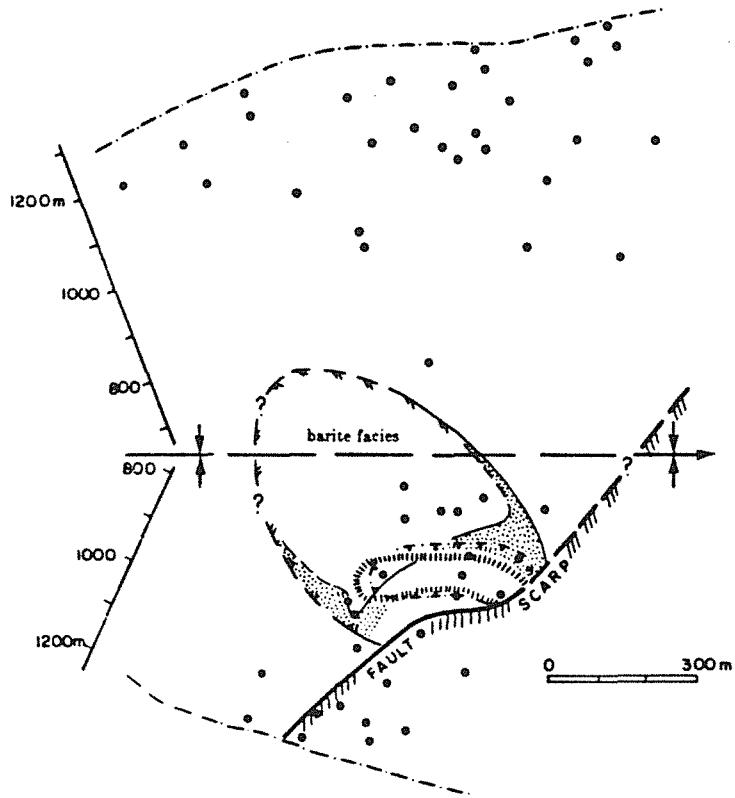
-  extent of stratiform horizon (known, inferred)
-  drill hole intersection where faulting/erosion complicates estimation of stratigraphic thickness of stratiform horizon
-  inferred scarp area of Jason fault during Late Devonian
-  stratigraphic thickness of stratiform horizon
-  intersection of drill hole with top of upper horizon

Figure 3.44d Isopach map of upper horizon (in meters).



LEGEND



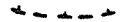




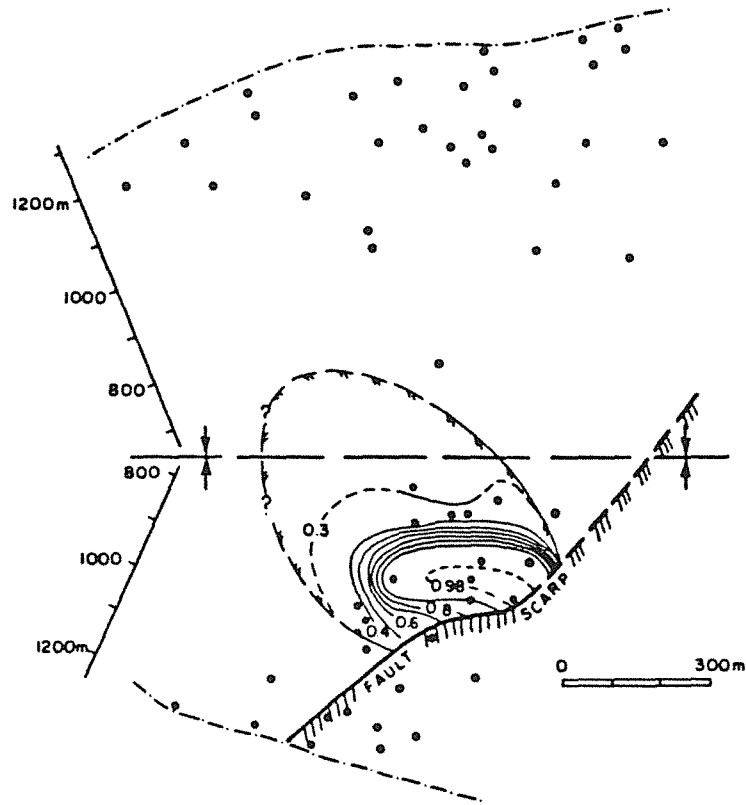
-  extent of stratiform horizon (known, inferred)
-  extent of barite-sulfide facies
-  extent of Pb-Zn-Fe facies
-  extent of pyrite facies
-  extent of predominance of quartz-sulphide facies
-  inferred scarp area of Jason fault during Late Devonian
-  extent of iron carbonate facies

Figure 3.44e Distribution of stratiform facies in lower horizon.



LEGEND

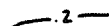

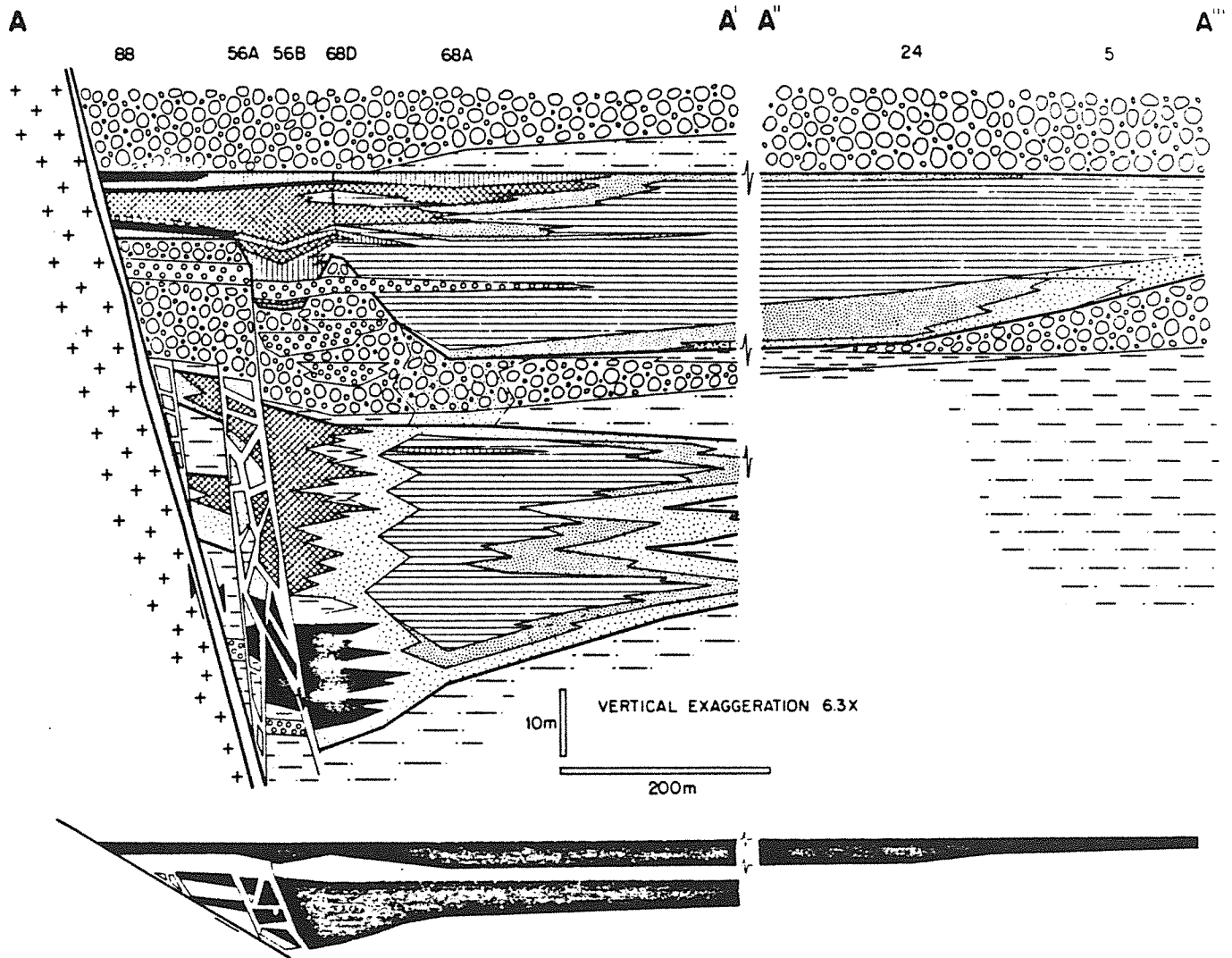



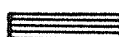

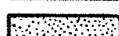

-  Pb/Pb+Zn ratio of stratiform horizon based on averaged drill intercepts
-  inferred scarp area of Jason fault during Late Devonian

Figure 3.44f Contour map of averaged Pb/Pb+Zn values for drill hole intersections of lower horizon.



Stratiform Facies

-  **Pyrite Facies**
-  **Iron Carbonate Facies**
-  **Pb-Zn-Fe Sulfide Facies**
-  **Barite-Sulfide Facies**
-  **Quartz-Sulfide Facies**
-  **Quartz Facies**
-  **stratiform mineralization breccia**

Terrigenous Lithologies



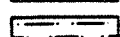

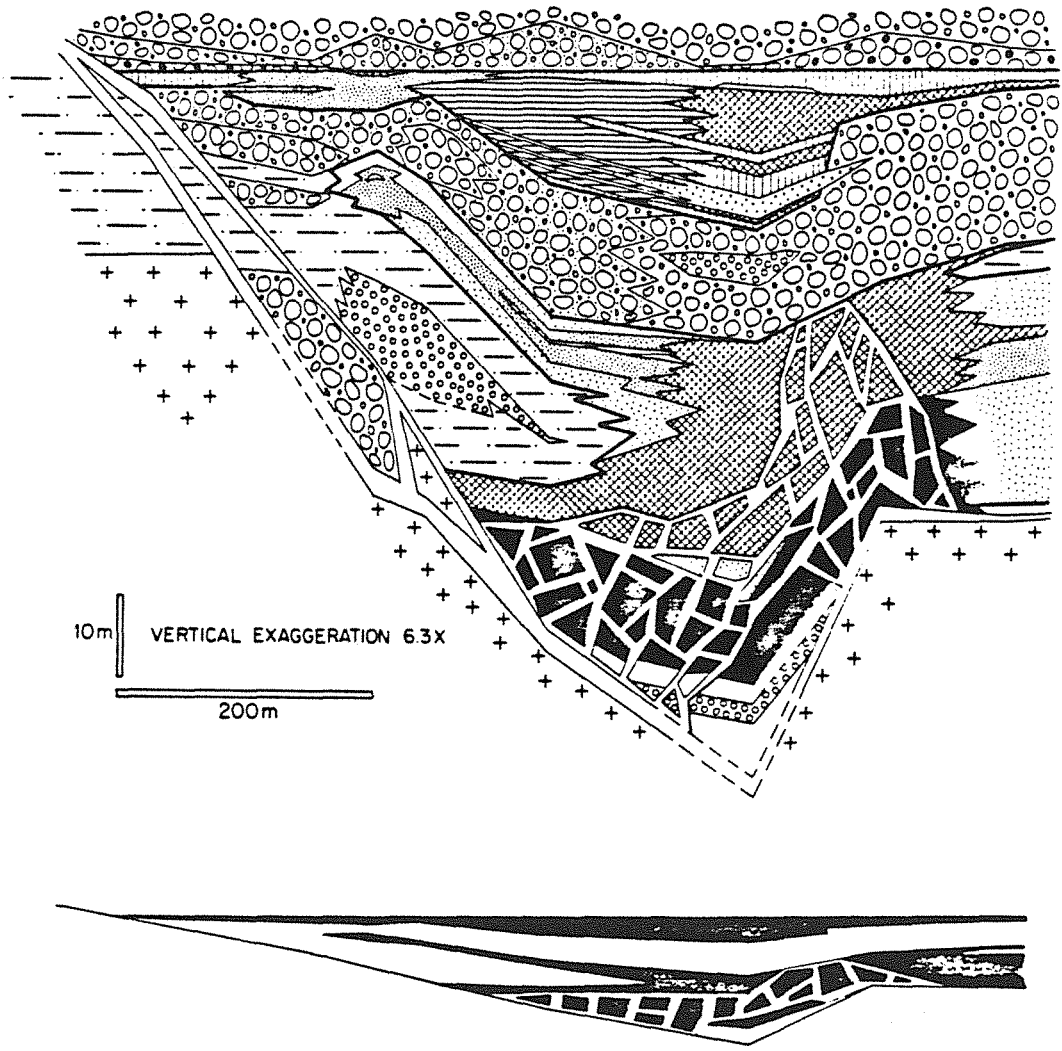



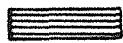
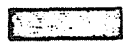


-  **Heterolithic Sedimentary Breccia**
-  **Conglomerate/Sandstone**
-  **Thin-bedded Siltstone, carbonaceous**
-  **Siliceous Argillite, carbonaceous**

Figure 3.45 Stratigraphic cross-section A-A' across the trend of the Jason Fault with 6.3X vertical exaggeration. Heavy black line encloses hydrothermal facies. True scale cross-section shown in black at base. Location of section indicated on Figure 3.44a.

B 41 51A 63B 63 87 56B 86A 86 B'



Stratiform Facies

-  Pyrite Facies
-  Iron Carbonate Facies
-  Pb-Zn-Fe Sulfide Facies
-  Barite-Sulfide Facies
-  Quartz-Sulfide Facies
-  Quartz Facies
-  stratiform mineralization breccia

Terrigenous Lithologies



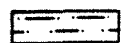
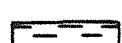
-  Heterolithic Sedimentary Breccia
-  Conglomerate/Sandstone
-  Thin-bedded Siltstone, carbonaceous
-  Siliceous Argillite, carbonaceous

Figure 3.46 Stratigraphic cross-section B-B' of proximal stratiform mineralization and breccia body along the trend of the Jason fault with 6.3X vertical exaggeration. Heavy black line encloses hydrothermal facies. True scale cross-section shown in black at base. Location of section indicated on Figure 3.44a.

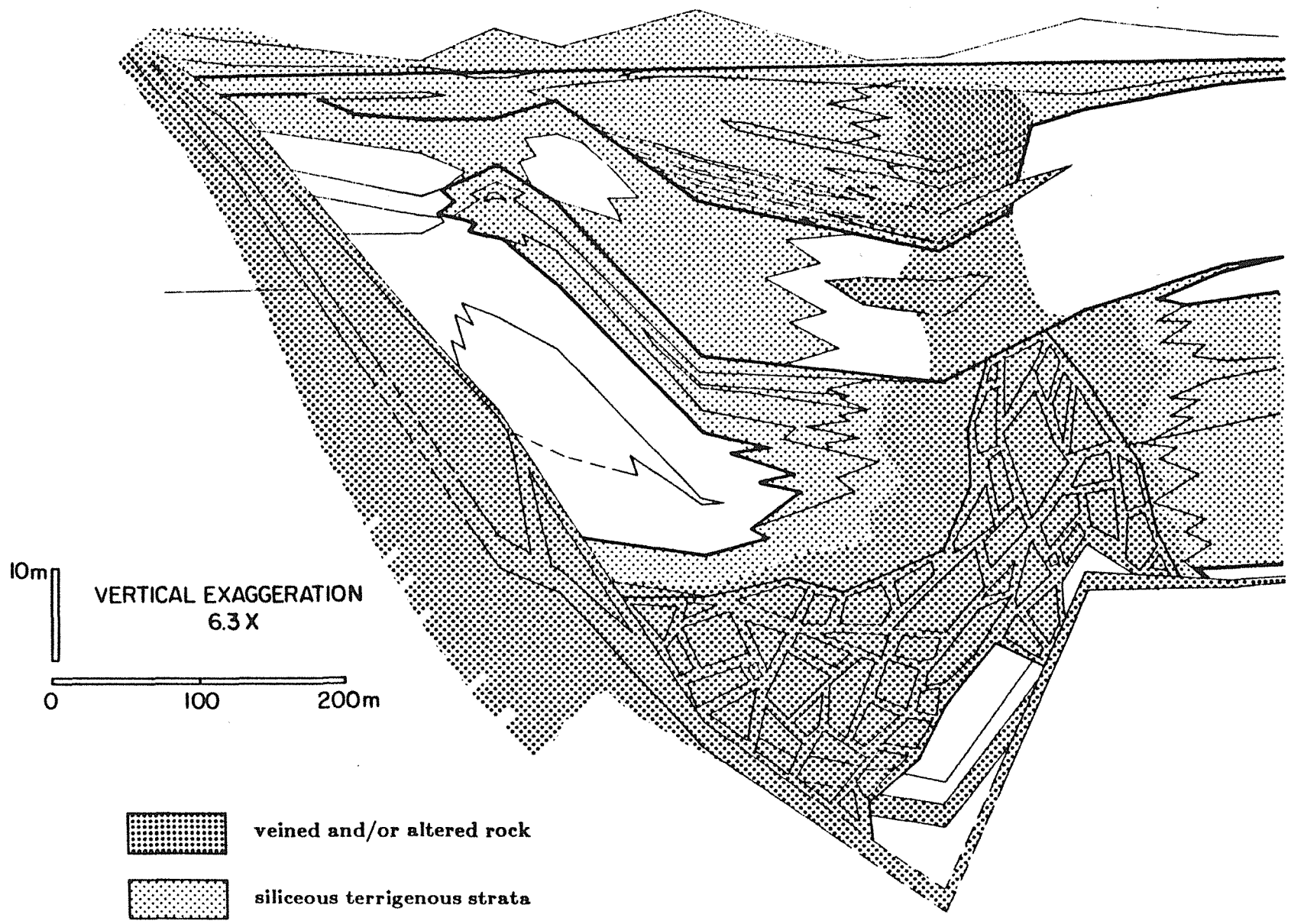


Figure 3.47 Stratigraphic cross-section B-B' with the distribution of veined or altered rock associated with the Jason fault, breccia body and proximal stratiform mineralization and the extent of siliceous terrigenous strata interbedded with or adjacent to the stratiform horizons is indicated. Heavy black line encloses hydrothermal facies.

carbonate facies of the lower horizon adjacent to the Jason fault.

The breccias are comprised of centimeter-scale angular fragments of siliceous siltstone (Fig. 3.48) and lesser fragments of siderite and pyrite beds within a matrix of siderite, pyrrhotite, pyrite, barian muscovite, quartz and minor sphalerite, chalcopyrite and galena (Fig. 3.49, 3.50). Siderite, pyrrhotite or pyrite may be the dominant mineral.

The breccia body cuts the stratiform mineralization of the lower horizon and hence postdates it. Disseminated and vein pyrrhotite +/- chalcopyrite, carbonate-muscovite-sulfide veins, disseminated muscovite rosettes and sericitized argillaceous beds are abundant adjacent to the breccia body in the iron carbonate facies. The compositional similarity of non-stratiform mineralization (e. g. pyrrhotite, barian muscovite) in the adjacent lower horizon to the breccia matrix suggests these minerals are related to the formation of the breccia body.

Jason Fault

The Jason fault is interpreted to have been active during the deposition of the stratiform horizons and was both the source of sedimentary breccias slumped from its submarine scarp as well as a conduit for rising metalliferous hydrothermal fluids that vented to form the stratiform horizon (Chap. 2).

The Jason fault is a 0.2 to 3m thick zone of pebble breccia to pebbly mudstone. Rounded to subangular clasts of siderite veins, argillite clasts veined by siderite, argillite and siltstone clasts occur in a matrix of clay and variable amounts of fine-grained quartz, siderite and barian muscovite (Fig. 3.51). In the deepest part of the fault intersected by drilling the matrix is very siliceous and carries up to 5 % disseminated pyrite, pyrrhotite, sphalerite and galena. Within the intermediate levels of the Jason fault, fine-grained barian muscovite occurs locally as a massive matrix to the fault. In the shallowest levels the matrix is unaltered silty mudstone. Disseminated fine-grained pyrite is common throughout the Jason fault, and exceeds 3 to 5 percent in the upper part of the fault.

Ankerite-siderite-muscovite-chalcopyrite-(pyrite) veins and breccia veins are abundant



Figure 3.48 Breccia body: Siliceous siltstone fragments within a matrix of siderite-muscovite-pyrrhotite. Field of view is 3.5 cm. DDH 56A.

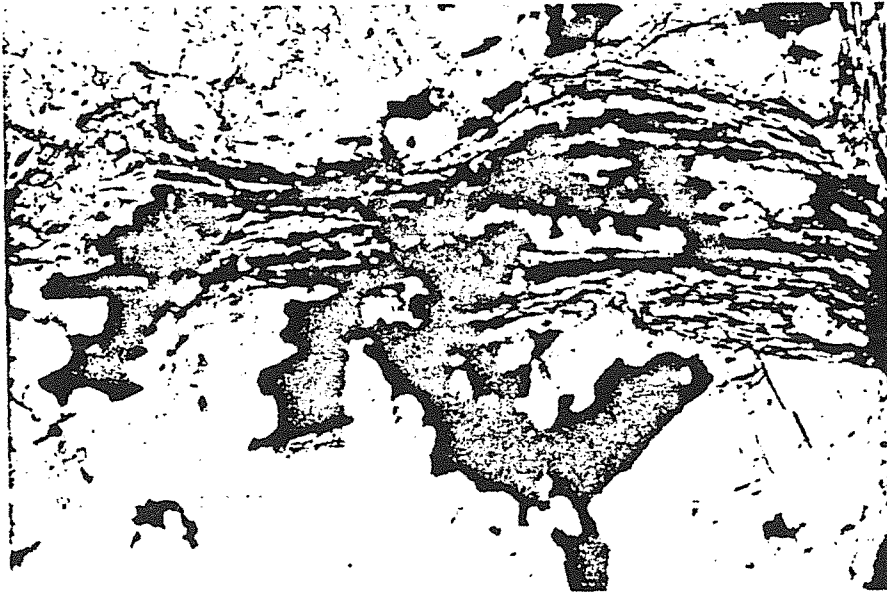


Figure 3.49 Breccia body: Vein of coarse-grained siderite-barian muscovite partially replaced by pyrrhotite (black). Field of view is 3 mm. Transmitted light. DDH 56A.



Figure 3.50 Breccia body: Fragments of silicified siltstone (medium grey) in matrix of siderite (grey) and pyrite (white). Rimming of siderite grains by pyrite suggests pyrite postdates siderite, pyrite pseudomorphs muscovite laths (black) within siltstone fragments. Field of view is 10 mm. Reflected light. DDH 86.



Figure 3.51 Jason fault: Clast of fine-grained siderite (medium grey) cut by irregular siderite-pyrrhotite-chalcopyrite-sphalerite-(pyrite) veinlet within fine-grained argillaceous quartz matrix (light grey). Clast is partially bound by stylolitic surfaces (black). Field of view is 10mm. Transmitted light. DDH 87.

within the Jason fault zone as well as in the footwall strata adjacent to the Jason fault (Fig. 3.47). These veins are characterized by a lack of an alteration selvage and are similar to fragmented veins with the Jason fault. Brecciated fragments of siderite +/- muscovite, pyrrhotite, sphalerite, chalcopyrite, galena veins occur within the Jason fault (Fig. 3.51).

STRATIFORM FACIES

The Jason stratiform deposit is composed of two stacked stratiform bodies. The lower horizon is an oval in plan view (Fig. 3.44e,f), and wedge-shaped in cross-section (Fig. 3.45). Pb/Pb+Zn ratios decrease rapidly away from the Jason fault.

The upper horizon is irregular in shape but becomes more extensive laterally away from the Jason fault (Fig. 6). The upper horizon is more sheet-like and extensive compared to the lower horizon (Fig. 7). The averaged Pb/Pb+Zn ratio of drill hole intercepts of the upper horizon decrease away from a maximum adjacent to the Jason fault; they also decrease away from a lead-rich corridor trending perpendicular to the Jason fault that coincides with the zone of maximum thickness of the upper horizon.

The two stratiform horizons can be divided into facies with individual facies characterized by a distinctive association of lamina types. Six stratiform facies are distinguished and named for their principal mineral constituent(s): pyrite, iron carbonate, Pb-Zn-Fe sulfide, barite-sulfide, quartz-sulfide and quartz.

Pyrite Facies

The pyrite facies is distinguished by a predominance of pyrite beds (Fig. 3.3) and occurs immediately adjacent to the Jason fault (Figs. 3.44b, 3.45, 3.46). Lead and zinc grades are typically low (i. e. %Pb+Zn < 5%) and lead to zinc ratios high (i. e. Pb/Pb+Zn = 0.7 to 0.9). In the upper stratiform horizon, beds of growth banded and massive pyrite beds 0.5 to 1.5 m thick thin abruptly away from the Jason fault. Pyrite beds are cut by abundant sulfide, quartz-sulfide and quartz veinlets and quartz breccia. Pyrite beds are interbedded with beds of the Pb-Zn-Fe sulfide facies and the iron carbonate facies; in the upper zone contacts

with other hydrothermal facies and terrigenous sediment are sharp while in the lower horizon adjacent to the breccia body interbedded siliceous siltstone beds are usually replaced by pyrite (Fig. 3.22).

Iron Carbonate Facies

The iron carbonate facies is dominated by ankerite or siderite beds (Fig. 3.3) and is characterized by the abundance of non-stratiform textural types. The iron carbonate facies is texturally and mineralogically diverse because of variations in the abundance of disseminated minerals, pods and veinlets within the carbonate beds. These include disseminated pyrrhotite and pyrite; quartz pods; and veinlets of carbonate-muscovite-sulfide, sulfide, carbonate-quartz-sulfide and pyrobitumen. The iron carbonate facies is characterized by a wide range of total Pb+Zn percent (3 to 25%) and very high Pb/Pb+Zn fractions (>0.95) (Fig. 14, 56A).

The iron carbonate facies occurs adjacent to the Jason fault (Figs. 3.44b, 3.45, 3.46, 3.52, 3.53). In the upper horizon it is interbedded with the Pb-Zn-Fe sulfide facies and interfingers laterally with the pyrite facies, barite facies and quartz-sulfide facies. Sharp bedding contacts occur with interbedded pyrite facies, Pb-Zn-Fe sulfide facies, and terrigenous sediments. However, the occurrence of abundant ankerite nodules within interbedded Pb-Zn-Fe sulfide beds interbedded with iron carbonate beds can cause the contacts between these two facies to be transitional. The contacts with the barite facies and quartz-sulfide facies are marked by the replacement of barite, quartz and sulfide by ankerite. In the lower horizon, the iron carbonate facies is adjacent to and cut by the breccia body. It overlies the pyrite facies and interfingers laterally with the quartz facies, quartz-sulfide facies, and less commonly, the barite facies.

The upper horizon is cut by abundant veinlets and non-stratiform minerals where it overlies the breccia body (Figs. 3.44b, 3.47). In contrast, the lateral fringe of the iron carbonate facies beyond the extent of the breccia body is characterized by massive to banded ankerite with only minor veins. Adjacent to the breccia body (Fig. 3.45, DDH 56B), disseminated pyrrhotite, and pyrrhotite veins and ankerite-quartz-galena veins are abundant

within the siderite beds of the lower horizon. Siltstone interbedded with these siderite beds are bleached in color and illite grains typical of laterally equivalent siltstones are recrystallized to coarser barian muscovite. Further from the breccia body siderite beds lack these sulfides and only pyrobitumen-quartz veins occur. Siltstone beds are siliceous, but show no other alteration.

Pb-Zn-Fe Sulfide Facies

The Pb-Zn-Fe sulfide facies is composed of massive strata of sphalerite, sphalerite-galena, galena and galena-pyrite centimeters to meters in thickness. Nodules of quartz or ankerite up to 10 mm in diameter are common; ankerite pods alone may comprise up to 30 % of the sulfide beds. It is interbedded along sharp contacts with the pyrite, the iron carbonate and the barite facies. The Pb-Zn-Fe facies occurs adjacent to the Jason fault in the upper horizon and is more extensive than the iron carbonate facies (Fig. 3.44b, 3.45, 3.46). Pb-Zn-Fe sulfide facies beds range from 30 to 45% Pb+Zn. With increasing distance from the Jason fault, sulfide lamina types are zoned from galena-pyrite to sphalerite-galena to sphalerite (Fig. 3.3). This is reflected by the decrease in Pb/Pb+Zn values from 0.9 near the fault to 0.35 in the distal-most parts of the facies. Beds of all laminae generally thin away from the Jason fault. The Pb-Zn-Fe sulfide facies does not occur in the lower horizon.

Barite Facies

The barite facies includes all strata where barite laminae are present. Where present, barite laminae are typically the predominant lamina type; lessor sphalerite, sphalerite-galena, quartz and carbonaceous quartz-pyrite strata are interbedded with the barite (Fig. 3.3). Disseminated celsian, ankerite and pyrite occur throughout the facies. The barite facies differs from the quartz-sulfide facies by the presence of barite laminae, the lessor abundance of laminated carbonaceous quartz beds and framboidal pyrite, and the higher average Pb/Pb+Zn value.

The barite facies is the most widespread facies within the stratiform horizons. It

comprises over three quarters of the drilled extent of the upper horizon (Figs. 3.44, 3.46, 3.52, 3.53). Towards the Jason fault, the barite facies interfingers with beds of the quartz-sulfide, iron carbonate and Pb-Zn-Fe sulfide facies. The contact of the barite facies with the quartz-sulfide facies is parallel to the 0.1 value contour of Pb/Pb+Zn value (Fig. 3.44c). The barite facies is overlain and underlain by either the quartz facies or quartz-sulfide facies.

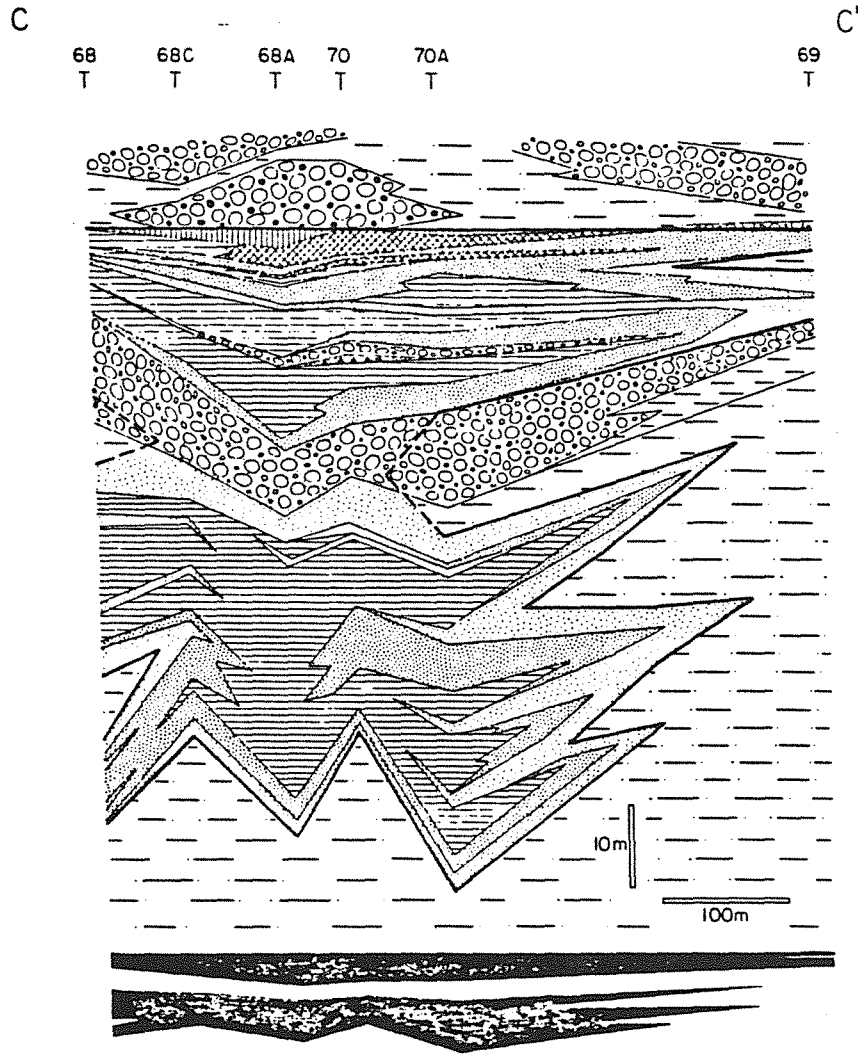
The barite facies is a much more extensive and homogeneous than those facies occurring adjacent to the Jason fault. However, within the barite facies the Pb/Pb+ Zn value of drill intercepts decreases systematically away from the Jason fault and away from a north trending (with respect to the Devonian orientation) corridor that lies at high angle to the Jason fault (Fig. 3.44).

Quartz-Sulfide Facies




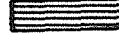



The occurrence of finely laminated sphalerite, quartz-sphalerite and quartz laminae and the absence of barite laminae distinguish the quartz-sulfide facies (Fig. 3.3). Organic-rich carbonaceous quartz-pyrite laminae comprise 50 to 80% of the strata in the distal part of the facies; towards the Jason fault these decrease in abundance and disappear. Disseminated framboidal pyrite, subhedral pyrite, celsian and ankerite/siderite are widespread; quartz bands are locally abundant. Discordant veinlets are rare. Quartz-sphalerite laminae are distinctive for their cyclic occurrence.

The quartz-sulfide facies comprises much of the distal portion of the upper stratiform horizon to the northeast, adjacent to the Jason fault. It interdigitates with the barite facies to the west and the iron carbonate facies toward the breccia body (Fig. 3.44b, 3.45, 3.52, 3.53). Strata of the quartz-sulfide facies also overlie and underlie the barite facies and in the lower horizon, the quartz-sulfide facies appears to envelope the barite facies.

Within the strata of the quartz-sulfide facies there is a zoning of organic carbon content, metal content and metal ratios. Where adjacent to the iron carbonate facies, the quartz-sulfide facies strata are distinguished by the absence of organic carbon and framboidal pyrite,



Stratiform Facies

-  **Pyrite Facies**
-  **Iron Carbonate Facies**
-  **Pb-Zn-Fe Sulfide Facies**
-  **Barite-Sulfide Facies**
-  **Quartz-Sulfide Facies**
-  **Quartz Facies**
-  **stratiform mineralization breccia**

Terrigenous Lithologies



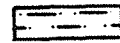
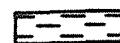
-  **Heterolithic Sedimentary Breccia**
-  **Conglomerate/Sandstone**
-  **Thin-bedded Siltstone, carbonaceous**
-  **Siliceous Argillite, carbonaceous**

Figure 3.52 Stratigraphic cross-section C-C' of distal stratiform mineralization in South zone area (south limb of Jason syncline) with 6.3X vertical exaggeration. True scale cross-section shown in black at base. Heavy black line encloses hydrothermal facies. Location of section indicated on Figure 3.44a.

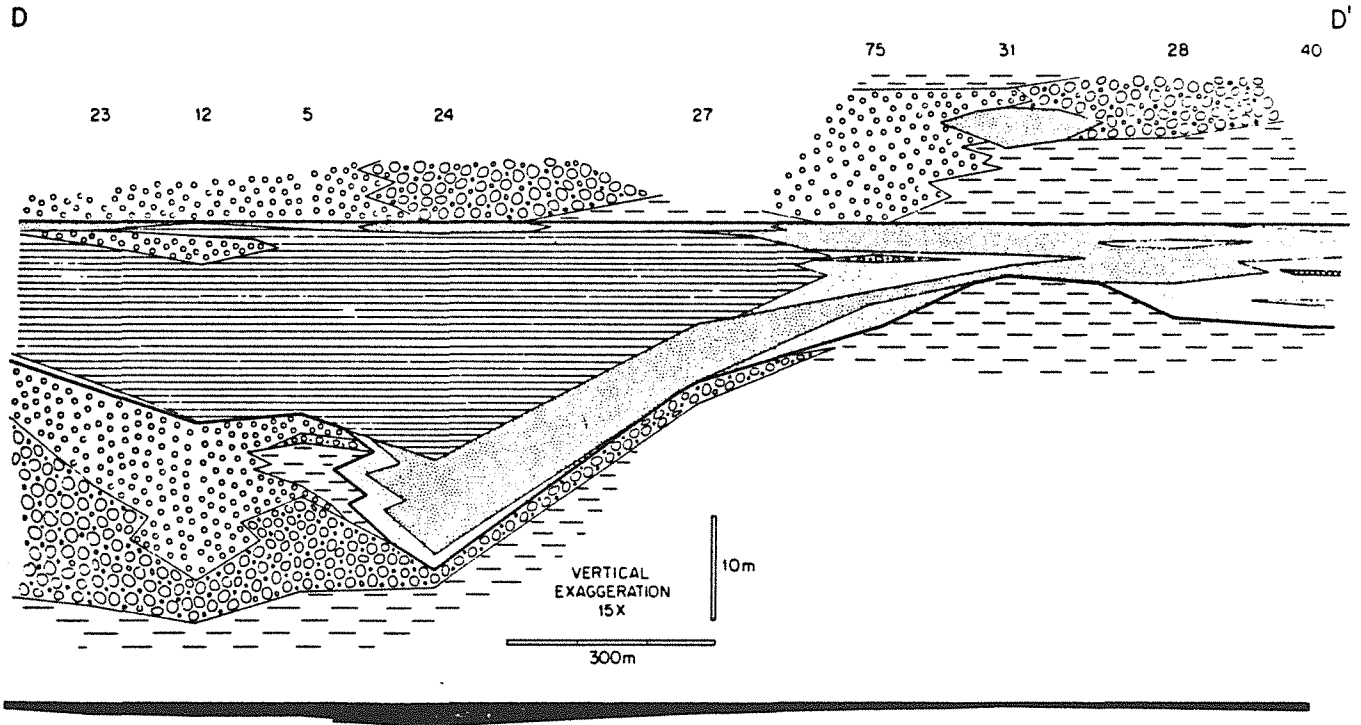


Figure 3.53 Stratigraphic cross-section D-D' of distal stratiform mineralization in Main zone area (north limb of Jason syncline) with 6.3X vertical exaggeration. Heavy black line encloses hydrothermal facies. Key same as in Figure 3.52. True scale cross-section shown in black at base. Location of section indicated on Figure 3.44a.

and have a low total pyrite content. These proximal quartz-sulfide strata average 3 to 7 percent Zn+Pb with Pb/Pb+Zn values of 0.09 to 0.25. Further from the breccia body the quartz-sulfide strata is rich in organic matter and has lower Pb/Pb+Zn values (0.03 to 0.08) though the percent Pb + Zn (2-7%) is similar to more proximal strata.

Quartz Facies

The quartz facies is defined by the presence of siliceous terrigenous sedimentary rocks and lack of barite or sulfide strata (Fig. 3.3). The quartz facies siliceous siltstone and argillite strata are similar to siliceous siltstone and argillite beds interbedded with the other stratiform facies. Typically the siliceous terrigenous strata are associated with abundant disseminated pyrite, celsian and hyalophane and ankerite/siderite (Fig. 3.28). Within the quartz facies there is a decrease in pyrite:siderite ratio away from the margins of the stratiform mineralization (Fig. 3.28).

The quartz facies is primarily a concordant body and forms a 1 to 5 m thick envelope overlying and underlying the barite and quartz-sulfide facies in the distal portion of the stratiform horizon (Figs. 3.45, 3.46, 3.52, 3.53) and may thicken at the margins of the deposit. This siliceous envelope is absent adjacent to the iron carbonate and pyrite facies near the Jason fault. The quartz facies has a discordant aspect within sedimentary breccias lying between the upper and lower stratiform horizons, a zone that connects the envelopes around the upper and lower horizons.

GRADED UNITS AND METAL CYCLES

Compositionally and texturally graded laminae and beds are a minor but widespread component of the stratiform ores. Three different graded units are recognized: sphalerite-quartz, sulfide-barite, and galena-sphalerite.

Graded quartz-sphalerite laminae up to 1.5 mm thick occur in the quartz-sulfide and barite sulfide facies; they are composed of faint fine-scale micro-laminae (0.01 to 0.1mm)

(Fig. 3.8). The thickest and most sphalerite-rich lamina commonly occur at the base of a cycle and are overlain by thinner alternating sphalerite-rich and quartz-rich quartz-sphalerite lamina.

The sulfide-barite cycles are comprised of sphalerite-galena laminae successively overlain by sphalerite-galena-barite laminae and uppermost barite laminae (Fig. 3.26). A cycle is typically 10 mm thick and occur where the barite facies interfingers with beds of the Pb-Zn-Fe sulfide facies.

Within the Pb-Zn-Fe sulfide facies, graded units of galena, sphalerite-galena and sphalerite laminae form bed sets that decrease upwards in thickness and in lead:zinc ratio. A typical graded unit is 0.4 m thick and composed of basal thick-bedded galena and galena-pyrite beds overlain by beds of sphalerite-galena that thin upwards and increase in sphalerite content. In the DDH 86A intersection of the upper horizon (Fig. 3.46), 7 stacked graded unit cycles occur over a 2 m interval; Pb/Pb+Zn decreases upward within each cycle as well as over the entire interval (Fig. 3.54).

The above descriptions allow the following generalizations to be made about graded cycles. The compositional and textural grading is characterized by: (a) an upward decrease in bed thickness within a laminae or bed set; (b) an upward change in the composition of the laminae that mimics the lateral mineralogical zoning within the stratiform body (e.g. galena to sphalerite, sulfide to barite, sphalerite to quartz); (c) laminae or beds that comprise the sets are typically polyminerallic, and the compositional grading reflects a systematic vertical change in the proportions of minerals within individual laminae or beds; (d) graded laminae and bed sets are best developed in the proximal part of the stratiform body; and (e) variation in the scale of graded units from millimeter scale cycles to meter scale cycles may result from similar processes but different rates or amounts of sedimentation.

Cyclic vertical changes, on a scale larger than graded units, also occur in the combined lead and zinc content and lead:zinc ratio within distal strata (Fig. 3.55). Such metal cycles, 2.5 to 5.0 m thick, occur in both the lower and upper stratiform horizons and are generally

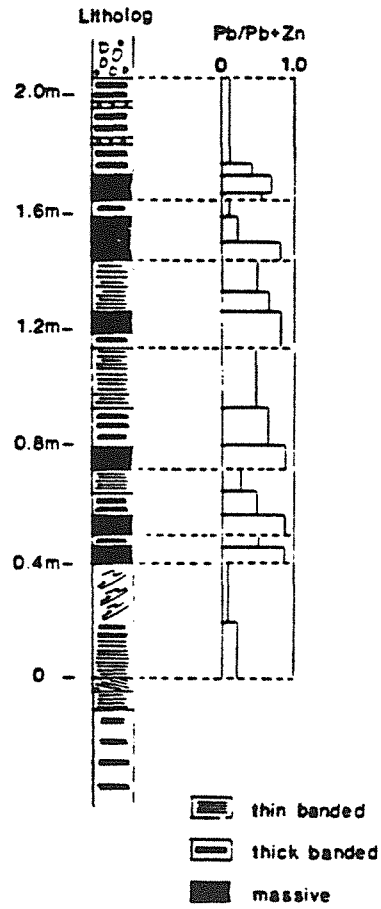


Figure 3.54 Lithological section of graded units of massive banded sphalerite-galena beds. DDH 86A- 667.7 669.25 m.

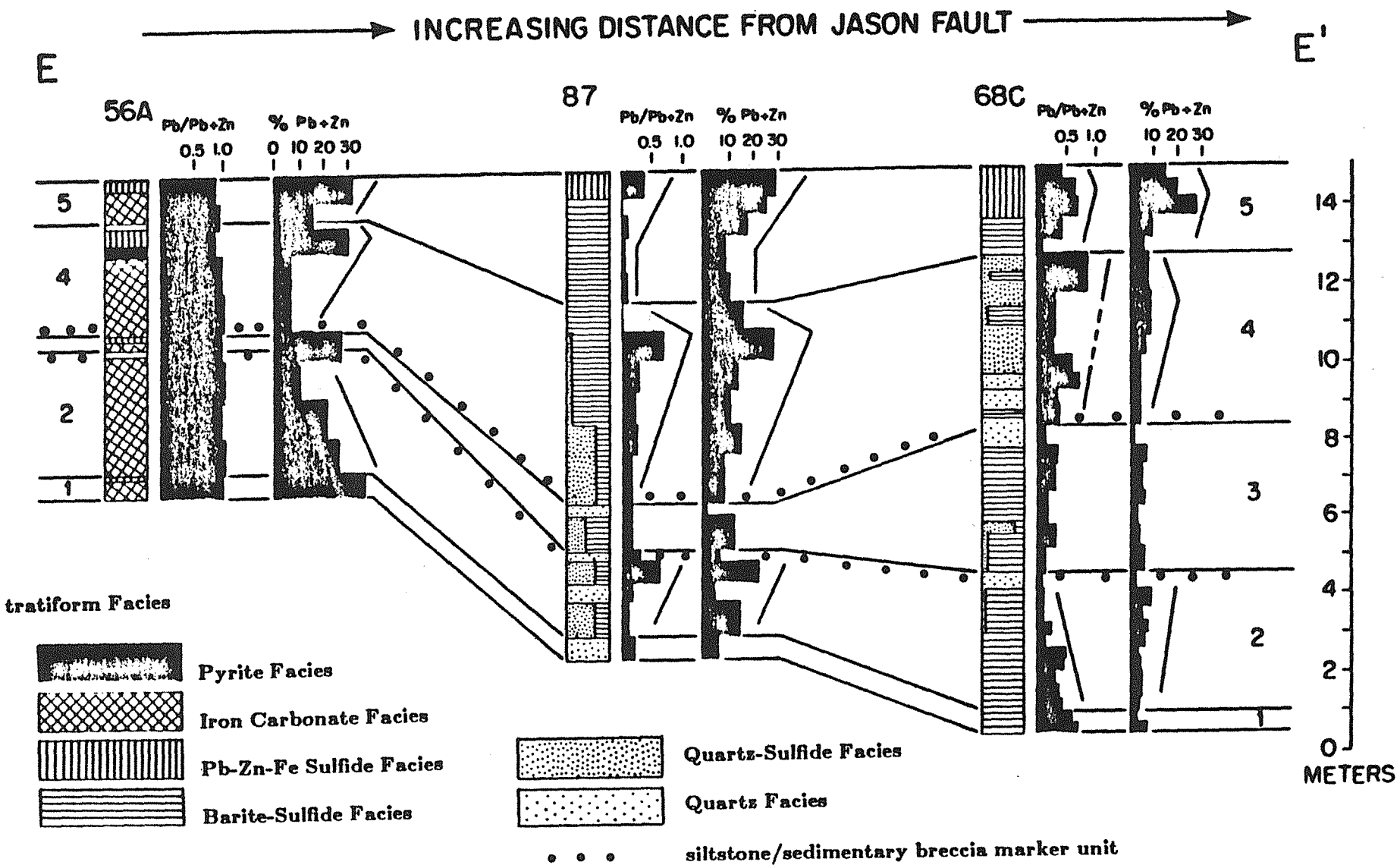


Figure 3.55 Correlation of metal cycles within iron carbonate, barite-sulfide and quartz-sulfide facies within upper stratiform horizon (DDH 56A, 87, 68C); the location of stratigraphic section E-E' is indicated on Fig. 3.44a. Stratigraphic lithologies indicate facies and proportions of facies within stratigraphic intervals; values of Pb/Pb+Zn and %Pb+Zn are indicated with black bars. Cycles of increasing %Pb+Zn and Pb/Pb+Zn are correlated between drill holes.

characterized by gradual upward decrease in %Pb+Zn and Pb/Pb+Zn followed by sharp decreases in total metal and Pb/Pb+Zn.

In the upper horizon, near the Jason fault, a cyclic repetition of iron carbonate facies and Pb-Zn-Fe sulfide facies beds occurs (Fig. 3.56). These cycles consist of (1) basal ankerite beds; (2) overlying Pb-Zn-Fe sulfide beds and (3) uppermost siliceous terrigenous sediment. Five such cycles ranging from 0.5 to 3 m in thickness comprise the central part of the iron carbonate facies (DDH 56A).

Metal cycles in the distal stratiform body, described previously, can be correlated with these iron carbonate:sulfide cycles (Fig. 3.55). Iron carbonate beds are laterally equivalent to the lead-poor, sulfide-poor bases of metal cycles; Pb-Zn-Fe sulfide facies beds are equivalent to lead-rich, sulfide-rich beds near the top of cycles.

STRONTIUM ISOTOPIC DATA

A suite of siderite, ankerite and barite samples were collected for strontium isotopic analysis. These included vein carbonates from the Jason fault, the footwall to the Jason fault, the breccia body and the proximal lower horizon as well as massive carbonate samples from beds in the lower and upper horizons. Barite laminae samples were collected to give vertical and lateral transects through the barite facies. Samples were submitted to Geochron Laboratories Ltd., Cambridge, Mass. for strontium isotopic analysis. Analysis of standard NBS-987 before and after analyses of both barites and carbonates averaged 0.71027 +/- .00003, and no adjustment was made.

The $^{87}\text{Sr}/^{86}\text{Sr}$ ratios ranged from 0.7729 to 0.7144 for barite samples and from 0.7137 to 0.7221 for carbonates (Fig. 3.59). Listed in order of decreasing $^{87}\text{Sr}/^{86}\text{Sr}$ ratio these samples are (Fig. 3.58): a) iron carbonates in the breccia body and the deep part of the Jason fault; b) massive proximal iron carbonate beds; c) iron carbonates in the shallow parts of the Jason fault; d) distal bedded iron carbonates and late carbonate-quartz-sulfide veins and e) laminated barite.

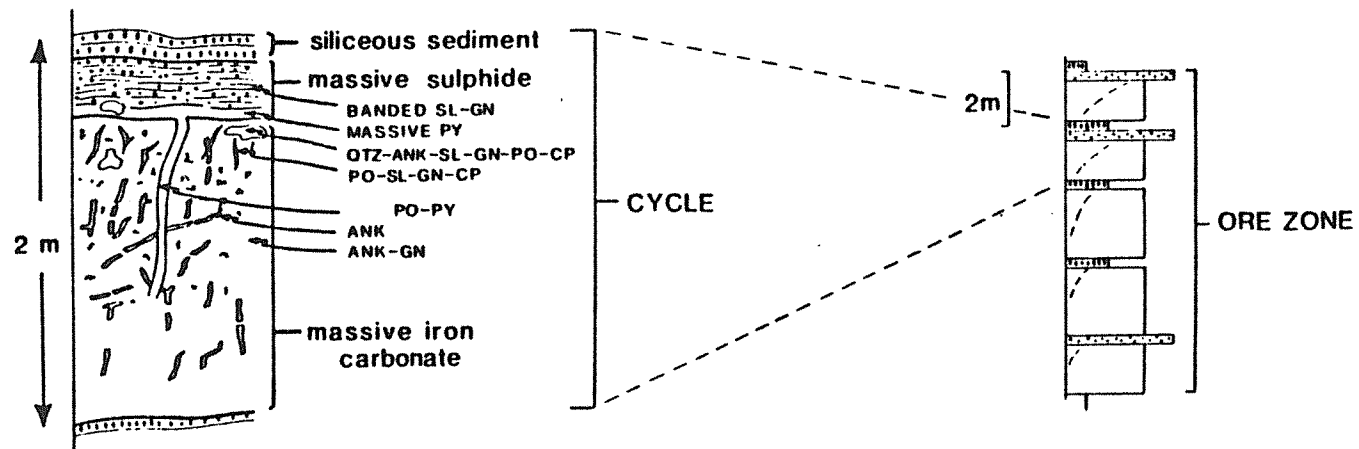


Figure 3.56 Schematic illustration of carbonate-sulfide cycle within the proximal part of the upper stratiform horizon. DDH 56A - 551-554 m. Abbreviations are: ANK, ankerite; CP, chalcopyrite; GN, galena; PO, pyrrhotite; PY, pyrite; SL, sphalerite.

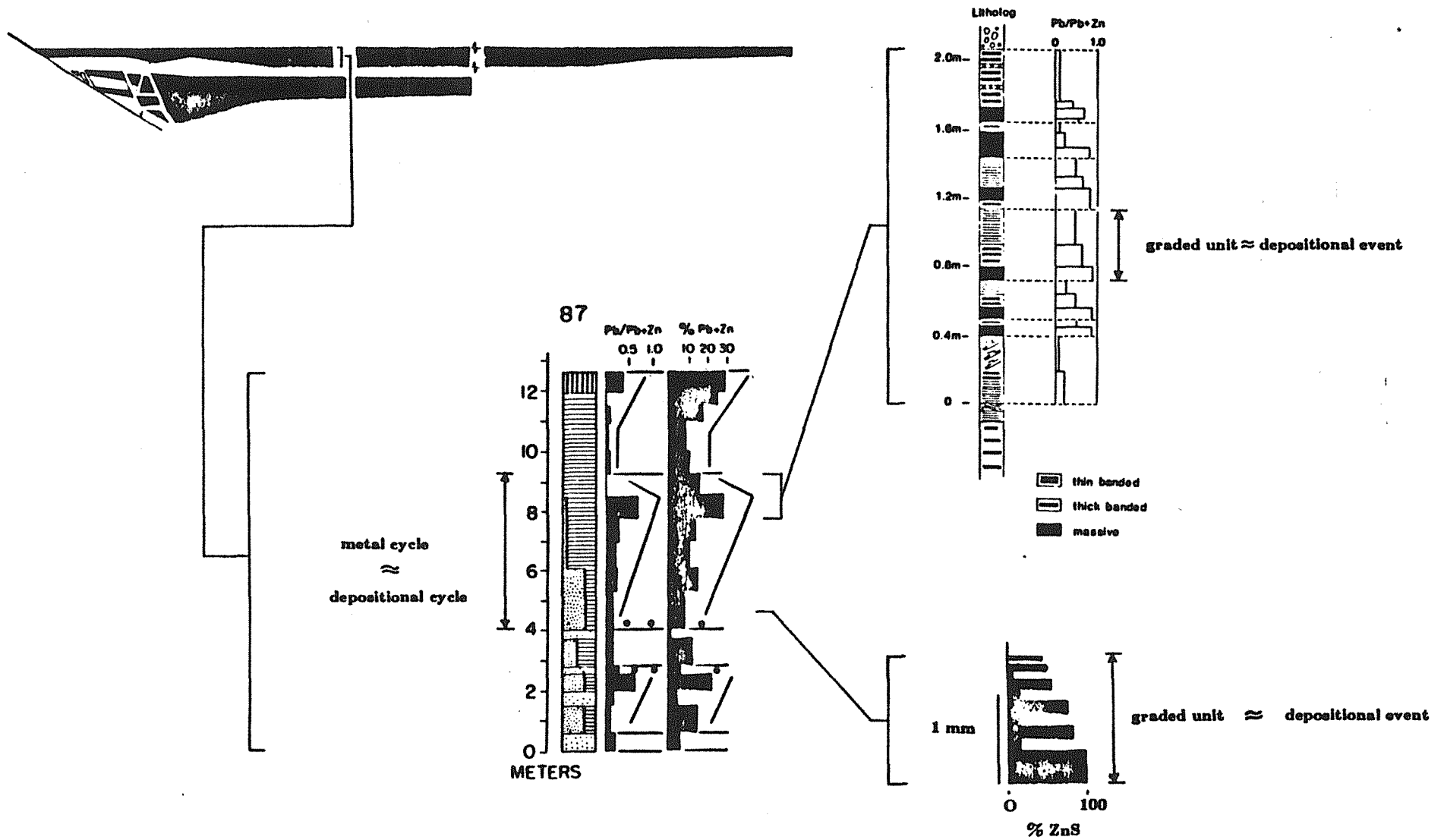


Figure 3.57 Relationship between graded units, depositional events, metal cycles, depositional cycles and the stratiform horizons. The setting of a graded sphalerite-quartz unit and graded sphalerite-galena units (Fig. 3.54) within larger metal cycles (Fig. 3.55) and the stratiform body (Fig. 3.45).

SEDIMENTARY ORIGIN OF THE STRATIFORM MINERALIZATION

Data from this study suggest the Jason deposit formed largely by exhalative processes on the seafloor based on (1) the resedimentation of sulfide beds; (2) the lack of terrigenous admixture in sulfide and barite strata; (3) the sedimentary character of laminae and beds; (4) the concordant nature of the stratiform body; (5) the distribution of mineralized veins and breccias; (6) the intercalation of stratiform minerals with mud-rich sediments.

Resedimented fragments of all hydrothermal strata types except iron carbonate beds are found. Resedimented textures include: (1) sulfide clasts within sulfide strata (Figs. 3.16,3.10); (2) terrigenous clasts within beds of sulfide strata (Fig. 3.23); (3) the truncation of stratiform beds at the top of the upper horizon by erosional surfaces and (4) clasts of stratiform sulfide within the sedimentary breccia beds overlying the upper horizon (Fig. 3.17). With respect to (3) and (4), sedimentary breccias both conformably and unconformably overlie the upper horizon; therefore the amount of downcutting by the sedimentary breccia was small. This argues for the existence of the stratiform sulfide on the seafloor prior to erosion.

The presence of sharp bedding contacts, stratiform and often planar lamination, lack of terrigenous admixture within sulfide, barite or iron carbonate strata, compositional and textural grading in some beds, and the absence of evidence for replacement of a terrigenous protolith by hydrothermal minerals in the distal parts of the orebody argue for a sedimentary origin of the bulk of the stratiform bodies.

Siltstone turbidites in the lower horizon are interbedded with beds of sulfide/sulfate strata; laterally equivalent turbidites outside the ore zone are interbedded with carbonaceous mudstone that represent hemipelagic sediment. Therefore, the hydrothermal sediments correlate laterally with hemipelagic matter outside the hydrothermal depocenter. The laterally extensive (>1000 m) and concordant nature of the stratiform horizons is compatible with a sedimentary mode of deposition. Except for resedimented veined clasts, veins and breccias only occur below the top of the upper horizon. The abrupt disappearance of veins at the top of the upper horizon suggests that the veining and brecciation took place when the

stratiform ores formed the seabottom.

The only evidence of replacement of terrigenous sedimentary strata by minerals that also occur in stratiform associations occurs adjacent to the breccia body where the breccia cuts the stratiform ores (e.g. iron carbonate replacement of siltstone beds). The lack of such replacement elsewhere suggests that the replacement represents alteration or remobilization associated with the formation of the breccia body.

An alternate model in which the stratiform body formed by the lateral infiltration of shallow sediments by hydrothermal fluids during diagenesis does not account for (1) the absence of sulfide and barite within the more permeable siltstone interbeds; and (2) the less extensive nature of the lower horizon with respect to the upper horizon in spite of being interbedded with coarser, and likely more permeable, sediments (siltstone turbidites versus shales). It is unlikely that fluids infiltrating laterally through such low permeability muds could remain at the same stratigraphic level for over 1 kilometer.

SEDIMENTATION BELOW A BRINE POOL

Types of Exhalative Environments.

Two end member types of hydrothermal exhalative environment are known within the modern ocean (Zierenberg, 1983). They are: (1) seawater mixing: hydrothermal precipitation +/- sedimentation from a buoyant plume discharged into ambient seawater (e.g. 21 N, East Pacific Rise) and (2) brine pool mixing: hydrothermal precipitation and sedimentation within a brine pool ponded in a topographic low on the seabottom (e.g. Atlantis II Deep, Red Sea). Strontium isotope data, stratigraphic relationships and the mineralogy of the deposit can be used to constrain the character of the exhalative environment during the formation of the Jason stratiform deposit.

Interpretation of Strontium Isotope Data

The large spread of strontium isotopic ratios in iron carbonates and barite samples from

the Jason suggest that the partial mixing of hydrothermal fluids and seawater took place during the precipitation of these iron carbonates and barite; listed in order of increasing degree of mixing with seawater, the setting of these samples are (Figs. 3.58, 3.59): a) the breccia body and veins within the deep part of the Jason fault; b) massive proximal iron carbonate beds with or without abundant veins; c) veins within the shallower part of the Jason fault; d) distal bedded carbonate beds and paragenetically late carbonate-quartz-sulfide veins and e) laminated barite. The apparent homogeneous character of the most radiogenic carbonates that occur in the fault and breccia body (i. e. 0.07221) suggests precipitation from a homogeneous and hence unmixed hydrothermal fluid.

Anhydrite precipitated within a seawater-mixing exhalative environment in the modern ocean show a range of values of $^{87}\text{Sr}/^{86}\text{Sr}$ up to the strontium isotopic value of ambient seawater (Albarede, 1981). This distribution is distinct from the $^{87}\text{Sr}/^{86}\text{Sr}$ values of anhydrite deposited within the present brine pool of the Atlantis II deep which show a distinct shift from ambient seawater values (Zierenberg and Shanks, in press).

Strontium isotopic ratios for barite samples from the Jason can be compared to these modern sulfates. The strontium isotopic composition of the ocean has changed with time; during the Late Devonian the $^{87}\text{Sr}/^{86}\text{Sr}$ ratio of seawater was approximately 0.7083 (Burke et al., 1983). This accords with the $^{87}\text{Sr}/^{86}\text{Sr}$ values of 0.7084 from Late Devonian age stratiform barite deposits in the eastern Yukon (pers. comm., W. Goodfellow, 1986) which are interpreted to have formed in seawater from the mixing of seawater with Ba-rich hydrothermal fluids. The range of strontium isotopic ratios in barite from the Jason deposit is very similar to that of the Atlantis II Deep; barite values cluster over a narrow range that

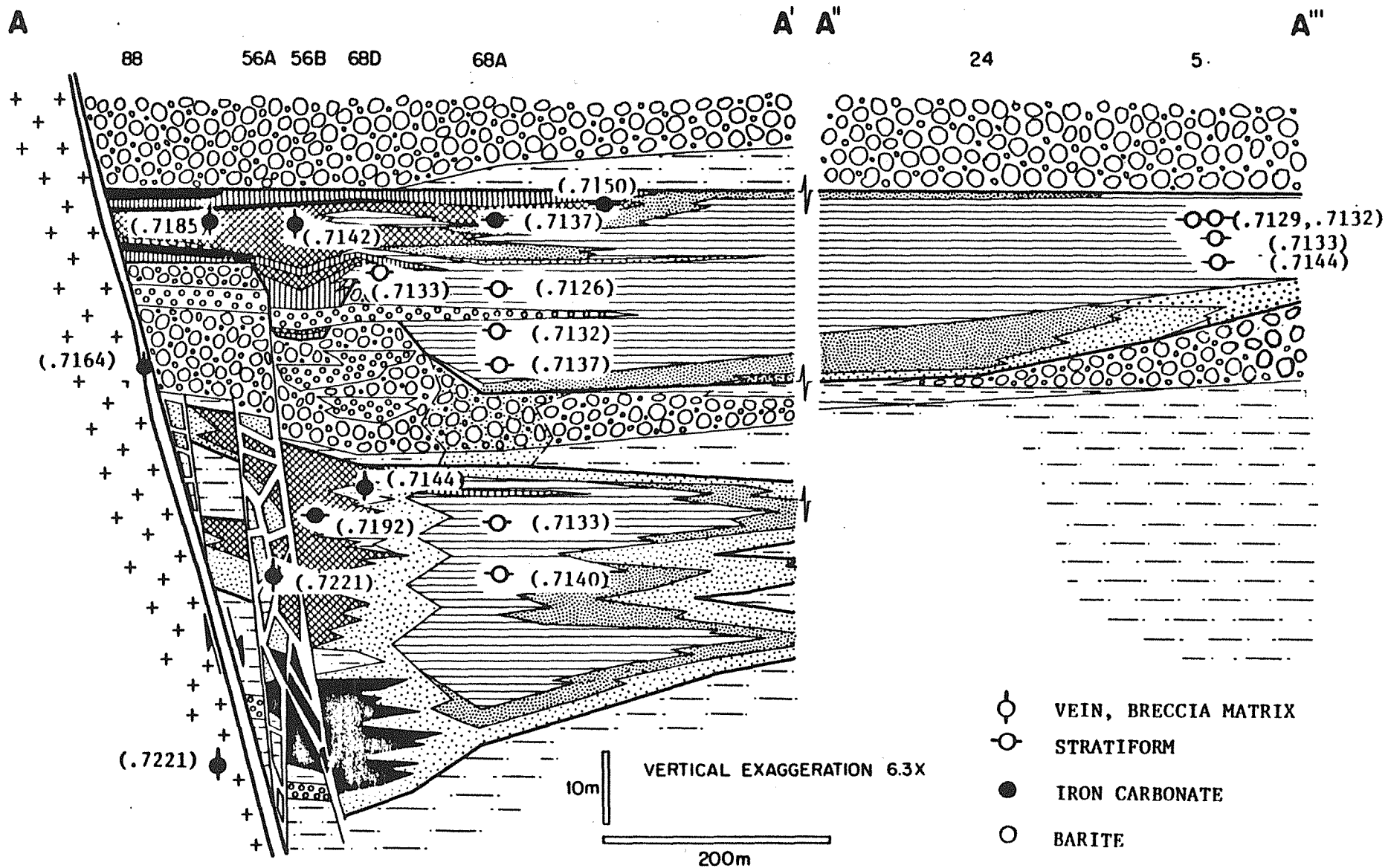


Figure 3.58 Stratigraphic cross-section A-A' (Fig. 3.45) with approximate locations of samples taken for strontium isotopic analysis. Samples not on section are projected to their approximate location.

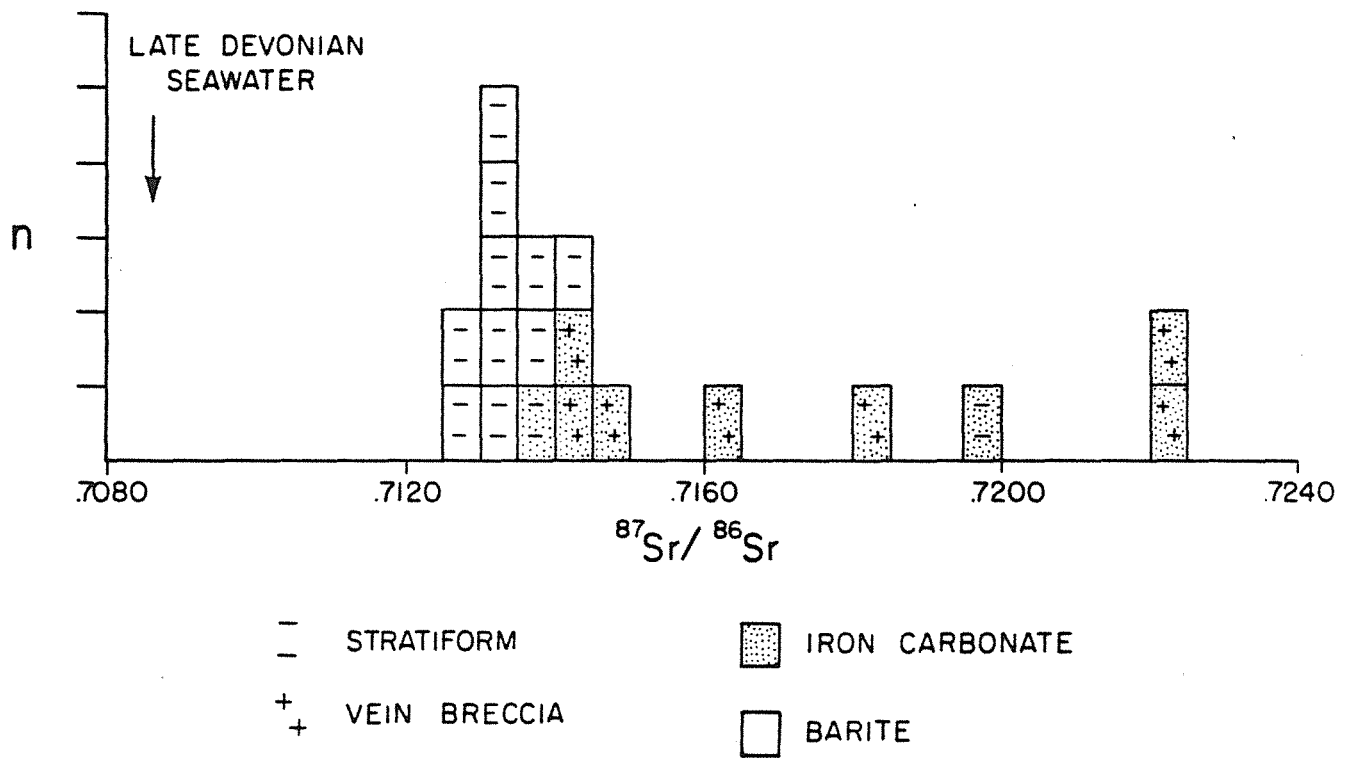


Figure 3.59 Histogram of $^{87}\text{Sr}/^{86}\text{Sr}$ values for iron carbonate and barite samples; strontium isotopic value for seawater of Late Devonian age is from Burke et al. (1982).

is distinct from that of Devonian seawater as well as that of the proposed hydrothermal fluid composition (i. e. 0.7221). Barite samples show little variation (0.7129 to 0.7144) regardless of stratigraphic position or lateral position within the barite facies. Thus the barite precipitated from a homogeneous fluid whose composition varied little in space or time yet was distinct from Devonian seawater. This suggests that barite precipitated from a well mixed water mass of composition intermediate between the hydrothermal fluid and seawater, such as a brine pool.

The broad scatter of strontium isotopic values in carbonate samples (Fig. 3.59) up to values equivalent to those of barite may indicate that the carbonates precipitated during various stages of subsurface mixing of the hydrothermal fluid with shallow connate fluids, i.e. Devonian seawater.

Textural Similarity to Modern Brine Pool Sediments

The only occurrence in the modern ocean of actively forming laminated and laterally extensive hydrothermal sediments similar to those in the Jason deposit occur below the brine pool of the Atlantis II deep within the axial rift zone of the Red Sea (Bischoff, 1969). These brine pools are the result of presently active hydrothermal discharge of very saline fluids; laminated metalliferous sediments extend over a 14 by 5 km area (Backer, 1972). In contrast, sulfide and sulfate associated with hydrothermal vent areas at 21° N EPR that discharge directly into seawater are characterized by very locally developed mounds and chimneys of massive to irregularly banded aggregates and lack laminated sediments (Goldfarb et al., 1983).

Stratigraphic Evidence for Bathymetric Control of Hydrothermal Deposition

As topographic lows are commonly noted immediately adjacent to active normal faults (Wallace, 1978), the occurrence of the Jason stratiform horizons immediately adjacent to an active synsedimentary fault (Chapter 2) suggests that sedimentation occurred within a bathymetric low at the base of the fault. The decrease in thickness of the upper horizon

away from the Jason fault (Fig. 3.45) suggests deposition within a trapdoor-style half graben. In addition, thickness variations of the upper horizon (Fig. 3.44d) indicate a trough-like depocenter parallel to the orientation of lobes of sedimentary breccia that underlie the upper horizon (Chapter 2) and at high angle to the trend of the Jason fault. Stratigraphic thinning of the stratiform mineralization coincident with thickening of the underlying sedimentary breccia beds occurs both near the Jason fault (Fig. 3.45; DDH 56A to DDH 68A) and in the distal part of the stratiform mineralization (Fig. 3.53; DDH 23 to DDH 24). The bathymetric relief of these lobes during hydrothermal deposition was likely equivalent to their present thickness, which near the Jason fault exceeds 20 m. Further away from the Jason fault and coincident with the thinning of these sedimentary breccia deposits, hydrothermal sedimentation was more laterally extensive (e.g. Main zone area). These data suggest that hydrothermal sediments preferentially accumulated between debris flow lobes within a trapdoor style half graben. Such bathymetric control of the distribution of hydrothermal sediments might be expected from a brine pool that was also confined to this bathymetric low.

Quartz-Rich Nature of Stratiform Mineralization

Quartz is virtually absent from smokers at 21 N, East Pacific Rise (Haymon and Kastner, 1981) even though hydrothermal fluids at 350° C are supersaturated with respect to quartz (Edmond et al., 1982). Thermodynamic modelling suggests that the mixing of these hydrothermal fluids with seawater does not lead to saturation with respect to amorphous silica in spite of the thermal quench, because the dilution with seawater offsets the decreasing solubility of the silica (Janecky and Seyfried, 1984). Kinetic effects impede quartz precipitation in water masses due to a lack of surface area for quartz nucleation (Rimstidt and Barnes, 1981) and the silica is dispersed into the water column. In contrast, the lower brine of the Atlantis II deep is saturated with respect to amorphous silica and is currently precipitating amorphous silica in the water column (Shanks and Bischoff, 1977); underlying

metalliferous sediments are rich in amorphous silica (Bischoff, 1969). Precipitation of amorphous silica is favored in this environment because (a) discharging hydrothermal fluids mix with brine pool waters that are saturated with respect to amorphous silica rather than undersaturated seawater and (b) the closed nature of the brine pool circulation prevents the dispersion of the silica until it precipitates. Thus, there is a marked difference in the depositional behavior of silica in seawater mixing versus brine pool mixing; quartz-rich exhalative mineralization such as at Jason suggests deposition within a brine pool environment.

Formation of a Brine Pool from Hot, Low Density Fluids

The presence of a brine pool requires that the ponded hydrothermal fluids be more dense than the ambient overlying seawater. However, calculations by Gardner (1985) from fluid inclusion studies at the Jason deposit indicate that the hydrothermal fluids were less dense than seawater (0.89 g/cc). This type of submarine discharge would be buoyant in seawater and form a widely dispersed deposit. This contradicts evidence presented above for the presence of a brine pool during deposition of the Jason mineralization.

An alternate possibility has been provided by recent hydrological modeling. Theoretical and experimental modeling of the fluid dynamics of hot saline fluids discharged into a submarine depression indicates that a heated fluid more saline but less dense than seawater will pool on the seabottom if it mixes upon discharge with a pre-existing brine pool (McDougall, 1984a,b). This modeling requires that the earliest hydrothermal discharge is denser than seawater so that a ponded layer forms. Once such a layer is formed it is no longer necessary for hydrothermal fluids to be more dense than seawater to maintain the brine pool. A double diffusive interface develops at the top of the brine and fluxes of heat and salts occur across it. The large ratio of heat to salt flux maintains the high density of the ponded layer.

An early phase of dense brine discharge might be expected within a submarine exhalative system because early hydrothermal discharge migrating along a fault conduit at

shallow depths would be conductively cooled (versus cooling by mixing) by cold wall rock. Such cooling of a saline fluid will create a dense fluid. At Jason there is evidence for an early period of low temperature hydrothermal discharge. The lowest and hence earliest deposited hydrothermal strata in the upper horizon are thin beds of nodular barite that lack any associated sulfide mineralization. Sulfide deficient barite deposits in the Macmillan Pass area are interpreted as the product of hydrothermal fluid discharge at temperatures less than 100° C, based on mineral assemblages and interpreted mineral solubilities (Lydon et al., 1985).

Comparison to the Atlantis II Brine Pool

If the stratiform ores of the Jason deposit formed below a brine pool, then the Atlantis II deep provides a modern depositional analogue and can be used to provide insights into: (1) the hydrodynamics of brine circulation; (2) the mechanisms of precipitation and sedimentation of the hydrothermal minerals; and (3) the character of hydrothermal sediments. The lower brine within the stratified Atlantis II deep brine pool is up to 150 m thick and represents cooled (61.5 C) but undiluted discharge (Craig, 1969) of hydrothermal fluids that vented at temperatures up to 300 C (Zierenberg, 1983; Pottorf and Barnes, 1984). Upon discharge through the seafloor into the brine pool, the hot fluids rise buoyantly while mixing and cooling to temperatures close to the ambient brine pool temperature. At the density interface at the top of the lower brine mass, the hydrothermal plume is more dense than fluids in the overlying mixed seawater-brine transition zone and spreads laterally throughout the entire Atlantis II basin (Schoell, 1976). Though data are scant, it can be surmised that sulfides precipitated during quenching are entrained by this rising plume and transported upwards and laterally. Precipitation of hydrothermal sulfides occurs during mixing in the subsurface (e.g. chalcopyrite, pyrrhotite, cubanite), during early mixing in the brine pool (e.g. sphalerite, pyrrhotite, galena) and while mixing with the overlying more oxygenated transitional brine (e.g. barite) (Shanks and Bischoff, 1977; Pottorf and Barnes, 1983). The order of precipitation of sulfide phases is controlled by their relative solubilities during the mixing process; however deposition is controlled by the processes of hydrodynamic dispersion

and mechanical sedimentation. Laminated and bedded metalliferous muds that occur at the base of the brine pool are composed of amorphous, poorly crystalline and crystalline silica, iron montmorillinites, iron hydroxides, sulfides and carbonates (Bischoff, 1969) and are the result of sedimentation from the overlying brine (Shanks and Bischoff, 1977). Over 90 percent of the hydrothermal material is less than micron in size; though rare fragments of cubanite-pyrrhotite up to 30 microns in diameter occur within the sediments must represent subsurface minerals carried by the discharging fluids to the seafloor (Pottorf and Barnes, 1983). Water content of the hydrothermal muds exceeds 90 percent by weight (Bischoff, 1969).

The grain size in the bulk of the distal Jason stratiform facies varies from 5 to 40 microns (0.005-0.040 mm). Assuming that the original Jason hydrothermal sediments were sub-micron particles similar to those of the Red Sea brine pools, the present Jason stratiform mineralization reflects crystallization and recrystallization during diagenesis and later regional sub-greenschist grade metamorphism. Therefore the present mineral textures reflect this diagenetic and metamorphic overprint and some aspects of the primary hydrothermal sediment have been obscured.

TEMPORAL AND SPATIAL MODEL FOR MINERALIZATION

If the timing of mineral deposition is compared to the timing of terrigenous sedimentation and secondly to the Mesozoic age deformation, then 3 stages of mineral deposition can be deduced. Stage 1 mineral deposition coincided with terrigenous sedimentation; Stage 2 postdated terrigenous sedimentation but pre-dated deformation and largely represents early diagenetic mineral growth and; Stage 3 was synchronous with or postdated deformation of Mesozoic age.

Paragenesis Within Distal Stratiform Body

Strata types in the distal stratiform body are characterized by xenomorphic granular aggregates that reflect equilibrium textures formed during diagenetic or metamorphic recrystallization. The sphalerite, galena, barite and quartz represent the earliest mineralizing

event (Stage 1) and are interpreted to have formed as sediments synchronously with the interbedded terrigenous sediments (Fig. 3.60). Framboidal pyrite and some component of the disseminated euhedral/subhedral pyrite may belong to Stage 1 if they represent crystallization in the water column as has been noted in the Black Sea. Quartz and pyrite continued to form after Stage 1; quartz bands, quartz-cemented siltstones and mudstones, and probably most of the subhedral/euhedral pyrite formed during Stage 2. Disseminated celsian, pyrite, ankerite and siderite are euhedral in shape and appear to postdate earlier stratiform mineralization or terrigenous sediments. Planar extension quartz veins in siliceous terrigenous beds likely formed concurrent with folding and extension of the stratiform deposit on the limb of the tight Jason syncline during Mesozoic deformation (Stage 3).

Paragenesis In Proximal Stratiform Body, Breccia Body and Fault

In the proximal stratiform body, the bulk of the sphalerite, galena, pyrite, siderite and ankerite that comprise the hydrothermal strata are Stage 1 minerals. However, there is abundant replacement of these Stage 1 minerals and various replacement reactions are evident: sphalerite by chalcopyrite, pyrite by sphalerite and galena, pyrrhotite by pyrite, siderite by ankerite, and ankerite and siderite by pyrrhotite and galena. This younger mineralization is interpreted as Stage 2. Irregular nodules of pyrite, quartz and ankerite formed during Stage 2; the increase in average grain size of Stage 1 minerals towards the breccia body and Jason fault suggests recrystallization during Stage 2.

A consistent paragenetic order of Stage 2 veinlets occurs within the fault footwall, fault, breccia body and the proximal stratiform mineralization (Fig. 5b). This paragenesis is: (1) carbonate veinlets; (2) carbonate-muscovite-sulfide veinlets; (3) sulfide veinlets and associated pyrrhotite and galena replacement of carbonate; (4) carbonate-quartz-sulfide veinlets. The early carbonate veinlets (siderite/ankerite) include fine-grained siderite in the Jason fault and matrix of the breccia body, and also as coarse-grained ankerite veins. Carbonate-muscovite-

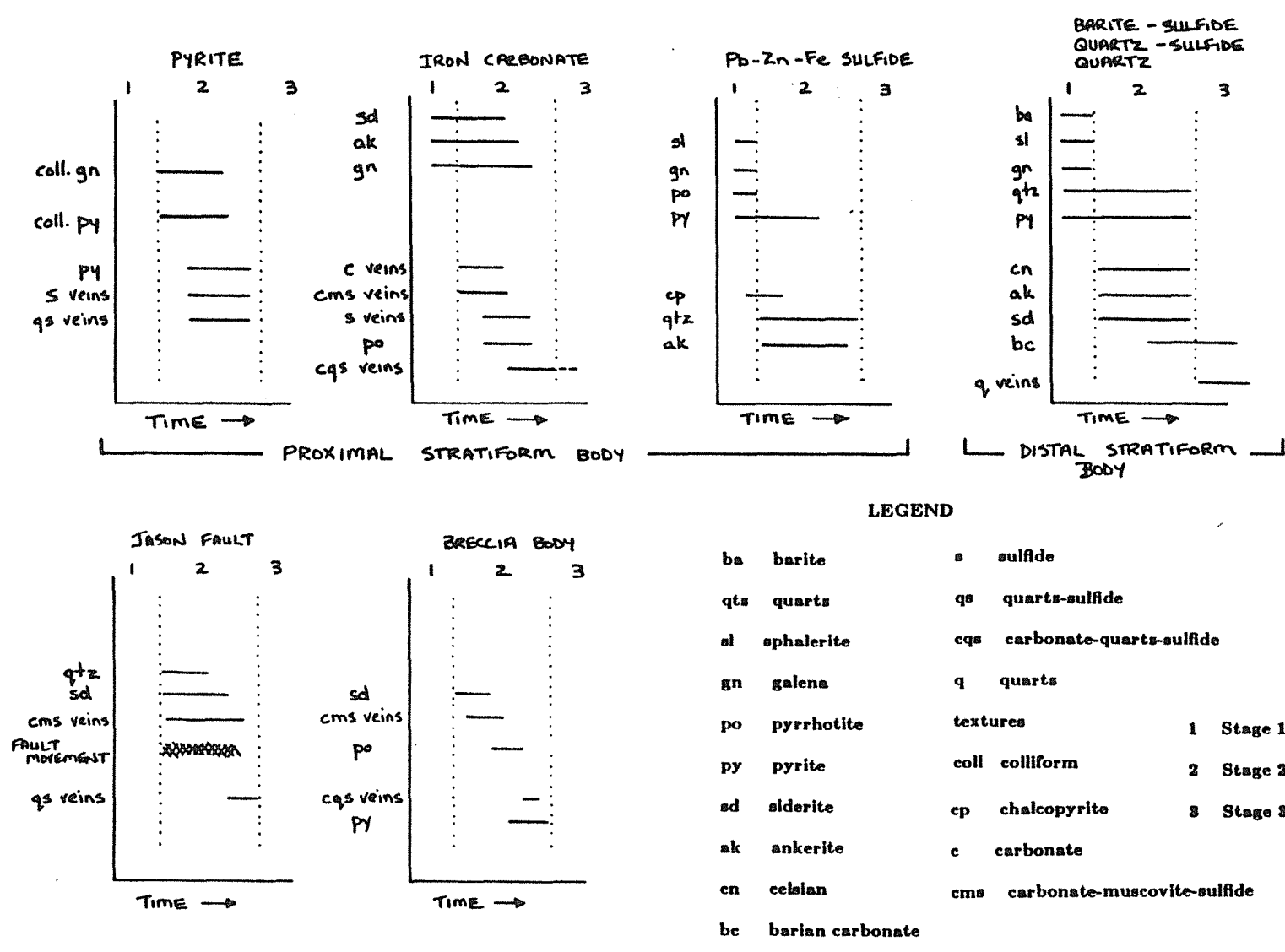


Figure 3.60 Paragenetic order of minerals within the Jason fault, breccia body and stratiform facies.

sulfide veinlets change vertically over tens of feet from a medium-grained siderite-muscovite assemblage at depth (e.g. fault, breccia body) to a fine-grained massive muscovite-ankerite-sphalerite assemblage at shallower levels. Sulfide veinlets are also vertically zoned from a chalcopyrite-pyrrhotite assemblage in the breccia body and adjacent lower horizon to sphalerite-galena-pyrrhotite and pyrite-pyrrhotite in the upper horizon. Disseminated pyrrhotite +/- galena replacement, quartz rich vein sets and disseminated pyrite replacement are more abundant within the stratiform mineralization than in the deeper breccia zone or fault.

Variation in the Depositional Environments: Hydrothermal Facies

Subsurface Environment, Vent Complex

A close genetic tie between hydrothermal fluids that formed the Stage 2 minerals in the breccia body and veinlets in the stratiform horizon and the hydrothermal fluids that formed the Stage 1 stratiform horizons is suggested by: (1) the zone of abundant Stage 2 veinlets in the upper horizon coincides with the extent of and the underlying breccia body as well as with the highest Pb/Pb+Zn values in the Stage 1 stratiform ores (Fig. 6b); (2) the irregular and pod-like character of the bulk of the Stage 2 veinlets suggests they formed prior to the lithification of the strata they cut; and (3) the absence of such Stage 2 veinlets and breccias within strata overlying the upper stratiform horizon indicating that they formed prior to the deposition of these overlying sediments; (4) Stage 2 iron carbonate veinlets in the footwall of the Jason fault have Sr isotopic values identical to those of iron carbonates in the matrix of the breccia body; and (5) the brecciation of all siderite veins within Jason fault suggests formation of veins synchronous with fault movement during the Late Devonian (Chapter 2).

The predominant occurrence of Stage 2 discordant mineralization within the proximal stratiform mineralization as disseminated grains, pods and irregular discontinuous veinlets indicates that the host ankerite-siderite beds were permeable and unlithified during this mineralization event. The nodular shape of Stage 2 quartz pods is similar to the texture of

anhydrite nodules growing within the metalliferous sediments of the Atlantis II deep that are described by Zierenberg and Shanks (1983). More throughgoing Stage 2 veinlets are only common later in the paragenetic sequence; this implies that with time a progressive induration of the vent area sediments occurred.

Widespread metasomatism of the vent area is evident from the abundant pyrrhotite and galena replacement of iron carbonate and widespread ankerite and quartz growth. Discordant ankerite and quartz occurs as pods and irregular veinlets of ankerite and pods of quartz within the massive ankerite or ankerite-galena beds, as pods of ankerite and quartz in Pb-Zn-Fe facies beds interbedded with the iron carbonate facies beds and as banded beds that replace adjacent barite facies and quartz-sulfide facies strata at the periphery of the iron carbonate facies. Massive carbonates cut by abundant ankerite veinlets have very radiogenic Sr ratios (0.7175-0.7195) which indicate that these carbonates were precipitated largely in the subsurface prior to the mixing of hydrothermal fluids with brine pool fluids.

The scatter of initial Sr values (0.7221-0.7135) for Stage 2 vein carbonates suggest that significant mixing occurred between hydrothermal fluids and shallow connate fluids below the seafloor. The strontium isotopic ratio of ankerite in late stage ankerite-quartz-galena veins is equivalent to values in iron carbonate and barite strata. This is very surprising and raises the possibility that convected brine pool fluids may have been the dominant fluid during late stage vein deposition.

The presence of mineralogical zoning present in Stage 2 veinlet sets may reflect a subsurface thermal gradient due to subsurface mixing. Stage 2 pyrrhotite+/-galena-sphalerite-chalcopyrite-pyrite veinlets are zoned from a pyrrhotite-chalcopyrite assemblage in the breccia body to pyrrhotite in the lower horizon adjacent to the breccia body to pyrrhotite-galena-sphalerite-chalcopyrite and pyrrhotite-pyrite in the upper horizon. This pyrrhotite-rich deposition is interpreted to reflect one period of veining that formed during the deposition of the upper horizon and was superposed on the underlying lower horizon near the breccia body. The occurrence in a core sample of a pyrrhotite-pyrite vein merging

upwards with an overlying pyrite bed (Fig. 3.56) is interpreted to indicate that the fluids that precipitated the pyrrhotite +/- sphalerite-galena-chalcopyrite-pyrite in the subsurface as veins or as the replacement of carbonate continued upwards and exhaled into seawater to form massive sulfide beds of pyrite.

Vertical changes also occur in carbonate-muscovite-sulfide veins; muscovite becomes more abundant and finer-grained upwards. Massive fine-grained clays may reflect rapid precipitation of neoform clays (McLeod and Stanton, 1984) due to quenching of the hydrothermal fluids via subsurface mixing.

Iron Carbonate Facies

The origin of siderite or ankerite beds is ambiguous due to their recrystallized and coarse-grained nature; however they likely are analogies of manganosiderite sediments in the Atlantis II deep (Pottorf and Barnes, 1983). Iron carbonate beds peripheral to the vent area are massive in nature, stratiform in character and similar in strontium isotopic composition to stratiform barite. All of this suggest that iron carbonate was deposited as a sediment on the seafloor. The very radiogenic character of vent area massive carbonates is likely due to metasomatism of these early formed carbonate sediments by discharging fluids. The abundance of discordant mineralization in the central part of the iron carbonate facies in the upper horizon and its location above the breccia body indicates it was a zone of vertical fluid flow and discharge into the overlying seawater. Galena-rich carbonate beds in which galena is interstitial to carbonate grains suggests formation as galena-rich carbonate sediments; subsequent recrystallization and crystal growth of carbonate grains resulted in the interstitial position of the galena.

Pyrite Facies

The occurrence of the pyrite facies immediately adjacent to the Jason fault in the upper horizon as well as its massive thick-bedded nature and the abundance of veins and breccias indicates that it represents part of the vent area for the stratiform body. The sharp contacts of massive beds with interlayered terrigenous sediments and the abundance of resedimented

pyrite (Fig. 3.16) indicate pyrite formed as accumulations on the seafloor.

The growth banded and colliform fine-grained pyrite is interpreted to have formed by precipitation of pyrite and galena from venting fluids within the top of a sulfide mound as has been described for ocean ridge vent mounds (Goldfarb et al., 1983). Growth band textures are interpreted to reflect insitu precipitation on a substrate within the sediment pile. These colliform textures are very similar to fine-grained pyrite-galena-sphalerite intergrowths illustrated by Eldridge et al. (1983) from the outer margin of Kuroko massive sulfide deposits. The abundance of veins indicate vertical fluid flow and subsurface precipitation of quartz, sphalerite, galena and chalcopyrite; the recrystallization of fine-grained pyrite and galena to medium-grained pyrite associated with these veins suggests prograde metasomatism of earlier, more peripheral precipitates as has been described for Kuroko deposits (Eldridge et al., 1983).

The absence within the pyrite facies of any iron carbonate veinlets that are so ubiquitous within the iron carbonate facies suggest that during the formation of the pyrite vent complex the fluid chemistry was different than during the formation of the iron carbonate vent complex. The iron carbonate facies is likely the exhalative equivalent of the early siderite and iron carbonate-muscovite-sulfide veinlet sets. The pyrite facies (+/- Pb-Zn-Fe sulfide facies) is the exhalative equivalent of the later pyrrhotite +/- sphalerite, galena, chalcopyrite, pyrite vein set. This is supported by the observation that pyrrhotite-pyrite veinlets cut iron carbonate beds and merge upwards into a massive pyrite bed in core.

The origin of the pyrite facies in the lower horizon is more ambiguous because of the superposed metasomatism associated with the breccia body. However, the concordance of the pyritic facies, the occurrence of floating clasts of chert within massive pyrite suggestive of resedimentation of sulfide and general interbedded character of siltstone beds with pyrite are taken to suggest a sedimentary origin similar to the upper horizon. The local replacement of siltstone beds by pyrite (Fig. 3.22) is interpreted to be the result of the reaction of pyritic sediments with later infiltrating hydrothermal fluids during formation of the breccia body.

Pb-Zn-Fe Facies

Pb-Zn-Fe sulfide facies beds are interbedded both with vent-related facies and also with more distal laminated facies. Their thicker bedded and commonly poorly laminated character suggest formation as a rapidly deposited, proximal sediment (Fig. 3.61). Rapid deposition of sphalerite and galena likely occurred from either the initial lateral spread of the plume along the top of the brine pool (Fig. 3.61, 10) or density flow of sphalerite- and galena-rich bottom-hugging density flows (Figure 3.61, 8) formed by plume collapse (cf., Turner and Gustafson, 1978). The discontinuous nature of the sphalerite-galena laminae also may reflect reworking and erosion in a turbulent environment proximal to the hydrothermal vent. The widespread resedimentation of this facies must indicate deposition on a slope, perhaps of the fault scarp or the vent mound. Fault activity and high pore water pressures adjacent to the vent area may have acted as destabilizing forces. The entire ore zone adjacent to parts of the Jason fault (e.g. DDH 41) are comprised of massive Pb-Zn-Fe sulfide and resedimented Pb-Zn-Fe sulfide. Pyrite clasts may reflect entrainment and transport of pyritic vein walls by discharging fluids; such processes have been invoked to explain 100 micron grains of pyrrhotite within much finer grained hydrothermal sediments in the Atlantis II deep (Pottorf, 1983).

It is unlikely that the coarser-grained nature of the Pb-Zn-Fe sulfide facies with respect to more distal sediments reflects the sedimentation of coarser grains close to the vent area; rather, post-depositional recrystallization of sulfides by percolating hydrothermal fluids in the vent area may have enhanced recrystallization. The consistent average grain size within beds, the abundance of nodular mineralization and the coarsening of sulfides adjacent to the quartz and ankerite nodules supports this interpretation. Such widespread recrystallization of early fine-grained sulfides and barite related to vent proximal prograde hydrothermal activity that deposited the Kuroko deposits is recognized by Eldridge et al., 1983.

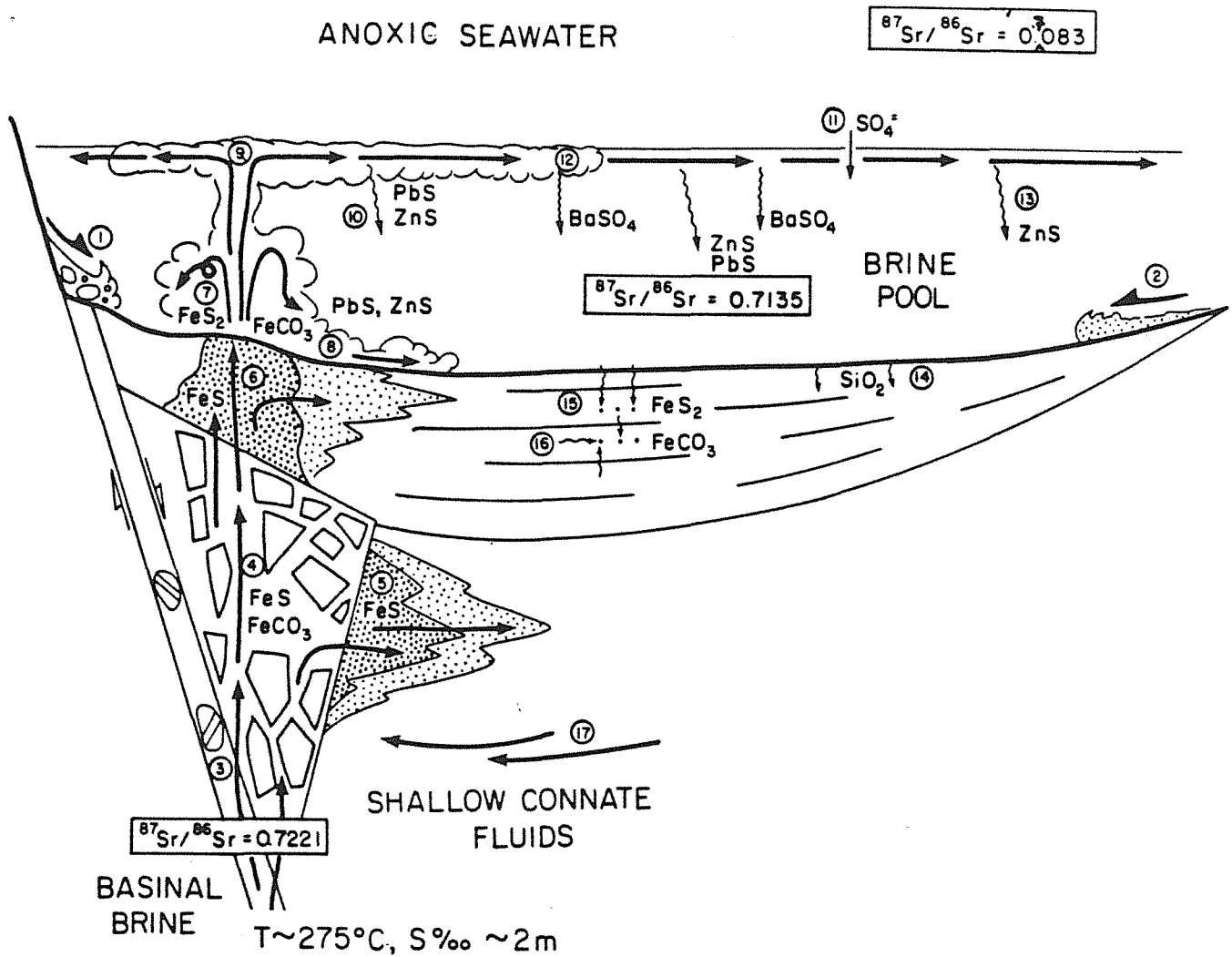


Figure 3.61 Schematic cross-section of brine pool environment adjacent to the Jason fault scarp illustrating hydrothermal, sedimentary and hydrographic processes. Representative processes are numbered: (1) debris flow from Jason scarp; (2) silt-rich turbidity flow, distal scarp source; (3) ascent of hot metalliferous brine on fault during periods of fault activity; (4) brecciation of indurated sediments, precipitation of iron carbonates, barian muscovite and pyrrhotite; (5) lateral infiltration of fluids into adjacent sediments; (6) recrystallization and replacement of vent complex sediments by iron carbonates and pyrrhotite; (7) venting and rapid mixing of hydrothermal fluids with ambient brine pool waters causing rapid precipitation and sedimentation of pyrite and siderite on the vent mound; (8) quenching causes rapid precipitation of galena and sphalerite, episodic collapse of hydrothermal plume due to mixing that causes negative buoyancy (cf., Turner and Gustafson, 1978), sedimentation of galena and sphalerite as graded sulphide beds from turbidity clouds; (9) bouyant rise of hydrothermal plume to top of brine pool; (10) lateral spread of plume causes rapid sedimentation of entrained sulfide; (11) diffusion of seawater sulfate into brine pool; (12) precipitation of barite from mixing of brine pool sulfate and barium in hydrothermal fluid; (13) exhaustion of barium or sulfate supply, continued precipitation/sedimentation of sphalerite and minor galena in most distal portion of brine pool; (14) diffusion of silica into pore waters of sediments causing precipitation of quartz/amorphous silica; (15) diagenetic formation of pyrite via sulfate-reduction in shallow sediments; (16) diagenetic formation of iron carbonates due to methanogenesis in sediments; (17) inflow of carbonate-rich connate fluids (CO_2 derived from methanogenesis or thermal maturation of shallow organic matter) causing precipitation of iron carbonates in vent complex.

Barite Facies

Sulfur isotope data suggest that the source of sulfate in the barite was Late Devonian seawater (Gardner, 1983). The distinctly more radiogenic strontium isotopic ratios of barite as compared to seawater argue that the barite precipitated within the brine pool. The absence of barite in the vent area is consistent with a lack of barite precipitation prior to lateral spread of the hydrothermal plume. At the periphery of the vent area, the occurrence of barite at the top of graded sulfide-barite beds suggests that (1) barite precipitated later than sulfides in the mixing process of one discharge cycle or (2) that the settling velocity of barite was less than that of the sulfides. The very finely laminated and planar character of barite strata suggests deposition below a very quiet watermass.

Very finely laminated hydrothermal sediments in the quartz-sulfide facies are interbedded with organic-rich laminae. The disappearance of organic-rich laminae towards the vent area coincides with the appearance of barite laminae (Fig. 3.3) and suggests that the barite sedimentation rate greatly exceeded the sedimentation of hemipelagic organic matter, or that organic matter was not stable within the barite facies. Barite laminae occur in the same position relative to interlaminated sphalerite and quartz-sphalerite laminae as do laterally equivalent organic-rich laminae in the more distal portions of the deposit; this textural equivalence of organic matter and barite deposition, and the fact that organic matter is interpreted to represent a steady-state hemipelagic rain, may suggest that barite deposition was also steady state and continuous rather than episodic. Given this scenario, a continuous rain might be punctuated by episodic and rapid bursts of sphalerite, or quartz-sphalerite deposition.

Interlaminated barite and sulfide is noted in other stratiform Pb-Zn deposits (e.g. Tom, Cirque, Anvil, Lady Loretta) and is distinct from stratiform deposits with a sulfide-barren barite body adjacent to a massive sulfide body (e.g. Meggan, Rammelsberg, GDR, Silvermines). The interlamination of laminae reflecting different redox states is also noted in the Atlantis II deep where manganosiderite is interlayered with sulfide layers.

Pottorf (1983) interprets this interbanding to reflect precipitation at the anoxic-oxic interface at the top of the brine pool. A lowering of the interface due to diffusion and mixing results in reaction of dissolved species from the lower brine with oxidants of the transition zone and precipitation of manganosiderite. The effect of raising the interface results in precipitation or more reduced minerals, such as sulfides. In the case of the Jason this would require a sulfate-bearing ambient seawater and sulfate-depleted brine pool in spite of evidence for regional anoxia in the Lower Earn "sea" as argued by Goodfellow and Jonnason (1984). Therefore such a brine pool characterized by volumetric fluctuation might yield interlaminated barite-sulfide. In the model described above, sulfide deposition is restricted to the extent of the brine pool while barite could precipitate from a transitional and more extensive water mass overlying the brine pool. If such a brine pool were stable through time (constant volume) the result might be massive sulfides juxtaposed laterally against massive barite. The greater lateral distribution of sulfide versus barite in the Jason deposit is problematic and not understood; in the Meggan deposit barite flanks the sulfide body.

Quartz-Sulfide Facies

A sedimentary origin for sphalerite and quartz-sphalerite laminae within the quartz-sulfide facies is suggested by: (1) the occurrence of clasts of these laminae within sedimentary breccias interbedded with quartz-sulfide beds and in conglomerate lens; and (2) the nature of asymmetric quartz-sphalerite microlaminae cycles and (3) the finely laminated character. Laminated carbonaceous quartz-pyrite laminae are interpreted as hemipelagic deposition because of the high organic content, association with radiolaria, and low clay content. Massive carbonaceous quartz-pyrite beds likely represent resedimented muds and siliceous, organic-rich oozes based on the presence of floating silt-sized terrigenous clasts. The origin of the high quartz content of carbonaceous quartz-pyrite beds is ambiguous; though it may represent the sedimentation of a siliceous ooze, it more likely represents diagenetic cementation from silica-saturated porewaters immediately below the seabottom (see Quartz Facies).

The transition from barite strata lacking organic material (barite-sulfide facies) to carbonaceous strata lacking barite (quartz-sulfide facies) coincides with a marked thinning of the stratiform body (Figs. 3.46, 3.53). The coincidence of this thinning with the appearance of a significant abundance of organic, non-hydrothermal, hemipelagic laminae suggest that a marked decrease in depositional rates was associated with the disappearance of barite laminae. Organic-rich quartz-sulfide facies strata in the upper horizon occur peripheral to the barite facies and the depositional trough as defined by greater thickness and greater $Pb/Pb+Zn$ fraction of the stratiform ores. This trough likely represents the flow path of brines moving away from the vent area.

Quartz-sphalerite strata proximal to the vent facies are distinct from similar composition but more distal laminae and are characterized by a greater $Pb/Pb+Zn$ fraction, a greater thickness of the sphalerite laminae, the presence of laminae cycles, and the absence of organic matter and framboidal pyrite. These characteristics indicate longer or more rapid sulfide deposition events than in the more distal organic-rich portion of the facies. The absence of organic matter may reflect the lack of preservation of organic matter after deposition due to higher diagenetic temperatures or the swamping of the biogenic input by rapid hydrothermal deposition.

The rate of organic accumulation in the distal quartz-sulfide facies relative to that in the laterally equivalent regional strata is unclear. Organic-rich strata are associated with some stratiform deposits (e.g. Meggan, McArthur River); increased organic content may reflect higher preservation potential in a locally reduced sub-environment, discharge of organic-rich hydrothermal fluids or locally enhanced biological activity. The content of organic matter in the metalliferous sediments of the Atlantis II Deep is similar to that in sediments outside the brine pool, yet the hydrothermal sedimentation rate greatly exceeds the sedimentation rate outside the brine pool indicating greater rates of organic accumulation within the Atlantis II brine pool than outside it. As the Atlantis II brine pool is abiotic due to the high salinity and metal concentration of the brine, this higher organic accumulation

rate is interpreted to reflect the absence of bacterial degradation of organic matter on the seabottom and during early diagenesis. At Jason, the presence of pyrobitumen in veins in the subsurface of the vent area indicates transport of organic matter by the hydrothermal system; organic matter transported in the hydrothermal fluids therefore may have been deposited as sediment with the other hydrothermal sediments.

Framboidal pyrite may form in the water column as noted in the anoxic watermass of the Black Sea or during diagenesis within the sediment (Berner, 1972). At Jason, the exclusive association of framboids with organic-rich chert layers suggest they formed during diagenesis through the coupled reaction of sulfate reduction and oxidation of organic matter.

Quartz Facies

Quartz occurs as a major or accessory phase in laminae (e.g. quartz-sphalerite laminae) as well as in veinlets (e.g. carbonate-quartz-sulfide) in the vent complex. However, the great bulk of the quartz in the ore horizons occurs as silicified terrigenous sediments interbedded with or enveloping the stratiform body. Apparently the quartz precipitated largely as a cement within the pore space of quartz-rich terrigenous sediments rather than as a siliceous sediment in the brine pool. The thinning of beds across a silicification front noted in core (Chap.2) indicates that this silicification occurred at shallow depths of burial prior to compaction of the sediments. This high ratio of diagenetic versus sedimentary silica deposition is also noted in Kuroko ores by Ohmoto and others (1983), who suggest that the precipitation of quartz is highly favored within porous sediments rather than seawater due to the high surface area for quartz nucleation provided by the former. These authors interpret the tetsusekiei ore (silica + hematite + barite) of the Kuroko deposits as silicified tuffs and mudstones.

Pore space silicification may result from the diffusion of silica into the pore space of the shallowest sediment from the overlying silica-saturated brine pool waters. Discordant zones of silicification may represent lateral infiltration of silica saturated hydrothermal fluids from zones of discharge.

ZONATION

If it is accepted that there is quantitative precipitation of metals during venting into a brine pool, then no zoning would be expected unless some physical segregation process were to operate. This might be thought to be contradicted by Kuroko deposits which are zoned yet have been interpreted as exhalative sedimentary deposits; however recent work shows this zoning is due to subsurface replacement whereby early formed minerals deposited on the periphery of the vent area are subsequently replaced by minerals in equilibrium with a thermally prograding hydrothermal system (Eldridge et al., 1983). However, the Jason and other stratiform sediment-hosted deposits form via sedimentation of hydrothermal strata that young upwards, rather than by replacement. Therefore, if zoning is observed in this vertical sequence then one must invoke changes in the character of discharge or invoke physical processes. In the former case the change in discharge composition can be ruled out because of the occurrence of fine-graded beds of a mm scale. It is unconceivable that a change in composition of hydrothermal discharge could occur on such a scale. Also, individual beds are zoned with respect to Pb/Pb+Zn suggesting segregation processes were operative during sedimentation.

At Jason there is evidence for zoning due to two independent mechanisms. There is zoning within the vent complex formed via replacement of earlier formed minerals that is similar to that noted within the Kuroko ores. There is also zoning of the stratiform ores that is due to physical processes within the brine pool. The superposition of these two zoning mechanisms results in more complex patterns than in Kuroko deposits.

EVIDENCE FOR GRAVITATIONAL SORTING AS A CONTROL ON MINERAL DEPOSITION

The tendency for laminae to be dominated by a single mineral in the distal portions of the deposit, lateral zoning of lead to zinc ratios of the stratiform ores, and the presence of compositional grading in laminae and beds indicate segregation of differing minerals occurred during the sedimentation process.

Strata Dominated by Single Minerals

Most laminae in the stratiform ores have a dominant phase that comprises 70 to 90 percent of the laminae. This monominerallic tendency may reflect either segregation during sedimentation or later during diagenesis. Some element of diagenetic segregation cannot be ruled out; however textures interpreted to reflect diagenetic segregation distinguished from laminae by their coarser grain size and discontinuous nature. Therefore, it is likely that the monominerallic nature of laminae represents depositional segregation.

Segregation within the brine pool could result from episodic nucleation of different minerals (Lydon, 1983) or the separation of co-precipitated minerals during suspension fall due to different settling velocities of different minerals. Modeling by Lydon (1983) indicates that the co-precipitation of minerals from a hydrothermal fluid undergoing physiochemical change within a brine pool environment will result in laminae dominated by a single phase as is outlined below. In order to overcome the energetics of nucleation due to the absence of seed crystals within the brine pool, the fluid must exceed saturation with respect to a mineral before precipitation occurs. Therefore, saturation-supersaturation-precipitation cycles will occur. Precipitation of minerals will be episodic and the amount of precipitation will reflect the degree of supersaturation achieved prior to precipitation. Sedimentation of a single phase will result if precipitation events for different minerals happen not to coincide.

Differential settling velocities of minerals may also provide an effective segregation mechanism. Stokes law states that a sphere of radius, a , and density contrast with the surrounding fluid, $\Delta\rho$, will settle at a velocity (cm/sec) V , through a fluid of viscosity, μ according to the equation:

$$V = \frac{2\Delta\rho g a^2}{9\mu}$$

where g is acceleration due to gravity. The settling velocity is therefore proportional to $\Delta\rho$, the density contrast of a mineral and the fluid. Assuming a temperature of the brine pool equal to that of the Atlantis II deep ($60^\circ C$), a 2M brine would have a density of 1.05 g/cc. Therefore the $\Delta\rho$ of different minerals would be as follows: galena (6.5), barite (3.4),

sphalerite (3.0), quartz (1.6). Using $\mu = 0.01$ poise, $g = 980$ cm²/sec, and $a = 5$ microns, settling velocities of minerals would range from 0.020 cm/sec for sphalerite to 0.036 cm/sec for galena. Coincidental precipitation of sphalerite and galena of the same grain size would result in galena-rich sediments overlain by sphalerite-rich sediments. The degree of the differentiation would be related to the thickness of the fluid that the particles settled through and the amount of turbulence within that fluid. In a brine pool environment, because fluids discharged from the vent area buoyantly rise to the top of the brine pool and spread laterally, particulates settling from this spreading flow would fall through the entire thickness of the brine pool which in the case of the Atlantis II deep is over 100 m.

Thicker, polyminerallic nature of laminae near the vent area.

At the Jason, beds and laminae near the vent area are distinctively thicker and less dominated by a single mineral as compared to laminae in the distal portions of the deposit. Thicker beds likely reflect higher sedimentation rates. The less segregated nature of minerals may be related to a shorter settling distance due to sedimentation from the lower part of the plume, sedimentation from turbulent fluids which prevented sorting, or the co-precipitation of phases within the steep physiochemical gradients above the vent area. Minerals that precipitate during the vertical rise of the hydrothermal fluids are prevented from settling by the vertical flow rate; Solomon and Walshe (1979) calculate that a vertical flow rate of 0.5 cm/sec will prevent the settling of all sulfide particulate matter less than 10 microns in diameter. In the area of initial lateral spread of the hydrothermal plume a sharp reduction in the vertical velocity will occur resulting in high rates of sedimentation.

Compositionally and Texturally Graded Units

Within graded units of galena-sphalerite, the vertical change from thick-bedded galena-rich beds at the base to thinning upward sphalerite-galena beds with increasing sphalerite content (Fig. 3.54) is similar to the lateral decrease in galena/sphalerite ratio and decrease in bed thickness away from the vent area that occur on an orebody scale. This comparison

suggests that the depositional processes at the base of a graded bed are similar to those that dominate in the proximal area while the processes controlling deposition in the top of the graded bed are those that dominate in the distal part of the deposit. Therefore, the base might represent rapid deposition of the least soluble or heaviest particulates, while the top represents slower deposition of more soluble or lighter particulates. The proximal portion of the ore deposit can be viewed as a composite of the bases of depositional events whereas the distal portion of the deposit is a composite of the tops of depositional events. This is analogous to turbidity flow deposition where the finer (more soluble, less dense) fraction bypasses the proximal depositional area, while the proximal depositional area is dominated by the deposition of coarser-grained (heavier, less soluble) sediments.

Modeling of fluid discharge by Turner and Gustafson (1978) indicates that steady state discharge can result in pulsatory collapse of the hydrothermal plume; such collapse events result in dense brine (and particulate) flow away from the vent. Depositional cycles such as graded galena-sphalerite ore sphalerite-quartz laminae or beds could represent the waning flow regime of such turbidity flows in which the massive base represents traction fallout from a bottom hugging turbidity flow or rapid suspension fallout from a turbulent cloud. Laminae or beds within cycles may reflect a series of successively waning turbulent pulses within the turbulent flow event.

TEMPORAL FLUCTUATIONS IN HYDROTHERMAL DISCHARGE

The vertical stratigraphy of the stratiform ores preserves the history of hydrothermal discharge during the formation of the deposit. Although all components of the sedimentary record may not be recorded within the sedimentary record, it is at least a partial record. In the vent area the sedimentary record is metasomatized by venting fluids obscuring some of the original sedimentary record. The distal part of the deposit reflects deposition from a more mixed hydrothermal fluid and consequently may lack a record of smaller discharge fluctuations. Therefore, it is considered that the portion of the deposit just distal of the vent area likely represents the most complete record of the hydrothermal activity. The 87 drill

hole intersected this part of the deposit.

Vertical changes in the stratiform facies and metal ratios within the Jason stratiform ores attest to a history of fluctuating hydrothermal discharge (Fig. 3.55). Three metal cycles can be correlated throughout much of the distal mineralization of the upper stratiform horizon. Where DDH 87 intersects the barite facies adjacent to the vent area, 2.5 to 5 m thick cycles are characterized by gradual upward increase in %Pb+Zn and Pb/Pb+Zn value followed by rapid decrease in both %Pb+Zn and Pb/Pb+Zn. The lower, lead poor, low total sulfide part of each cycle has a high quartz to barite ratio; the lead-rich, high total sulfide upper part of each cycle is quartz poor. Each cycle represents early quartz-sphalerite dominant sedimentation followed by barite deposition and increasing galena deposition.

The deposition of the sulfide facies of the hydrothermal sediments within the Atlantis II deep brine pool coincided with the maximum extent of the brine pool (Backer and Richter, 1973), suggesting sulfide deposition during periods of maximum discharge.

HIGH RATES OF HYDROTHERMAL SEDIMENTATION

Organic matter is not present in most of the stratiform body and only in the very finely laminated distal ores is much interbedded organic matter present. The appearance of organic-rich laminae coincides with the disappearance of barite laminae towards the periphery of the deposit (Fig. 3.3.) suggesting that the cumulative deposition rate of barite, sulfide and carbonate greatly exceeded and therefore diluted the hemipelagic biogenic sedimentation. The calculated hydrothermal sedimentation rate in the Atlantis II deep also greatly exceeds normal marine sedimentation rates; within the brine pool depositional rates are 50 cm/1000 years, about 3 times the normal marine sedimentation rate outside the deeps.

DURATION OF HYDROTHERMAL ACTIVITY

The great volume of hydrothermal sedimentary rock in the stratiform horizons requires the discharge of a large volume of hydrothermal fluid. The lack of hemipelagic sediment interbedded with the bulk of the stratiform hydrothermal sediments, the active tectonic and

sedimentological setting, and the high fluid temperatures suggest rapid accumulation rates of the hydrothermal sediments. In the Atlantis II deep, up to 30 meters of sediments (75 % water) have accumulated during the past 25,000 years (Hackett and Bischoff, 1973). After compaction, this would represent an accumulation rate of 7.5 m / 25,000 years or 30 cm / 1000 years. This sedimentation rate is three times the rate of deposition outside the brine pool. Assuming similar rates of sedimentation, the Jason hydrothermal sediments would have accumulated in about 150,000 years.

Using the Atlantis II deep sedimentation rates, the deposition of metal cycles 2.5 to 5 m thick would represent 8,000 to 17,000 years. This concurs with the expectation that the duration of hydrothermal activity at Jason is intermediate between volcanogenic massive sulfide deposits (associated with rapidly cooled high-level intrusions) and the very large tonnage, low grade stratiform mineralization at Howards Pass, Yukon. Using heat flow and hydrodynamic considerations, Cathles (1983) suggests that Kuroko deposits were deposited in less than 5000 years and probably in 100 years. Based on biostratigraphic evidence, Goodfellow and Jonnason (in press) suggest that mineralization at Howards Pass spanned a period from 1 to 3 m.y. in the brine pool (Pottorf and Barnes, 1983).

CONCLUSIONS

The Jason deposit is characterized by its deep marine setting, very active tectonic environment, high temperature hydrothermal fluids and stratiform ores that overlie and are adjacent to a paleo-vent area. The data presented in this study of the Jason deposit support the theory that the Jason deposit formed in a submarine exhalative environment. It is likely that an exhalative model is appropriate for other sheetlike stratiform deposits formed within deep marine, siliciclastic basins (e.g. Rammelsberg, Sullivan, Selwyn basin deposits) as concluded by past workers such as Hannak, 1981; Hamilton et al., 1982; and Goodfellow and Jonnason, in press.

Lateral infiltration of the hydrothermal fluids into the shallow sediments appears to have been limited to an area immediately adjacent to the paleo-vent area body and does not

appear to provide a mechanism to form laminated ores as described by Williams (1978).

The interlamination of barite and sulfide and the relatively greater lateral distribution of sulfide versus barite at the Jason deposit is characteristic of many Late Devonian age stratiform sulfide deposits in northwestern Canada. In contrast, coeval deposits elsewhere either lack barite (e.g. Triumph, Idaho; Lik, Alaska) or barite occurs as massive bodies peripheral to a massive sulfide body (e.g. Meggan and Rammelsberg, GDR). The former group of deposits are interpreted to have formed in very reduced watermasses that lacked sulfate as argued by Forrest (1983); the latter group have features which suggest a layered brine pool in which barite precipitation occurred in an upper, more oxidized, mixed layer but only accumulated where that upper brine impinged on the seafloor to form a 'bath-tub ring' (R. Zierenberg, pers. comm. 1986). The limited distribution of barite with respect to sulfide at Jason might suggest the more rapid depletion of barium or sulfate than zinc or sulfide during mixing.

Because hydrothermal fluids quench immediately during discharge into a water mass (Solomon and Walshe, 1979), it is difficult to attribute the well developed zoning of galena and sphalerite throughout the stratiform ores to the differential solubilities of zinc and lead complexes. However, the greater settling rate of galena versus sphalerite particulate could explain the preferential occurrence of galena near the vent area as well as in rapidly deposited beds at the base of galena-sphalerite cycles. The possibility is proposed that similar metal zoning in other stratiform deposits (e.g. Sullivan; Hamilton et al., 1983) also may be related to differential settling rates.

The occurrence of the Jason stratiform ores at the stratigraphic level of the earliest sedimentary breccias derived from the Jason fault indicates that hydrothermal activity commenced during earliest fault movement (Chapter 2). The size (thickness and lateral extent) and abundance of sedimentary breccias increases upwards from the stratigraphic level of the lower horizon to the thick sedimentary breccia units overlying the upper horizon. The intimate connection between fault activity and hydrothermal activity would suggest that

seismic pumping or rupture of overpressured strata by fault movement was likely the mechanism of hydrothermal discharge.

The estimated duration of hydrothermal activity for the formation of the Jason deposit (~ 150,000 years) is much greater than that proposed by Cathles (1983) for the Kuroko massive Cu-Zn sulfide deposits but significantly less than the 1 to 3 m.y. duration proposed for the Howards Pass stratiform Pb-Zn deposit (Goodfellow and Jonnason, in press); this accords with the smaller tonnage, general lack of interbedded hemipelagic sediments, and active tectonic setting of the Jason deposit with respect to the Howards Pass deposit.

Study of the Jason also provides insight into processes of a submarine hydrothermal vent area. Mineralization in the vent area was characterized by recrystallization and replacement of early formed hydrothermal sediments by later formed minerals related to discharging hydrothermal fluids. The crude spatial zoning of an outer zone of recrystallization, an intermediate zone of carbonate replacement and an inner pyrrhotite replacement of carbonate is texturally analogous to the zoned model of increasing metasomatism toward the core in Kuroko deposits (Eldridge et al., 1983). The general similarity of Kuroko paleo-vent textures to the Jason vent suggests that common vent processes existed; however, Kuroko deposits represent direct hydrothermal discharge into seawater (Ohmoto et al., 1983) and hence they lack a flanking sheet of laminated hydrothermal sediments resulting from the containment of hydrothermal solutes by a brine pool. The dispersion of solutes into the water column of seawater exhalative hydrothermal systems such as the Kuroko deposits in part may explain their much smaller tonnage with respect to stratiform Pb-Zn deposits.

At the Jason deposit, a link is proposed between sub-seafloor mixing of hydrothermal fluids prior to exhalative discharge and the abundance of discordant 'footwall' mineralization. Large and Finlow Bates (1980) have ascribed the development of footwall mineralization associated with stratiform deposits to boiling during discharge due to shallow water exhalative activity. However, study of fluid inclusions in vent complex veins at the Jason deposit

(Gardner, 1983) did not indicate that boiling occurred. There is also a lack of fluid inclusion evidence for boiling at the Silvermines deposit (Samson and Russell, 1982), yet footwall discordant veins and disseminations in the footwall of the stratiform bodies is extensive. Though the data are sparse, there is no documented evidence for boiling during formation of any stratiform deposit. An alternate possibility is suggested here; the presence or absence of footwall alteration/mineralization is tied to the structural setting of the discharge zone and the degree of subsurface mixing and hence mineral precipitation in the vent area.

This study provides the numerous lines of evidence for the formation of the Jason stratiform deposit within a brine pool environment. The hydrodynamic model of MacDougall (1984) provides a mechanism for forming brine pools from hot, low density hydrothermal fluids. This model overcomes the apparent contradiction from fluid inclusion evidence that suggests that the fluids were less dense than seawater and incapable of forming a brine pool. This study presents data that early, low temperature discharge preceded higher temperature discharge as required in the McDougall model for brine pool formation and supports the validity of the McDougall model for brine pool formation.

If an exhalative origin can be demonstrated for other deposits, this study suggests several criteria that can be applied to determine whether or not they may have formed within a brine pool environment: quartz-rich nature, Sr isotopic ratios of stratiform ores that distinct from coeval seawater, and control of mineral deposition and sediment thickness by bathymetric features. Strontium isotopic analysis has application to the barite- and/or carbonate-rich stratiform deposits. The use of quartz content as a criteria for formation of stratiform mineralization within a brine pool has broad potential application because it is a simple and easily evaluated criteria. The common association of bedded "chert" with stratiform Pb-Zn deposits (Large, 1981) argues that many stratiform deposits likely formed within brine pool environments. Evidence for bathymetric control of the distribution of stratiform ores can also support a sedimentary origin as has been applied at the Silvermines deposit (Taylor, 1984).

REFERENCES

- Abbott, G., Structure and stratigraphy of the MacMillan fold belt: evidence for Devonian faulting, *Dept. Ind. Affairs Northern Development, Open File Rept.*, 16 p., 16, 1982.
- Abbott, J. G., Geology of the MacMillan Fold Belt 105 O - S.E. and parts of 105 P - S.W. (3 maps 1:50,000 and legend), *Open File*, 1983.
- Abbott, J. G., S. P. Gordey, and D. J. Tempelman-Kluit, Setting of stratiform sediment-hosted lead-zinc deposits in Yukon and northeastern British Columbia, *C. I. M. M., Spec. Vol., Mineral Deposits of the Northern Cordillera*, in press.
- Albarede, F., A. Michard, J. F. Minster, and G. Michard, $^{87}\text{Sr}/^{86}\text{Sr}$ ratios in hydrothermal waters and deposits from the East Pacific Rise at 21N, *Earth and Planetary Science Letters*, 55, 229-236, 1981.
- Ansdell, K. M., Fluid inclusion and stable isotope study of the Tom Ba-Pb-Zn deposit, Yukon Territory, M. Sc. Thesis, University of Alberta, Edmonton, 123 p., 1985.
- Badham, J. P. N., Shale-hosted Pb-Zn deposits: products of exhalation of formation waters?, *Trans. Instn. Min. Metall.*, 90, B70-B76, 1981.
- Bailes, R.J., D.W. Blackadar, and B.W. Smee, Stratiform lead-zinc-silver deposits, Jason prospect, Macmillan Pass, Yukon, *Abstracts with programmes, C.I.M. Symposium on Mineral deposits of the northern Cordillera*, pp. 16, Whitehorse, 1983.
- Bailes, R. J., B. W. Smee, D. W. Blackadar, and H. D. Gardner, Geology of the Jason lead-zinc-silver deposits, Macmillan Pass, Yukon Territory, in *Mineral Deposits of the Northern Cordillera: Canadian Inst. Mining Metall., Spec. Vol.*, edited by J. Morin, in press.
- Barton, P. B., Jr., Some ore textures involving sphalerite from the Furutobe mine, Akita Prefecture, Japan, *Mining Geology*, 28, 293-300, 1978.
- Berner, R. A., Sedimentary pyrite formation, *Am. Jour. Sci.*, 268, 1-23, 1970.
- Berry, W. B. N., and P. Wilde, Progressive ventilation of the oceans, *Amer. Jour. Sci.*, 278, 257-275, 1978.
- Bischoff, J. L., Red Sea geothermal brine deposits: their mineralogy, chemistry, and genesis, in

- Hot Brines and Recent Heavy Metal Deposits in the Red Sea*, edited by E. T. Degens and D. A. Ross, pp. 368-401, Springer, 1969.
- Blake, M. C., Jr., R. H. Campbell, T. W. Dibble, T. W. Dibble, Jr., D. G. Howell, T. H. Nilsen, W. R. Normark, J. C. Vedder, and E. A. Silver, Neogene basin formation in relation to plate-tectonic evolution of the San Andreas fault system, California, *Amer. Assoc. Petroleum Geologists Bull.*, 62, 344-372, 1978.
- Bouma, A. H., *Sedimentology of Some Flych Deposits*, 168 p., Elsevier, Amsterdam, 1962.
- Briggs, R. C., and H. C. Troxell, Effect of Arvin-Techapi earthquake on spring and stream flow, *Calif. Div. Mines Bull.* 171,, 81-98, 1955.
- Burke, W. H., R. E. Denison, E. A. Hetherington, R.B. Koepnick, H. F. Nelson, and J. B. Otto, Variation of seawater $^{87}\text{Sr}/^{86}\text{Sr}$ throughout Phanerozoic time, *Geology*, 10, 516-519, 1982.
- Carne, R.C., Geological setting and stratiform lead-zinc-barite mineralization, Tom Claims, Yukon Territory, *Open File Rept. EGS 1979-4*, 30, 1979.
- Carne, R. C., and R. J. Cathro, Sediment exhalative (sedex) zinc-lead-silver deposits, northern Canadian cordillera, *Canadian Mining Metall. Bull.*, 75, 66-78, 1982.
- Cathles, L. M., An analysis of the hydrothermal system responsible for massive sulfide deposition in the Hokuroku basin of Japan, *Econ. Geol. Mon.* 5, 439-487, 1983.
- Craig, H., Geochemistry and origin of Red Sea brines, in *Hot Brines and Recent Heavy Metal Deposits in the Red Sea*, edited by E. T. Degens and D. A. Ross, pp. 208-242, Springer, 1969.
- Craig, J. R., and D. J. Vaughan, *Ore microscopy and ore petrology*, 406 p., John Wiley and Sons, New York, 1981.
- Dawson, K.M., and M.J. Orchard, Regional metallogeny of the northern cordillera: Biostratigraphy, correlation and metallogenic significance of bedded barite occurrences in eastern Yukon and western District of Mackenzie, *Current Research, Part C, Geological Survey of Canada, Paper 82 - 1C*, pp. 31-38, 1982.
- Demaison, G. J., and G. T. Moore, Anoxic environments and oil source bed genesis, *American Assoc. Petrol. Geologists Bull.*, 8, 1179-1209, 1980.

- Edmond, J. M., K. L. Von Damm, R. E. McDuff, and C. I. Measures, Chemistry of hot springs on the East Pacific Rise and their effluent dispersal, *Nature*, 297, 187-191, 1982.
- Eisbacher, G., Devonian-Mississippian sinistral transcurrent faulting along the cratonic margin of western North America: a hypothesis, *Geology*, 11, 7-10, 1983.
- Eldridge, C. S., P. B. Barton, Jr., and H. Ohmoto, Mineral Textures and their bearing on formation of the Kuroko orebodies, *Econ. Geol. Mon. 5*, 241-281, 1983.
- Fischer, A. G., and M. A. Arthur, Secular variations in the pelagic realm, *S.E.P.M. Spec. Pub.*, 25, 19-50, 1977.
- Forrest, K., Geological and isotopic studies of the Lik deposit and the surrounding mineral district, Delong Mountains, western Brooks Range, Alaska, Ph. D. Thesis, , University of Minnesota, 1983.
- Gardner, H. D., Petrologic and geochemical constraints on genesis of the Jason Pb-Zn deposits, Yukon Territory, M.S. Thesis, , University of Calgary, 1983.
- Gardner, H. D., and I. Hutcheon, Geochemistry, mineralogy and geology of the Jason Pb-Zn deposits, Macmillan Pass, Yukon, Canada, *Econ. Geol.*, 80, 1257-1276, 1985.
- Giordano, T. H., and H. L. Barnes, Lead transport in Mississippi Valley-type ore solutions, *Econ. Geol.*, 76, 2200-2211, 1981.
- Goldfarb, M. S., D. R. Converse, H. D. Holland, and J. M. Edmond, The genesis of hot spring deposits on the East Pacific Rise, 21 N, *Econ. Geol. Mon. 5*, 184-197, 1983.
- Goodfellow, W. D., and I. R. Jonasson, Ocean stagnation and ventilation defined by 34S secular trends in pyrite and barite, Selwyn Basin, Yukon, *Geology*, 12, 583-586, 1984.
- Gordey, S. P., Stratigraphy of southeastern Selwyn Basin in the Summit Lake area, Yukon Territory and Northwest Territories, *Current Research, Part a*, 13-16, 1979.
- Gordey, S. P., *Stratigraphy, structure and tectonic evolution of southern Pelly Mountains in the Indigo Lake area, Yukon Territory*, 44p., Geological Survey of Canada, 1981.
- Gordey, S. P., J. G. Abbott, and M. J. Orchard, Devono-Mississippian (Earn Group) and younger strata in east-central Yukon, *Geol. Surv. Canada, Paper 82-1B*, 93-100, 1982.

- Hackett, J., and J. L. Bischoff, New data on the stratigraphy, extent, and geologic history of the Red Sea geothermal deposits, *Econ. Geol.*, *68*, 553-564, 1973.
- Hamilton, J. M., D. T. Bishop, H. C. Morris, and O. E. Owens, Geology of the Sullivan orebody, Kimberley, B. C., Canada, in *Precambrian sulfide deposits (H. S. Robinson Memorial Volume)*, edited by R. W. Hutchinson, C. D. Spence and J. M. Franklin, pp. 597-625, Geol. Assoc. Canada Special Paper 25, 1982.
- Haymon, R. M., and M. Kastner, Hot spring deposits on the East Pacific Rise at 21 N: preliminary description of mineralogy and genesis, *Earth Planet. Sci. Lett.*, *59*, 363-381, 1981.
- Henley, R. W., and P. Thornley, Some geothermal aspects of polymetallic massive sulphide formation, *Econ. Geol.*, *v. 714*, p. 1600-1612, 1979.
- Janecky, D. R., and W. E. Seyfried, Jr., Formation of massive sulfide deposits on oceanic ridge crests: Incremental reactions models for mixing between hydrothermal solutions and seawater, *Geochim. Cosmochim. Acta*, *48*, 2723-2738, 1984.
- Lambert, I. B., The McArthur zinc-lead-silver deposit: features, metallogensis and comparisons with some other stratiform ores, in *Handbook of stratabound and stratiform ore deposits*, edited by K. H. Wolf, pp. 535-585, Elsevier, Amsterdam, 1976.
- Large, D. E., Sediment-hosted submarine exhalative lead-zinc deposits - a review of their geological characteristics and genesis, in *Handbook of strata-bound and stratiform ore deposits, 9, Regional studies abroad*, edited by K. H. Wolf, pp. 469-507, Elsevier, Amsterdam, 1981.
- Lenz, A. C., Ordovician to Devonian history of northern Yukon and adjacent District of Mackenzie, *Bulletin of Canadian Petroleum Geology*, *2*, 321-361, 1972.
- Lydon, J.W., Chemical parameters controlling the origin and deposition of sediment-hosted stratiform lead-zinc deposits, in *Short Course on sediment-hosted lead-zinc deposits*, edited by D. F. Sangster, pp. 175-250, Mineral. Assoc. Canada, 1983.
- Lydon, J. W., W. D. Goodfellow, and I. R. Jonasson, A general genetic model for stratiform baritic deposits of the Selwyn Basin, Yukon Territory and District of Mackenzie, *Current Research, Part A, Geological Survey of Canada, Paper 85-1A*, pp. 651-660, 1985.

- Mahon, W. A. J., G. D. McDowell, and J. B. Finlayson, Carbon dioxide: Its role in geothermal systems, *New Zealand Journal of Science*, 23, 133-148, 1980.
- McDougall, T. J., Fluid dynamic implications for massive sulphide deposits of hot saline fluid flowing into a submarine depression from below, *Deep Sea Research*, 2, 145-170, 1984.
- Morimoto, R., K. Nakamura, Y. Tsuneishi, J. Osaka, and N. Tsunoda, Landslides in the epicentral area of the Matsushiro earthquake swarm - Their relationship to the earthquake fault, *Bull. Earthq. Res. Inst.*, 45, 241-263, 1967.
- Nardin, T. R., B. D. Edwards, and D. S. Gorsline, Santa Cruz basin, California borderland: Dominance of slope processes in basin sedimentation, *SEPM Special Publication*, no. 27, 209-221, 1979.
- Ohmoto, H., M. Mizukami, S. E. Drummond, C. S. Eldridge, V. Pisutha-Arnond, and T. C. Lenagh, Chemical processes of Kuroko formation, *Economic Geology Monograph* 5, pp. 570-604, 1983.
- Parrish, J. T., Upwelling and petroleum and source beds with reference to the Paleozoic, *Amer. Assoc. Petrol. Geologists Bull.*, 66, 750-774, 1982.
- Pottorf, R. J., and H. L. Barnes, Mineralogy, Geochemistry, and Ore genesis of hydrothermal sediments from the Atlantis II deep, Red Sea, in *Economic Geology Monograph* 5, edited by H. Ohmoto and B. J. Skinner, pp. 198-223, 1983.
- Revelle, R., and K. O. Emery, Barite concretions from the ocean floor, *Geol. Soc. America Bull.*, 62, 707-724, 1951.
- Rimstidt, J. D., and H. L. Barnes, The kinetics of silica-water reactions, *Geochim. et Cosmochim. Acta*, 44, 1683-1699, 1980.
- Russell, M. J., Fluid inclusion data from Silvermines base-metal-baryte deposits, Ireland, *Inst. Mining Metallurgy Trans.*, 92, sec. B., B67-71, 1983.
- Sato, T., Behaviors of ore-forming solutions in seawater, *Mining Geology*, 22, 31-42, 1972.
- Sawkins, F. J., Ore genesis by episodic dewatering of sedimentary basins: Application to giant Proterozoic lead-zinc deposits, *Geology*, 12, 451-454, 1984.

- Schoell, M., and M. Hartmann, Detailed temperature structure of the hot brines in the Atlantis II deep area (Red Sea), *Marine Geology*, 14, 1-14, 1973.
- Scotese, C. R., and et al., Paleozoic base maps, *Jour. Geol.*, 87, 217-277, 1979.
- Shanks, W. C., III, and J. L. Bischoff, Ore transport and deposition in the Red Sea geothermal system: a geochemical model, *Geochim. Cosmochim. Acta*, 41, 1507-1519, 1977.
- Sibson, R.H., J. McM. Moore, and A.H. Rankin, Seismic pumping--a hydrothermal fluid transport mechanism, *Geol. Soc. London Jour.*, 191, 653-659, 1975.
- Smith, C. L., Geological setting of Jason and Tom deposits, Macmillan Pass area, Eastern Yukon, *Summary of presentation, Whitehorse Geoscience Forum 1978*, 6, 1977.
- Smith, C.L., Sediment-hosted stratiform lead-zinc-silver deposits, in *Revolution in the Earth Sciences- advances in the past half-century, proceeding of a symposium held at Carleton College, Northfield, Minnesota*, edited by S.J. Boardman, Kendall Hunt Publishing Company, Dubuque, Iowa, 1983.
- Solomon, M., and J. L. Walshe, The formation of massive sulfide deposits on the sea floor, *Econ. Geol.*, 74, 797-813, 1979.
- Stanton, R. L., *Ore Petrology*, 713 p., McGraw-Hill, New York, 1972.
- Taylor, S., Structural and paleotopographic controls of lead-zinc mineralization in the Silvermines orebodies, Republic of Ireland, *Econ. Geol.*, 79, 529-548, 1984.
- Teal, P. R., and S. E. Teal, *Geology and sedimentary interpretation of the Macmillan Pass area (Jason and Tom properties), Yukon territory, unpublished company report*, 35 p., 1978.
- Templeman-Kluit, D. J., Transported cataclasite, ophiolite and granodiorite in Yukon: evidence of arc-continent collision, *Geological Survey of Canada Paper 79-14*, 27p, 1979.
- Turner, J. S., and L. B. Gustafson, The flow of hot saline solution from vents in the sea floor -- some implications for exhalative massive sulphide and other ore deposits, *Econ. Geol.*, 73, 1082-1100, 1978.
- Turner, R. J. W., Geology of the South Zone deposits, Jason proerty, Macmillan Pass area, Yukon, *Yukon Exploration and Geology 1983*, 105-114, 1984.

- Wentworth, C. K., A scale of grade and class terms for clastic sediments, *Jour. Geol.*, 90, 377-392, 1922.
- Williams, N., Studies of the base-metal sulfide deposits at McArthur River, Northern Territory, Australia I: The Cooley and Ridge deposits, *Econ. Geol.*, 78, 1005-1056, 1978a.
- Winn, R.D., R.J. Bailes, and K.I. Lu, Debris flows, turbidites and lead-zinc sulfides along a Devonian submarine fault scarp, Jason prospect, Yukon Territory, in *Deep-water clastic sediments, a core workshop*, edited by C.T. Seimers, R.W. Tillman and C.R. Williamson, pp. 396-416, Soc. Econ. Paleontologists Mineralogists, 1981.
- Yoshioka, R., O. Setsuo, and Y. Kitano, Calcium chloride type water discharge from Tatsushiro area in connection with swarm earthquakes, *Geochemical Journal*, 4, 61-74, 1970.
- Zierenberg, R. A., and W. C. Shanks, III, Isotopic constraints on the origin of the Atlantis II Deep metalliferous sediments, and the smectite geothermometer, *Geochim. Cosmochim. Acta*, (in press).
- Zierenberg, R. A., and W. C. Shanks, III, Mineralogy and geochemistry of epigenetic features in metalliferous sediment, Atlantis II deep, Red Sea, *Econ. Geol.*, 78, 57-72, 1984.